AFWAL-TR-80-3141
Part I

INVESTIGATION OF HIGH-ANGLE-OF-ATTACK MANEUVER-LIMITING FACTORS

Part I: Analysis and Simulation

DONALD E. JOHNSTON
DAVID G. MITCHELL
THOMAS T. MYERS
SYSTEMS TECHNOLOGY, INC.
13766 SOUTH HAWTHORNE BOULEVARD
HAWTHORNE, CALIFORNIA 90250

DECEMBER 1980

TECHNICAL REPORT AFWAL-TR-80-3141, PART I
Final Report for Period May 1976 — July 1980

Approved for public release; distribution unlimited.

FLIGHT DYNAMICS LABORATORY
AIR FORCE WRIGHT AERONAUTICAL LABORATORIES
WRIGHT-PATTERSON AIR FORCE BASE, OHIO 45433

NOTICE

This report has been reviewed by the Office of Public Affairs (ASD/PA) and is releasable to the National Technical Information Service (NTIS). At NTIS, it will be available to the general public, including foreign nations.

This technical report has been reviewed and is approved for publication.

Michael E Bise
MICHAEL E. BISE, Project Engineer
Control Dynamics Branch
Flight Control Division

R.O. Anderson
R. O. ANDERSON, Chief
Control Dynamics Branch
Flight Control Division

FOR THE COMMANDER

ROBERT C. ETTINGER, Colonel, USAF
Chief, Flight Control Division

"If your address has changed, if you wish to be removed from our mailing list, or if the addressee is no longer employed by your organization please notify AFWAL/FIGC, W-PAFB, OH 45433 to help us maintain a current mailing list."

AIR FORCE/56780/13 July 1981 — 440

(11) TR-80-3141-PT-1

UNCLASSIFIED

SECURITY CLASSIFICATION OF THIS PAGE (*When Data Entered*)

REPORT DOCUMENTATION PAGE

READ INSTRUCTIONS BEFORE COMPLETING FORM

1. REPORT NUMBER
(18) AFWAL-TR-80-3141, Part I

2. GOVT ACCESSION NO.
AD-A101 646

3. RECIPIENT'S CATALOG NUMBER

4. TITLE (*and Subtitle*)
(6) INVESTIGATION OF HIGH-ANGLE-OF-ATTACK
MANEUVER ~~[illegible] FACTORS~~ Limiting Factors.
Part I. Analysis and Simulation.

5. TYPE OF REPORT & PERIOD COVERED
(9) Final Report,
May 1976 - July 1980,

6. PERFORMING ORG. REPORT NUMBER
(30)

7. AUTHOR(s)
(10) Donald E. Johnston, David G. Mitchell,
and Thomas T. Myers

8. CONTRACT OR GRANT NUMBER(s)
(15) F33615-76-C-3072

9. PERFORMING ORGANIZATION NAME AND ADDRESS
Systems Technology, Inc.
13766 South Hawthorne Boulevard
Hawthorne, California 90250

10. PROGRAM ELEMENT, PROJECT, TASK AREA & WORK UNIT NUMBERS
PE 62201F
(12) 203

11. CONTROLLING OFFICE NAME AND ADDRESS
AFWAL/FIGC
Air Force Wright Aeronautical Laboratories
Air Force Systems Command
Wright-Patterson AFB, OH 45433

12. REPORT DATE
(11) DEC 80

13. NUMBER OF PAGES
203

14. MONITORING AGENCY NAME & ADDRESS (*if different from Controlling Office*)
(16) 2403 (17) 05

15. SECURITY CLASS. (*of this report*)
UNCLASSIFIED

15a. DECLASSIFICATION/DOWNGRADING SCHEDULE

16. DISTRIBUTION STATEMENT (*of this Report*)

Approved for public release; distribution unlimited.

17. DISTRIBUTION STATEMENT (*of the abstract entered in Block 20, if different from Report*)

18. SUPPLEMENTARY NOTES

19. KEY WORDS (*Continue on reverse side if necessary and identify by block number*)

High AOA, flying qualities, stall/departure, simulation

20. ABSTRACT (*Continue on reverse side if necessary and identify by block number*)

The high-angle-of-attack, low-speed stall/departure characteristics of the F-4J and F-14A are analyzed, using a six-degree-of-freedom mathematical model with nonlinear aerodynamics. Cause-effect relationships are investigated for maneuver limiting factors including wing rock, nose slice, and rolling departures. Cross-derivatives of $\mathcal{L}'_{\dot{\alpha}}$, $N'_{\dot{\alpha}}$, and M_β alter key transfer function

(continued) > cont.

DD FORM 1 JAN 73 1473 EDITION OF 1 NOV 65 IS OBSOLETE

340415

UNCLASSIFIED

SECURITY CLASSIFICATION OF THIS PAGE (*When Data Entered*) cont.

parameters. A piloted simulation validates analytic predictions and demonstrates that departure warning, susceptibility, and severity are strongly influenced by the static cross-derivatives. A connection between roll numerator parameter values and pilot perception of departure susceptibility and severity is identified. Potential modifications for the high AOA sections of the MIL-F-8785B Flying Qualities Specification are proposed: a criterion for the real part of the roll numerator root, further recommendations for minimizing departure susceptibility and certain sideslip influences, and a flying quality rating form for assessing departure and recovery characteristics.

Part I, Analysis and Simulation, presents a summary of the complete investigation and results. Part II, Piloted Simulation Assessment of Bihrle Departure Criteria, presents a detailed comparison of analytical prediction and piloted simulation results for a specific set of programmed control deflections. Part III, Appendices — Aerodynamic Models, contains the detailed aerodynamic models employed in the F-4J and F-14A high-angle-of-attack analysis and validation and the equations of motion, aerodynamic models, control system configurations, etc., employed in the piloted simulation.

FOREWORD

This research was sponsored by the Air Force Wright Aeronautical Laboratories, Air Force Systems Command, under Contract F33615-76-C-3072, Work Unit 24030514. Mr. Gary K. Hellmann was the initial project monitor. This responsibility was later transferred to Mr. Michael E. Bise (AFWAL/FIGC). Support of the piloted simulation was also provided by the Naval Air Development Center where Mr. Mark Stifel served as project monitor. The analytic work was performed at Systems Technology, Inc., Hawthorne, California. The work was performed during the period 13 May 1976 through 30 July 1980. The STI Technical Director was Mr. I. L. Ashkenas. Mr. D. E. Johnston was Principal Investigator and STI Project Engineer. The piloted simulation was accomplished at the McDonnell Aircraft Co., St. Louis, Missouri. The report manuscript was submitted in September 1980.

The authors wish to express acknowledgment and thanks to their many coworkers for contributions, both general and detailed, in the program: at STI, Mr. G. L. Teper for invaluable aid in accomplishing the digital simulation, Mr. T. T. Myers for development and validation of the F-4 and F-14 aerodynamic models and for most of the initial analytic support, and Mr. R. H. Hoh for checkout and accomplishment of the piloted simulation. Mr. Hoh also served as one of the subject pilots. At MCAIR, Mr. H. Passmore directed setup and operation of the piloted simulation. Special thanks are due to Lt. Col. R. M. Cooper, Maj. J. A. Fain, Jr., and Maj. J. Jannarone of the 6510th Test Wing and Maj. P. Tackabury of the Test Pilot School, Edwards Air Force Base, for their contribution in refining the high angle of attack flying quality rating scale and their professional approach in accomplishing the sometimes tedious simulation experiments.

Finally, appreciation is extended to Mr. P. Kelly of Grumman Aircraft Co. and Mr. M. Humphreys of the Naval Air Test Center for support in obtaining much of the F-14 data and information, to Mr. R. Wood of the Air Force Flight Test Center for invaluable comments and suggestions concerning the flying quality rating scale, and to Mr. R. Woodcock (AFWAL/FIGC) for his careful critique and editorial refinement of this final report.

TABLE OF CONTENTS

TABLE OF CONTENTS (Concluded)

LIST OF ILLUSTRATIONS

LIST OF ILLUSTRATIONS (Continued)

LIST OF ILLUSTRATIONS (Continued)

LIST OF ILLUSTRATIONS (Continued)

LIST OF ILLUSTRATIONS (Concluded)

LIST OF TABLES

DEFINITION OF AXIS SYSTEMS

Unless otherwise indicated, all moment coefficients and derivatives are referenced to the fuselage-centerline-oriented body system of axes. All longitudinal force coefficients and derivatives are referenced to the flight path (or wind) system of axes. These axis systems are defined in the sketch below.

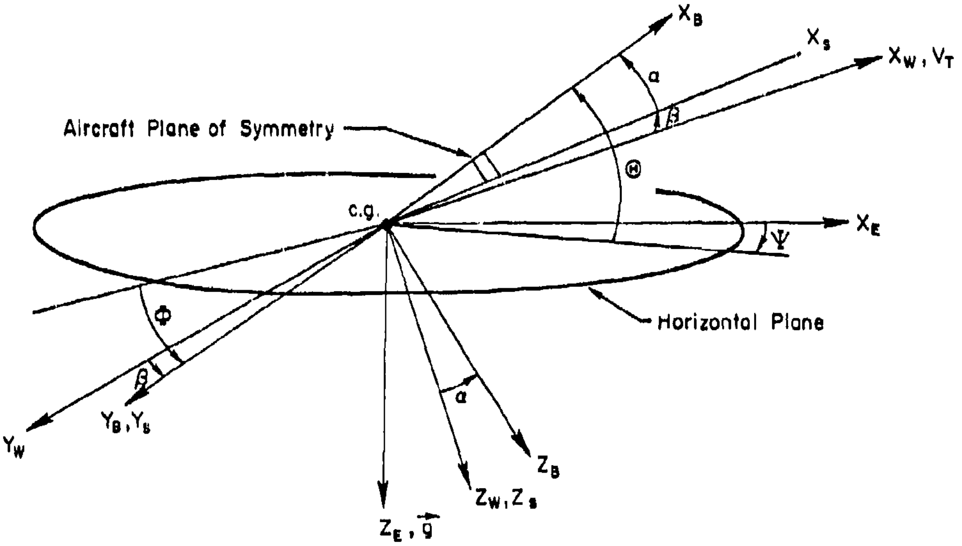

LIST OF SYMBOLS

a_y'	Body-mounted lateral accelerometer signal, ft/sec^2
A_i	Root locus gain of transfer function numerator, N_δ^i
AOA	Angle of attack
b	Wing reference span, ft
$\bar{c}$	Wing mean aerodynamic chord, ft
c.g.	Center of gravity
C_D	Dimensionless drag coefficient
℄	Aircraft fuselage centerline
CAS	Calibrated airspeed, kt
C_ℓ	Dimensionless body axis rolling moment coefficient
C_{ℓ_i}	Change in C_ℓ with change in variable, i
C_L	Dimensionless stability axis lift coefficient
C_{L_i}	Change in C_L with change in variable, i
C_m	Dimensionless body axis pitching moment coefficient
C_{m_i}	Change in C_m with change in variable, i
C_n	Dimensionless body axis yawing moment coefficient
C_{n_i}	Change in C_n with change in variable, i
$C_{n_{\beta_{dyn}}}$	Stability axis dynamic directional stability parameter defined as $C_{n_{\beta_{dyn}}} = C_{n_\beta} \cos \alpha - (I_z/I_x)C_{\ell_\beta} \sin \alpha$, with coefficients and inertias in body-centerline-oriented axes
C_y	Dimensionless body or stability axis side force coefficient
C_{y_i}	Change in C_y with change in variable, i
D	Total drag, $\bar{q}SC_D$, lb

LIST OF SYMBOLS (Continued)

F_{LS}	Lateral stick force, lb
F_P	Rudder pedal force, lb
g	Gravitational acceleration, 32.2 ft/sec^2
H (or h)	Reference altitude, ft
HDD	Head-down display
HUD	Head-up display
i	Aircraft state variable, e.g., α, β, θ, ϕ, V_T; or control variable, δ
Im	Imaginary part of complex second-order mode, $\omega\sqrt{1 - \zeta^2}$, rad/sec, or imaginary axis
I_x, I_y, I_z, I_{xz}	Moments of inertia about x-, y-, and z-body centerline-oriented axes, and product of inertia about x-z body axes, respectively, slug-ft^2
K	Root locus gain term
K_{xf}	Crossfeed gain for $\delta_{stk} \rightarrow \delta_r$ crossfeed, deg/in.
K_{δ_a}	Gain for $\delta_{stk} \rightarrow \delta_a$ control, deg/in.
L	Total lift, $\bar{q}SC_L$, lb
$\mathcal{L}_i$, M_i, N_i	Aerodynamic rolling, pitching, and yawing moment about aircraft I_{xx}, I_{yy}, I_{zz} principle axes due to variable, i
$\mathcal{L}'_i$	Total aerodynamic rolling moment about aircraft body axis other than principal axis, $\mathcal{L}'_i = [(\mathcal{L}_i + I_{xz}N_i/I_x)/(1 - I_{xz}^2/I_xI_z)]$
$\mathcal{L}'_{i_{dyn}}$	$\mathcal{L}'_i \cos \alpha + N'_i \sin \alpha$
$\mathcal{L}'_\alpha$	$\beta_o[\partial^2(\mathcal{L}')/\partial(\beta)\partial(\alpha)] = \beta_o(\bar{q}Sb/I_x)C'_{\ell_{\beta\alpha}}$
L_1	Aileron command travel limit for roll rate command augmentation, deg
L_2	Command travel limit for δ_r with $\delta_{stk} \rightarrow \delta_r$ crossfeed, deg
LCDP	Lateral control divergence parameter, $C_{n_\beta} - C_{\ell_\beta}(C_{n_\delta}/C_{\ell_\delta})$

LIST OF SYMBOLS (Continued)

LHP	Left half-plane
m	Aircraft mass, slugs
M	Mach number
n_z	Normal acceleration at center of mass, $-a_z$, g units
N'_i	$N'_i = [(N_i + I_{xz} \mathcal{L}_i/I_z)/(1 - I_{xz}^2/I_x I_z)]$
$N'_{i_{dyn}}$	$N'_i \cos \alpha - \mathcal{L}'_i \sin \alpha$
N'_α	$\beta_o[\partial^2(N')/\partial(\beta)\partial(\alpha)] = \beta_o(\bar{q}Sb/I_z)C'_{n_{\beta\alpha}}$
$N_{\beta_{dyn}}$	Dimensionalized form of $Cn_{\beta_{dyn}}$; equivalent to N'_β in stability axis
N^i_δ	Numerator of state variable i to control variable δ transfer function
$N^{i_1 i_2}_{\delta_1 \delta_2}$	Coupling numerator for effect of control variables (δ_1, δ_2) on state variables (i_1, i_2)
p_c	Roll rate command
p, q, r	Total inertial angular body axis roll, pitch, and yaw velocity, respectively, rad/sec
PIO	Pilot-induced oscillations
PSG	Post-stall gyrations
$\bar{q}$	Dynamic pressure, $(1/2)\rho V_T^2$, lb/ft^2
Re	Real part of complex second-order mode, $\zeta\omega$
RHP	Right half-plane
s	Laplace operator
S	Reference wing area, ft^2
SRI	Stick-rudder interconnect
T_R	Roll subsidence time constant

LIST OF SYMBOLS (Continued)

T_R^{θ}	Time constant of root of the aerodynamically cross-coupled numerator $N^{\theta}_{\delta_{stab}}$ corresponding to roll mode in Δ
T_s	Spiral time constant
T_{θ_3} or T_s^{θ}	Time constant of root of the aerodynamically cross-coupled numerator $N^{\theta}_{\delta_{stab}}$ corresponding to spiral mode in Δ
T_{ϕ_1}	Time constant of non-minimum phase N^{ϕ}_{δ} root
T_{ϕ_2}	Time constant of minimum phase N^{ϕ}_{δ} root
u, v, w	Perturbation velocities along the x, y, and z wind axes, respectively, ft/sec
V_T	Total aircraft inertial translational velocity, ft/sec
W	Aircraft weight, lb
X_i, Y_i, Z_i	Incremental change in wind-axis components of total force (aerodynamic, gravity, and thrust) due to incremental change in in state variable quantity i
Y_i^*	Y_i/V_{T_0}
Y_{θ}	Transfer function for pilot model closing the pitch loop
Y_{ϕ}	Transfer function for pilot model closing the roll loop
Z_p	Kinematic roll coupling term in $\dot{\alpha}$ equation, $\beta_0 \cos \alpha_0$
Z_r	Kinematic yaw coupling term in $\dot{\alpha}$ equation, $\beta_0 \sin \alpha_0$
α	Angle of attack, deg
β	Sideslip angle, deg
γ	Longitudinal flight path angle, deg
δ	Control deflection, e.g., δ_{stab}, δ_a, δ_r, δ_{stk}, δ_D
δ_{stk}	Lateral stick deflection, $8.08\ \delta_a + 11.6\delta_{sp}$, in.
Δ	Transfer function denominator

LIST OF SYMBOLS (Continued)

ζ	Damping ratio
λ	Lateral flight path angle, deg
Λ	Wing sweep angle, deg
ξ	Thrust angle with respect to body centerline axis
τ	Time response lag, sec
ϕ, θ, ψ	Euler angles between gravity-oriented inertial axis and aircraft body axis,deg
ω	Frequency, rad/sec; with subscript, modal undamped natural frequency
ω_p^ϕ	Natural frequency of complex roots of the aerodynamically cross-coupled numerator $N^\phi_{\delta_{stk}}$ corresponding to ω_p in Δ
ω_{sp}^ϕ	Natural frequency of complex roots of the aerodynamically cross-coupled numerator $N^\phi_{\delta_{stk}}$ corresponding to ω_{sp} in Δ

Subscripts

a	Aileron
coupl	Coupled lateral-longitudinal
d	Dutch roll
D	Differential stabilizer
lat	Lateral
long	Longitudinal
max	Maximum
o	Trim or steady state
p	Phugoid
r	Rudder

LIST OF SYMBOLS (Concluded)

R	Roll
RS (or SR)	Coupled roll-spiral
s	Spiral (or stabilator)
sp	Short period (or spoiler)
stab	Stabilator

SECTION I

INTRODUCTION

A. BACKGROUND

For modern military aircraft, manageable flight at high, near-stall angles of attack is a key effectiveness and safety factor. The safe angles of attack and sideslip attainable in level and maneuvering flight often represent the important differences in both offensive/defensive capability and accident histories of otherwise equivalent aircraft. In the past generation of fighter aircraft, surprise loss of control departure generally has been of concern as a key maneuver-limiting factor. The more recent generation has emphsized design for departure resistance but not necessarily prevention. Many operational pilots desire the capability to depart the aircraft on command as a last-ditch defensive maneuver, since departure is generally violent with unpredictable results from the attacker's viewpoint. The key element then revolves around departure resistance (or susceptibility), warning, severity, and recoverability. Accordingly, the issue of improved utility and safety at high angles of attack has been re-recognized as an area of fruitful research and development.

The recent upsurge in interest has resulted in numerous studies devoted to identifying the safety-related maneuver-limiting phenomena inherent in:

- Buffet
- Pitchup or "dig-in"
- Roll reversal
- Wing rock
- Nose slice
- Rolling departure — snap roll

Some of these phenomena are perturbations about a steady flight condition (e.g., buffet, wing rock), which not only limit tracking capability (as shown in Reference 1) but also may serve as warning of approaching "departure" from controlled flight (e.g., nose slice, rolling departure). The more interesting and mysterious of these phenomena are the latter, and considerable effort has been expended in correlating the angles of attack at which such behavior occurs with various aerodynamic stability and control parameters (e.g., References 2-4). Such open-loop "correlations," while useful, are not so satisfying or instructive as the more positive identification of causal factors offered by the methods developed in Reference 5.

The difficulty is in identifying causal relationships in the complex interactive pilot/vehicle situation during uncoordinated flight, where aerodynamic cross-coupling can compound vehicle dynamic characteristics. The previous (Reference 5) analysis and pilot simulation showed the static aerodynamic cross-coupling coefficients $\mathcal{L}'_{\alpha}$ and N''_{α} to contribute to closed-loop nose-slice departure susceptibility and severity in the A-7 aircraft. It represented an initial successful and promising new attack on an old problem. But configuration differences among aircraft types, models and even loadings have been observed to produce gross differences in behavior through changed aerodynamics and inertial characteristics. Thus it is desirable that the same methods be applied to additional high-performance fighter aircraft having widely differing high AOA handling characteristics to see if further cause-effect relationships can be identified.

Accordingly, the stated or implied goals of this program are to:

- Identify key design parameters that limit high-angle-of-attack maneuverability for contemporary high-performance attack and fighter-type aircraft.
- Postulate fundamental aerodynamic and control system design methodologies that will alleviate the limiting conditions.
- Formulate handling qualities requirements for high AOA maneuvering flight to be incorporated in MIL-F-8785C, the military flying qualities specification for piloted airplanes.

B. TECHNICAL APPROACH

The research encompassed four major technical areas. The first was devoted to development and validation of aerodynamic models for two fighter aircraft having significantly different high AOA maneuver-limiting characteristics. The two aircraft selected, the F-4J and the F-14A, were found to represent almost opposite extremes in their range of departure susceptibility and severity. Attention was then turned to investigation of maneuver-limiting characteristics of each airframe and identification of causal relationships based on quasi-linear* analysis at symmetric and asymmetric ($\beta \neq 0$) flight conditions. The causal parameters were varied to alter the dynamic characteristics of each airframe at high AOA. Predicted characteristics were checked utilizing complete six-degree-of-freedom (6 DOF) models with nonlinear aerodynamics, and any differences between the quasi-linear frozen point analytic predictions and the nonlinear model results were resolved.

The second task involved development of methods, criteria, and an associated pilot rating scale, for evaluation of handling qualities when approaching controllability limits. Previous analysis and simulation (Reference 5) has demonstrated that the Cooper-Harper handling quality rating scale is inapplicable for departure/recovery flight situations. Therefore, a new pilot rating scale is required specifically for high angles of attack.

The third task, pilot simulation, was performed to evaluate the influence of intentionally varied maneuver-limiting characteristics (wing rock, nose slice, etc.) under different normal flying situations such as training flights and air combat tracking tasks; to identify key

---

*It is recognized that these linear analysis techniques are applied to phenomena which may be nonlinear in nature. However, the intent of the study is to investigate in an understandable manner the conditions which can lead to or precipitate rapid changes in motion, as opposed to analyzing the fully developed large angle phenomena. Therefore, piecewise linearity is appropriate — but care should be taken in attempting to extrapolate the results.

flying quality parameters in terms of departure resistance, warning, severity, and recovery for possible inclusion in the flying qualities specification; and to exercise and refine as necessary the new pilot rating scale.

The fourth task involved assessment and correlation of results of the simulation with other applicable results and data; and formulation of high AOA maneuvering flight generalized design guides and flying qualities criteria for incorporation into MIL-F-8785C.

SECTION II

AIRCRAFT HIGH AOA DYNAMIC CHARACTERISTICS

This section presents condensed results of an extensive analysis of the high AOA dynamic characteristics of the two example aircraft. The F-4J is treated first, followed by the F-14A. The high AOA characteristics of each aircraft are described as determined in flight test and operational deployment. The analytical models are briefly summarized and example comparisons shown to demonstrate the match obtained with the actual aircraft.

Results of linear, frozen-point dynamic analysis at a series of symmetric and asymmetric ($\beta \neq 0$) flight conditions are summarized. This analysis provides insight to potential causal factors behind undesirable characteristics at high AOA, showing examples of advantages and limitations of such analysis when applied to situations in which aerodynamics are obviously quite nonlinear. In particular, this section identified lateral-directional static aerodynamic cross-coupling as a key factor in determining high AOA stability and controllability characteristics.

A. F-4J ANALYSIS

The F-4J model of the F-4 family was selected because a previously validated aerodynamic model (Reference 6) was in hand. However, all versions of the aircraft with an unslatted leading edge wing are reported to exhibit quite similar high AOA flying characteristics: increasing AOA produces buffet of increasing severity, increasingly adverse yaw, wing rock, mild pitch-up, stall, and finally departure. A representative trimmed lift curve with onset of these handling phenomena is shown in Figure 1 from Reference 7. Above about 11 deg AOA, aileron adverse yaw becomes significant and rudder is used for roll control.

Wing rock appears primarily as a rolling-sideslipping motion. It is often described by pilots as a divergent dutch roll which is easily

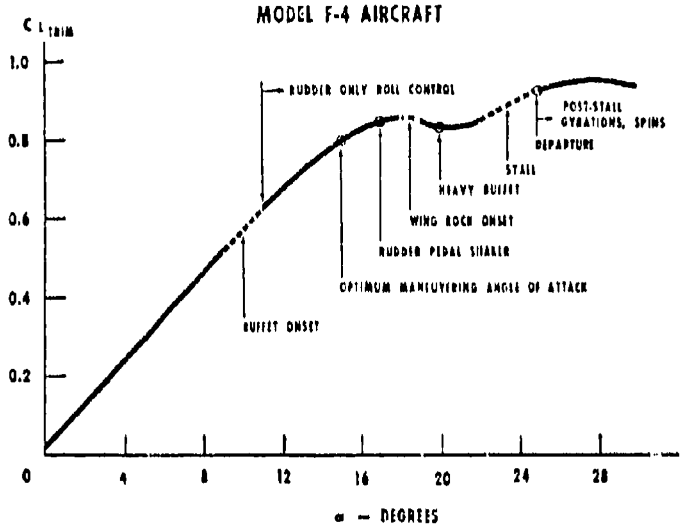

Figure 1. Basic F-4 Trimmed Lift Curve (from Ref. 7)

aggravated or caused by pilot lateral stick inputs. The angle of attack for onset and the severity actually depend upon several factors, including c.g. location, roll inertia or loading (clean vs. external stores), gear and flap settings, etc. It is generally more pronounced at light weight, with low roll inertia, and at forward c.g. The oscillations generally require 10 sec or more of sustained high AOA to develop. Amplitudes can be large enough (±30 deg ϕ and ±10 deg β) to interfere with tracking performance, or to be highly uncomfortable when escorting considerably slower aircraft.

The mild pitch-up is alleviated by a pitch rate damper but does result in some lightening of stick forces. It has been described by some pilots as a "dig-in" during slow turns. Possibly it is more of a stall warning cue than a maneuver-limiting problem.

Departure is described variously as nose slice, roll departure, or both. Its onset also appears to depend upon c.g. location and aircraft inertia variations. Although shown in Figure 1 to occur at considerably higher AOA than wing rock, departure is not necessarily preceded by wing rock — especially if AOA is rapidly increased.

1. Analytic Model

The F-4J aerodynamic model (Reference 6) was derived from three excellent but separate data sources (References 8-10). It was assembled to model as closely as possible the F-4J sub- and transonically for a moving-base simulation used to train U.S. Navy pilots in air combat maneuvering. It therefore had to be a very good representation of the complete aircraft in high AOA maneuvering up through stall. The instructor pilots pronounced the simulation "credible and realistic of actual F-4J handling characteristics."

The history of development of the complete aerodynamic model and the data package is presented in Part III, Appendix I. In brief, the aerodynamic coefficients represent the following flight regime:

$$0 < \alpha < +110 \text{ deg}$$

$$-30 < \beta < +30 \text{ deg}$$

For this analysis the look-up table data were restricted to low Mach (<0.4) and a single altitude (h = 15,000). Weight and inertia characteristics representative of partially full internal fuel tanks, an empty 600 gal centerline tank, and missile pylons on wing stations 2 and 8 have been assumed.

Conventional 6 DOF equations plus kinematic terms are employed with the moment equations in body centerline axes, the force equations in wind axes, and aircraft orientation angles in standard Euler axes. The nonlinear equations of motion, aerodynamic force and moment equations, auxiliary equations, etc., are detailed in Appendix I (Part III).

A block diagram of the basic flight control and augmentation mechanization is presented in Figure 2. Aircraft control is exerted through horizontal stabilator (δ_{stab}), rudder (δ_r), aileron (δ_a), and spoiler (δ_{sp}) surfaces. The aileron and spoiler systems are interconnected such that lateral deflection of the control stick produces downward

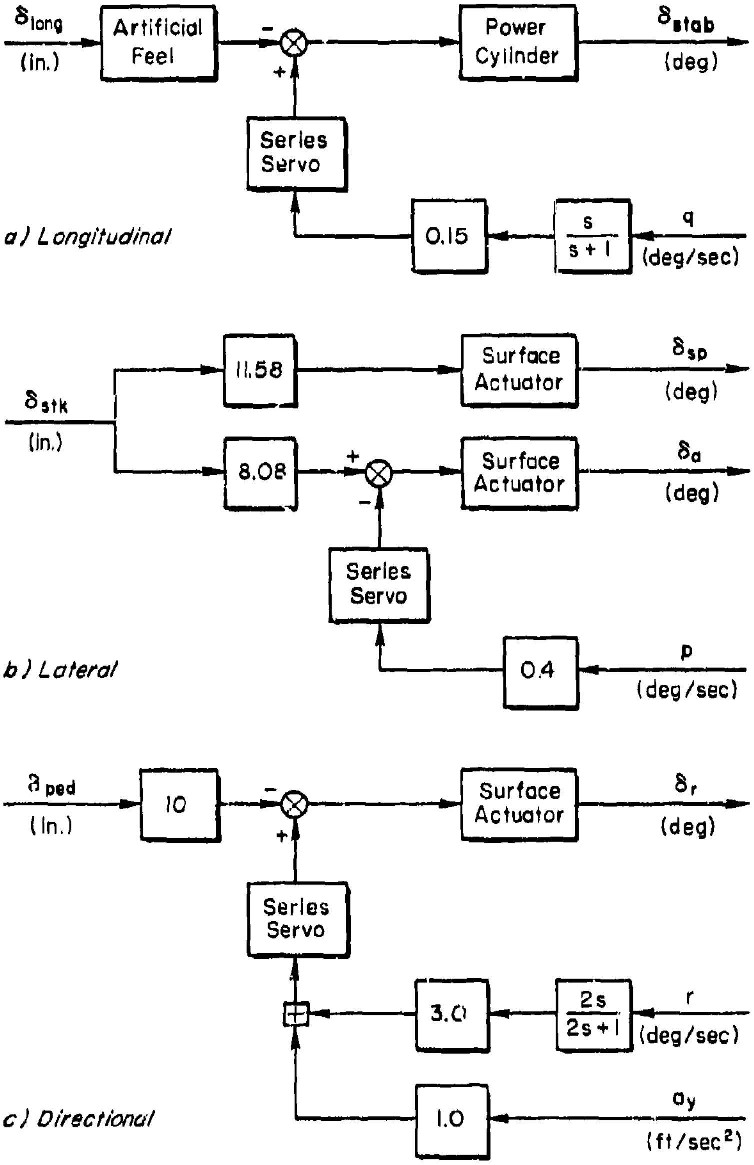

Figure 2. F-4J Flight Control System

deflection of one aileron and upward deflection of the opposite spoiler. Stability augmentation is provided in all three axes, but it is common practice for the pilot to turn the roll damper off during high AOA maneuvering. The complex artificial feel system was not modeled in this analysis and simulation.

2. Model Validation

As a part of the checkout and acceptance test, the simulation based on the Reference 6 aerodynamic data was flown through various offensive and defensive air combat maneuvers, stalls, and departures by Navy instructor pilots, who indicated that it adequately represented the F-4J handling and performance. This provided the first gross validation of the aerodynamic model.

Actual flight test traces of F-4J high AOA dynamic responses are not available to compare against those of the mathematical models. The available high AOA flight traces are from an F-4E stall/post-stall flight test (Reference 11). However, Reference 12 indicates that all hard-wing models of the F-4 have approximately the same stall/departure characteristics. The F-4E has a nose section approximately 5 ft longer than the F-4J; this could cause some difference in side force due to asymmetric vortex shedding at high AOA (Reference 13). In addition the flight test vehicle was equipped with a spin chute, had a reinforced aft fuselage structure to handle the spin chute loads, and is presumed to have offsetting ballast in the nose. Thus, its pitch and yaw inertia characteristics are quite different from the F-4J, as shown in Table 1. This difference is assumed to have minor influence on the sequence of stall/departure characteristics with increasing AOA. The larger yaw inertia and longer nose (greater vortex shedding) of the F-4E could be offsetting departure susceptibility factors. But the inertia differences should produce measurable differences in dynamic response parameters such as dutch roll frequency, response to control inputs, and angular rates associated with departure. For example, scaling parameters by the ratio of inertias gives ratios of ω_{sp} and ω_d of 1.11.

TABLE 1. COMPARISON OF F-4E AND F-4J WEIGHTS AND INERTIAS

	F-4E (Reference 11)	F-4J
℄ stores	Empty tank	Empty tank
Wing stores	Pylons 1, 2, 8, 9	Pylons 2, 8
W (lb)	40,000	37,000
c.g. (% $\bar{c}$)	28.1	29.3
I_x (slug-ft^2)	27,500	23,850
I_y (slug-ft^2)	157,000	127,400
I_z (slug-ft^2)	180,600	146,000
I_{xz} (slug-ft^2)	5,500	2,210

Example comparisons between the F-4E test results and the nonlinear 6 DOF F-4J math model are shown in Figures 3-5. Figure 3 shows the F-4E at a nearly steady AOA averaging about 23 deg. The rudder trace indicates that the yaw damper is on. The wing rock starts as a divergent dutch roll but then appears to limit at approximately 40-50 deg roll amplitude with a ϕ/β ratio between 2 and 3. Also the divergence grows linearly, instead of exponentially as it would at constant ζ. During the large, constant-amplitude ϕ and β oscillation, the AOA trace shows a small oscillation at twice the frequency of the lateral oscillation.

Figure 4 is the F-4J simulation trimmed to $\alpha_0 = 23$ deg and disturbed by a lateral stick pulse. Here the dutch roll also diverges almost linearly for about three cycles and then becomes limited in amplitude. The ϕ/β ratio is about 3 during the limit cycle. An oscillation develops in the AOA trace, again with a frequency double that of the lateral oscillation. The characteristics are remarkably similar except for the period of the oscillations. The higher frequency of the F-4E oscillations is most likely due to a higher dynamic pressure. In Figure 3 the

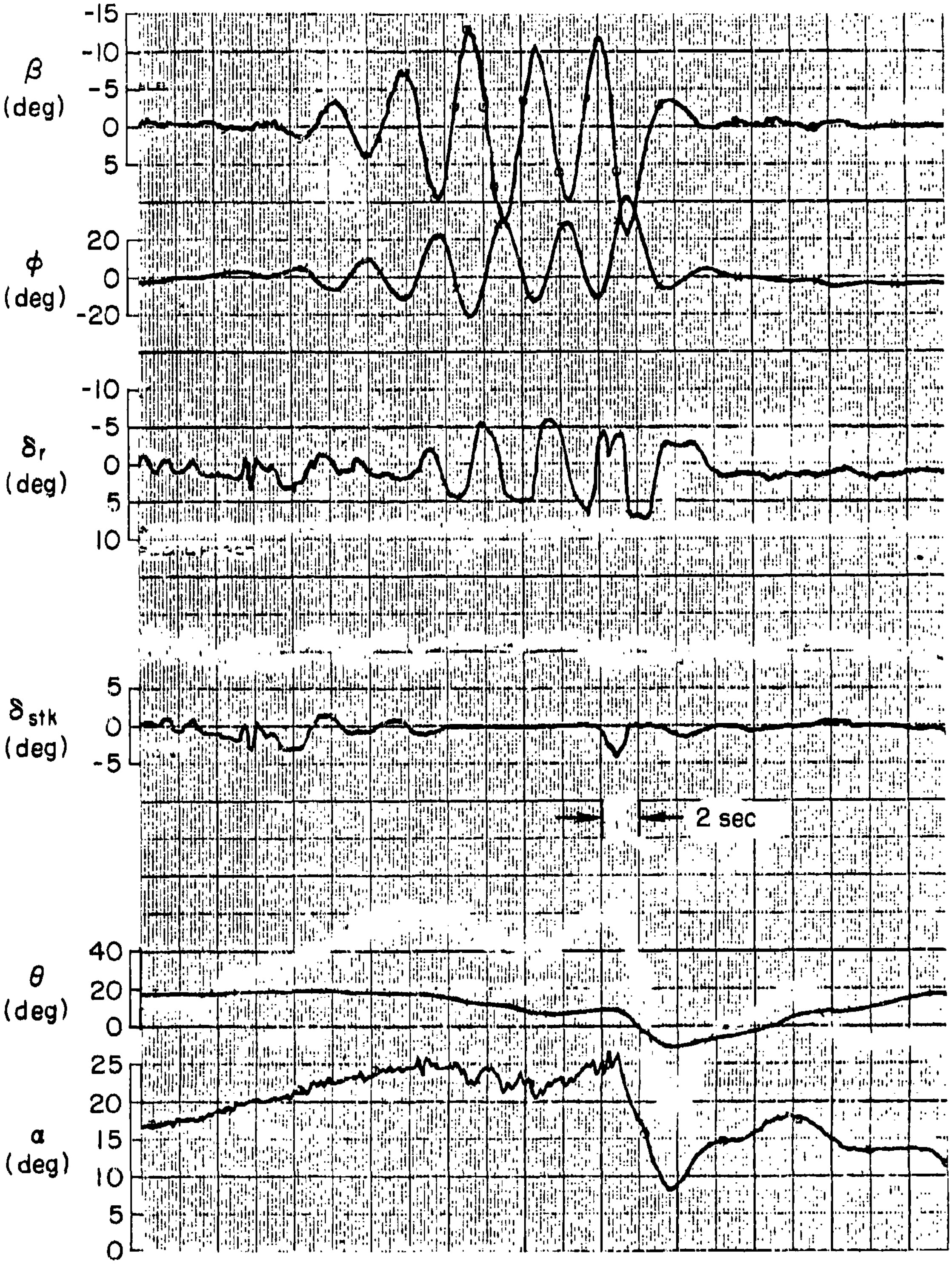

Figure 3. F-4E Flight Test Pullup and Steady Wing Rock

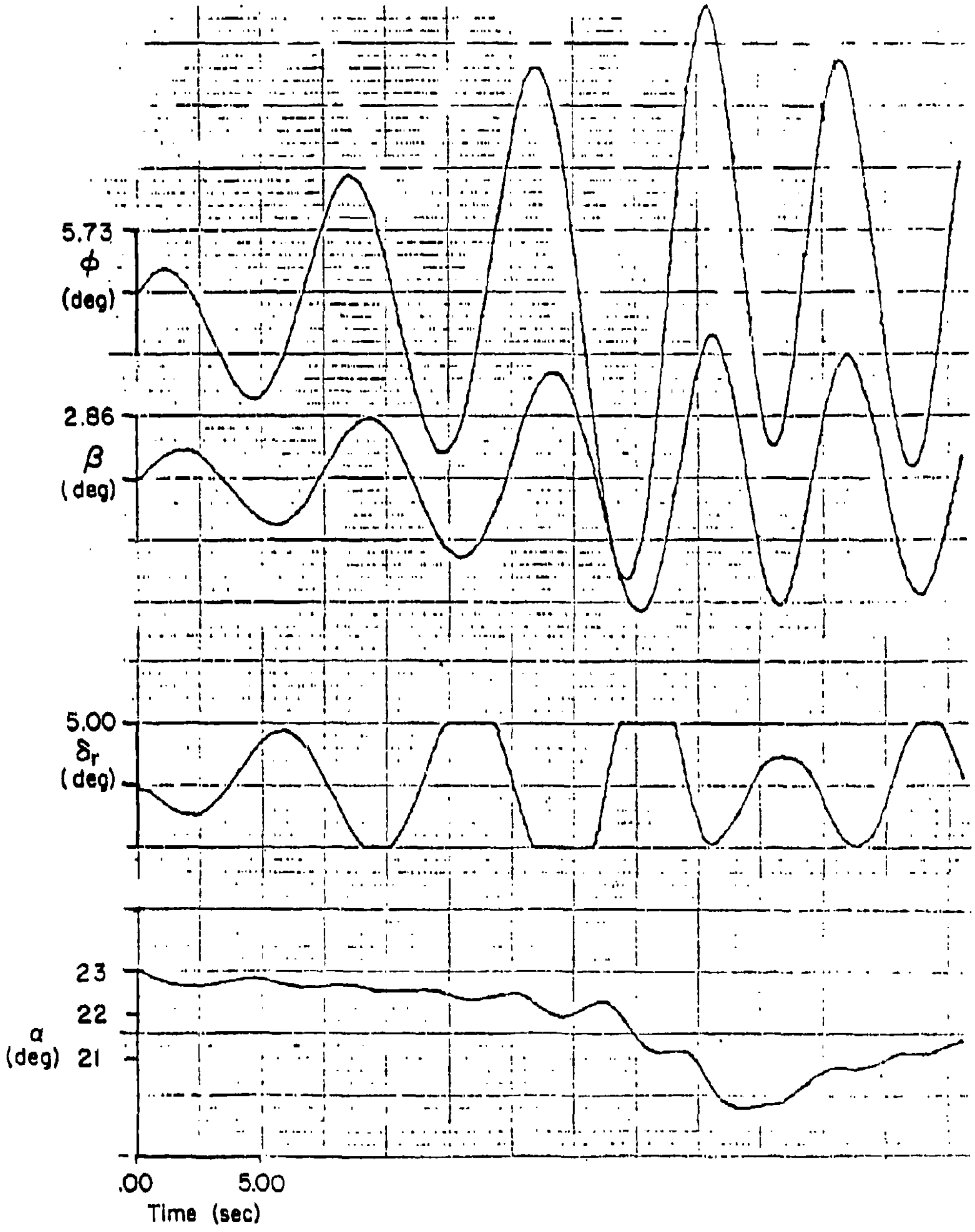

Figure 4. F-4J Model Wing Rock at α_0 = 23 deg, β_0 = 0; Pitch and Yaw SAS On

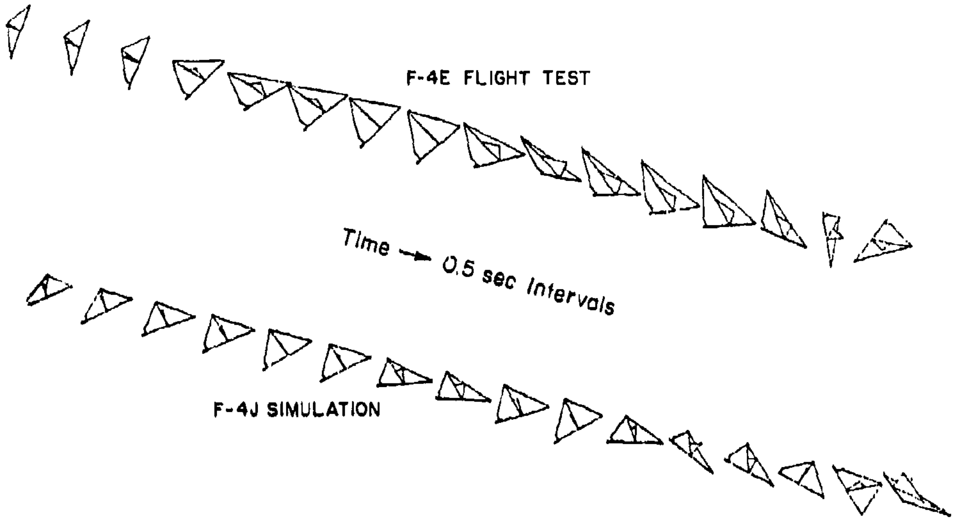

Figure 5. Departure During Left Turn

aircraft was pulled up to $\alpha \triangleq 23$ deg within about 10 sec and then held at this AOA for about 15 sec. The initial Mach number was not indicated. In Figure 4 the model was trimmed at an initial speed corresponding to $\alpha_0 = 23$ deg. If all other factors were exactly the same, the difference in frequency shown here would be accounted for with only a 30 percent difference in speed.

The computer-generated images of Figure 5 show a comparison of the F-4E aircraft and the F-4J model departures from a wind-up turn to the left. The departure onset is quite similar. Both depart with a nose slice away from the turn accompanied by a roll oscillation. The F-4E ends up with more of a rolling departure, while the F-4J ends with more of a yaw departure (nose slice). This difference in final motion is probably influenced greatly by the differences in inertias. The F-4E has 24 percent higher yaw inertia and 7.3 percent higher ratio of yaw to roll inertia. Thus it could be expected to be more resistant to yaw departure and prone to roll departure.

Since our main interest is in modeling and establishing causal relationships leading to high AOA maneuver-limiting factors rather than modeling post-stall gyration and spin, the foregoing match of the nonlinear wing rock behavior and nose slice onset is considered to be one validation of the aerodynamic model. Appendix I of Part III and portions of the analysis and simulation to be presented later offer additional validation.

One key aspect is that the aerodynamic model demonstrates both limit cycle wing rock and nose slice departure without introducing artificial hysteresis in aerodynamic coefficients (Reference 14), drastic changes in roll damping (Reference 10), or contrived elevator control asymmetry (Reference 15).

3. Dynamic Analysis

In high AOA maneuvering flight it is not uncommon for the aircraft to be in asymmetric ($\beta \neq 0$) flight — either intentionally or unintentionally. Previous studies (e.g., References 5, 16-18) have shown that static aerodynamic cross-coupling due to sideslip can have significant influence on aircraft stability and dynamic characteristics and possibly the departure characteristics. For example, Figures 6-8 reflect the pitch, roll, and yaw aerodynamic moments, respectively, for our F-4J model as a function of α and β. For simplicity the aerodynamic moments were assumed symmetric with sideslip. Over the region $15 < \alpha < 25$ deg pitching moment is significantly influenced by sideslip, and rolling and yawing moments due to sideslip vary greatly with AOA. This is the same AOA region in which the various maneuver-limiting characteristics of the F-4 are exhibited. Thus, in the analysis to follow, attention will be devoted to examining the possible influence of static aerodynamic cross-coupling on high AOA maneuver-limiting factors. Aircraft open-loop stability characteristics will be analyzed first, and then closed-loop piloted control aspects will be determined.

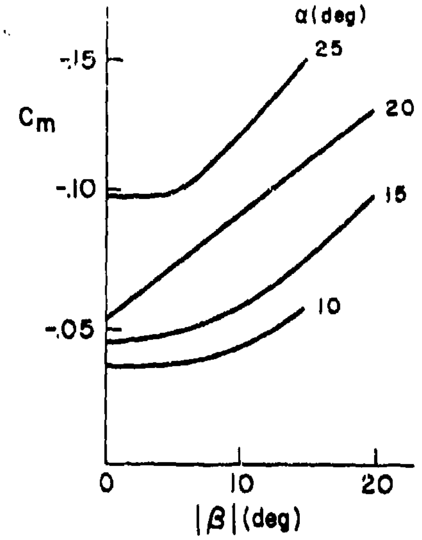

Figure 6. F-4J Pitch Coefficient Variation with α, β

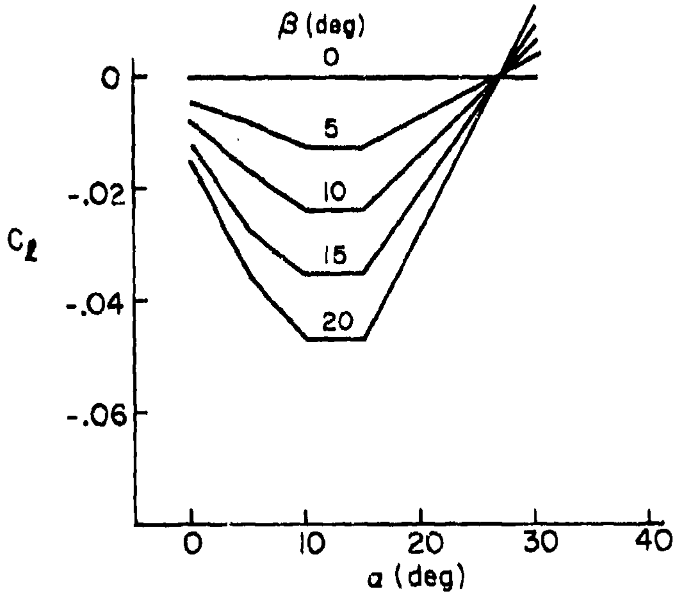

Figure 7. F-4J Roll Coefficient Variation with α, β

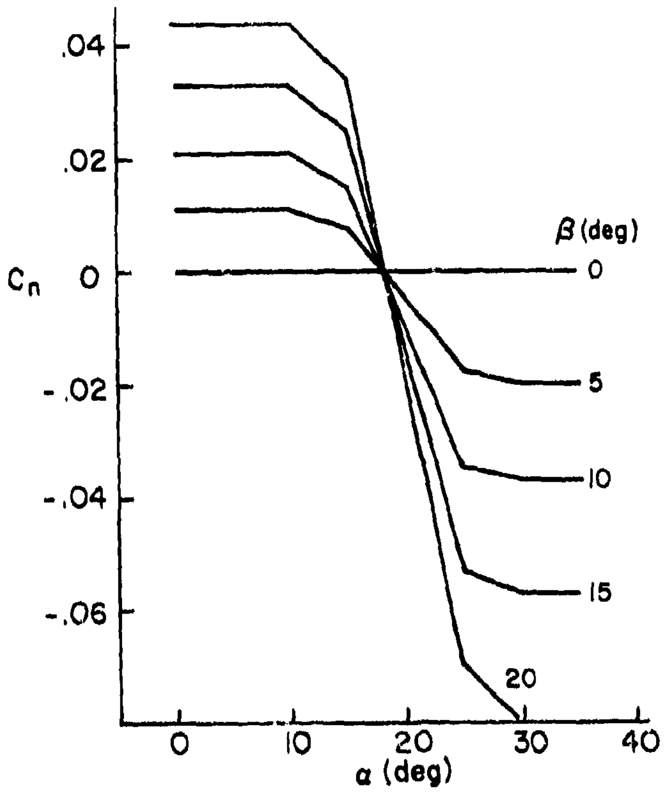

Figure 8. F-4J Yaw Coefficient Variation with α, β

a. Open-Loop Dynamic Characteristics

Figure 9 presents a locus of longitudinal short-period and lateral dutch roll root migrations with AOA in wings-level, symmetric, 1-g flight at an altitude of 15,000 ft. These dynamic parameters represent symmetric, linearized, fixed-operating-point conditions. With increasing AOA the dutch roll mode is seen to progress from a lightly damped stable mode to oscillatory divergence and, finally, to a pair of aperiodic divergences while the longitudinal short period remains relatively unchanged.

Also shown in the figure is the AOA at which the dynamic stability parameter $Cn_{\beta_{dyn}}$ becomes zero. At lower AOA the parameter is positive,

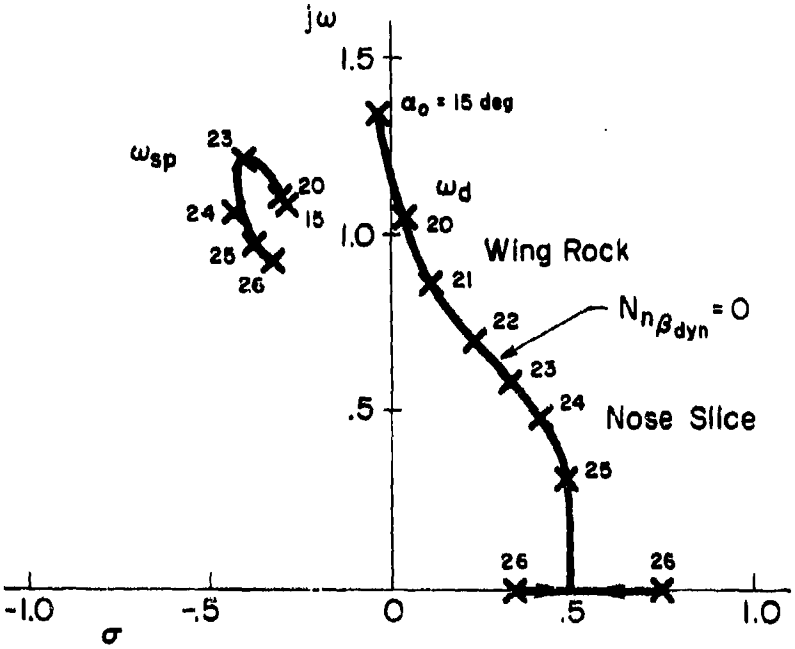

Figure 9. F-4J Lateral-Longitudinal Short-Period Root Migration with α; $\beta_o = 0$

indicating directional dynamic stability. At high AOA the parameter is negative, indicating directional dynamic instability. The AOA regions below and above $Cn_{\beta_{dyn}} = 0$ are identified as wing-rock and nose-slice regions, which correlate quite well with the AOA ranges identified with these characteristics in the F-4E flight test, Figure 10 (from Reference 19).

The influence of non-zero sideslip at trim on the dutch roll and short-period frequencies and damping is reflected in Figure 11. The 6 DOF aircraft was trimmed to 1.5 and 5.5 deg sideslip and linearized transfer function parameters obtained. These indicate that the dutch roll is destabilized and the short-period stabilized by steady sideslip. Thus there is an apparent interchange of damping between the two modes while the overall system damping remains essentially constant.

Unfortunately, comparison of dynamic characteristics predicted by linear frozen-point analysis in Figures 9 and 11 with the actual flight

Symbol	Gross Weight (lb)	Aim Normal Load Factor (g)	Symbol	Gross Weight (lb)	Aim Normal Load Factor (g)
⊙	40,500	1.0	★	35,200	2.0
⊡	40,000	1.0	●′	34,800	3.0
△	39,400	1.0	⊡′	40,000	1.0
▼	39,200	1.0	△′	39,700	2.0
◆	39,000	1.5	▽′	38,700	2.0
◗	39,200	2.0	◇′	43,500	1.0
◒	37,100	1.0	◿′	43,200	1.0
◿	36,500	1.0	◺′	42,700	2.0
◺	36,200	1.0	◁′	42,200	3.0
◥	35,700	1.0	☆′	41,700	3.0
			⊙′	41,300	1.0

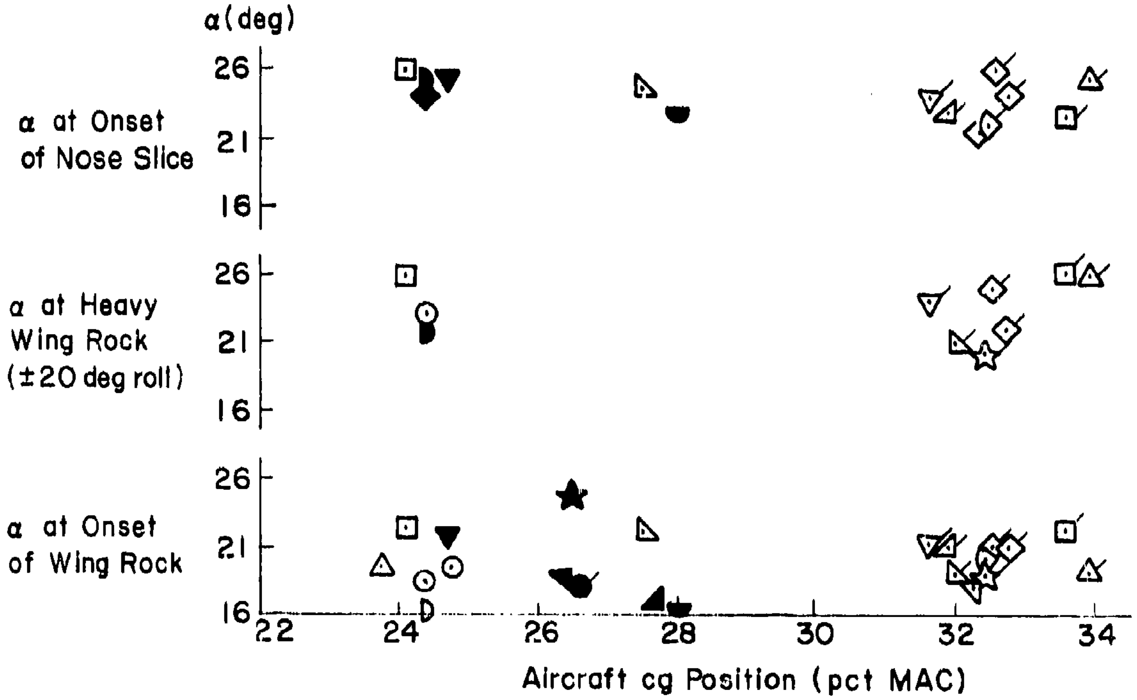

Figure 10. F-4E Stall Approach Characteristics (From Ref. 19)

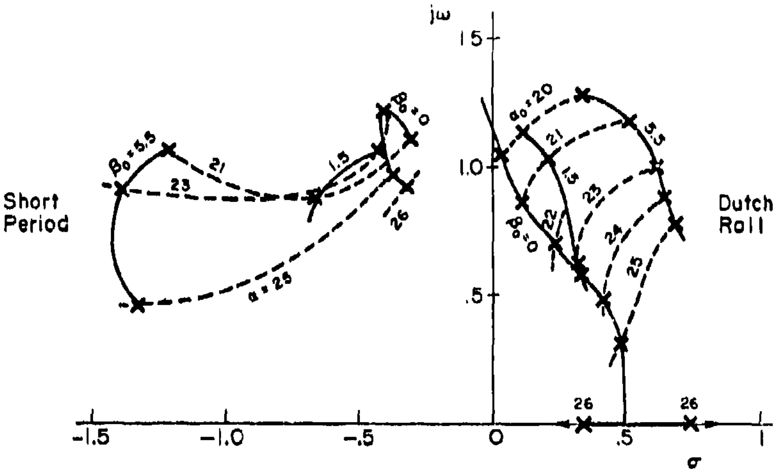

Figure 11. F-4J 6 DOF Linearized Equation; Lateral-Longitudinal Root Migration with α and β

traces of Figure 3 or nonlinear 6 DOF model traces of Figure 4 shows several significant differences. The wing rock linear analysis predicts a dutch roll divergence of increasing amplitude as α, β, or both are increased, and a longitudinal short-period with a frequency quite close to the dutch roll frequency, but heavily damped. The traces of Figures 3 and 4 show the dutch roll divergence bounded in amplitude and a low-damped longitudinal oscillation at about twice the dutch roll frequency.

Figure 12 shows a similar set of nonlinear time response characteristics for the open-loop 6 DOF nonlinear model trimmed to $\alpha_0 = 21$ deg and $\beta_0 = 0$ deg and excited with an aileron pulse. From Figure 12 it is apparent that the longitudinal oscillation results from rectifying the lateral oscillation and the sharp peaks of pitching acceleration coincide with sideslip passing through zero. Thus, the nonlinear-type behavior appears to be caused by lateral-longitudinal coupling due to sideslip.

A nine-by-nine matrix of aerodynamic and kinematic terms for coupled, non-symmetric flight obtained from the partial derivative expansion of the nine equations of motion is presented in Figure 13.

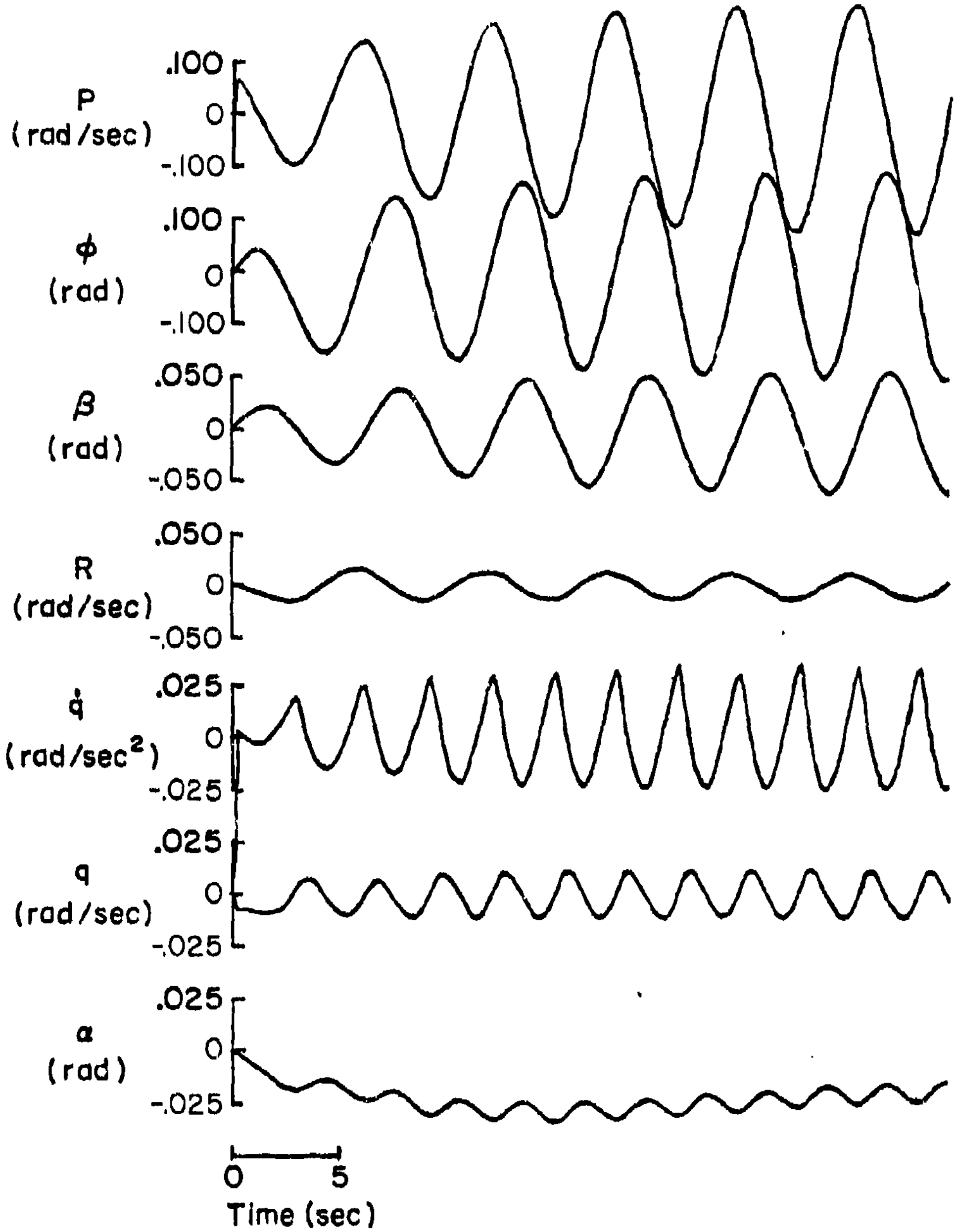

Figure 12. F-4J Open-Loop Nonlinear Airframe Response to Pulse Aileron; $\alpha_0 = 21$ deg, $\beta_0 = 0$ deg

$$
\begin{bmatrix}
\substack{(s-X_u)\\ {[s+.048]}} & \substack{-X_w V_{T_o}\\ {[-21.76]}} & & \substack{-X_\beta\\ {[1.21]}} & & & \substack{-g\,\beta_o\cos\theta_o\\ {[-.787]}} & \substack{g\cos\gamma_o\\ {[32.19]}} & \\
\substack{\frac{-Z_u}{V_{T_o}}\\ {[.0006]}} & \substack{(s-Z_w)\\ {[s+.067]}} & -1 & & \substack{\beta_o\cos\alpha_o\\ {[.024]}} & \substack{\beta_o\sin\alpha_o\\ {[.009]}} & & & \\
 & \substack{-M_\alpha\\ -M_{\dot\alpha}Z_{\dot w}\\ {[1.0]}} & \substack{s-M_q\\ -M_{\dot\alpha}\\ {[s+.659]}} & \substack{-M_\beta\\ {[.812]}} & & & & & \\
 & \substack{-Y_\alpha/V_{T_o}\\ {[-.002]}} & & \substack{(s-Y_v)\\ {[s+.067]}} & \substack{-\sin\alpha_o\\ {[-.359]}} & \substack{\cos\alpha_o\\ {[.933]}} & \substack{\frac{-g}{V_{T_o}}\cos\theta_o\\ {[-.098]}} & \substack{\frac{-g}{V_{T_o}}\beta_o\cos\gamma_o\\ {[-.003]}} & \\
 & \substack{-\mathcal{L}'_\alpha\\ {[-.844]}} & & \substack{-\mathcal{L}'_\beta\\ {[3.44]}} & \substack{(s-\mathcal{L}'_p)\\ {[s+.51]}} & \substack{-\mathcal{L}'_r\\ {[-1.25]}} & & & \\
 & \substack{-N'_\alpha\\ {[.572]}} & & \substack{-N'_\beta\\ {[.705]}} & \substack{-N'_p\\ {[-.004]}} & \substack{(s-N'_r)\\ {[s+.312]}} & & & \\
 & & & & -1 & \substack{-\tan\theta_o\\ {[.3396]}} & s & \substack{\frac{-r_o}{\cos^2\theta_o}\\ {[.0116]}} & \\
 & & -1 & & & & \substack{r_o\\ {[-.0104]}} & s & \\
 & & & & & \substack{\frac{-1}{\cos\theta_o}\\ {[-1.056]}} & & \substack{\frac{-r_o\sin\theta_o}{\cos^2\theta_o}\\ {[.0037]}} & s
\end{bmatrix}
\begin{bmatrix}
u\\ \alpha-\alpha_c\\ q\\ \beta-\beta_o\\ p-p_o\\ r-r_o\\ \phi\\ \theta-\theta_o\\ \psi-\psi_o
\end{bmatrix}
=
\begin{bmatrix}
\substack{X_{\delta_{stab}}\\ {[-.093]}} & & \substack{X_{\delta_r}\\ {[.001]}}\\
\substack{Z_{\delta_{stab}}/V_{T_o}\\ {[-.0006]}} & & \\
\substack{M_{\delta_{stab}}+\\ M_{\dot w}Z_{\delta_{stab}}\\ {[-.037]}} & \substack{M_{\delta_{stk}}\\ {[-.009]}} & \\
 & & \substack{Y_{\delta_r}/U_o\\ {[.0001]}}\\
 & \substack{\mathcal{L}_{\delta_{stk}}\\ {[.033]}} & \substack{\varepsilon_r\\ {[.005]}}\\
 & \substack{N_{\delta_{stk}}\\ {[-.0003]}} & \substack{\varepsilon_r\\ {[-.006]}}\\
 & & \\
 & & \\
 & &
\end{bmatrix}
\begin{bmatrix}
\delta_{stab}\\ \delta_{stk}\\ \delta_r
\end{bmatrix}
$$

Assumes: $\alpha_o = \gamma_o = \phi_o = 0$, β_o small ($\sin\beta_o = \beta_o$; $\cos\beta_o = 1$);
negligible terms omitted.

Figure 13. Matrix for Coupled Equations with $\beta_o \neq 0$

The major derivatives and kinematic terms are identified in literal form and, for comparison with Figure 12, have been evaluated at $\alpha_o = 21$ deg and $\beta_o = 1.5$ deg. The principal cross-coupling at this small sideslip angle is seen to be due to M_β, $\mathcal{L}_{\alpha}'$ and N_{α}'. The influences of these derivatives on actual vehicle dynamic response can best be seen through the use of eigenvectors and vector polygons.

Figure 14 contains the eigenvectors for the dutch roll and short-period modes. These show both modes to be dominated by roll, sideslip, and pitch, with the difference between the modes being primarily motion phasing and damping. For example, in the dutch roll, q and β are nearly 180 deg out of phase, while in the short-period they are nearly in phase. However, the short-period is so well damped ($\zeta_{sp} \doteq 0.6$) that it would influence only the first second or two of the time responses shown in Figure 12. Therefore, the observed time responses must be due entirely to the dutch roll.

Vector polygons for the four principal motion equations are presented in Figure 15. Each polygon represents a force or moment equation. The polygon's sides show the contributions of each motion variable to the total acceleration. Vector lengths are a product of the appropriate stability derivatives and eigenvectors evaluated at the dutch roll frequency. The predicted motion is mostly rolling ($\dot{p}$), with sideslip ($\dot{\beta}$), and pitching ($\dot{q}$) about the same magnitude, and with comparatively little yawing ($\dot{r}$). The polygons for $\dot{\alpha}$ and $\dot{u}$ are so small that they can be neglected. The vector polygons provide the first insight to the causes for the change in modal response characteristics. The $\dot{p}$ vector polygon shows phasing of the $\mathcal{L}_{\alpha}'\alpha$ vector opposite to that for the $\mathcal{L}_{p}'p$ vector. Thus the aerodynamic cross-coupling coefficient, $\mathcal{L}_{\alpha}'$, in effect opposes the normal aerodynamic damping term, $\mathcal{L}_{p}'$, and therefore increases the rolling tendency of the aircraft. Since the aerodynamic cross-coupling coefficients increase in magnitude as the trim sideslip increases, one can readily visualize that at higher sideslip angles, $\mathcal{L}_{\alpha}'$ can actually become greater than $\mathcal{L}_{p}'$. Then one could expect the model to exhibit a roll divergence for large α and β perturbations.

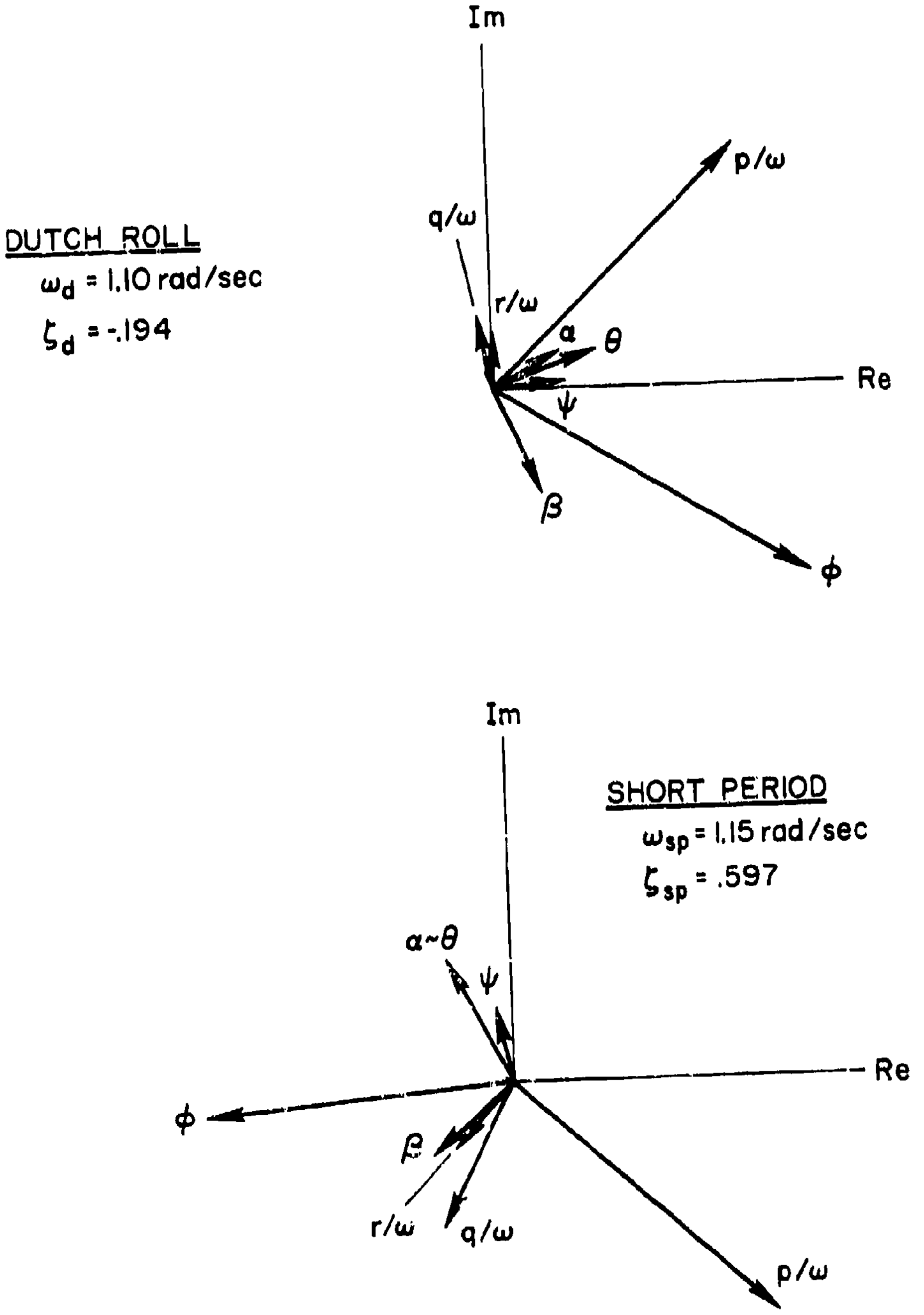

Figure 14. F-4J Eigenvectors; α_0 = 21 deg, β_0 = 1.5 deg

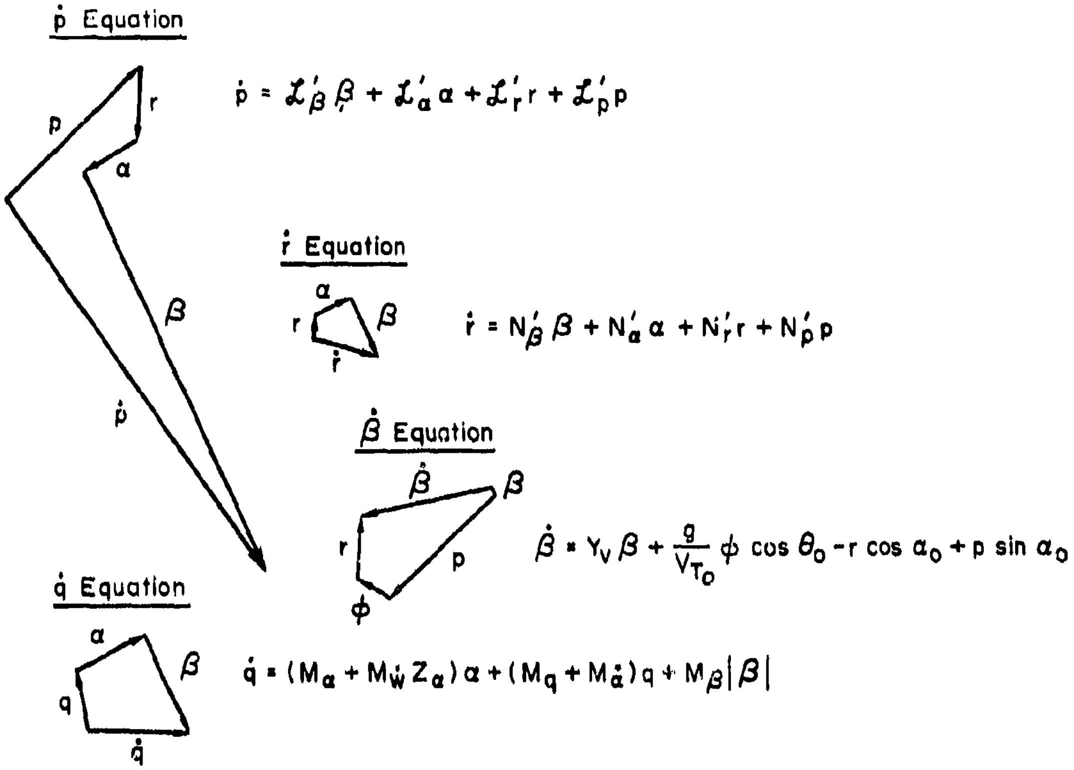

Figure 15. F-4J Force Vector Polygons; $\alpha_0 = 21$ deg, $\beta_0 = 1.5$ deg

The $\dot{\beta}$ vector polygon indicates that this vehicle motion derives primarily from the kinematic coupling of roll rate about the body centerline axis at the elevated AOA.

In the $\dot{r}$ vector polygon the p vector is missing because the aerodynamic coefficient N_p' is negligible at this flight condition. The vector $N_\alpha'\alpha$ has a relatively large component in phase with $N_r'r$ so that the aerodynamic cross-coupling from longitudinal into lateral augments the natural yaw damping and thus contributes to reducing body-axis yawing motion. All of this contributes to the dominance of roll and sideslip in the Figure 12 wing rock.

Finally the $\dot{q}$ vector polygon shows that the $M_\beta\beta$ vector is of opposite phase and is larger in magnitude than the damping vector derived from the aerodynamic derivatives $M_q + M_{\dot{\alpha}}$. Thus the sideslip-induced pitching moment overpowers the normal aerodynamic damping and forces the double frequency oscillation observed in the time traces. M_β changes sign with β (Figure 6). Since pitch inertia is considerably larger than roll inertia for this aircraft, a transfer of energy from the unstable lateral mode into the stable longitudinal mode may be a contributing factor in bounding the lateral-directional mode divergence. The influence of reducing C_{m_β} is shown in Figure 16. In this case, C_{m_β} is small but not zero. Comparing these traces with those of Figure 12 demonstrates the strong influence M_β has in bounding the lateral divergence.

It is concluded for our model that the roll/sideslip oscillation starts as a divergent dutch roll with small sideslip excursions. As sideslip increases, coupling causes a nonlinear behavior which bounds the divergence. Thus F-4J wing rock, per se, is a nonlinear phenomenon dominated by static aerodynamic lateral-longitudinal cross-coupling. Further, the vector polygons show that except for $\mathcal{L}_p'$ the damping derivatives do not have a significant influence on high AOA dynamic characteristics.

This analysis has also shown that one must exercise caution in the use or interpretation of open-loop transfer function parameters even when obtained from 6 DOF fixed operating point conditions. Such parameters are limited to relatively small sideslip conditions such as onset to wing rock or departure and hence better reflect susceptibility to these maneuver-limiting factors rather than describing the resulting vehicle motion.

b. Closed-Loop Dynamic Characteristics

The closed-loop dynamic characteristics of any system are strongly influenced by transfer function numerator roots (zeros) in or near the range of the desired bandwidth of control. When controlling any motion variable with any controller, the numerator zeros of that transfer function attract denominator (open-loop) poles. Hence these zeros alter closed-loop stability and modal response characteristics of the vehicle in proportion to the tightness (gain) of the loop closure. Thus certain

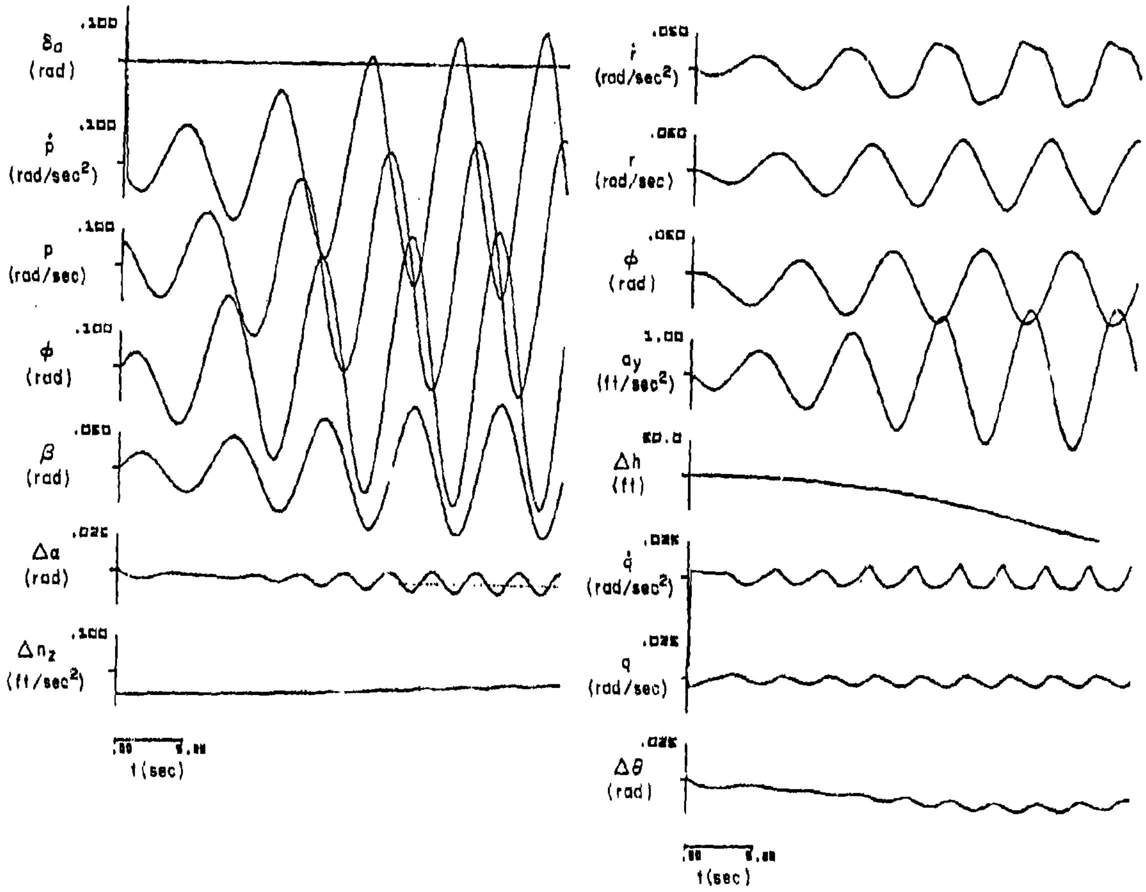

Figure 16. Open-Loop Wing Rock with C_{m_β} Small;
α_o = 21 deg, β_o = 0 deg

zeros can become high AOA maneuver-limiting factors in that they cause or influence closed-loop roll reversal, wing rock (lateral PIO), and departure (nose slice or roll). This observation applies to loops closed both by the pilot and by automatic feedback systems. The key numerators for piloted control are $N^{\phi}_{\delta_{stk}}$, $N^{\phi}_{\delta_r}$, and $N^{\theta}_{\delta_{stab}}$. The F-4J augmentation systems are of little concern due to limited SAS authorities and very low loop gains at high AOA and low dynamic pressure.

Lateral stick control of roll. Under normal low AOA flight situations, the 3 DOF equations produce a transfer function

$$\frac{\phi(s)}{\delta_{stk}(s)} = \frac{N^{\phi}_{\delta_{stk}}}{\Delta}$$

$$N^{\phi}_{\delta_{stk}} = A_{\phi}[s^2 + 2\zeta_{\phi}\omega_{\phi}s + \omega^2_{\phi}]$$

$$\Delta = (s + 1/T_s)(s + 1/T_R)(s^2 + 2\zeta_d\omega_d s + \omega^2_d)$$

with values of ω_{ϕ} and $\zeta_{\phi}\omega_{\phi}$ in the vicinity of those for the dutch roll mode, ω_d and $\zeta_d\omega_d$. With this loop closure the zeros attract (modify) the dutch roll, causing the closed-loop root locus (with increasing feedback gain K) to take on a form typified by the sketch below.

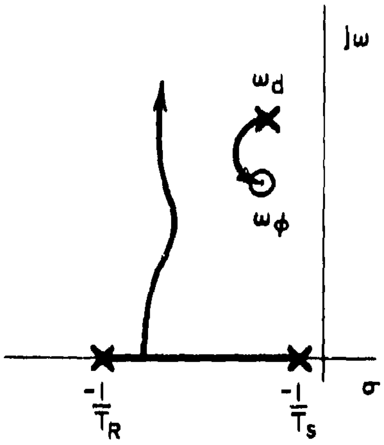

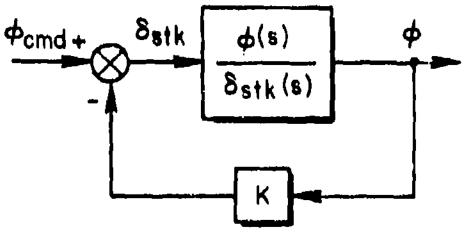

As AOA is increased, ω_ϕ^2 generally decreases and can become negative in value. When this occurs, $N_{\delta_{stk}}^{\phi}$ is of the form

$$N_{\delta_{stk}}^{\phi} = A_\phi\left(s + \frac{1}{T_{\phi 1}}\right)\left(s + \frac{1}{T_{\phi 2}}\right)$$

where one root is positive and one is negative. With the high AOA shift in open-loop denominator roots, the root locus often takes on the form shown below.

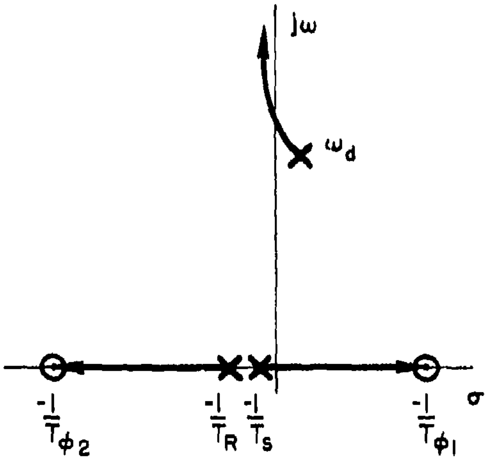

In this case the spiral root, $-1/T_s$, is driven toward the right half-plane (RHP) zero and a first-order instability (divergence) results. The rate of divergence depends upon how far the zero lies in the RHP and how tightly the loop is closed.

Migration of the F-4J open-loop zeros with AOA at zero sideslip is reflected by the solid lines in Figure 17, which indicate an almost linear decrease in ω_ϕ^2 (at constant damping) with increase in AOA up to $\alpha \doteq 18$ deg. Above this angle, ω_ϕ^2 is negative and the RHP root location is quite AOA-sensitive. Also noted on the figure are the regions associated with wing rock and nose slice from Figure 10. Wing rock occurs

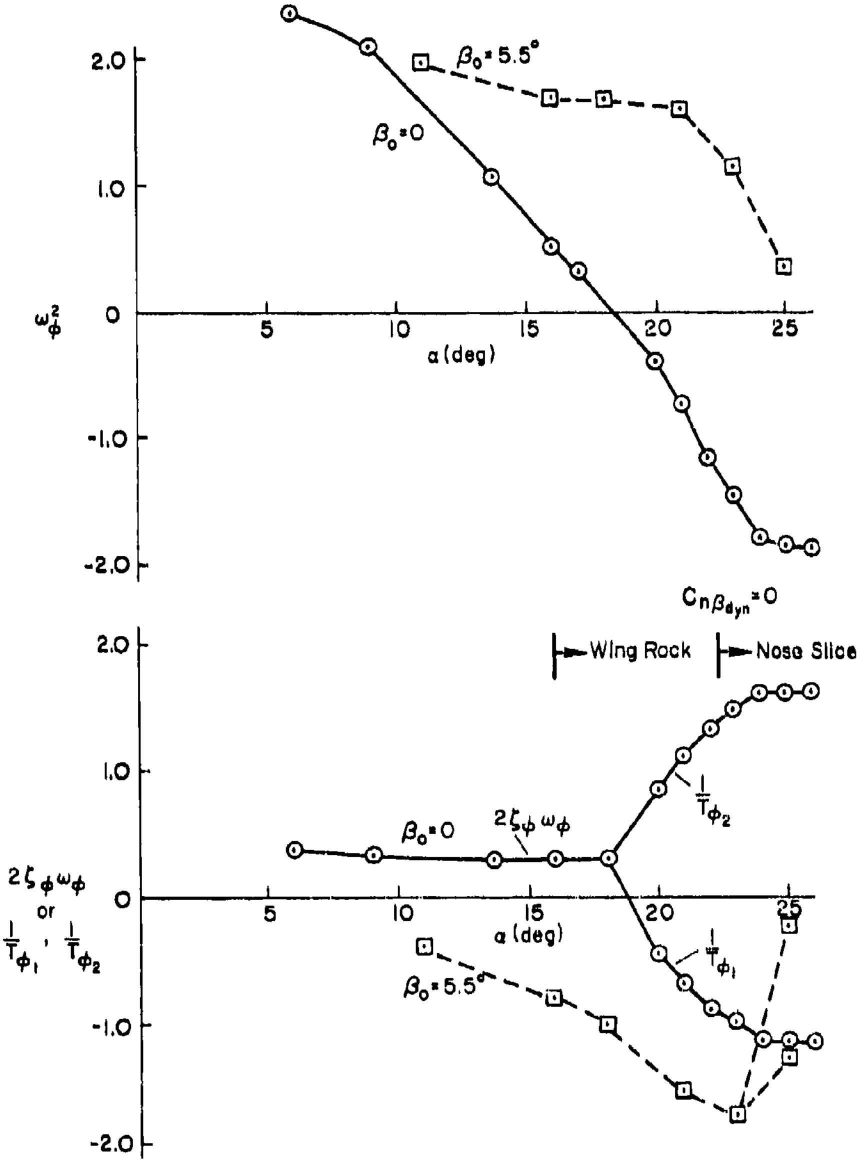

Figure 17. $N^{\phi}_{\delta_{stk}}$ Root Migration with AOA; F-4J

in the region where ω_ϕ^2 is small; nose slice occurs in the region where $1/T_{\phi_1}$ is large and negative.

Actually, negative ω_ϕ^2 reflects steady-state roll opposite to that commanded by stick deflection. This is generally due to large adverse aileron yaw, since (after Reference 20)

$$\omega_\phi^2 \doteq N'_\beta - \frac{N'_{\delta_{stk}}}{\mathcal{L}'_{\delta_{stk}}} \mathcal{L}'_\beta$$

where $\delta_{stk} = 8\delta_a + 11.6\delta_{sp}$. At high AOA, N'_β is small, $\mathcal{L}'_\beta$ is large negative, and $N'_{\delta_{stk}}$ determines the sign of ω_ϕ^2. Adverse (negative) $N'_{\delta_{stk}}$ then tends to produce negative ω_ϕ^2 and the RHP zero. In physical terms, adverse yaw produces sideslip and, in turn, roll reversal due to $\mathcal{L}'_\beta\beta$. It thus becomes apparent that the nose slice region identified in Figure 17 may be related to strong adverse aileron yaw and the <u>magnitude</u> of the RHP zero.

The dashed lines of Figure 17 show the values of ω_ϕ^2 and $2\zeta_\phi\omega_\phi$ (or $1/T_{\phi_1}$, $1/T_{\phi_2}$) for $\beta_o = 5.5$ deg. Whereas increasing AOA at $\beta = 0$ causes ω_ϕ^2 to decrease steadily and finally become negative, when $\beta \neq 0$ the aerodynamic cross-coupling causes ω_ϕ^2 to stay positive and close to the dutch roll mode but the damping ratio, ζ_ϕ, becomes negative (see sketch below).

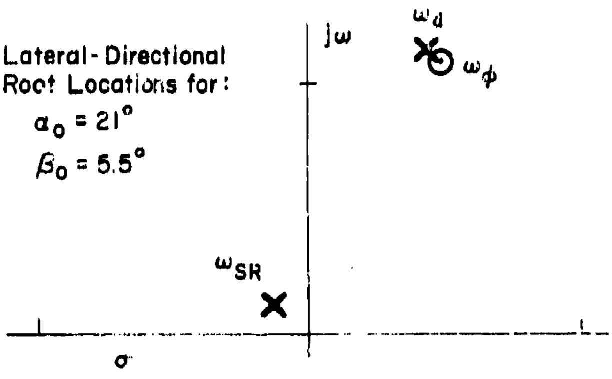

The promixity of ω_ϕ and ω_d means low residue for the dutch roll mode in roll control with stick when $\beta \neq 0$. Thus sideslip should reduce the roll content of the unstable dutch roll mode; this is consistent with the observed bounding of the roll oscillation divergence in Figures 4 and 16.

Rudder control of roll. When the region of adverse aileron yaw is reached, roll control is maintained via rudder. This produces yaw and sideslip-induced roll in the same direction and thus much more rapid turning than just yawing moment and side force would produce. The rudder-to-roll numerator, $N^{\phi}_{\delta_r}$, is of the form

$$N^{\phi}_{\delta_r} \doteq A_{\phi_r}\left(s + \frac{1}{T_{\phi_{r_1}}}\right)\left(s + \frac{1}{T_{\phi_{r_2}}}\right)$$

One root is always positive (RHP) as shown in Figure 18. The RHP zero results from adverse roll due to $\mathcal{L}'_{\delta_r}$. It is apparent from Figure 18 that the zeros of $N^{\phi}_{\delta_r}$ are not greatly influenced by either AOA or sideslip.

Again this control structure portends closed-loop instability since some pole must be driven toward the RHP zero. However, these zeros lie at high frequencies relative to the low-frequency bandwidth normally achieved with rudder control via the pilot's legs. Rudder-to-roll control handling qualities are normally dominated by the low-frequency spiral and roll subsidence modes, and at high AOA these remain stable and well behaved. While this type of control is "unnatural," it does not result in roll stability problems at low gain closures.

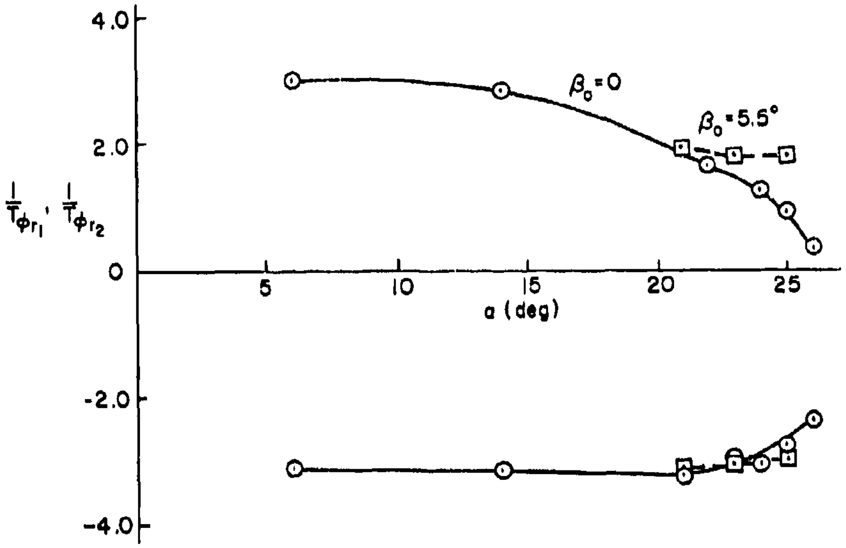

Figure 18. $N^{\phi}_{\delta_r}$ Root Migration with AOA; F-4J

Stabilator control of pitch. Closed-loop control of pitch attitude becomes pertinent to maneuver-limiting if and when the numerator for stabilator control of pitch, $N^{\theta}_{\delta_{stab}}$, has zeros in the RHP. At zero sideslip the transfer function is of the form

$$\frac{\theta(s)}{\delta_{stab}(s)} = \frac{N^{\theta}_{\delta_{stab}}}{\Delta}$$

$$N^{\theta}_{\delta_{stab}} = A_{\theta}\left(s + \frac{1}{T_{\theta_1}}\right)\left(s + \frac{1}{T_{\theta_2}}\right)$$

$$\Delta = [s^2 + 2\zeta_p\omega_p s + \omega_p^2][s^2 + 2\zeta_{sp}\omega_{sp}s + \omega_{sp}^2]$$

On the F-4J, $1/T_{\theta_2}$ decreases with increasing AOA and finally couples with $1/T_{\theta_1}$ to form a complex pair which almost cancels the longitudinal phugoid mode. Thus these zeros remain well behaved. However, when there is sideslip so that static aerodynamic cross-coupling becomes significant, the numerator contains additional zeros related to lateral-directional modes.

It was discovered (Reference 5) that such coupling in the A-7 aircraft produced an RHP zero, $1/T_{\theta_3}$, and subsequent pilot control of pitch attitude via the stabilator caused a closed-loop directional divergence which has the appearance of a nose slice. A similar situation exists in the F-4J aircraft. Figure 19 presents pole and zero locations for $\alpha_o = 23$ deg and $\beta_o = 5.5$ deg. The coupled 6 DOF equations (Figure 19a) produce two real zeros (one RHP, one LHP), one complex pair which nearly cancels the phugoid, and one higher-frequency complex pair.

The source of the low-frequency zeros can be determined by eliminating the velocity equation, which should reduce the phugoid mode to a first-order pole at the origin and eliminate the speed numerator zero, $1/T_{\theta_1}$. It may be observed in Figure 19b that the only change is in the phugoid dipole pair which became first-order as expected.

Next, as in Reference 5, the cross-coupling terms $\mathcal{L}'_{\alpha}$ and N'_{α} are set to zero in the 6 DOF equations to identify the lateral-directional modes. This is shown in Figure 19c where the pole-zero cancellations show the two real zeros to be related to the roll subsidence, $1/T_R$, and spiral, $1/T_s$, modes and the higher-frequency complex zeros to be related to the dutch roll.

Figure 20 is a system survey for closure of the pitch attitude loop for the augmented* (SAS on) airframe at this same trim condition. The lower figure is a root locus and the upper figure is a Bode-siggie (Reference 20). The root locus shows the migration of roots from the

---

*The slight difference in airframe dynamic parameters between Figures 20 and 11 indicates the very minor influence of the SASs at high AOA and low dynamic pressure conditions.

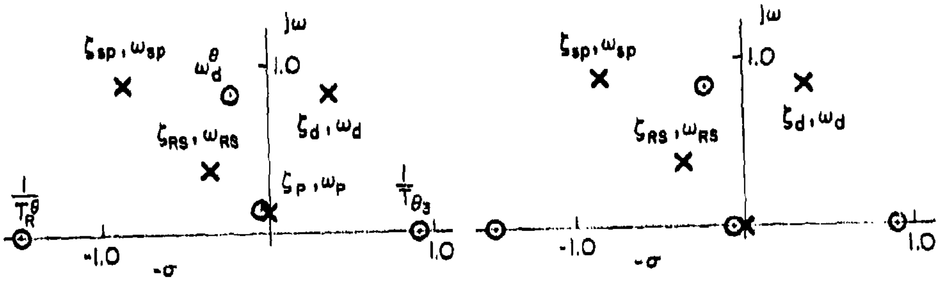

a) 6 DOF Coupled

b) 5 DOF ($\dot{V}_T = 0$) Coupled

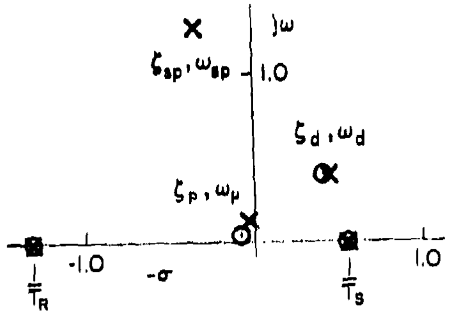

c) 6 DOF Coupled, $N'_{\alpha} = \mathcal{L}'_{\alpha} = 0$

Figure 19. Effect of Lateral-Longitudinal Coupling on $N^{\theta}_{\delta_{stab}}/\Delta$ Roots; $\alpha_o = 23$ deg, $\beta_o = 5.5$ deg

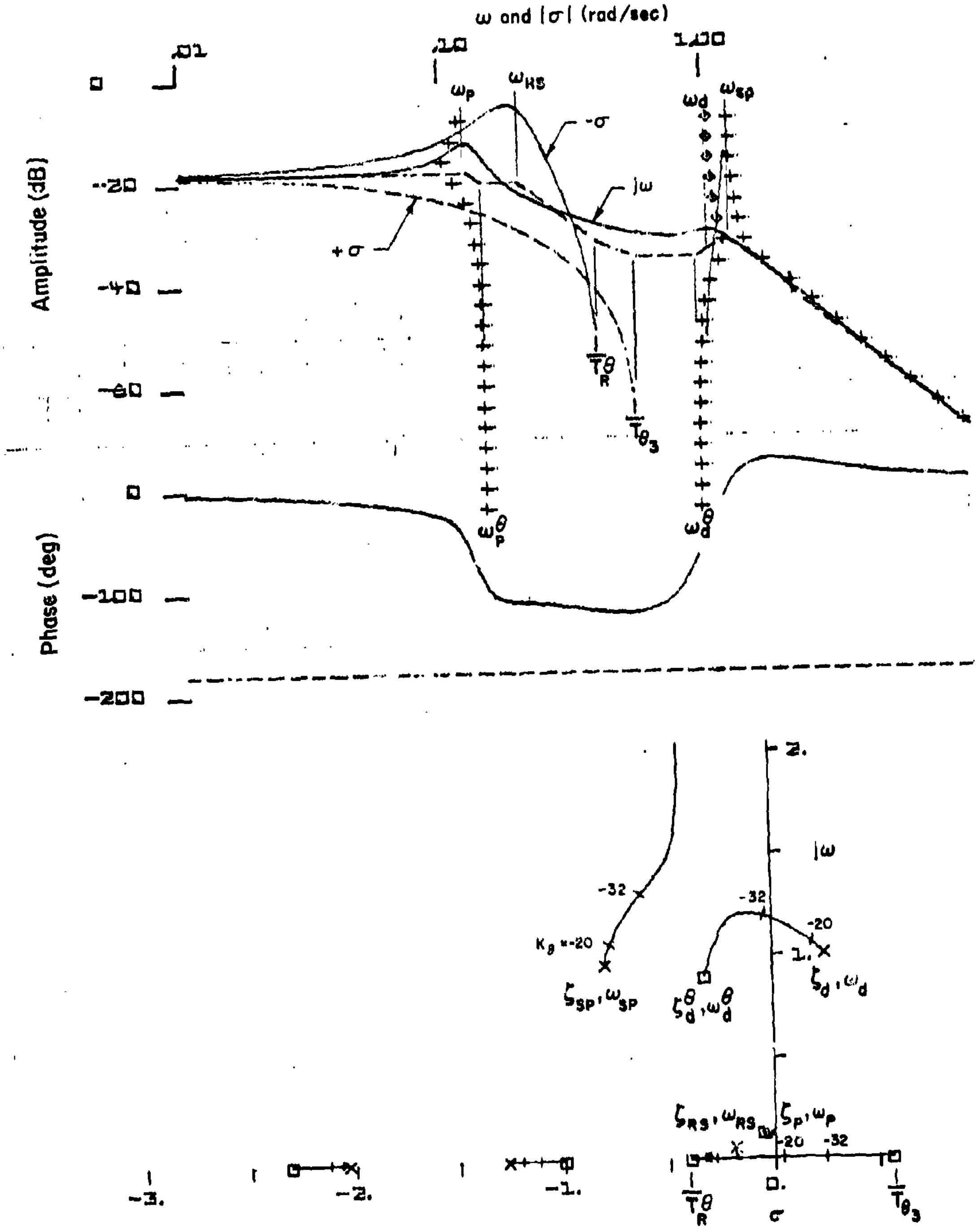

Figure 20. System Survey for $\theta \rightarrow \delta_{stab}$ Closure; $\alpha_o = 23$ deg, $\beta_o = 5.5$ deg

open-loop poles toward the open-loop zeros as gain is increased. It provides information concerning closed-loop frequency and damping as a function of gain but does not provide information concerning sensitivity to gain change. The Bode-siggie presents the open-loop transfer function amplitude and phase as functions of frequency where the amplitude is evaluated for $s = j\omega$ (Bode) and $s = \sigma$ (siggie). The ✛ symbols identify migration of complex LHP closed-loop pole frequency with increasing gain (Bode-root locus, Reference 20) and the ◈ symbols similar migration of closed-loop poles in the RHP. Closed-loop first-order roots lie at the intersection of the gain closure lines and the σ amplitude curves. Thus these survey plots allow identification of closed-loop roots at a specific gain value, and sensitivity of root value to changes in gain.

In order to provide any pitch attitude control whatsoever, the loop gain must be sufficiently high that the closure line crosses the Bode plot below the -20 dB low-frequency asymptote, i.e., with a gain 20 dB or greater. Generally the crossover will be at or above the short-period frequency —— again in the vicinity of -30 to -40 dB. The root locus plot has tick marks showing closed-loop root locations for gains of 20 and 32 dB. This shows that the root moving toward $1/T_{\theta_3}$ has already reached the RHP, and divergence, with the gain at 20 dB. By 32 dB the first-order divergence has a time constant of 4 sec. Thus any attempted control of pitch attitude results in a divergence. This divergence is due to lateral-longitudinal coupling and is evidenced in a lateral motion.

Figure 21 shows values for the real zeros $1/T_{\theta_3}$ and $1/T_R^{\theta}$ at $\beta_0 = 5.5$ deg and α_0 from 21 to 25 deg. These indicate that at non-zero sideslip and AOA increasing above 20 deg $1/T_{\theta_3}$ rapidly moves to negative values which portend closed-loop first-order divergence time constants as low as 1 sec. Again this coincides with the nose slice region observed in flight test.

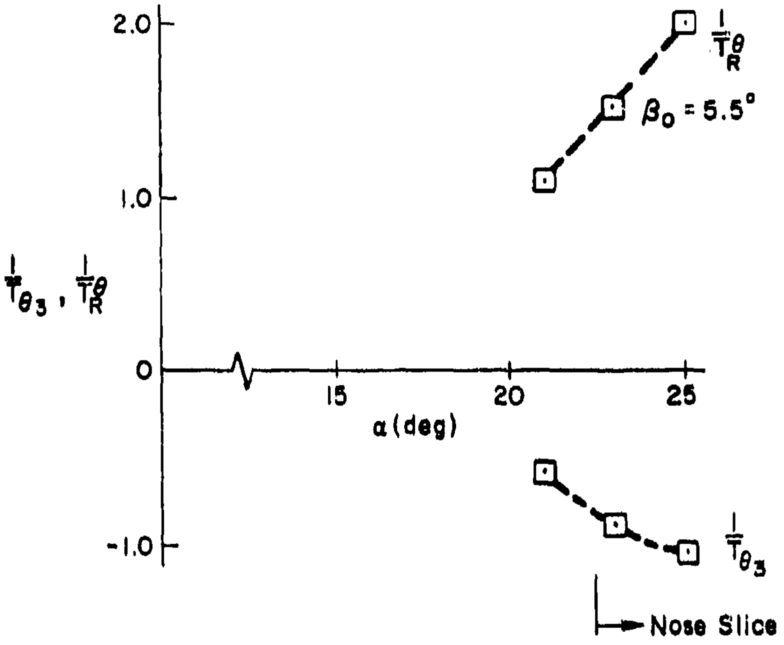

Figure 21. $N^{\theta}_{\delta_{stab}}$ First-Order Root Migrations with AOA; F-4J

Coupling numerators. When the aircraft is in asymmetric, sideslipping flight, any control action in the longitudinal axis influences the lateral-directional numerator and vice versa. This can be illustrated as follows:

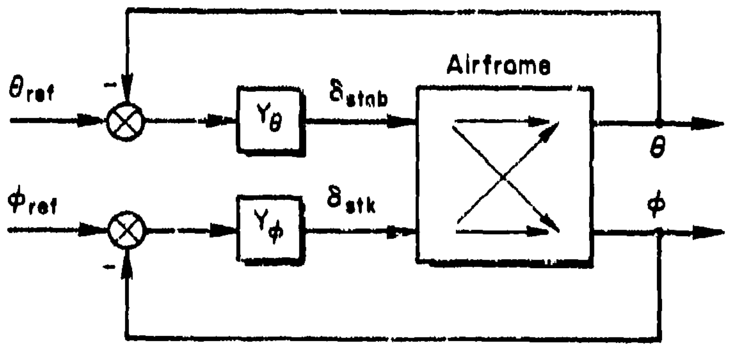

The effective transfer function for each control loop becomes

$$\frac{N^{\theta}_{\delta_{stab}}}{\Delta} = \frac{N^{\theta}_{\delta_{stab}} + Y_{\phi} N^{\theta\,\phi}_{\delta_{stab}\delta_{stk}}}{\Delta}$$

$$\frac{N^{\phi}_{\delta_{stk}}}{\Delta} = \frac{N^{\phi}_{\delta_{stk}} + Y_{\theta} N^{\theta\,\phi}_{\delta_{stab}\delta_{stk}}}{\Delta}$$

where $N^{\theta\,\phi}_{\delta_{stab}\delta_{stk}}$ is the numerator term due to cross-coupling effects.* Both the θ and ϕ numerators are modified by the same coupling numerator; the extent of the influence depends upon how tightly the other loop is being closed. This influence can be determined by treating the effective numerator as a closed-loop system and identifying the migration of numerator roots as the loop gain (Y_{ϕ} or Y_{θ}) is varied, e.g., the roots of the θ numerator are obtained from

$$N^{\theta}_{\delta_{stab}} = N^{\theta}_{\delta_{stab}} + Y_{\phi} N^{\theta\,\phi}_{\delta_{stab}\delta_{stk}} = 0$$

$$1 + \frac{Y_{\phi} N^{\theta\,\phi}_{\delta_{stab}\delta_{stk}}}{N^{\theta}_{\delta_{stab}}} = 0$$

The uncoupled numerator roots become the poles of this system and the coupling numerator roots are the zeros. The root migration is controlled by the pilot gain, Y_{ϕ}. For the Figure 20 example case of $\alpha_o = 23$ deg, $\beta_o = 5.5$ deg, the transfer function is

$$\frac{Y_{\phi} N^{\theta\,\phi}_{\delta_{stab}\delta_{stk}}}{N^{\theta}_{\delta_{stab}}} = \frac{-.0029(-1.35)(1.69)[.993;\ .102]Y_{\phi}}{-.0352(-.896)(1.49)[.404;\ .148][.267;\ .851]}$$

---

*The reader is referred to page 163 et seq. of Reference 20 for a thorough development and treatise of multiloop control systems analysis.

where first-order factors $(s + a)$ are represented by (a) and second-order factors $[s^2 + 2\zeta\omega_n s + \omega_s^2]$ by $[\zeta;\ \omega_n]$. Assuming Y_ϕ to be a simple positive gain, this produces a root locus of the form shown in the sketch below. Thus pilot control of the roll attitude loop via aileron and spoiler causes the RHP zero of the pitch numerator to move further into the RHP because the root of the coupling numerator lies beyond $1/T_{\theta_3}$.

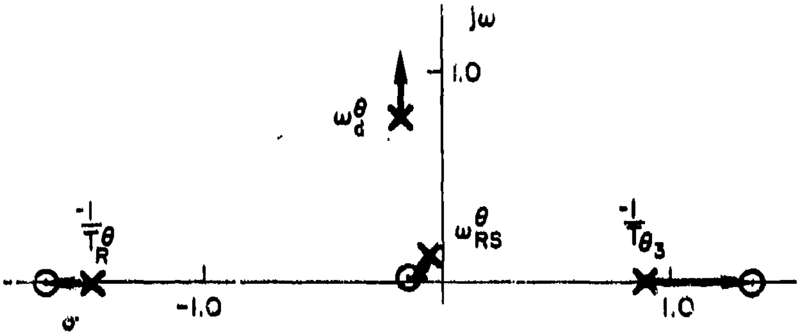

Similarly, pilot control of pitch attitude via stabilator alters the roll numerator as

$$\frac{Y_\theta N^{\theta\ \phi}_{\delta_{stab}\delta_{stk}}}{N^\phi_{\delta_{stk}}} = \frac{-.0029(-1.35)(1.69)[.993;\ .102]Y_\theta}{.0834[.487;\ .135][-.808;\ 1.07][.906;\ 1.62]}$$

which, for Y_θ assumed a simple negative gain, produces a root locus of the form sketched below. This results in the RHP ω_ϕ complex pair being driven to the real axis with one root eventually moving further into the RHP while the other moves into the LHP.

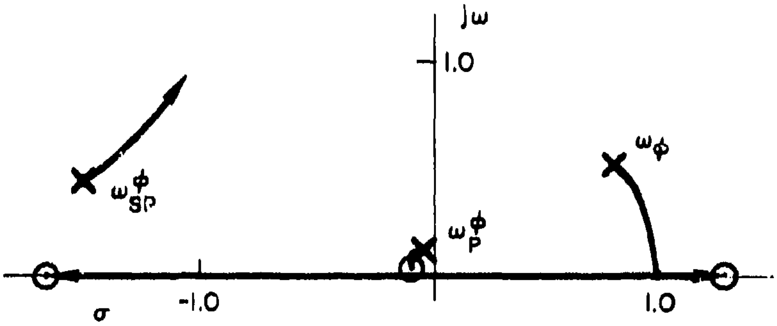

Thus in each instance the influence of the coupling numerator is definitely not beneficial; the coupling can further degrade closed-loop control in both axes.

Since F-4 pilots are normally instructed to use rudder to roll at high AOA, the influence of this control technique may be observed from the transfer functions (again at $\alpha_o = 23$ deg, $\beta = 5.5$ deg):

$$\frac{Y_{\phi} N^{\theta\ \phi}_{\delta_{stab}\delta_r}}{N^{\theta}_{\delta_{stab}}} = \frac{-.009(1.77)(-3.03)[.180;\ .148]Y_{\phi}}{-.0352(-.896)(1.49)[.404;\ .148][.267;\ .851]}$$

$$\frac{Y_{\theta} N^{\theta\ \phi}_{\delta_{stab}\delta_r}}{N^{\phi}_{\delta_r}} = \frac{-.009(1.77)(-3.04)[.180;\ .148]Y_{\theta}}{.00417(1.80)(-3.04)[.180;\ .148][.277;\ 1.20]}$$

Use of rudder to roll modifies the pitch numerator in much the same manner as does use of aileron and spoiler. This can be seen by comparing values of the coupling numerator terms. On the other hand, pitch control has little influence on the rudder roll numerator because nearly all numerator and denominator roots cancel. Thus it appears that this control strategy produces the most consistent closed-loop lateral-directional dynamic properties at high AOA and non-zero sideslip, which also might be a reason pilots do not mind using this technique.

<u>Summary</u>. This analysis has shown several areas in which control-numerator dynamic parameters can become maneuver-limiting factors for the F-4J. These limits are generally associated with zeros migrating to the RHP at high AOA in asymmetric ($\beta \neq 0$) flight.

The RHP zero of $N^{\phi}_{\delta_{stk}}$ is due to adverse "aileron" yaw ($N^{\psi}_{\delta_{stk}}$ negative) and results in roll reversal. The attendant sideslip causes the ϕ zeros to shift toward the dutch roll poles. This proximity reduces the roll contribution in the dutch roll mode and produces a nonlinear bounding of dutch roll (or wing rock) oscillation amplitude.

One RHP zero exists in $N^{\phi}_{\delta_r}$ whether the aircraft is in asymmetric flight or not. However, that root is at a frequency sufficiently above the region in which rudder control is generally exerted that it does not pose a closed-loop stability problem.

An RHP zero can occur in $N^{\theta}_{\delta_{stab}}$ due to aerodynamic cross-coupling with non-zero sideslip. This zero results in a first-order divergence mode if stabilator control of pitch attitude is attempted.

Asymmetric flight also produces lateral-longitudinal control coupling that further aggravates these undesirable RHP zero locations of the key θ and ϕ numerators.

Thus the aerodynamic cross-coupling associated with sideslip tends to dominate the F-4J high AOA flying qualities. Values of the cross-coupling derivatives evaluated at $\beta_o = 5.5$ deg and a range of AOA are shown in Figure 22. Comparing these with the root migrations in Figures 9 and 11 demonstrates their significance. The regions where large shifts in dynamic parameters occur coincide with large magnitude of cross-coupling derivatives. Also, it should be noted that the magnitude of the cross-coupling derivatives is directly proportional to the magnitude of sideslip.

The foregoing analytic results must be viewed with some caution since it was shown that linearized, fixed-operating-point dynamic parameters do not necessarily reflect the actual open-loop dynamics of the nonlinear airframe. On the other hand, the apparent correlation between bounding of dutch roll divergence and movement of ω_ϕ zeros with

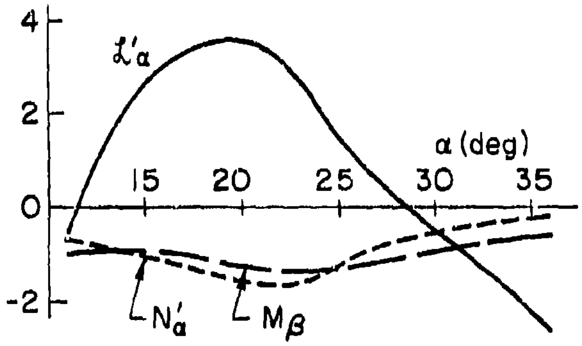

Figure 22. F-4J Static Aerodynamic Cross-Coupling Derivatives; $\beta_o = 5.5$ deg

sideslip, and the AOA region for nose slice observed in actual flight with the region where the RHP zeros of $N^{\theta}_{\delta_{stab}}$ and $N^{\phi}_{\delta_{stk}}$ are large is quite encouraging.

B. F-14A ANALYSIS

The F-14A configuration does not have wing leading-edge slats. This aircraft has variable wing sweep; at $M < 0.5$ the wings are in the full forward ($\Lambda = 22$ deg) position. The unaugmented airframe is classified as departure resistant, but it can be departed (References 21 and 22). It remains laterally stable and longitudinally controllable at full aft stick (AOA approximately 50 deg with wings forward). It has a mild dutch roll instability starting at about 15 deg AOA. The oscillations are aggravated if the pilot attempts to oppose the motion with either lateral stick or rudder. The dutch roll mode becomes stable again at about 23-25 deg AOA. Roll reversal due to adverse yaw from the aileron and differential horizontal stabilizer also starts at about 18 deg AOA. Prolonged deflection of the lateral stick at $\alpha > 20$ deg will result in a departure, characterized by a rapid increase in "adverse" yaw rate, which may develop into a series of uncommanded rolls with the appearance of snap rolls. At low speed, departure can occur at AOA as low as 21 deg. The departure characteristics are a function of wing sweep, c.g. location, and Mach number. The airplane will spin and has a non-recoverable flat spin mode.

1. Analytic Model

The F-14A aerodynamic model was derived from several sources (References 23-27). The data base was taken from the NASA/Langley Differential Maneuvering Simulator (DMS) report of Reference 23. This fixed-base piloted simulation was considered by Grumman test pilots to provide a valid representation of high AOA dynamic characteristics observed in early flight tests. However, time traces obtained from these same aerodynamic data did not match available flight test records. Therefore the data were modified on the basis of information obtained from other references, discussions with F-14 aerodynamicists at Grumman, and finally, as necessary to match available flight test data.

The resulting aerodynamic model, together with supportive documentation for each aerodynamic coefficient, is detailed in Part III, Appendix II. The data cover the range:

$$0 < \alpha < 55 \text{ deg}; \; -20 < \beta < +20 \text{ deg}$$

at low Mach (0.2). At this low speed the variable-sweep wing is nominally in its full forward (Λ = 22 deg) position, so wing sweep influence is not included.

Based upon the F-4J analysis, the key high AOA aerodynamic moments are $C_\ell(\alpha,\beta)$, $C_n(\alpha,\beta)$ and $C_m(\alpha,\beta)$. The roll moment (Figure 23) is seen to remain essentially constant for $\alpha > 15$ deg and $\beta < 10$ deg, as opposed to the F-4J's significant decrease in $C_\ell(\alpha,\beta)$ for $\alpha > 15$ deg (Figure 7). The yaw moment (Figure 24) is similar to the F-4J's (Figure 8) for $\alpha < 17$ deg, but for $\alpha > 17$ deg both the slopes with respect to α and the maximum values with respect to β are approximately half those of the F-4J. The combination of less negative C_{n_β} and larger negative $C\ell_\beta$ produces positive values of the dynamic stability parameter $C_{n_{\beta_{dyn}}}$ throughout the 55 deg AOA range.

The pitch moment with sideslip (Figure 25) is also similar to that of the F-4J over the range $10 < \alpha < 25$ deg, where it is negative. However, above $\alpha = 35$ deg, C_{m_β} becomes positive.

Weight, c.g., and moments and product of inertia for the clean (no external stores) aircraft were provided by Grumman. These are shown in Table 2 with F-4J values for comparison. All inertias are in the fuselage centerline reference axis system. Aircraft dimensions are also presented for comparison.

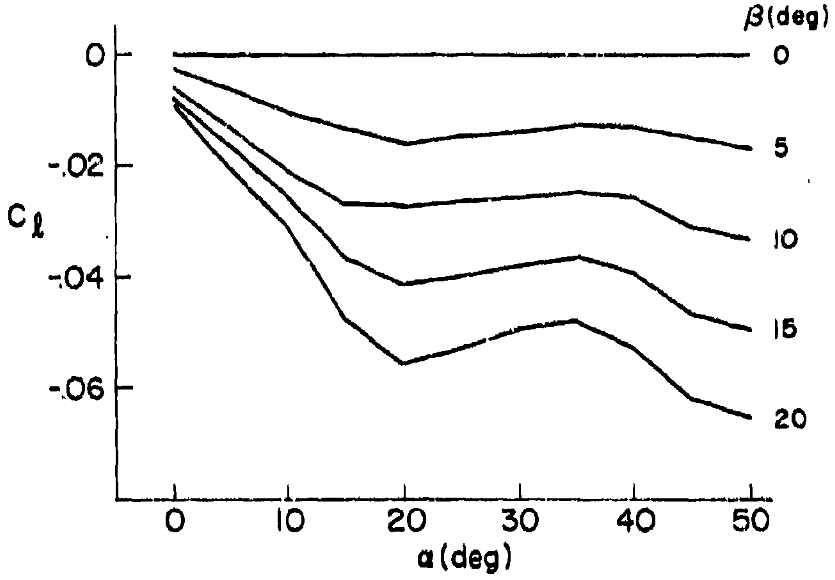

Figure 23. F-14A Roll Coefficient Variation with α, β

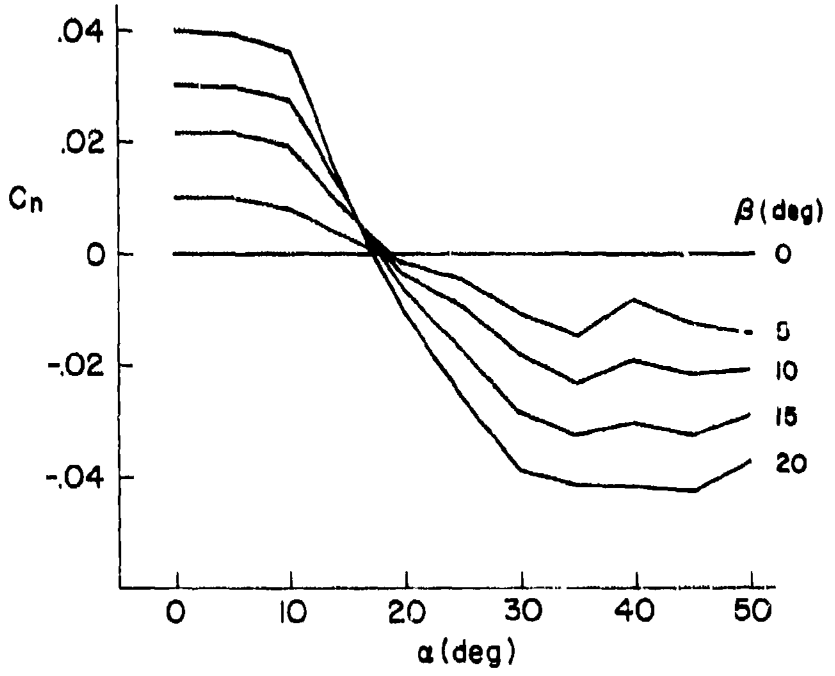

Figure 24. F-14A Yaw Coefficient Variation with α, β

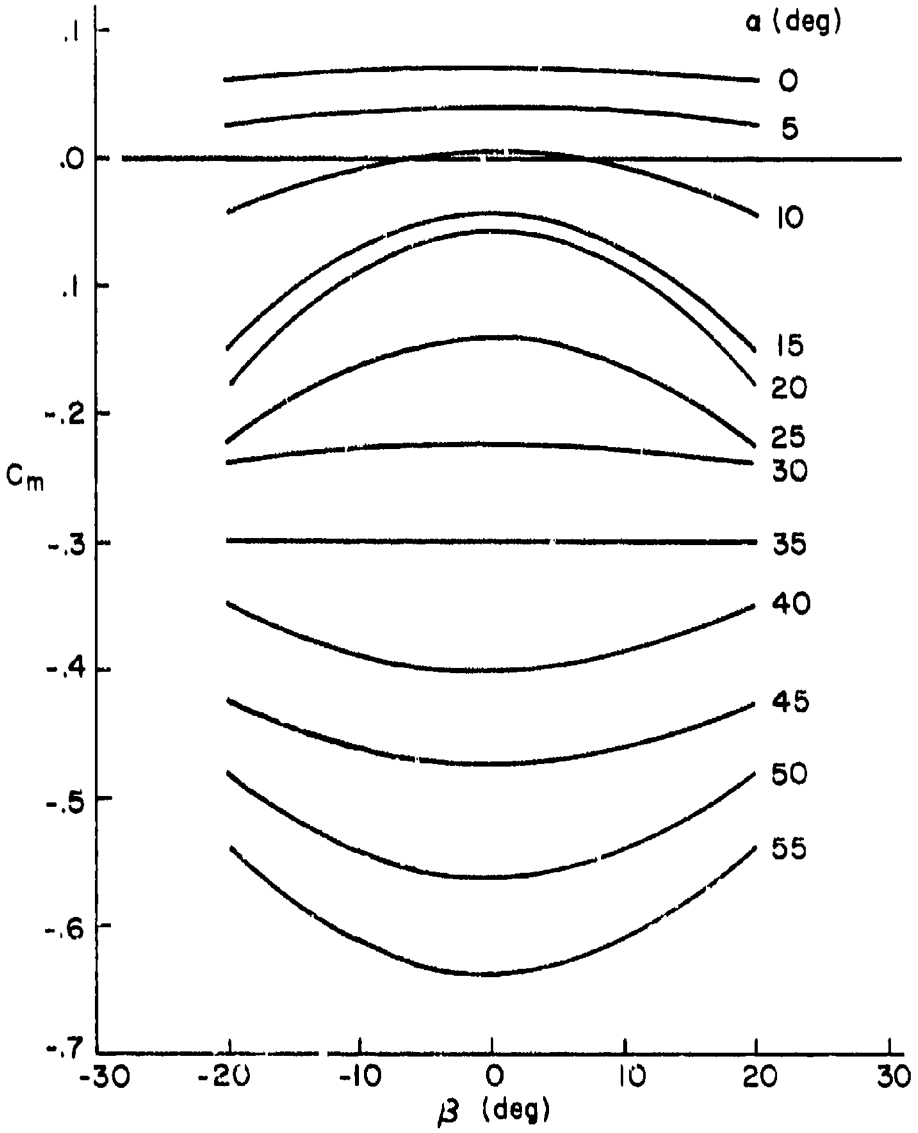

Figure 25. F-14A Pitch Coefficient Variation with α, β

TABLE 2

COMPARISON OF F-14A AND F-4J WEIGHTS, INERTIAS, AND DIMENSIONS

Parameter	F-14A	F-4J
W (lb)	46,950	37,000
c.g. (% $\bar{c}$)	16.0	29.3
I_x (slug-ft^2)	58,950	23,850
I_y (slug-ft^2)	225,600	127,400
I_z (slug-ft^2)	285,000	146,000
I_{xz} (slug-ft^2)	-3030	2210
Λ (deg)	22	45
S (ft^2)	565	530
b (ft)	64.1	38.67
$\bar{c}$ (ft)	9.8	16.04

The inertia differences between the vehicles are large. Although the F-14A is some 27 percent heavier than the F-4J with comparable fuel loading, the inertias range from 77 to 147 percent higher and the product of inertia is of opposite sign. This has considerable influence on the ratios of aerodynamic to kinematic terms in the model and greatly influences coupling effects, as will be shown later.

Aircraft control is exerted through a horizontal stabilizer (δ_{stab}), twin rudders (δ_r), spoilers (δ_{sp}), and differential horizontal (δ_D) surface deflections. Simplified block diagrams of the flight control and augmentation systems are shown in Figures 26-28. The longitudinal system contains a feel system (spring cartridge, variable gearing ratio, bobweights), a limited-authority pitch rate SAS, and a surface actuator. However, the analysis and simulation are based on a simple fixed stick-to-surface gain and pitch rate SAS.

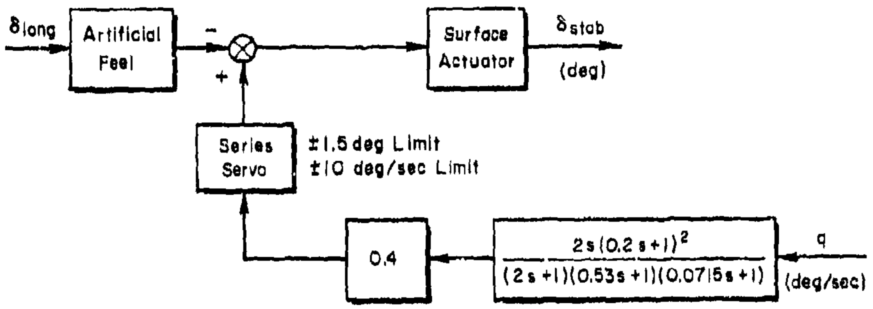

Figure 26. F-14A Longitudinal Control System

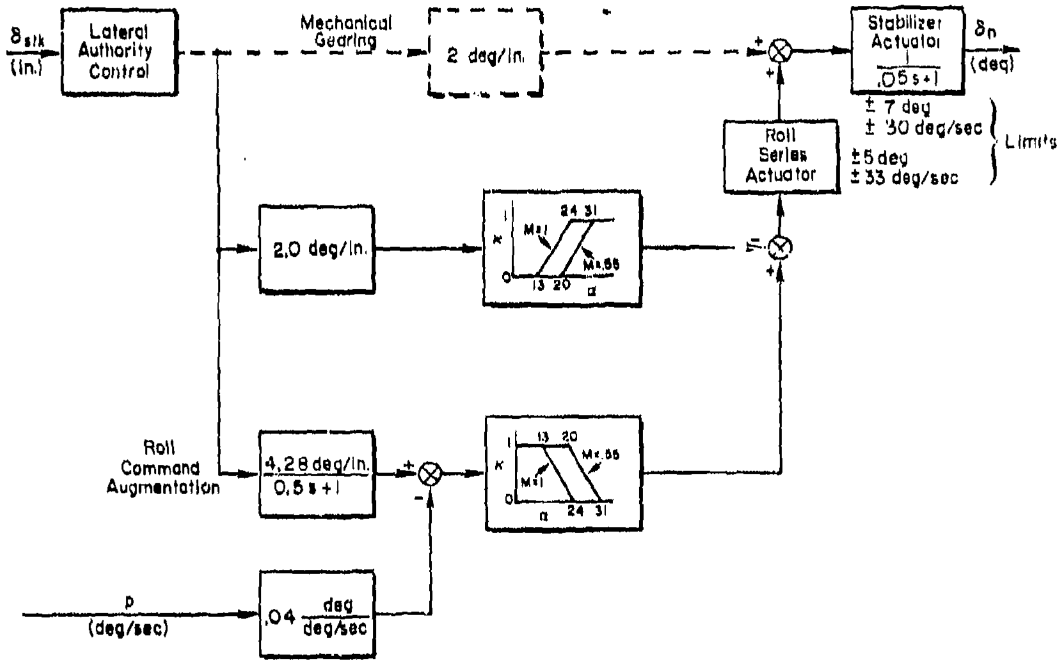

Figure 27. F-14A Lateral Control System

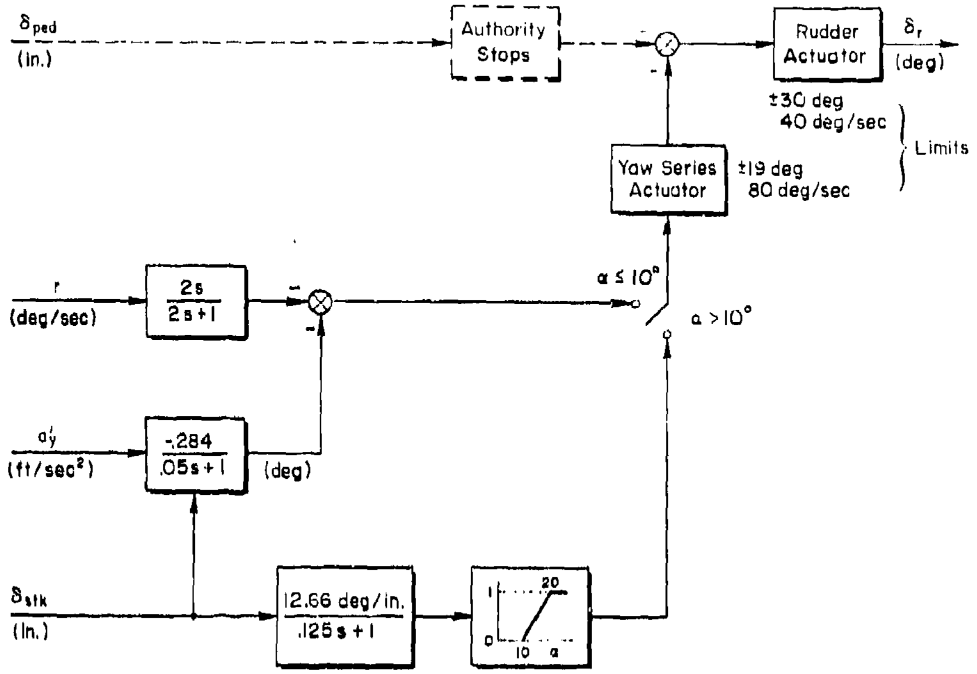

Figure 28. F-14A Directional Control System

The lateral system (Figure 27) has a roll rate command augmentation system (CAS) in parallel with a mechanical stick-surface link. At high AOA the spoilers are ineffective and all roll control is obtained through differential horizontal, δ_D. The roll rate CAS operates only through the differential horizontal, and the electrical path gains are varied with AOA such that the CAS command and feedback fades to zero when $20 < \alpha < 31$ deg and, simultaneously, the electric stick-surface path fades in to cancel all but ±2 deg of mechanical path surface command. Thus, for $\alpha > 31$ deg there is no roll rate damping augmentation and the pilot can only command ±2 deg of differential horizontal surface.

The rudder system (Figure 28) contains a fixed gain mechanical link from pedals to surface actuators, a conventional yaw damper with yaw rate and lateral acceleration feedback, and a lateral stick-to-rudder crossfeed (SRI). At $\alpha > 10$ deg the yaw SAS is cut out and the SRI faded in. The SRI signal, passed through a first-order lag filter (break frequency 8 rad/sec), reaches full gain at $\alpha > 20$ deg. Above $\alpha = 20$ deg full lateral stick deflection produces 19 deg of rudder deflection.

Thus for the AOA region of interest, $\alpha > 20$ deg, the airframe is essentially unaugmented in the lateral-directional axes and the control stick effectively moves the stabilator for pitching and twin rudders for rolling.

2. Model Validation

F-14A flight test data covering the appropriate AOA region were provided by the aircraft manufacturer (Reference 28). Unfortunately, the data were extracted from tests of three aircraft having slightly different weights, inertias, flight control systems, and flight test instrumentation. Since the flight test goals involved flight control and leading edge flap system development rather than identification of basic airframe dynamics, most runs were contaminated by SAS effects, pilot control inputs, or configuration influences. The model validation therefore was based on general response matching of a few short time "windows" of bare-airframe response or relatively uncontaminated traces, plus observation that the sequence of dynamic characteristic changes with increasing AOA described previously was indeed achieved.

Figure 29 presents results of a static longitudinal validation check based upon a 1-g stall in which AOA is increased steadily from 10 deg to almost 40 deg with a ramp horizontal stabilizer input. The circled points reflect the excellent agreement for horizontal stabilizer inputs required to achieve the noted AOA trim condition at 35,000 ft altitude with the aerodynamic model.

Figure 30 is a short time-slice of the divergent dutch roll at approximately 15 deg AOA. Motion is excited by a lateral stick doublet which, through the SRI, produces both differential horizontal and rudder doublets. Both the yaw and roll rate SASs are then turned off, and the subsequent oscillation represents the "bare" airframe in the lateral-directional sense. As with the F-4J, the envelope of the oscillation

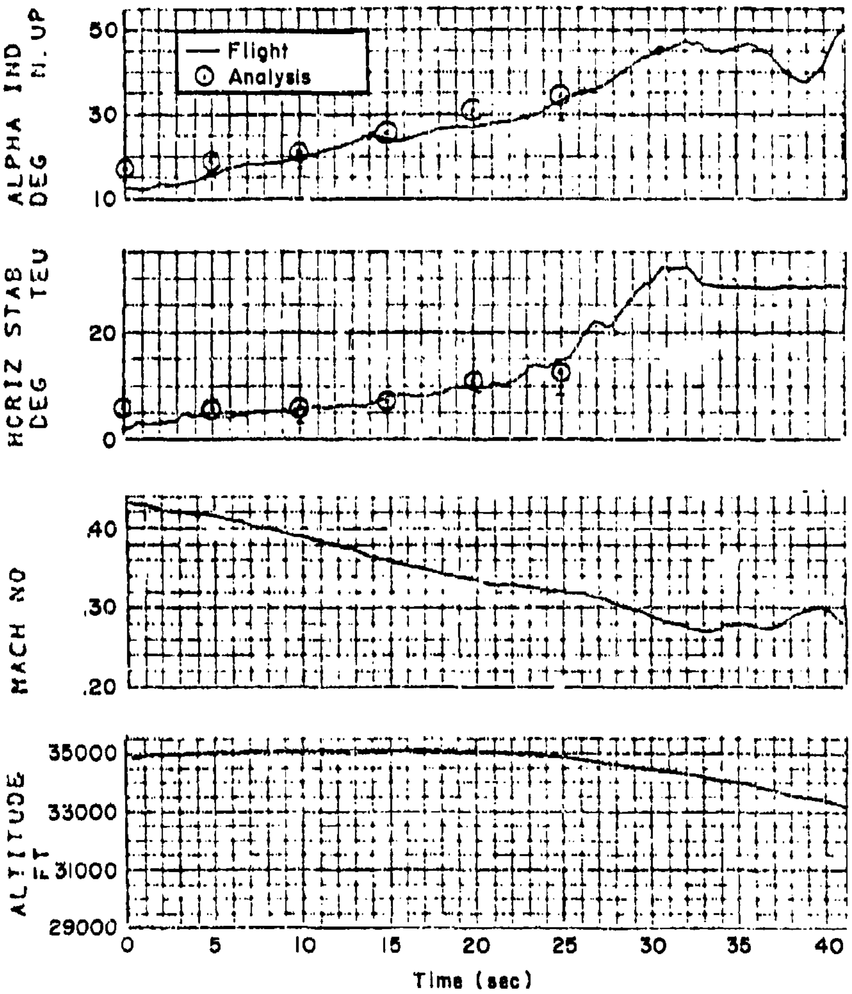

Figure 29. F-14A Longitudinal Static Trim Comparison

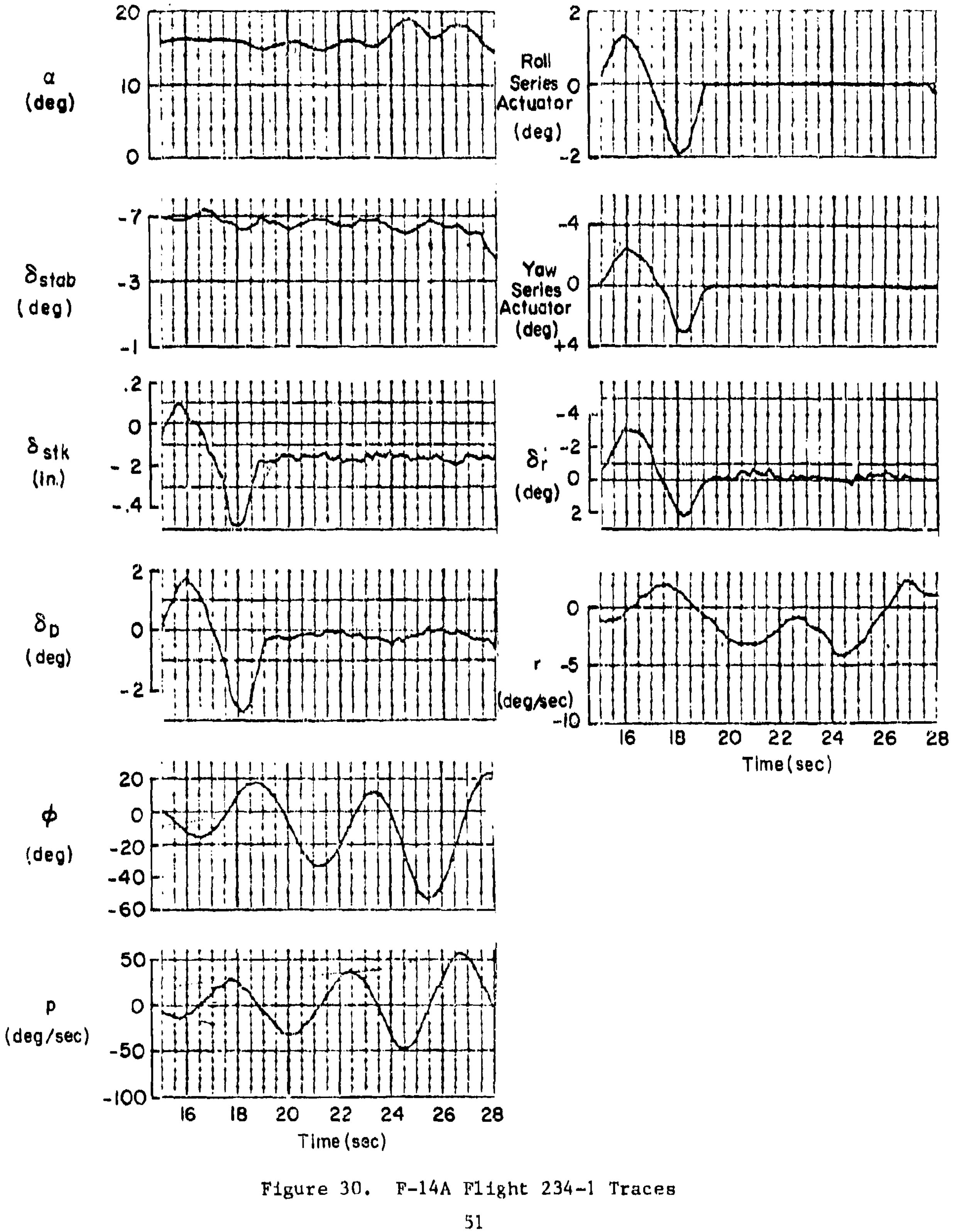

Figure 30. F-14A Flight 234-1 Traces

seems to grow linearly rather than exponentially, which indicates nonlinear damping. Also, the AOA trace shows an oscillation at twice the dutch roll frequency. The motion on the δ_{stab} trace indicates the pitch SAS was on and responding to the longitudinal oscillation.

Figure 31 presents time traces for the F-14 aerodynamic model trimmed at 15 deg AOA and excited by aileron and rudder doublets similar to Figure 30. This also shows an almost linear, rather than exponential, growth in dutch roll amplitude. The frequency and cycles to double amplitude are the same as in Figure 30. The small-amplitude AOA oscillation also is precisely twice the frequency of the dutch roll.

Figure 32 presents another short time-slice in which AOA is maintained at 18 ± 2 deg. In this angle of attack region the SAS gain schedule shows that the yaw SAS should be off and the roll SAS on. However, comparison of the yaw rate and rudder position traces indicates that the rudder is correlated with yaw rate at approximately the magnitude and phase angle that would result from the yaw damper. Since the rudder pedal and lateral stick are both constant and very small, the aircraft response is essentially that of the controls-fixed augmented airframe. This dutch roll oscillation is essentially the same, indicating that the yaw SAS is quite ineffective at this AOA and airspeed.

Other comparisons which can be made among Figures 30, 31, and 32 are summarized below:

	F-14A		Model
Parameter	Figure 32	Figure 30	Figure 31
Period of oscillation (sec)	4.5	4.5	4.5
Cycles to double	2	2	2
ϕ/β (deg/deg)	2	*	2
p/r	25	**	22.5
α (deg)	18 ± 2	15	15

*β trace not available. **r trace contaminated.

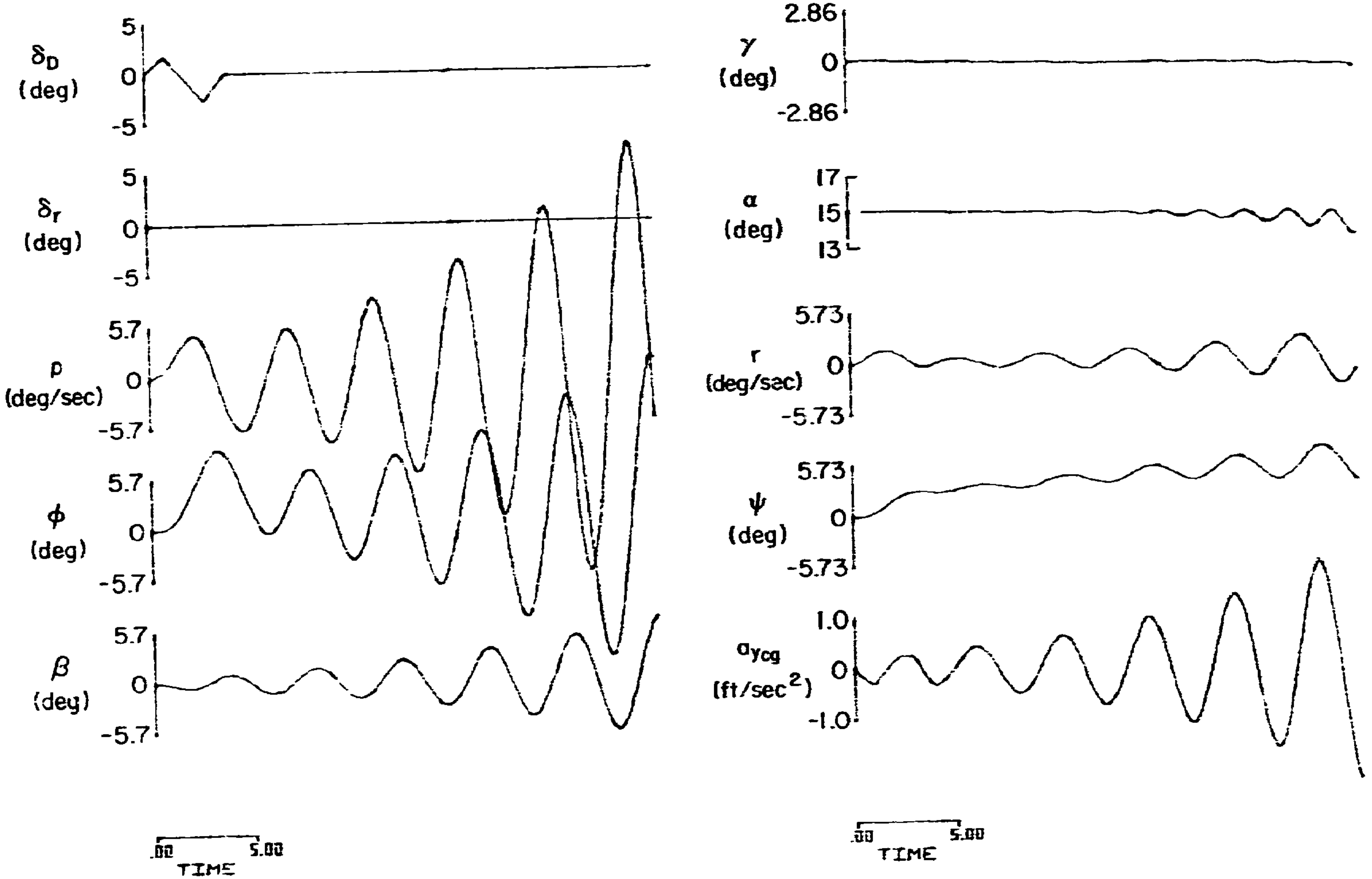

Figure 31. F-14A Model Match of Flight 234-1

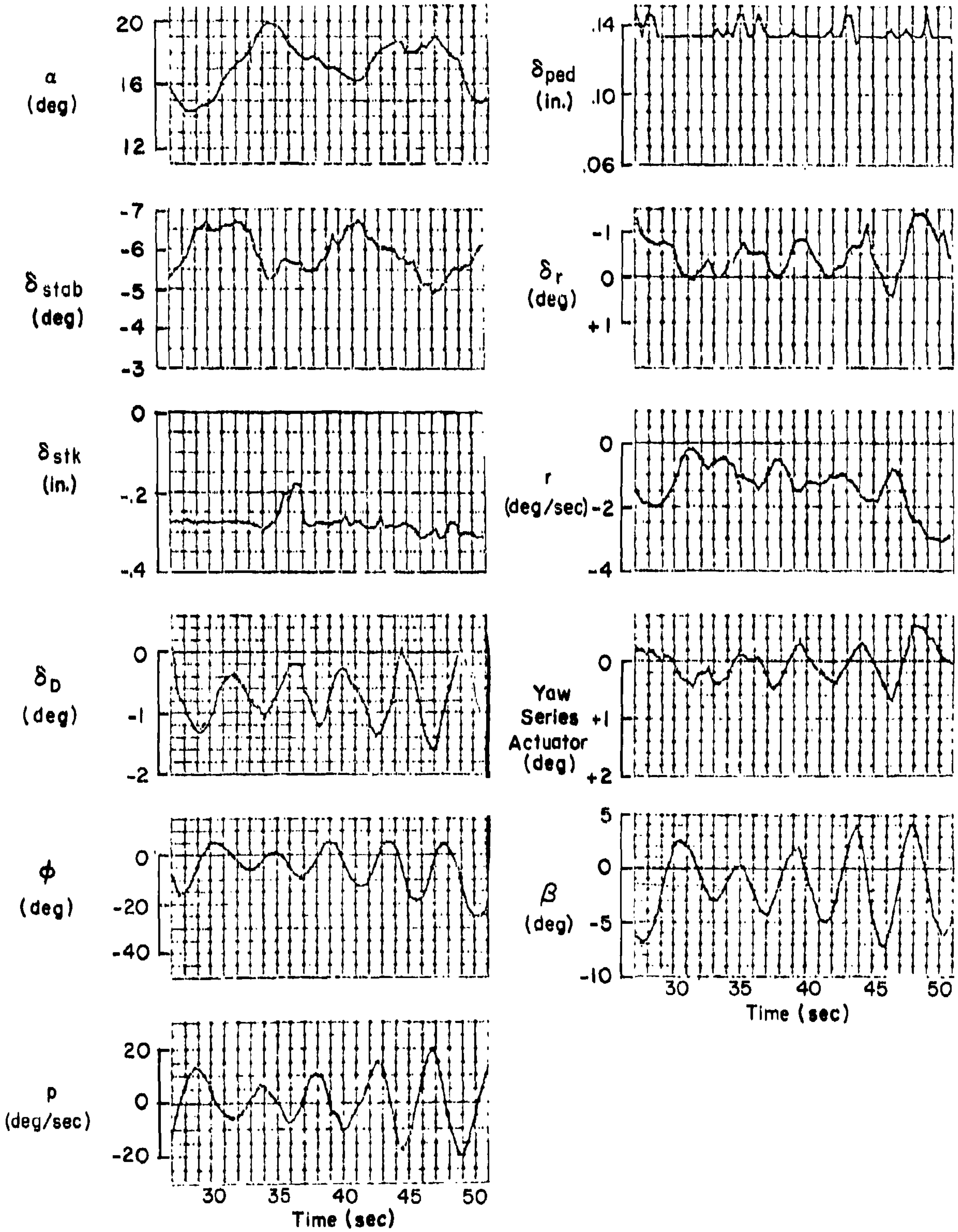

Figure 32. F-14A Flight 243 Traces

Taken together, the foregoing is considered an acceptable match between actual and simulated airframe dynamics in the region of 15 deg AOA where the dutch roll divergence and wing rock are most pronounced.

Figure 33 shows a pullup initiated from wings-level flight in which AOA is steadily increased from 13 to 38 deg at about 0.75 deg/sec. A lateral stick oscillation is introduced at about 15 deg AOA. The stick is then centered and the SASs turned off at about 18 deg AOA. A small rudder ramp is then introduced, possibly to counter the slow roll-off in bank angle. Simulation traces for a matching pullup with similar stick and rudder inputs are shown in Figure 34. Both Figures 33 and 34 show a divergent dutch roll. However, the amplitude appears to increase linearly rather than exponentially, again reflecting nonlinear damping. Both sets of traces show the period of oscillation to increase from about 4.5 sec to over 5.5 sec as AOA approaches 30 deg. Again there is good agreement between the actual flight and simulation responses.

3. Dynamic Analysis

The principal shortcomings of the F-14A bare-airframe flight characteristics at high AOA are wing rock (unstable dutch roll) and roll reversal. Otherwise the airplane is quite docile. It is departure-resistant, but can be departed if lateral control deflection is sustained without large accompanying rudder. Thus, the following discussion will be devoted to identifying potential factors underlying these key differences between the F-14A and F-4J.

a. Open-Loop Dynamic Characteristics

A survey plot of root migration with angle of attack for the range $15 < \alpha < 30$ deg and $\beta = 0$ is shown in Figure 35. This indicates excellent lateral-directional agreement with the previously reported high AOA flight characteristics and with the flight traces of Figures 30, 31, and 33. The dutch roll mode becomes divergent at just under 15 deg AOA and stays unstable until approximately 22-23 deg AOA. This is the region of reported wing rock. Above 23 deg AOA the dutch roll is stable and well

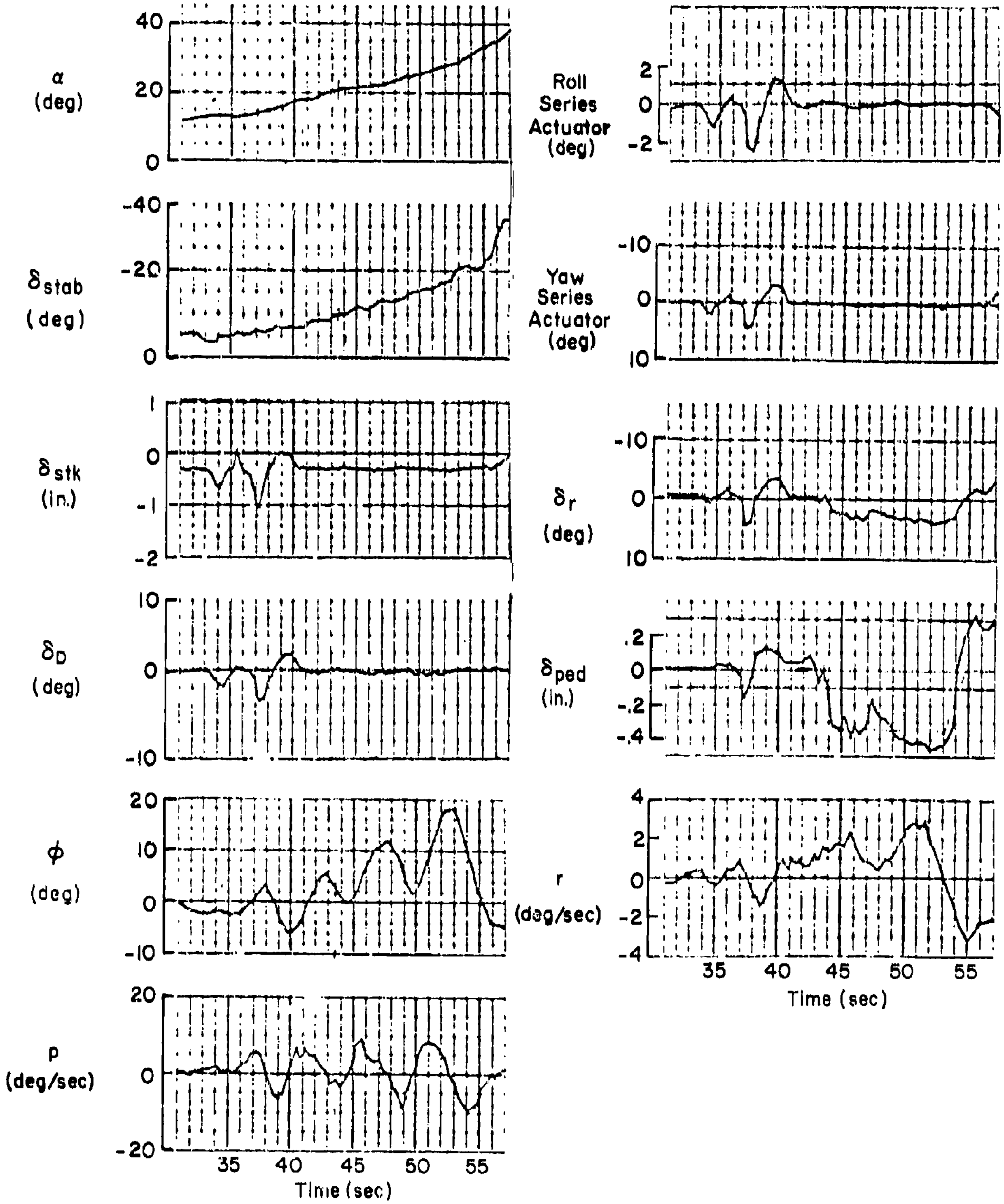

Figure 33. F-14A Flight 236-1 Pullup

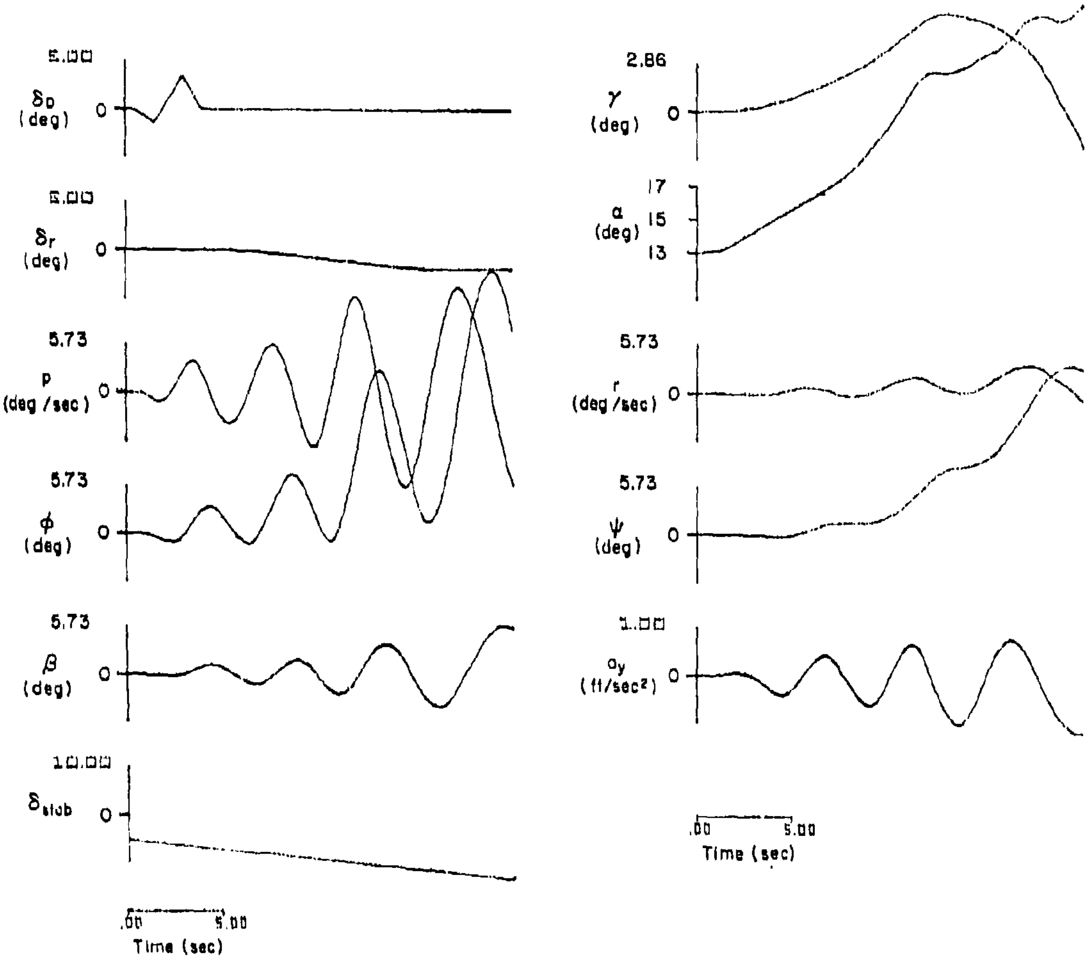

Figure 34. F-14A Model Simulation of Flight 236-1 Pullup

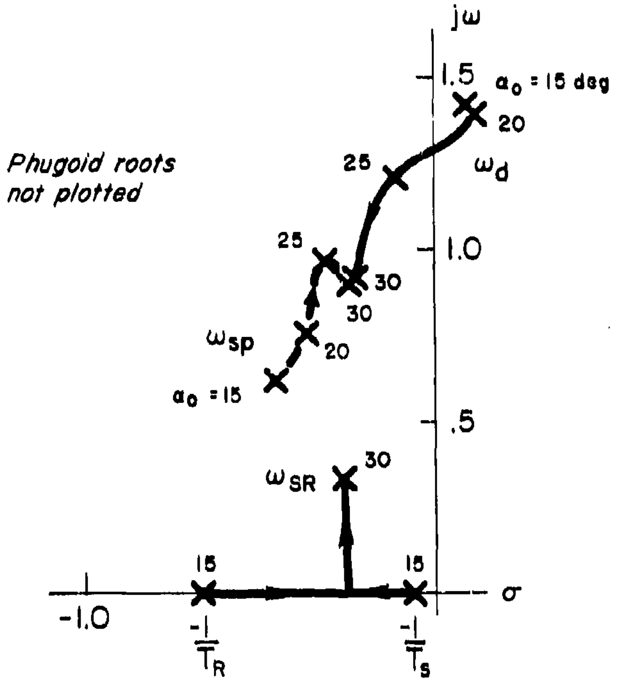

Figure 35. F-14A Root Migrations with AOA

damped but the coupled roll-subsidence and spiral becomes oscillatory. The AOA at which $N_{\beta_{dyn}} = 0$ is not shown on this plot because it remains positive (as shown in Figure 36).

The longitudinal short-period mode exhibits relatively low frequency and high damping at 15 deg AOA. Frequency then increases and damping decreases with increasing AOA until the dutch roll and short-period are about equal at 30 deg AOA. Note that this is not in agreement with the flight traces for 15 deg AOA (Figure 30), which showed a short-period frequency twice that of the dutch roll.

Referring back to Figure 25, 15 deg AOA is where Cm_β is a maximum. Thus, cross-coupling through M_β may again create pitch frequency coupling and contribute to the nonlinear dutch roll damping, as was the case with the F-4J. However for $\beta \neq 0$ the shift in the Figure 35 root locations is so small as to be negligible, and this is not the same as with the F-4J.

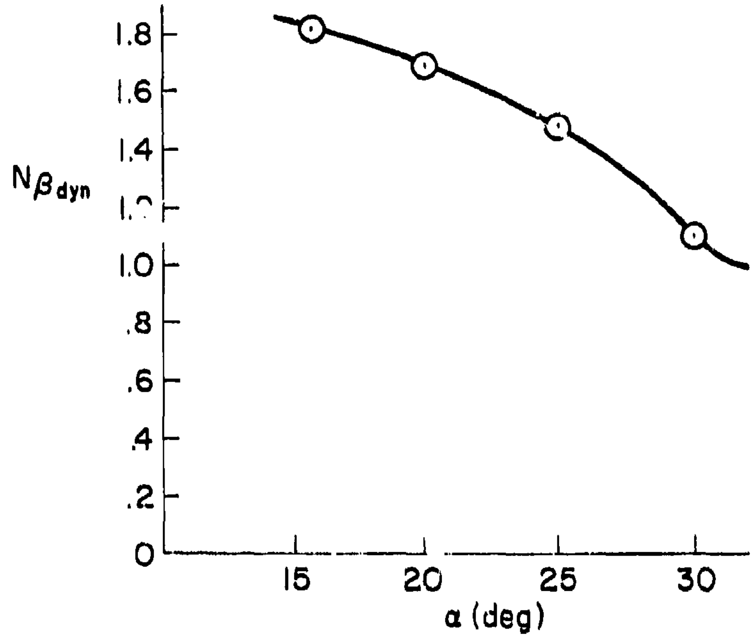

Figure 36. $N_{\beta_{dyn}}$ Variation with AOA; F-14A

Eigenvectors for the coupled dutch roll and short-period modes of the 6 DOF airframe at $\alpha_0 = 20$ deg and $\beta_0 = 1.5$ deg are shown in Figure 37. There is essentially no longitudinal coupling into the dutch roll mode and only slight lateral coupling (mainly rolling motion) into the short-period mode. These eigenvectors are noticeably different from those for the F-4J (see Figure 14) at a similar flight condition.

Vector polygons for the dutch roll mode at this flight condition are shown in Figure 38. The $\dot{p}$ equation indicates that $\mathcal{L}_\beta'$ and $\mathcal{L}_p'$ completely dominate rolling motion. All damping derives from $\mathcal{L}_p'$; there is no cross-coupling influence from $\mathcal{L}_{\dot{\alpha}}'$. All terms in the $\dot{r}$ equation have been doubled to make this polygon legible. The relative size of the $\dot{p}$ and $\dot{r}$ polygons indicates that in this AOA region static and dynamic yawing force and moment terms are negligible in the dutch roll mode. However, the yawing moment that does exist derives primarily from N_p'. The $\dot{q}$ equation has significant magnitude compared to the $\dot{p}$ equation. The key is the dominance of the $M_\beta|\beta|$ term which, as with the

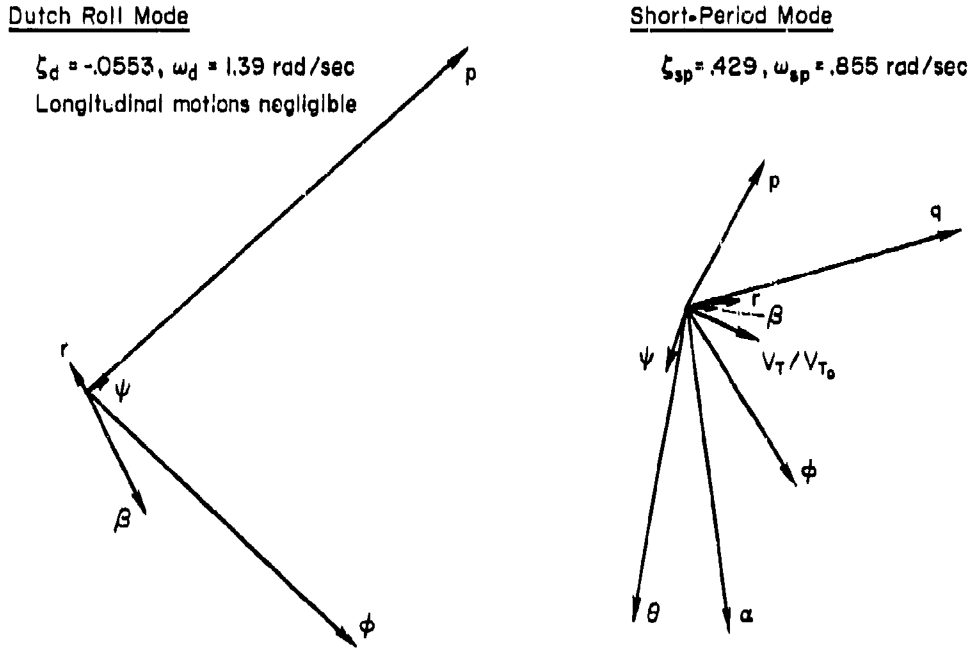

Dutch Roll Mode

$\zeta_d = -.0553$, $\omega_d = 1.39$ rad/sec

Longitudinal motions negligible

Short-Period Mode

$\zeta_{sp} = .429$, $\omega_{sp} = .855$ rad/sec

Figure 37. F-14A Eigenvectors;
$\alpha_0 = 20$ deg, $\beta_0 = 1.5$ deg

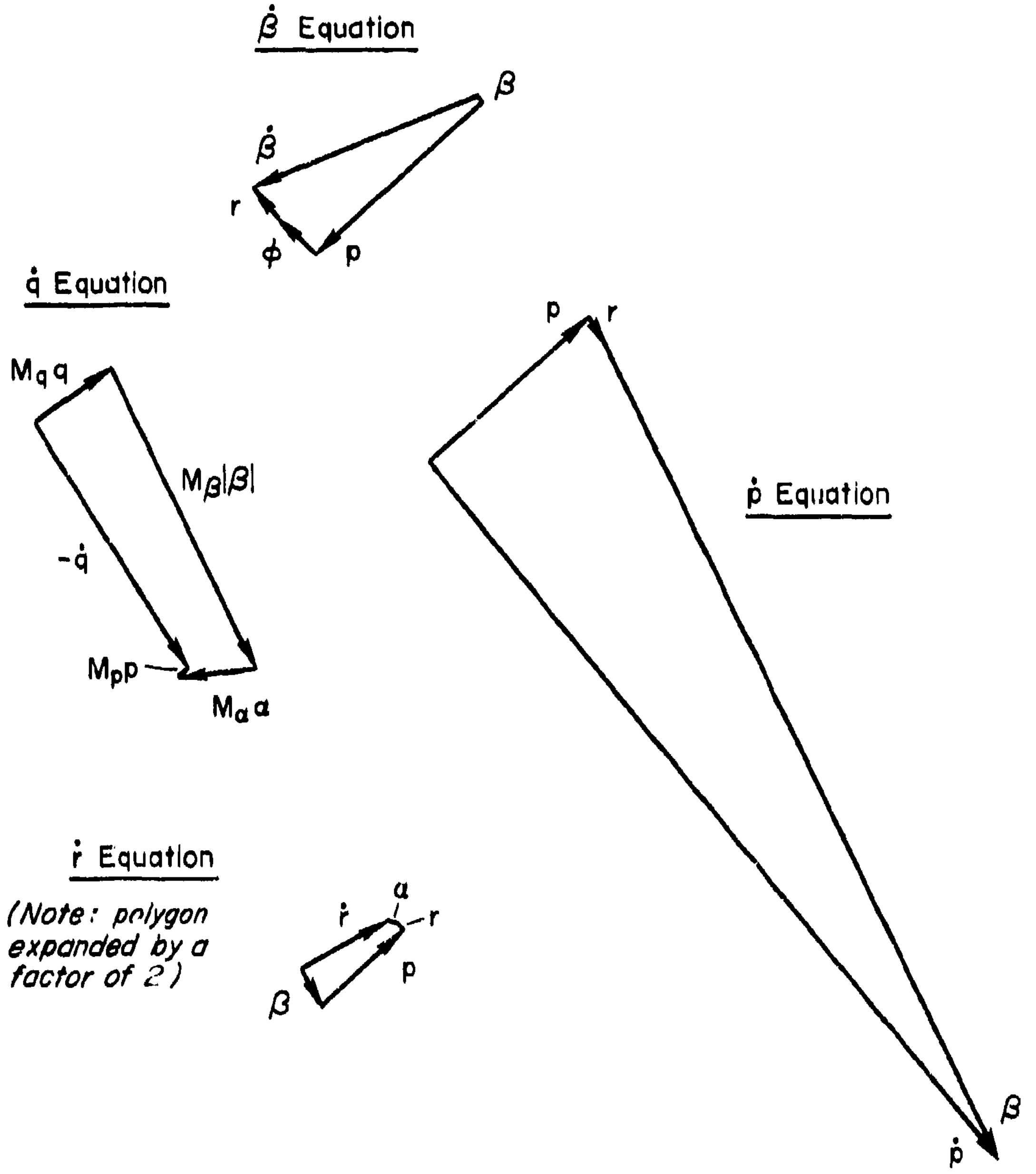

(Note: polygon expanded by a factor of 2)

Figure 38. F-14A Vector Polygons for Dutch Roll Mode; α_o = 20 deg, β_o = 1.5 deg

F-4J, indicates that coupling from the lateral into the longitudinal produces the frequency doubling effect.

Based upon the above argument, it is concluded that the F-14A wing rock is due to a divergent dutch roll which derives from very low damping in roll, $\mathcal{L}_p'$, rather than lateral-longitudinal cross-coupling (since the open-loop lateral-directional dynamic characteristics are relatively insensitive to sideslip). The principal static aerodynamic cross-coupling is a transfer of energy from rolling-sideslipping motion into pitch motion and this, as with the F-4J, results in frequency doubling into pitch and may contribute to amplitude bounding of the wing rock.

b. Closed-Loop Dynamic Characteristics

Lateral stick control of roll. Figure 39 presents the key parameters for the numerator $N^{\phi}_{\delta_D}$. The lower plot indicates that the movement of one zero into the RHP with increasing AOA is not as rapid for this airframe as for the F-4J (see Figure 17). However, departure can occur where one of the real roots is large negative. This plot also demonstrates that the roll numerator zeros are quite insensitive to sideslip when compared to the F-4J.

Rudder control of roll. Same $N^{\phi}_{\delta_r}$ characteristics as for the F-4J.

Stabilator control of pitch. The potential for divergence lies with the RHP zero, $1/T_{\theta_3}$, in $N^{\theta}_{\delta_{stab}}$. Figure 40 is a plot of $1/T_{\theta_3}$ at $\beta_o = 4$ deg over a range of AOA. Note that the parameter scale factor is an order of magnitude less than the one used for the F-4J in Figure 21, and the largest value (approximately -0.01) is *two* orders of magnitude less than for the F-4J (equal to -1.0). Thus, pilot control of pitch attitude should have no noticeable coupling into the lateral-directional modes for the F-14A.

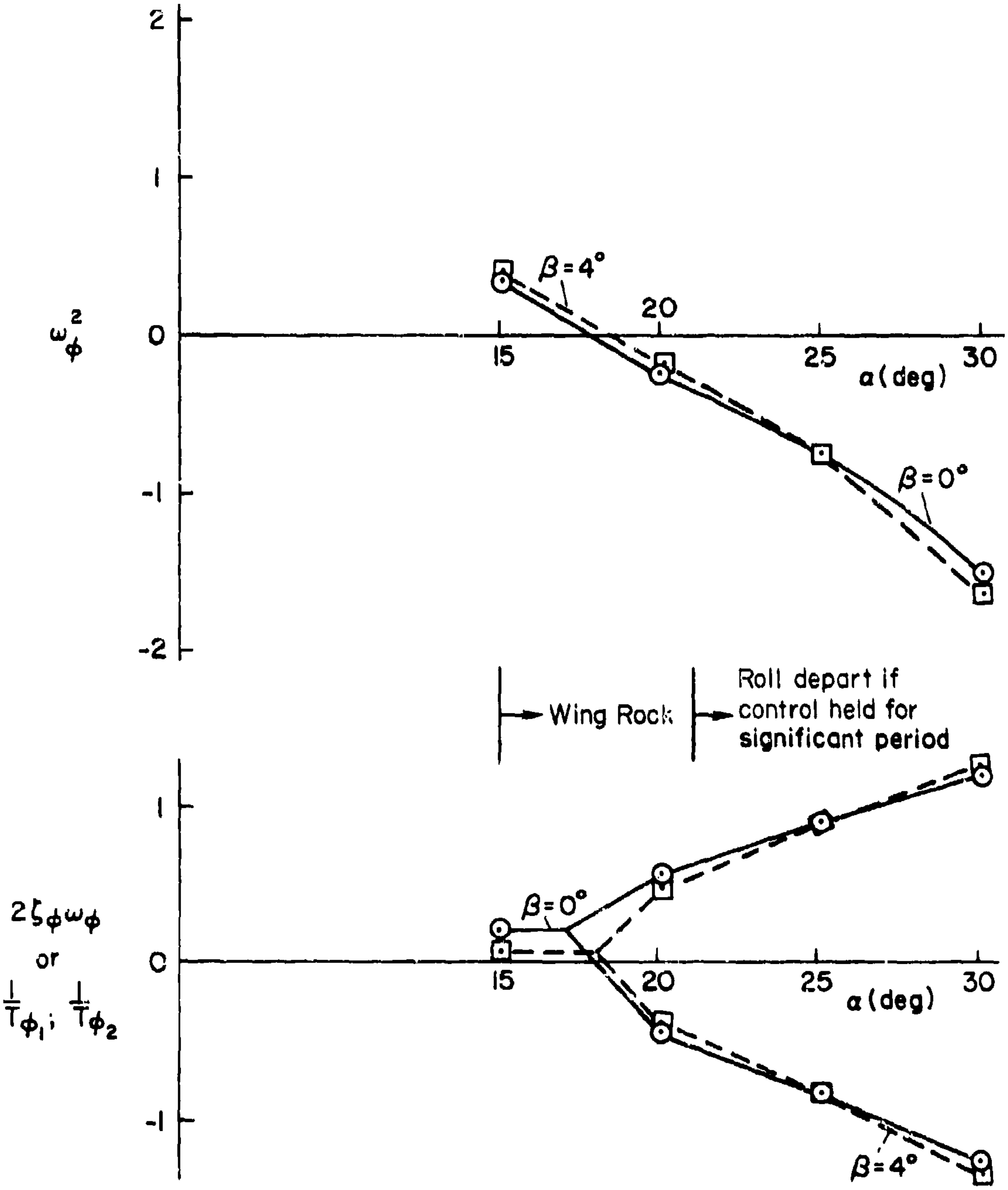

Figure 39. $N^{\phi}_{\delta_D}$ Root Migration with AOA; F-14A

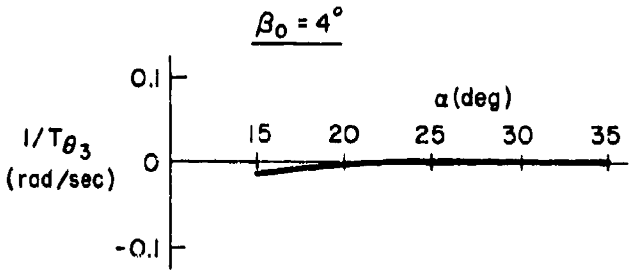

Figure 40. $N^{\theta}_{\delta_{stab}}$ First-Order Root Migration with AOA, F-14A

Coupling numerator. The lead coefficient (gain term) for the F-14A coupling numerator, $N^{\theta\ \phi}_{\delta_{stab}\delta_D}$, is, for all practical purposes, zero. Thus closure of either loop (pitch or roll) has essentially no influence on the other.

Summary. The F-14A exhibits somewhat better open-loop static and dynamic stability than does the F-4J. It also has considerably less lateral-longitudinal static cross-coupling in asymmetric flight, and hence little change or degradation in dynamic parameters with sideslip. The static aerodynamic cross-coupling derivative values at $\beta_0 = 4$ deg and $15 < \alpha < 30$ deg are presented in Figure 41. Comparison

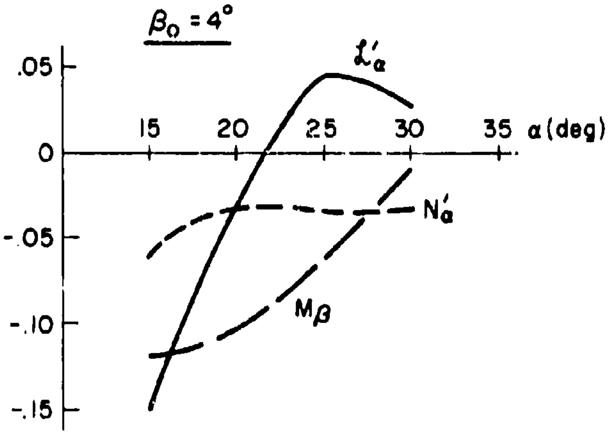

Figure 41. F-14A Static Aerodynamic Cross-Coupling Derivatives

of these values with those for the F-4J (Figure 22) shows a drastic difference between the two aircraft.

The most significant maneuver-limiting factor for the F-14A appears to be roll reversal associated with movement of one root of the roll numerator, $N^{\phi}_{\delta_D}$, into the RHP as AOA is increased. The F-14A exhibits a more gradual shift of this root with AOA than does the F-4J.

SECTION III

AERODYNAMIC CROSS-COUPLING INFLUENCES

The previous section showed a significant migration of denominator and numerator roots for the F-4J due to aerodynamic cross-coupling at $\beta_o = 5.5$ deg. In this section literal analytic expressions are developed to examine in greater detail the influences of specific cross-coupling coefficients on the airframe characteristic (open-loop) modes and the key piloted control numerators for roll due to lateral stick and pitch due to stabilator deflections.

With lateral-longitudinal cross-coupling, at least 5 DOF equations of motion (e.g., Figure 13) must be used for analysis. As a result, the wealth of existing knowledge on the dynamics of vehicles in three (or fewer) degrees of freedom is not adequate, and qualitative insight into the motions of the aircraft is sacrificed.

The important cross-coupling terms in the equations of motion identified empirically by Porter and Loomis (Reference 29) and Johnston and Hogge (Reference 5) are both aerodynamic and kinematic. Effects of cross-coupling on the characteristic aircraft modes were evaluated by Hamel (Reference 16) by applying servo analysis techniques to a 5 DOF aircraft mathematical model.

The approach applied next will follow and expand upon that utilized by Hamel.

A. CHARACTERISTICS MODES

Analysis of an uncoupled ($\beta \equiv 0$) airframe is relatively straightforward. Approximations to the classical 3 DOF lateral or longitudinal expressions can be developed for a wide range of airframe and flight conditions (e.g., Reference 20).

However, sideslip characteristically introduces cross-coupling, both kinematic and aerodynamic. Then the only clear simplification one can apply is the assumption of constant forward velocity, thereby removing the velocity equation and associated terms (see Figure 13). This can be justified since forward velocity changes comparatively slowly. No significant coupling occurs due to velocity, and its effect is primarily on the low-frequency characteristics (i.e., the phugoid mode). The three kinematic equations of Figure 13 can be resolved and substituted in the Z, M, and Y equations to reduce the number of equations to five.

Hamel takes five-degree-of-freedom equations of motion "using body axes which have the x-axis initially aligned with the flight path"; from the context we interpret that for initial sideslip, the x-axis is aligned with the projection of the flight path vector onto the plane of symmetry. In expanding the characteristic determinant he separates out the effects of the aerodynamic coupling terms $\mathcal{L}_{\acute{\alpha}}$, $N_{\acute{\alpha}}$ and M_β (neglecting any other coupling between the longitudinal set and the lateral-directional set) thus:

$$\Delta = \Delta_{long}\Delta_{lat} + K(\beta_o)\Delta_{coupl}$$

The uncoupled ($\beta_o \equiv 0$) denominator terms are

$$\Delta_{long} = s^2 + 2\zeta_{sp}\omega_{sp}s + \omega_{sp}^2$$

$$\Delta_{lat} = (s + 1/T_s)(s + 1/T_R)(s^2 + 2\zeta_d\omega_d s + \omega_d^2)$$

Hamel defines the classical longitudinal (short period) and lateral-directional (spiral, roll subsidence, dutch roll) by approximate factors (Reference 20). The coupling component, $K(\beta_o)\Delta_{coupl}$, can be manipulated to represent a sum of two terms:

$$K(\beta_o)\Delta_{coupl} = \mathcal{L}_{\acute{\alpha}}\beta_o s(s + 1/T_o)(s^2 + 2\zeta_o\omega_o s + \omega_o^2)$$

$$+ M_\beta N_{\acute{\alpha}}\beta_o(s + 1/T_1)(s + 1/T_2)$$

The approximate factors for these coupling terms are reproduced (in the notation of this report) in Table 3.

TABLE 3. COUPLING NUMERATOR FACTORS

$$1/T_o = -M_q$$

$$2\zeta_o\omega_o = -Y_\beta - N'_r + (N'_\alpha/\mathcal{L}'_\alpha)\mathcal{L}'_r$$

$$\omega_o^2 = N'_\beta + Y_\beta N'_r - (N'_\alpha/\mathcal{L}'_\alpha)(\mathcal{L}'_\beta + Y_\beta\mathcal{L}'_r)$$

$$1/T_1 = -\mathcal{L}'_p + (\mathcal{L}'_\alpha/N'_\alpha)(N'_p - g/U_o)$$

$$1/T_2 = T_1 g/[U_o(\mathcal{L}'_\alpha/N'_\alpha)(N'_r - \mathcal{L}'_r)]$$

The roots of the coupling component are evaluated by applying servo analysis techniques for obtaining the roots of a characteristic equation, setting it into the form

$$1 + \frac{M_\beta(N'_\alpha/\mathcal{L}'_\alpha)(s + 1/T_1)(s + 1/T_2)}{s(s + 1/T_o)[s^2 + 2\zeta_p\omega_o s + \omega_o^2]} = 0$$

Figure 42 is a root locus plot for this equation. In this instance $\zeta_o > 1$ and $\omega_o^2 < 0$. The "closed-loop" roots for this case are

$$K(\beta_o)\Delta_{coupl} = \mathcal{L}'_\alpha\beta_o(s + .404)(s + .47)$$

$$\times [s^2 + 2(-.48)(1.87)s + (1.87)^2]$$

This same technique can be applied on a larger scale to find the roots for the coupled characteristic modes, i.e., the roots of the relationship

$$1 + \frac{K(\beta_o)\Delta_{coupl}}{\Delta_{long}\Delta_{lat}} = 0$$

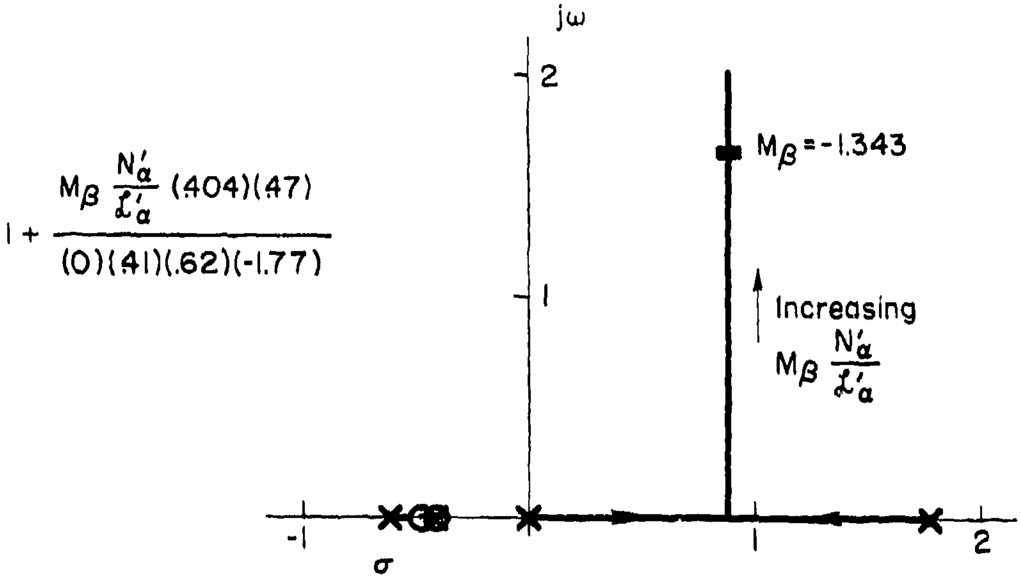

Figure 42. Migration of Roots of $K(\beta_o)\Delta_{coupl}$ with Increasing M_β (α_o = 21 deg, β_o = 5.5 deg)

Figure 43 is a root locus plot for this expression showing the migration of ω_{sp} and ω_d with increasing $\mathcal{L}'_{\alpha}\beta_o$. Note that $1/T_s$ and $1/T_R$ are essentially cancelled by zeros obtained from the approximate factors and the preceding "closure."

The actual 6 DOF roots of the F-4J α_o = 21 deg, β_o = 5.5 deg case are shown by the dashed lines and △ symbols in Figure 43. There is fair agreement between the simplified and exact loci for the dutch roll but not for the other modes. The problem, it appears, lies with the location of the first-order coupling zeros. If these were to lie closer to the origin, the ω_{sp} and ω_d loci would be rotated counterclockwise and $1/T_s$ and $1/T_R$ would be driven to the right. It is not surprising that the approximate factors employed here do not precisely predict the F-4J root shift since they were developed in Reference 16 for an airframe configuration considerably different from the F-4J. However, they do demonstrate the trends and show specifically that:

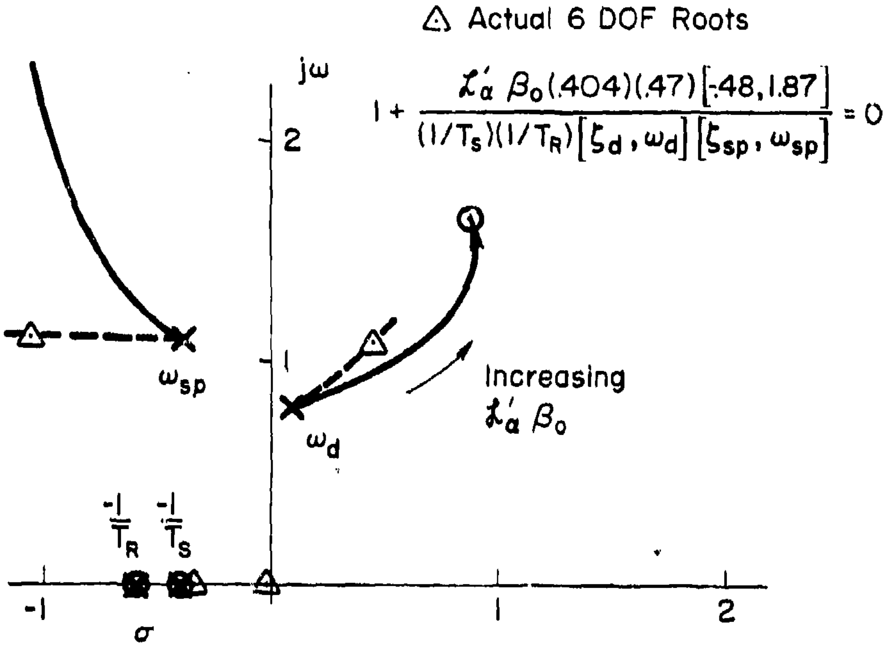

Figure 43. Migration of Roots of Characteristic Modes as Cross-Coupling Increases; $\alpha_o = 21$ deg, $\beta_o = 5.5$ deg

- The location of the roots of $K(\beta_o)\Delta_{coupl}$ (Figure 42) and hence the direction of the root shift in Figure 43, is controlled by the sign and magnitude of $M_\beta(N'_\alpha/\mathcal{L}'_\alpha)$.
- The magnitude of root shift in Figure 43 is controlled by the sign and magnitude of $\mathcal{L}'_\alpha\ \beta_o$.

B. $N^{\phi}_{\delta_{stk}}$ NUMERATOR

The first step in identifying the influences of cross-coupling terms on the key numerator for lateral piloting control, $N^{\phi}_{\delta_{stk}}$, require elimination of all insignificant terms. This is accomplished by a series of simplifying steps. The 6 DOF characteristic poles and the zeros for the numerator $N^{\phi}_{\delta_{stk}}$ are shown in Figure 44, again for the F-4J at $\alpha_o = 21$ deg, $\theta_o = 5.5$ deg. Figure 44a represents a case for which the cross-coupling terms are zero. At this high AOA the uncoupled numerator

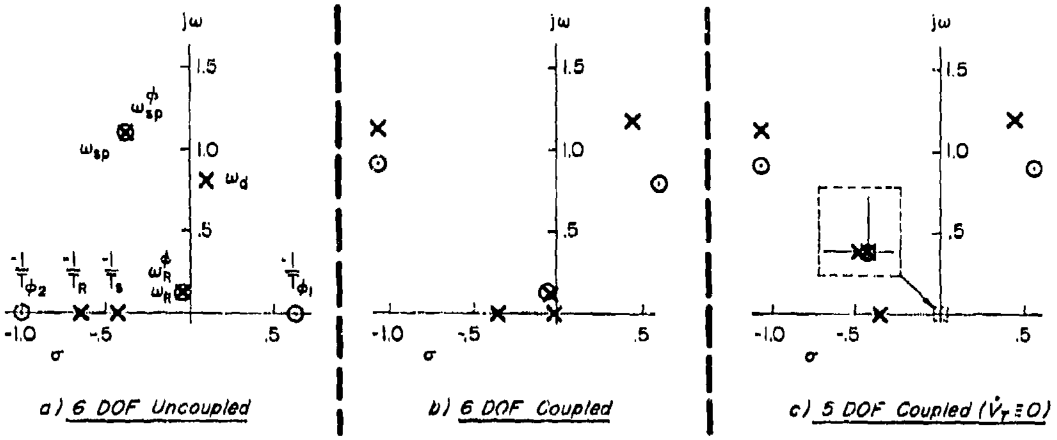

a) 6 DOF Uncoupled

b) 6 DOF Coupled

c) 5 DOF Coupled ($\dot{V}_T \equiv 0$)

Figure 44. $N^{\phi}_{\delta_{stk}}/\Delta$ Pole-Zero Locations, Coupled vs. Uncoupled, F-4J, $\alpha_0 = 21$ deg, $\beta_0 = 5.5$ deg

consists of two real roots, $1/T_{\phi_1}$ and $1/T_{\phi_2}$, non-minimum phase and minimum phase, respectively; and two complex pairs, ω^{ϕ}_{p} and ω^{ϕ}_{sp}, which exactly cancel the uncoupled longitudinal poles. With cross-coupling (Figure 44b) the first-order zeros couple into a complex pair located near the divergent dutch roll mode. In addition, the numerator counterpart to ω_{sp}, ω^{ϕ}_{sp}, has moved apart from the short-period poles. The effects of coupling on the phugoid numerator term, ω^{ϕ}_{p}, are neglible (see Figure 44b). This indicates that the velocity equation of Figure 13 may be eliminated. The phugoid then reduces to a first-order pole-zero pair at the origin, but all other roots are affected only slightly (Figure 44c). However, even with the V_T terms removed from Figure 13, and recognizing that the equations for the Euler angles ψ and θ contribute no significant kinematic coupling and can be deleted, a rather unwieldy six-by-six matrix still remains.

The matrix can be further reduced by use of time vectors evaluated for the particular mode of interest. Inspection of Figure 44b shows that the $N^{\phi}_{\delta_{stk}}$ zeros of greatest concern are the complex pair which lie in the right half-plane, near the already divergent dutch roll poles. Therefore further analysis of $N^{\phi}_{\delta_{stk}}$ will concentrate on this complex pair, and on the effects of cross-coupling in driving them off the real axis, where Figure 44a places the corresponding zeros of the uncoupled response.

For denominator roots the relative magnitude and phase of each motion variable in the mode corresponding to any particular real pole or pair of complex poles can be determined. The result can be expressed numerically as an eigenvector or graphically as phasors. In order to determine such characteristics for transfer function numerator roots, a pole is driven into each zero to be examined. The poles are driven into the zeros by closing a tight feedback loop, as shown in Figure 45. In Figure 44c the real poles are driven into the right half-plane pair of complex zeros. Actually the $(p/s)\delta_{stk}$ transfer function is utilized here rather than ϕ/δ_{stk} since the two are almost identical (compare Figures 44c and 45).

Figure 46 presents the resulting phasors for the closed-loop roll-spiral mode, ω'_{SR}, which approximates the numerator "mode" ω_ϕ. Using these phasors, vector polygons have been plotted for this mode (see Figure 46) from the equations of motion, Figure 13. Minor vectors

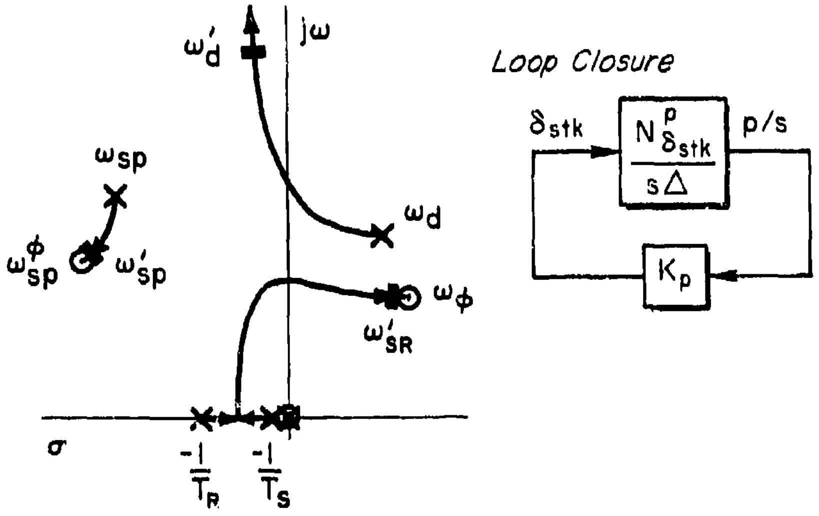

Figure 45. Closure of $p/s \rightarrow \delta_{stk}$ to Obtain Time Vectors, F-4J, $\alpha_0 = 21$ deg, $\beta_0 = 5.5$ deg

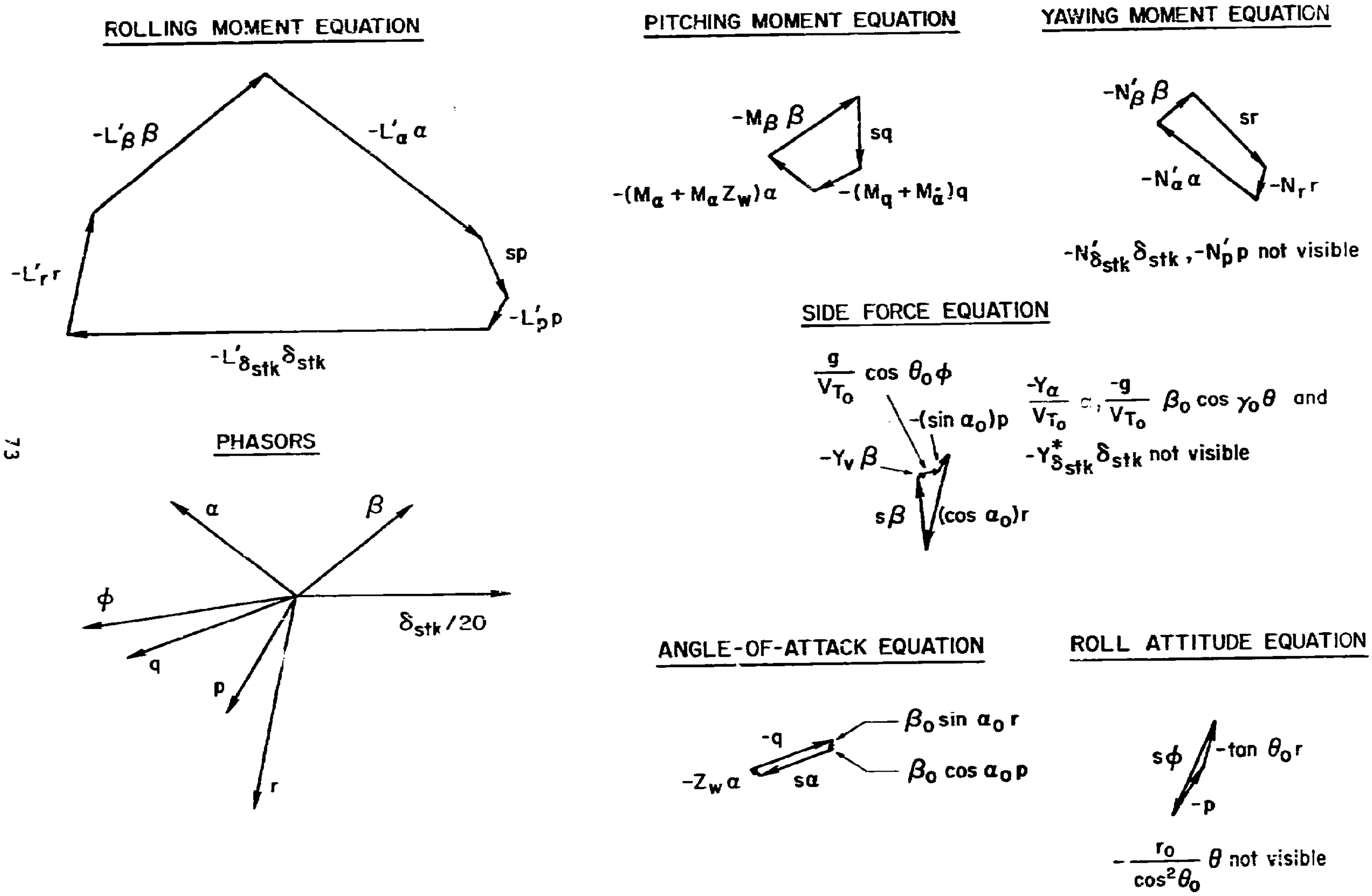

Figure 46. Vector Polygons for Closed-Loop ω'_{SR} (Approximating ω_ϕ), F-4J; α_o = 21 deg, β_o = 5.5 deg

correspond to negligible terms; small polygons indicate little contribution to the modal response. Examination of these vector polygons leads to elimination of a number of terms from the equations of Figure 13. Specifically, the kinematic equations are no longer needed, and so the matrix for approximation of the coupled numerator $N^{\phi}_{\delta_{stk}}$ reduces to the form shown in Figure 47. The derivatives Y_v, $N'_{\delta_{stk}}$, and Z_w are also minimal for this particular airframe and flight condition. However, under other circumstances they can be quite large, so they have been retained to obtain a more general expression for $N^{\phi}_{\delta_{stk}}$.

The determinant of this matrix may be developed as a combination of uncoupled longitudinal and lateral-directional terms plus cross-coupling terms, as follows:

$$
\begin{aligned}
N^{\phi}_{\delta_{stk}} \doteq \mathcal{L}'_{\delta_{stk}} \Bigg\{ & \left[s^2 - (Z_w + M_q + M_{\dot{\alpha}})s - (M_\alpha + Z_w M_q)\right] \\
& \times \left[s^2 + \left(\frac{N'_{\delta_{stk}}}{\mathcal{L}'_{\delta_{stk}}} \mathcal{L}'_r - N'_r - Y_v \right) s + \left(N'_\beta - \frac{N'_{\delta_{stk}}}{\mathcal{L}'_{\delta_{stk}}} \mathcal{L}'_\beta \right) \cos \alpha_o \right. \\
& \qquad \left. + Y_v \left(N'_r - \frac{N'_{\delta_{stk}}}{\mathcal{L}'_{\delta_{stk}}} \mathcal{L}'_r \right) \right] \\
& + M_\beta \cos \alpha_o \left(- \frac{N'_{\delta_{stk}}}{\mathcal{L}'_{\delta_{stk}}} \mathcal{L}'_\alpha + N'_\alpha \right) \Bigg\}
\end{aligned}
$$

This is of the form

$$N^{\phi}_{\delta_{stk}} \doteq \left(N_{\delta_{stk}}\right)_{coupled} + K_{\mathcal{L}} + K_N$$

where $\left(N^{\phi}_{\delta_{stk}}\right)_{uncoupled}$ consists of two second-order terms: a longitudinal term equivalent to the conventional short-period (denominator)

$$\begin{bmatrix} s - (M_q + M_{\dot{\alpha}}) & -M_\alpha - M_{\dot{\alpha}} Z_w & & & -M_\beta \\ -1 & s - Z_w & & & \\ & -\mathcal{L}'_\alpha & \mathcal{L}'_{\delta_{stk}} & -\mathcal{L}'_r & -\mathcal{L}'_\beta \\ & -N'_\alpha & N'_{\delta_{stk}} & s - N'_r & -N'_\beta \\ & & & \cos\alpha_o & s - Y_v \end{bmatrix} \begin{bmatrix} q \\ \alpha \\ p \\ r \\ \beta \end{bmatrix}$$

Figure 47. Matrix for Approximation of Coupled Numerator $N^{\phi}_{\delta_{stk}}$

approximation; and a lateral-directional term which is the 3 DOF $N^{\phi}_{\delta_{stk}}$ (with $Y^{\phi}_{\delta_{stk}} \equiv 0$) (Reference 20). The coupling "gain" terms are:

$$K_{\mathcal{L}} = -M_\beta \mathcal{L}'_\alpha \frac{N'_{\delta_{stk}}}{\mathcal{L}'_{\delta_{stk}}} \cos\alpha_o$$

and

$$K_N = M_\beta N'_\alpha \cos\alpha_o$$

Servo analysis techniques can now be utilized to examine the influence of each of the cross-coupling derivatives by writing the numerator in characteristic-equation form, i.e.,

$$N^{\phi}_{\delta_{stk}} \doteq \left(N^{\phi}_{\delta_{stk}}\right)_{uncoupled} + K_{\mathcal{L}} + K_N = 0$$

and examining the migration of the roots as each of the "gains" is varied.

Setting the coupling term K_N to zero, the characteristic equation may be written as:

$$1 + \frac{K_{\mathcal{L}}}{\left(N^{\phi}_{\delta_{stk}}\right)_{uncoupled}} = 0$$

Figure 48 is a system survey plot showing the effect of varying positive $\mathcal{L}'_{\alpha}$ on the uncoupled numerator $N^{\phi}_{\delta_{stk}}$. The upper plot is a root locus and the lower plot a Bode-siggie (see Section II) showing the influence of increasing (negative) gain. These indicate that the complex zero associated with the longitudinal short period, ω^{ϕ}_{sp}, is driven to higher frequencies parallel to the $j\omega$-axis; and the conventional roll zeros, $1/T_{\phi_1}$ and $1/T_{\phi_2}$, are driven apart. The influence of $\mathcal{L}'_{\alpha}$ is found to be negligible in this case, but this is due to a very small value of the ratio $N'_{\delta_{stk}}/\mathcal{L}'_{\delta_{stk}}$ (at the flight condition being evaluated) which is a factor in the "gain" term.

The prime contributor to cross-coupling influence on the F-4J roll numerator is $K_N = M_{\beta}N'_{\alpha} \cos \alpha_0$ as shown in Figure 49, which is a survey for the equation

$$1 + \frac{K_N}{N^{\phi}_{\delta_{stk}}\Big|_{K_{\mathcal{L}}}} = 0$$

where primes have been used to denote that $K_{\mathcal{L}}$ has already been accounted for, and double primes indicate that both $K_{\mathcal{L}}$ and K_N have been accounted for. K_N produces a locus opposite in direction to that of $K_{\mathcal{L}}$, since both are pure gains but have opposite sign. The root location is much more sensitive to changes in K_N, as the relative Bode amplitudes in Figures 48 and 49 show.

The "gains" $K_{\mathcal{L}}$ and K_N are functions of $\mathcal{L}'_{\alpha}$, N'_{α}, M_{β}, $N'_{\delta_{stk}}$, and $\mathcal{L}'_{\delta_{stk}}$. While $\mathcal{L}'_{\alpha}$ and N'_{α} have been stressed in the foregoing, it should be obvious that the influence of changes in magnitude of any of these derivatives can be equally represented by Figures 48 and 49. Changes in sign of any of the derivatives would reverse the direction of root migration in either case.

The results shown here represent the usual derivative signs that prevail as AOA increases toward stall, i.e., $\mathcal{L}'_{\alpha}$ positive, N'_{α} negative, and M_{β} negative. However, M_{β} depends upon several configuration details and can be either positive or negative (Reference 30). For the above signs, uncoordinated ($\beta \neq 0$) flight results in reduced dutch roll

$$1 + \frac{K_{\mathcal{L}}}{\left(N^{\phi}_{\delta_{stk}}\right)_{uncoupled}} = 1 + \frac{-M_{\beta}\,\frac{N'_{\delta_{stk}}}{\mathcal{L}'_{\delta_{stk}}}\,\mathcal{L}'_{\alpha}\cos\alpha_o}{(-.586)(.943)[.386,.978]}$$

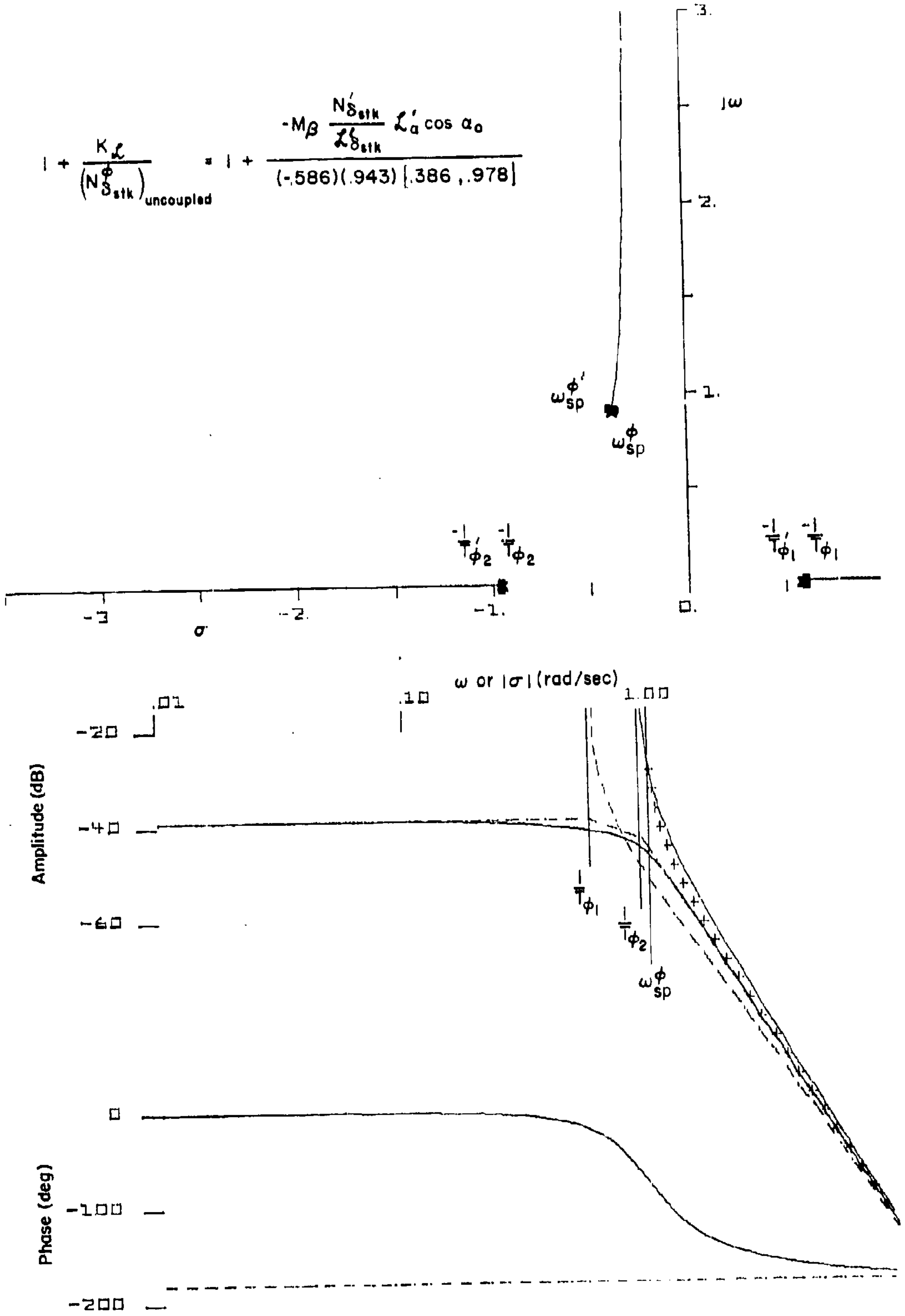

Figure 48. System Survey of Effect of $\mathcal{L}'_{\alpha}$ on $N^{\phi}_{\delta_{stk}}$; F-4J; $N'_{\alpha} = 0$, $\alpha_o = 21$ deg, $\beta_o = 5.5$ deg

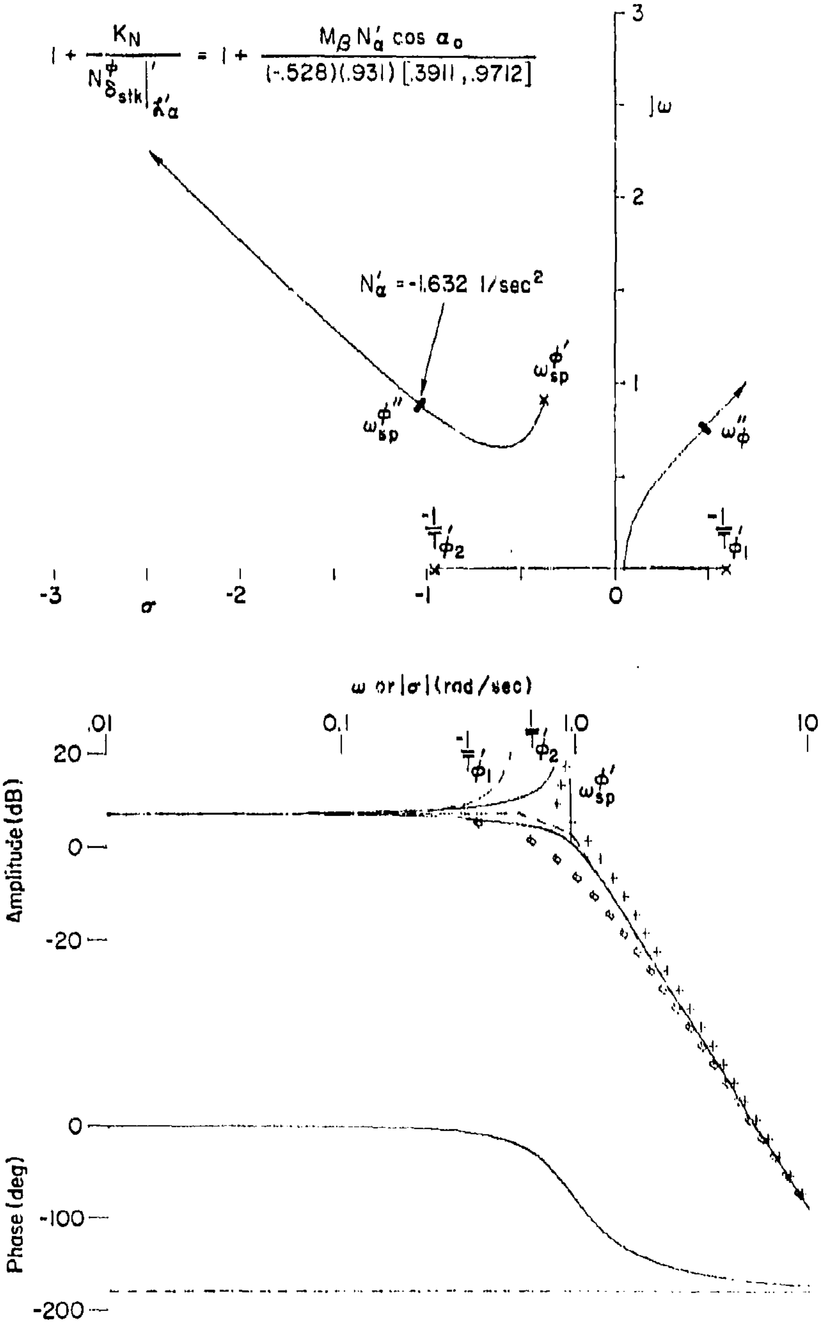

Figure 49. System Survey for Effect of N'_α on $N_{\delta_{stk}}$ (with $\mathcal{L}'_\alpha$ = 3.4251 1/sec^2), F-4J; α_o = 21 deg, β_o = 5.5 deg

stability (Figure 43 or 44) and a corresponding shift of the roll numerator zeros. These shifts portend increasing closed-loop roll control problems with sideslip (Figure 45).

The accuracy of the 5 DOF $N^{\phi}_{\delta_{stk}}$ approximation is evident from Table 4: the coupled, 6 DOF numerator has been matched almost identically. With this validation of the approximation, the following simple coupled approximate factors were developed for this flight condition (it must be stressed that these literal approximate factors apply to this aircraft and flight condition only,and may not be accurate for other situations). For the general form

$$N^{\phi}_{\delta_{stk}} = (s^2 + 2\zeta_{\phi}\omega_{\phi}s + \omega_{\phi}^2)(s^2 + 2\zeta^{\phi}_{sp}\omega^{\phi}_{sp}s + \omega^{\phi}_{sp})$$

$$2\zeta_{\phi}\omega_{\phi} \doteq -(N'_r + Y_v) - \sqrt{N'_{\alpha}M_{\beta}\cos\alpha_o}$$

$$\omega_{\phi}^2 \doteq N'_{\beta}\cos\alpha_o + \sqrt{N'_{\alpha}M_{\beta}\cos\alpha_o}$$

$$2\zeta^{\phi}_{sp}\omega^{\phi}_{sp} \doteq -(M_q + M_{\dot{\alpha}}) + \sqrt{N'_{\alpha}M_{\beta}\cos\alpha_o}$$

$$\omega^{\phi 2}_{sp} \doteq -M_{\alpha} + Z_w M_q + \sqrt{N'_{\alpha}M_{\beta}\cos\alpha_o}$$

Table 4 includes the values given by these approximate factors, indicating that they also are accurate and therefore encompass the key derivatives.

These literal factors clearly indicate that longitudinal-lateral cross-coupling in $N^{\phi}_{\delta_{stk}}$ is primarily through the product $N'_{\alpha}M_{\beta}$. If either derivative is zero, the cross-coupling terms disappear and the approximate factors become similar to the literal expressions for uncoupled lateral dutch roll and longitudinal short-period (Reference 20).

TABLE 4

$N^{\phi}_{\delta_{stk}}$ NUMERATOR APPROXIMATIONS

NUMERATOR	ζ_ϕ	ω_ϕ	ζ^{ϕ}_{sp}	ω^{ϕ}_{sp}
6 DOF coupled	-.531	.909	.778	1.361
5 DOF (approximate) coupled	-.533	.892	.766	1.370
Based on literal approximate factors	-.574	.940	.667	1.544

In addition, for non-zero N'_α and M_β the aircraft coupling is sensitive to sideslip since

$$N'_\alpha = \beta_o \frac{\partial^2 N'}{\partial\beta\partial\alpha} = \beta_o \frac{\bar{q}Sb}{I_z} C'_{n_{\beta\alpha}}$$

so that Figure 49 may be viewed as a locus of root migration with sideslip for constant $C_{n_{\beta\alpha}}$.

From the standpoint of vehicle design, any airframe changes which modify either of these cross-coupling derivatives can be expected to have a significant influence on high AOA flying qualities and departure characteristics.

C. $N^{\theta}_{\delta_{stab}}$ NUMERATOR

Analysis of the influence of aerodynamic cross-coupling on the numerator for longitudinal control, $N^{\theta}_{\delta_{stab}}$, uses an approach identical to that taken with $N^{\phi}_{\delta_{stk}}$. The first step is to make the development tractable by eliminating insignificant terms in the nine-by-nine matrix.

It was shown in Subsection II.A.3.b (Figure 19) that constraining velocity does little to change the zeros influenced by cross-coupling, i.e., $1/T_{\theta_3}$, $1/T^{\theta}_{R}$, and ω^{θ}_{d}. Additionally, we find from Figure 50 that the equations for the Euler angles ψ and θ can again be eliminated. This

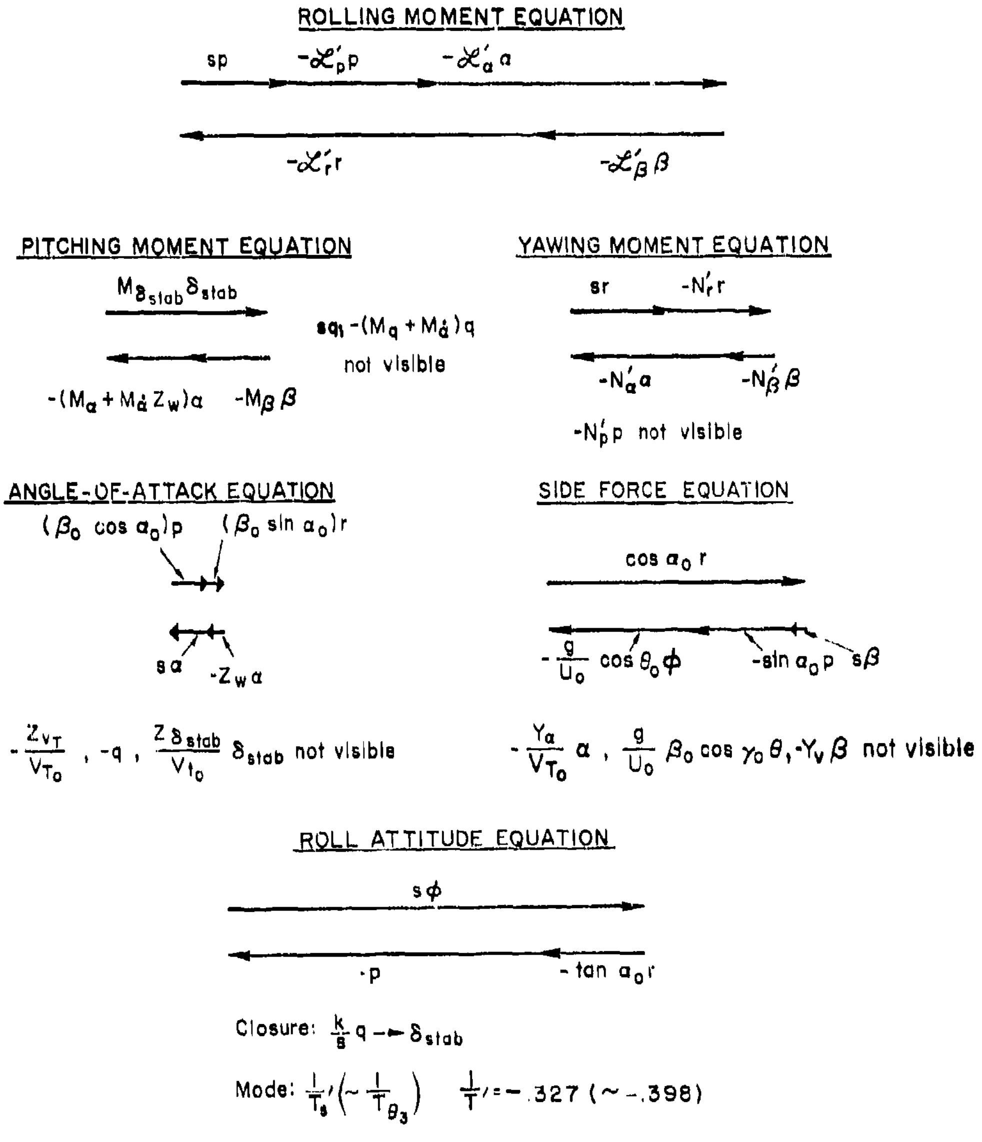

Figure 50. Time Vectors for Closed-Loop Mode $1/T_s'$ (Approximating $1/T_{\theta_3}$), F-4J; α = 21 deg, β = 5.5 deg

still leaves a six-by-six matrix which is too large and complex to work with comfortably.

Applications of time vectors, as was done with $N^{\phi}_{\delta_{stk}}$, is accomplished by closing a pitch rate loop with a feedback element of K/s (to obtain body-axis θ). Modal response coefficients are then calculated for the closed-loop pole driven into $1/T_{\theta_3}$, and the time vectors for each equation constructed as shown in Figure 50. Except for the α equation, few terms are small enough to be eliminated by inspection. Further, it seems unwise to restrict the general applicability of the results by eliminating the α equation. The main benefit of the time vectors is to demonstrate that the modal response for a root at $1/T_{\theta_3}$ contains considerably more lateral than longitudinal motion.

Thus, it is necessary to expand the complete six-by-six matrix of Figure 51 in literal form, evaluate each of the terms, and eliminate products of small numbers. The resulting polynomial is then separated into uncoupled and coupled terms to form the approximation:

$$\begin{aligned} N^{\theta}_{\delta_{stab}} \cong M_{\delta_{stab}} \Big[(s - Z_w) \Big\{ & s^4 - (\mathcal{L}'_p + N'_r + Y_v)s^3 + \big|\mathcal{L}'_p(N'_r + Y_v) + N'_r Y_v + N'_{\beta_{dyn}}\big| s^2 \\ & - \Big|\mathcal{L}'_p N'_\beta \cos\alpha_o + \mathcal{L}'_p N'_r Y_v + \frac{g}{V_{T_o}} \mathcal{L}'_{\beta_{dyn}} + (\mathcal{L}'_r N'_\beta - \mathcal{L}'_\beta N'_r) \sin\alpha_o\Big| s \\ & + \frac{g}{V_{T_o}} \Big|(\mathcal{L}'_\beta N'_r - N'_\beta \mathcal{L}'_r)\cos\alpha_o + \mathcal{L}'_p N'_\beta \sin\alpha_o\Big| \Big\} + \mathcal{L}'_\alpha Z'_p s \Big[s^2 - (N'_r + Y_v)s + \frac{N'_\beta}{\cos\alpha_o}\Big] \\ & + N'_\alpha Z_r s \Big[s^2 + \Big(\frac{\mathcal{L}'_r}{\tan\alpha_o} - Y_v - \mathcal{L}'_p\Big)s - \frac{\mathcal{L}'_\beta}{\sin\alpha_o} + Y_v\Big(\mathcal{L}'_p - \frac{\mathcal{L}'_r}{\tan\alpha_o}\Big)\Big]\Big] \end{aligned}$$

where in the "dynamic axis" system of Reference 18,

$$N'_{\beta_{dyn}} \equiv N'_\beta \cos\alpha_o - \mathcal{L}'_\beta \sin\alpha_o$$

$$\mathcal{L}'_{\beta_{dyn}} \equiv \mathcal{L}'_\beta \cos\alpha_o + N'_\beta \sin\alpha_o$$

$$\left[\begin{array}{c|c|c|c|c|c}
M_{\delta_{stab}} & -M_\alpha + M_{\dot{\alpha}} Z_w & & & -M_\beta & \\
\hline
\frac{M_{\delta_{stab}}}{V_{T_o}} & -Z_w & \beta_o \cos \alpha_o & \beta_o \sin \alpha_o & & \\
\hline
 & -\mathcal{L}'_\alpha & s - \mathcal{L}'_p & -\mathcal{L}'_r & -\mathcal{L}'_\beta & \\
\hline
 & -N'_\alpha & & s - N'_r & -N'_\beta & \\
\hline
 & & -\sin \alpha_o & \cos \alpha_o & s - Y_v & -\frac{g}{V_{T_o}} \cos \alpha_o \\
\hline
 & & -1 & -\tan \alpha_o & & s
\end{array}\right]
\left[\begin{array}{c}
q \\ \hline \alpha \\ \hline p \\ \hline r \\ \hline \beta \\ \hline \phi
\end{array}\right]$$

Figure 51. Matrix for Approximation of Coupled $N^{\theta}_{\delta_{stab}}$
($\phi_o = \gamma_o = 0$, $\theta = \alpha$, β_o Small)

The terms not containing cross-coupling derivatives are seen to separate into a first-order and quartic function of s. The first-order is the conventional literal approximation for the longitudinal zero $1/T_{\theta_2}$, i.e., $-Z_w$. The quartic contains all lateral-directional derivatives and, with the exception of the sin α_o terms, is the same as the conventional body-axis uncoupled lateral characteristic equation (Reference 20). This polynomial thus factors into the parameters ω_d, $1/T_R$, and $1/T_s$.

The first cross-coupling term involves $\mathcal{L}'_\alpha$ as the "gain," a free s, and a quadratic containing only yawing derivatives. The second cross-coupling expression has N'_α as a "gain," a free s, and a quadratic containing only rolling derivatives.

The kinematic terms Z_p and Z_r were negligible for $N^{\phi}_{\delta_{stk}}$, but here dictate the influence of the aerodynamic cross-coupling. As a result, coupling in the $\theta \rightarrow \delta_{stab}$ numerator is an explicit function of sideslip. It is interesting to note that M_β does not appear in the approximation; a quadratic coupling term involving $M_\beta Z_{\delta_{stab}}/V_{T_o}$ was found to be negligible.

The influence of the individual cross-coupling terms can again be observed by servo analysis methods, setting

$$(N^{\theta}_{\delta_{stab}})_{coupled} = (N^{\theta}_{\delta_{stab}})_{uncoupled} + (N^{\theta}_{\delta_{stab}})_{\mathcal{L}'_{\alpha}} + (N^{\theta}_{\delta_{stab}})_{N'_{\alpha}} = 0$$

and performing system surveys. The survey for

$$1 + \frac{(N^{\theta}_{\delta_{stab}})_{\mathcal{L}'_{\alpha}}}{(N^{\theta}_{\delta_{stab}})_{uncoupled}} = 0$$

is shown in Figure 52. The "poles" $1/T^{\theta}_{s}$ and $1/T_{\theta_2}$ couple to create a second-order closed-loop root, ω'_{θ_s}, which is on the $j\omega$-axis. The dutch roll "pole" is moved to the left half-plane, while $1/T^{\theta}_{R}$ is moved slightly to the left.

Figure 53 shows the additional movement when the cross-coupling due to N'_{α} is included. The latter moves things further in the same direction. However, it can be determined that the first-order coupled zero in the left half-plane comes from the roll subsidence mode and the zero farthest into the right half-plane (previously called $1/T_{\theta_3}$) comes from a coupling of the spiral mode and the conventionale $1/T_{\theta_2}$. Since the time vectors indicated this mode is dominated by lateral-directional motion it is now labeled $(1/T^{\theta}_{s})''$. The prime notation in Figures 52 and 53 is used to keep track of the number of "loops" being closed and the influence of each "closure." From here on the prime notation will be dropped and the lateral-longitudinal coupled zeros identified as ω^{θ}_{d}, $1/T^{\theta}_{R}$, $1/T^{\theta}_{s}$, etc.

Since each of the cross-coupling terms has similar influence on the migration of zeros, no insight is lost by combining the two coupling terms via the concept of the previously noted "dynamic" term $\mathcal{L}'_{\alpha_{dyn}}$. Then

$$1+\frac{\left(N^{\theta}_{\delta_{stab}}\right)_{\mathcal{L}'_{\alpha}}}{\left(N^{\theta}_{\delta_{stab}}\right)_{uncoupled}} = 1+\frac{\mathcal{L}'_{\alpha} Z_p(0)(-.664)(.963)}{(.131)(.375)(.764)[-.107,.762]}$$

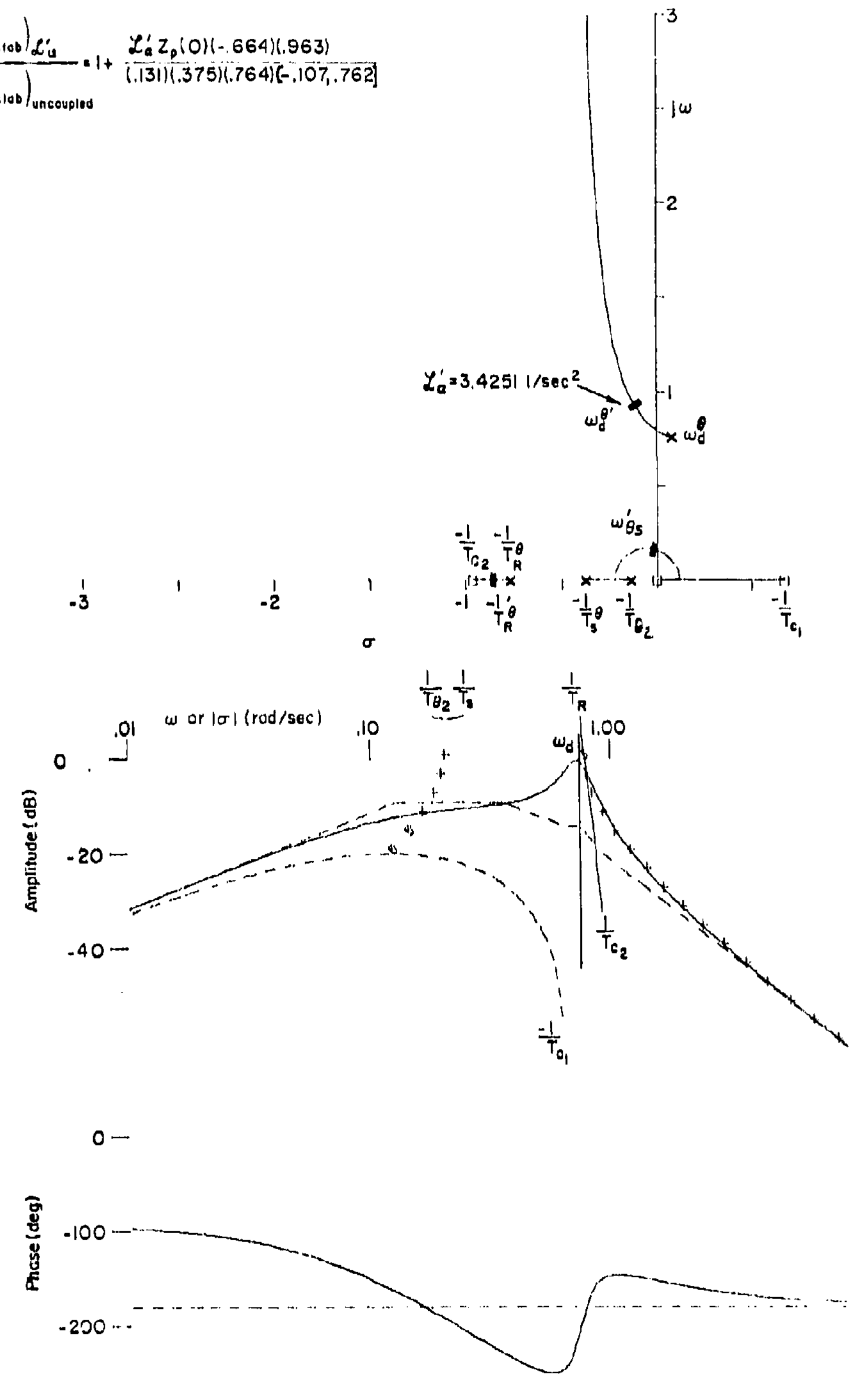

Figure 52. System Survey for Effect of $\mathcal{L}'_\alpha$ on $N^{\theta}_{\delta_{stab}}$; $N'_{\dot{\alpha}}$ = 0; α = 21 deg, β = 5.5 deg

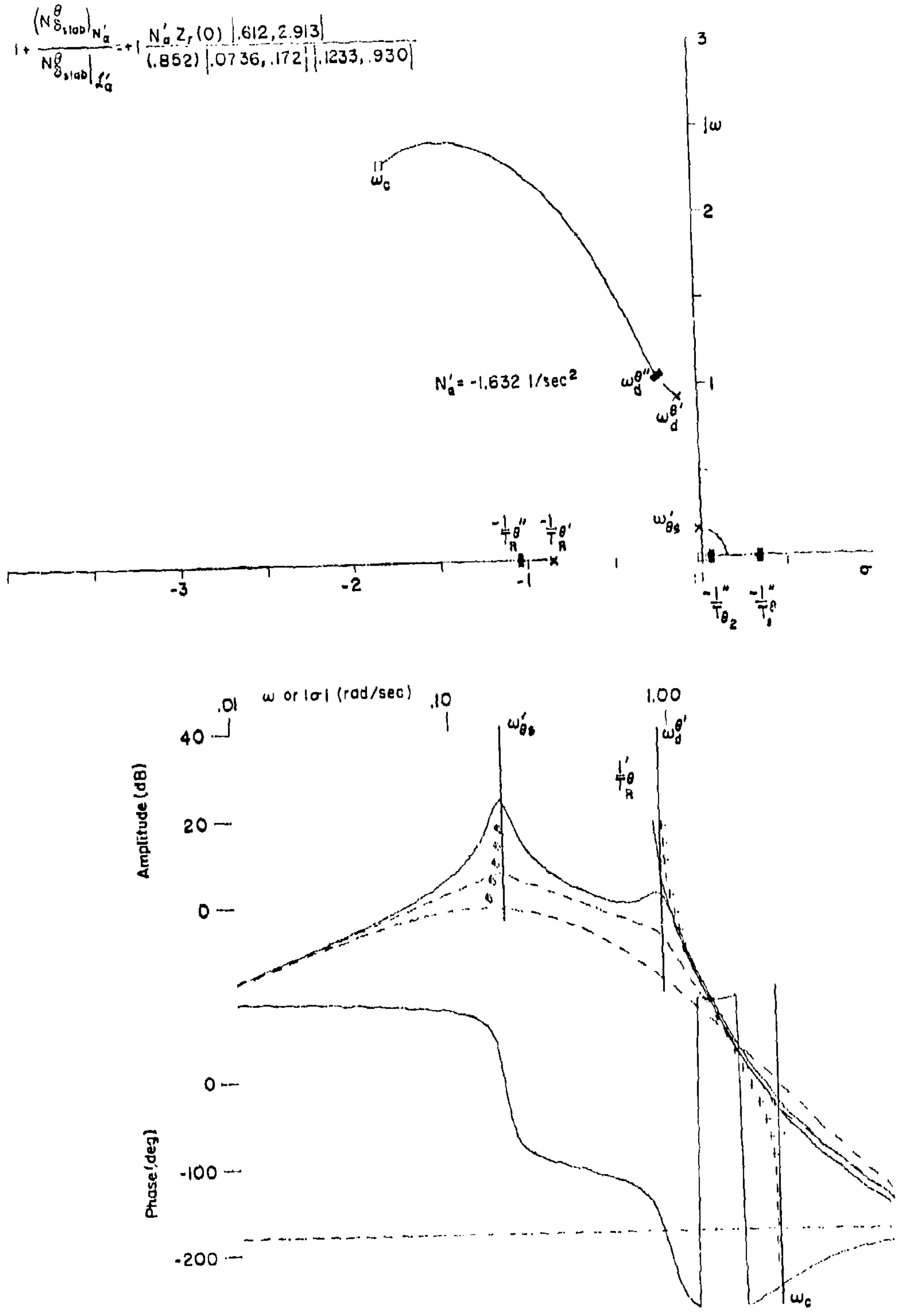

Figure 53. System Survey for Effect of N'_α on $N^{\theta}_{\delta_{stab}}$; $\mathcal{L}'_\alpha$ = 3.4251 1/sec²; F-4J; α = 21 deg, β = 5.5 deg

$$
\begin{aligned}
\left(N^{\theta}_{\delta_{stab}}\right)_{coupled} &= \left(N^{\theta}_{\delta_{stab}}\right)_{\mathcal{L}'_{\alpha}} + \left(N^{\theta}_{\delta_{stab}}\right)_{N'_{\alpha}} \\
&= \mathcal{L}'_{\alpha_{dyn}}\beta_o s \left[s^2 + \frac{1}{\mathcal{L}'_{\alpha_{dyn}}} \left\{ -\mathcal{L}'_{\alpha}(N'_r + Y_v)\cos\alpha_o \right.\right. \\
&\quad \left. + N'_{\alpha}\left[\mathcal{L}'_r \cos\alpha_o - (\mathcal{L}'_p + Y_v)\sin\alpha_o\right]\right\} s \\
&\quad \left. + \frac{1}{\mathcal{L}'_{\alpha_{dyn}}}\left[\mathcal{L}'_{\alpha}N'_{\beta} - N'_{\alpha}\mathcal{L}'_{\beta} - Y_v(\mathcal{L}'_r\cos\alpha_o - \mathcal{L}'_p \sin\alpha_o)\right]\right]
\end{aligned}
$$

The system survey for the combined coupling influence on $N^{\theta}_{\delta_{stab}}$ is shown in Figure 54; the coupled roots, of course, are the same.

Finally, it should be noted that aerodynamic cross-coupling in the numerator $N^{\theta}_{\delta_{stab}}$ is a direct function of sideslip squared. Since $\mathcal{L}'_{\alpha}$ is proportional to $C'_{\ell_{\beta_{\alpha}}}(\beta_o)$ and N'_{α} is proportional to $C'_{n_{\beta_{\alpha}}}(\beta_o)$, the "gain" term is

$$
\begin{aligned}
\mathcal{L}'_{\alpha_{dyn}}\beta_o &\sim \left(C'_{\ell_{\beta_{\alpha}}}\beta_o \cos\alpha_o + C'_{n_{\beta_{\alpha}}}\beta_o \sin\alpha_o\right)\beta \\
&\sim \left(C'_{\ell_{\beta_{\alpha}}} \cos\alpha_o + C'_{n_{\beta_{\alpha}}} \sin\alpha_o\right)\beta_o^2
\end{aligned}
$$

Thus the zero $1/T^{\theta}_{s}$ is drastically influenced by static aerodynamic cross-coupling and magnitude of sideslip.

D. SUMMARY

Literal analytic expressions have been developed to show the influence of static aerodynamic cross-coupling derivatives and asymmetric flight on denominator and numerator roots. The analysis has shown that the shift in denominator roots depends upon all three static cross-coupling derivatives, $\mathcal{L}'_{\alpha}$, N'_{α}, and M_{β}. The direction of root migration is controlled by the sign and magnitude of $M_{\beta}N'_{\alpha}/\mathcal{L}'_{\alpha}$. The magnitude of root migration is determined by $\mathcal{L}'_{\alpha}\beta_o$.

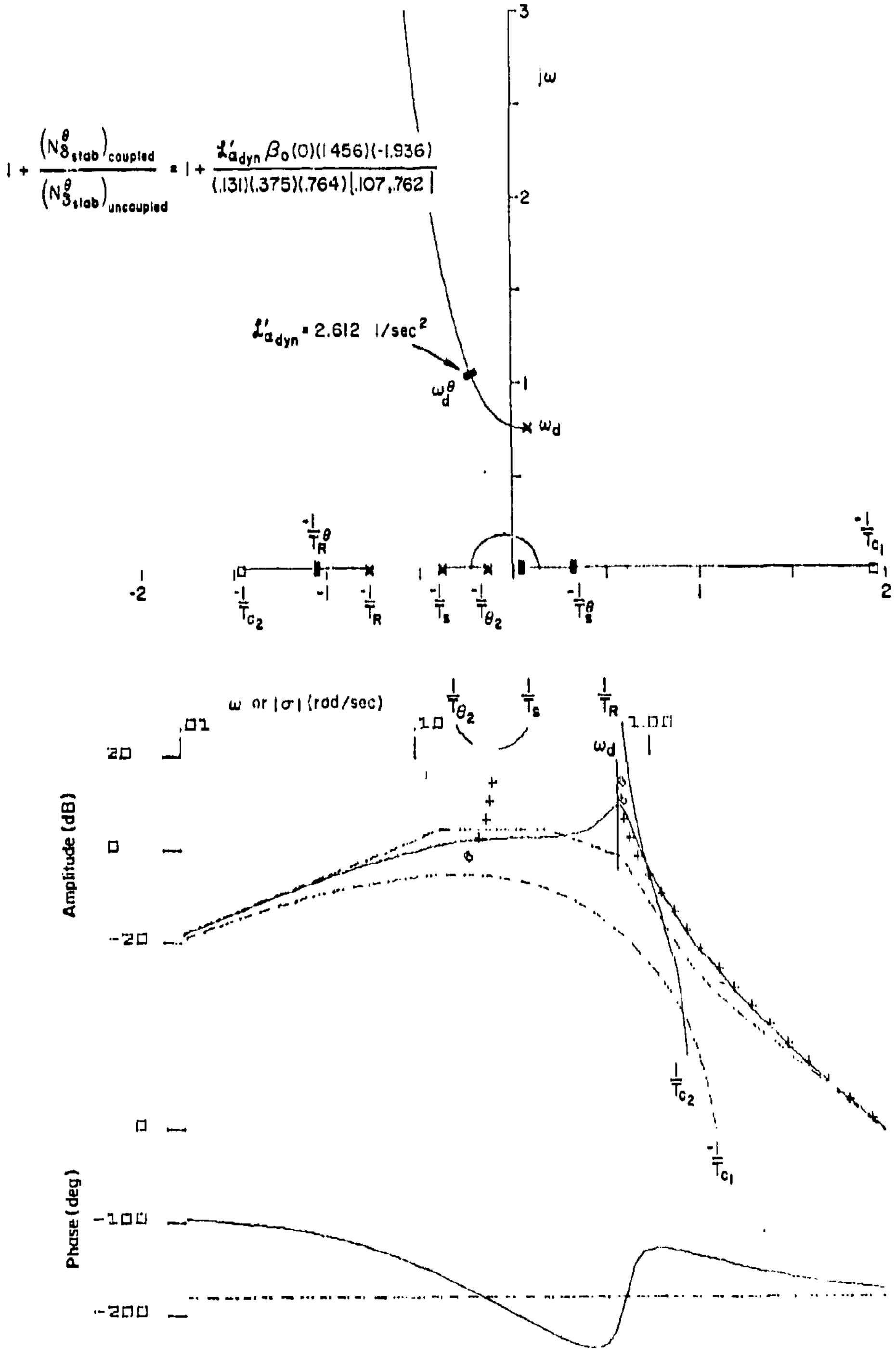

Figure 54. System Survey for Effect of Combined Cross-Coupling on $N^{\theta}_{\delta_{stab}}$; F-4J; α_o = 21 deg, β_o = 5.5 deg

For the F-4J the principal cross-coupling influence on the roll numerator, $N^{\phi}_{\delta_{stk}}$, is due to the term $N'_{\alpha} M_{\beta} \cos \alpha_0$. The literal approximate factors which describe the coupled numerator roots are

$$2\zeta_{\phi}\omega_{\phi} \doteq -(N'_r + Y_v) - \sqrt{N'_{\alpha} M_{\beta} \cos \alpha_0}$$

$$\omega^2_{\phi} \doteq N'_{\beta} \cos \alpha_0 + \sqrt{N'_{\alpha} M_{\beta} \cos \alpha_0}$$

$$2\zeta^{\phi}_{sp}\omega^{\phi}_{sp} \doteq -(M_q + M_{\dot{\alpha}}) + \sqrt{N'_{\alpha} M_{\beta} \cos \alpha_0}$$

$$\omega^{\phi 2}_{sp} \doteq -M_{\alpha} + Z_w M_q + \sqrt{N'_{\alpha} M_{\beta} \cos \alpha_0}$$

The pitch numerator, $N^{\theta}_{\delta_{stab}}$, is influenced by a more complicated combination of kinematic and aerodynamic terms. Existence of a first-order RHP zero depends upon

$$\frac{\mathcal{L}'_{\alpha} N'_{\beta} - \mathcal{L}'_{\beta} N'_{\alpha} - Y_v(\mathcal{L}'_r \cos \alpha_0 - \mathcal{L}'_p \sin \alpha_0)}{\mathcal{L}'_{\alpha} \cos \alpha_0 + N'_{\alpha} \sin \alpha_0} < 0$$

The above approximations may not apply to configurations significantly different from the F-4J.

SECTION IV

CONFIGURATIONS SELECTED FOR SIMULATION

The seven aerodynamic derivatives which have been shown to dominate open- and closed-loop dynamic characteristics at high AOA are summarized in Table 5. These are comprised of six static stability and cross-coupling derivatives and one dynamic damping derivative. Together they limit the useful flight envelope via roll reversal and wing rock tendencies, and they limit the safe flight envelope via departure susceptibility. One goal of the piloted simulation was to demonstrate this premise.

TABLE 5

KEY MANEUVER-LIMITING PARAMETERS

Negative N'_{δ_a} or N'_{δ_D}	Roll reversal
Positive M_β	Pitch up
$\mathcal{L}'_\beta$, $\mathcal{L}'_\alpha$, $\mathcal{L}'_p$ N'_β, N'_α M_β	Wing rock Nose slice Roll divergence

This section presents the vehicle aerodynamic configurations selected for the piloted simulation and the predicted high AOA dynamic characteristics.

Four "configurations" were obtained by altering the key aerodynamic coefficients of a baseline. The three altered configurations incorporated changes in, respectively, $C_{\ell_p}(\alpha)$, $C_\ell(\alpha,\beta)$, and $C_n(\alpha,\beta)$ combined with a change in C_{m_β}, to provide specific alteration of key open- and closed-loop parameters discussed in the preceding two sections. The attempt was to influence the denominator only, the numerator only, and the combined denominator and numerator, thereby to provide distinct variations in high AOA departure susceptibility, onset warning, and motion severity. The influence of artificially altering aerodynamic coefficients via a lateral-directional augmentation system was also investigated with two of the configurations.

A. AERODYNAMIC CONFIGURATIONS

1. Configuration A

The baseline case is identified as Configuration A. This F-4J-based configuration has been thoroughly reviewed in the preceding sections. The key open- and closed-loop dynamic parameters are summarized in Figure 55 for comparison with the other configurations discussed subsequently. Dutch roll and numerator root migrations are shown for increasing α at zero β (solid lines) and at 5.5 deg β (dashed lines). The solid triangle (▲) indicates the AOA above which $C_{n_{\beta_{dyn}}}$ becomes negative at zero β. Recalling the discussion in Section II about the shortcomings of linearized frozen point analysis, the important aspects to note here are:

- The low dutch roll damping at AOA below $C_{n_{\beta_{dyn}}} = 0$ (wing rock).
- ω_ϕ^2 or $1/T_{\phi_1}$ negative at AOA above 18 deg or at small β (roll reversal).
- $1/T_{\phi_1}$ and $1/T_s^0$ both large and negative when $\beta \neq 0$ (nose slice parameters).
- Dutch roll and roll numerator roots sensitive to sideslip.

The plots in the lower left corner indicate the magnitude of the aerodynamic coupling terms evaluated at 5.5 deg β. In the AOA range from 20 to 30 deg, $\mathcal{L}'_\alpha$ is of approximately the same magnitude as $\mathcal{L}'_\beta$ but is of opposite sign. In this same AOA range, N'_α is of about the same magnitude as N'_β and of the same sign. For this relatively mild sideslip condition (5.5 deg), the static cross-coupling derivatives are of equal magnitude to the basic static derivatives.

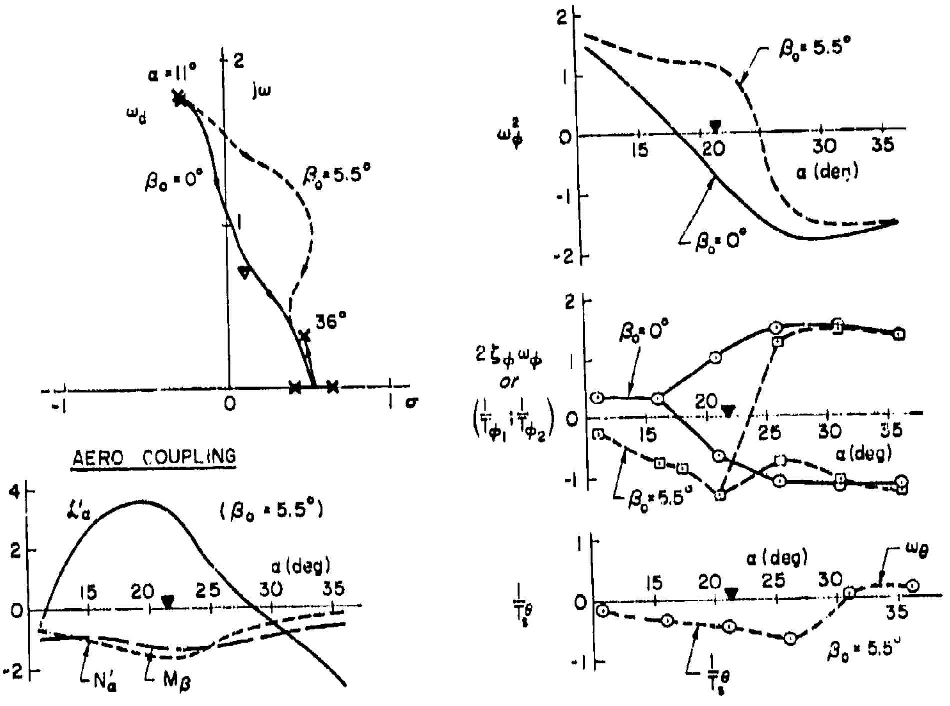

Figure 55. Key Parameters for Configuration A

2. Configuration B

For Configuration B the roll rate damping coefficient, C_{ℓ_p}, was made large, negative and essentially invariant over the range $10 < \alpha < 35$ deg (see $C_{\ell_{p2}}$, Figure 56). The object of this change is to increase the dutch roll damping and hence reduce the wing rock tendency. Since all other parameters remain unchanged, this should not alter the basic roll reversal tendency or the nose slice departure characteristics; but it should eliminate or reduce wing rock as a warning of impending departure. However, note again in Figure 57 the sensitivity of the dutch roll mode to sideslip. At $\beta = 5.5$ deg there is little difference between Configurations A (Figure 55) and B (Figure 57), which indicates that the influence of $\mathcal{L}'_p$ is small with respect to that of $\mathcal{L}'_\alpha$.

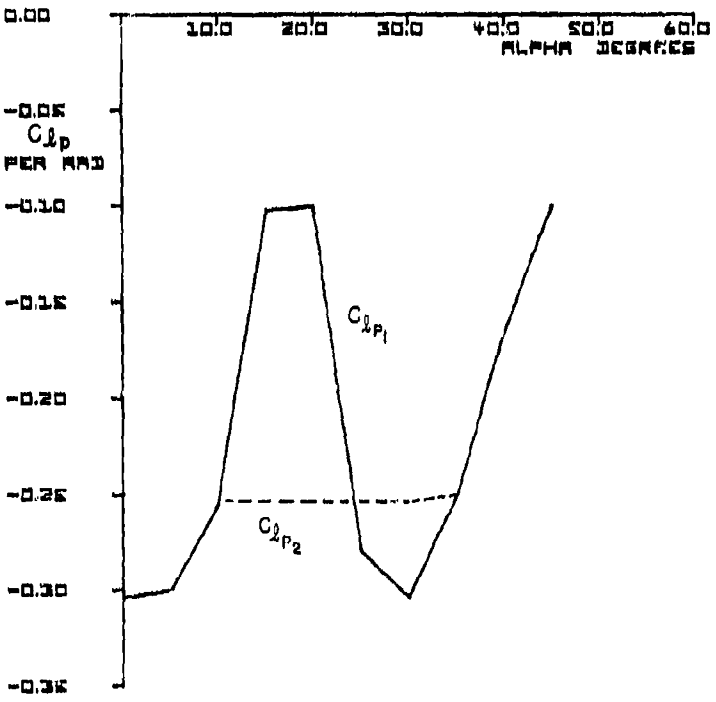

Figure 56. Change in C_{ℓ_p} for Configuration B

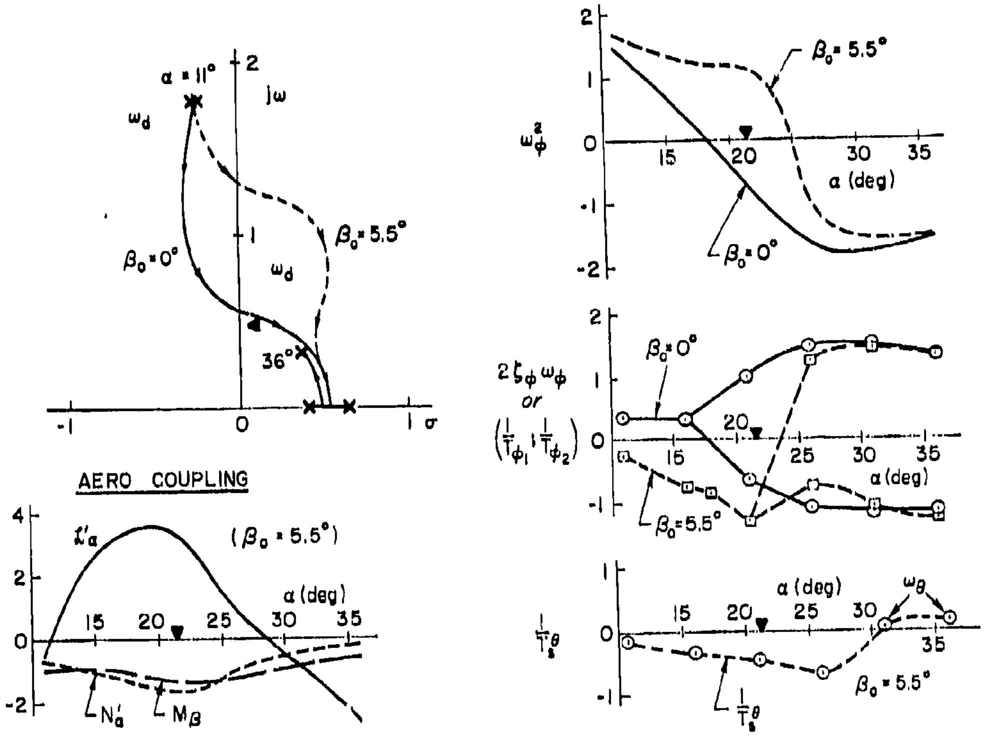

Figure 57. Key Parameters for Configuration B

3. **Configuration** C

For Configuration C the roll due to sideslip coefficient, C_{ℓ_β}, was altered (see Figure 58) to approximate that of the F-14A over the range $15 < \alpha < 45$ deg, taking into account the difference in roll inertias of the two aircraft, i.e.,

$$C_{\ell_{\beta_2}} \triangleq C_{\ell_{\beta_{F-14}}} \frac{I_{x_{F-4}}}{I_{x_{F-14}}}$$

Figure 59 presents the parameter plots for Configuration C. The upper left figure shows that the change introduced in C_{ℓ_β} and C_{ℓ_α} has shifted the dutch roll mode toward the left. It remains in the left half-plane for $\beta = 0$ and only bulges into the right half-plane over a small α range at $\beta = 5.5$ deg. A major difference in this configuration occurs in the roll subsidence and spiral modes, which in the previous

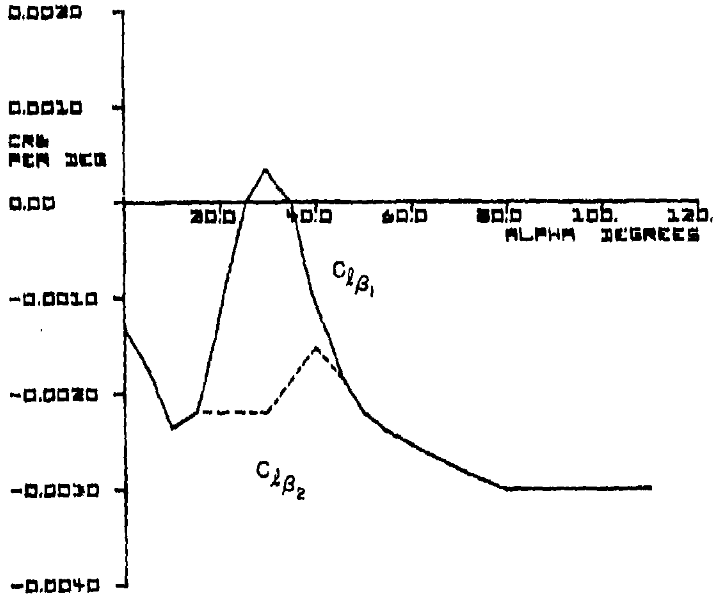

Figure 58. Change in C_{ℓ_β} for Configuration C

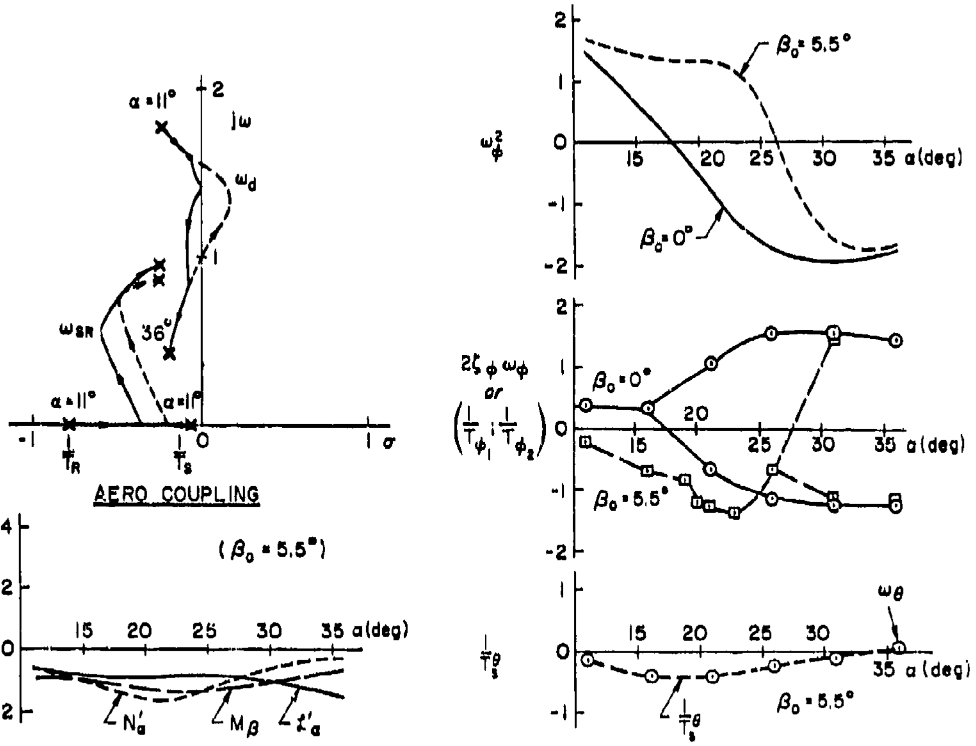

Figure 59. Key Parameters for Configuration C

cases have remained on the real axis and therefore have not been shown. In this case, $1/T_R$ and $1/T_s$ couple to form a "lateral phugoid" mode, ω_{SR}, as AOA increases. At 36 deg AOA the frequency of this mode is approximately twice that of the dutch roll, with approximately the same damping. Comparison of Figures 35, 39, and 59 show this to be a valid representation of F-14A root locations, but mode identity may be different.

Comparison indicates that increasing β shifts the ω_{SR} locus toward the right half-plane. However, both the dutch roll and lateral phugoid modes are now relatively unaffected by β.

The upper right-hand plot for ω_ϕ^2 is essentially the same for Configuration C as that for Configurations A and B. While this configuration has better open-loop stability, the closed-loop characteristics should be little different from the previous two configurations because the roll numerator roots are essentially unchanged.

Absence of the solid triangle symbol indicates that $C_{n_{\beta_{dyn}}}$ is positive throughout the AOA range.

The lower left-hand figure shows that the $\mathcal{L}'_{\alpha}$ term (which derives from the variation of C_{ℓ_β} with α) is small and negative. Since this configuration also has a large increase in $\mathcal{L}'_{\beta}$ (see Figure 58), the aerodynamic cross-coupling derivative $\mathcal{L}'_{\alpha}$ is now much smaller than $\mathcal{L}'_{\beta}$ throughout the angle-of-attack range. Comparing the values of $\mathcal{L}'_{\alpha}$ for Configurations A and C with the differences in denominator root migrations with β makes it apparent that $\mathcal{L}'_{\alpha}$ is the dominant parameter in shifting the Configuration A dutch roll mode into the right half-plane when $\beta \neq 0$. The lower right-hand plot of Figure 59 indicates that the change in $\mathcal{L}'_{\alpha}$ and $\mathcal{L}'_{\beta}$ has decreased $1/T_s^{\theta}$ at AOA above 20 deg.

4. Configuration D

For the fourth case the yaw due to sideslip coefficient, C_{n_β}, was modified to approximate that of the F-14 as shown by the dashed line in Figure 60. In addition, for this case only, the sign of C_{m_β} was reversed to provide positive pitch with sideslip. As predicted by the approximate factors of Section III, the result is an airframe quite insensitive to sideslip (Figure 61) and, most pertinently, having numerator roots ($1/T_{\phi_1}$ and $1/T_s^\theta$) which do not penetrate as far into the right half-plane.

Roll reversal is delayed until $\alpha > 20$ deg and $C_{n_{\beta_{dyn}}}$ remains positive until $\alpha \doteq 25$ deg.

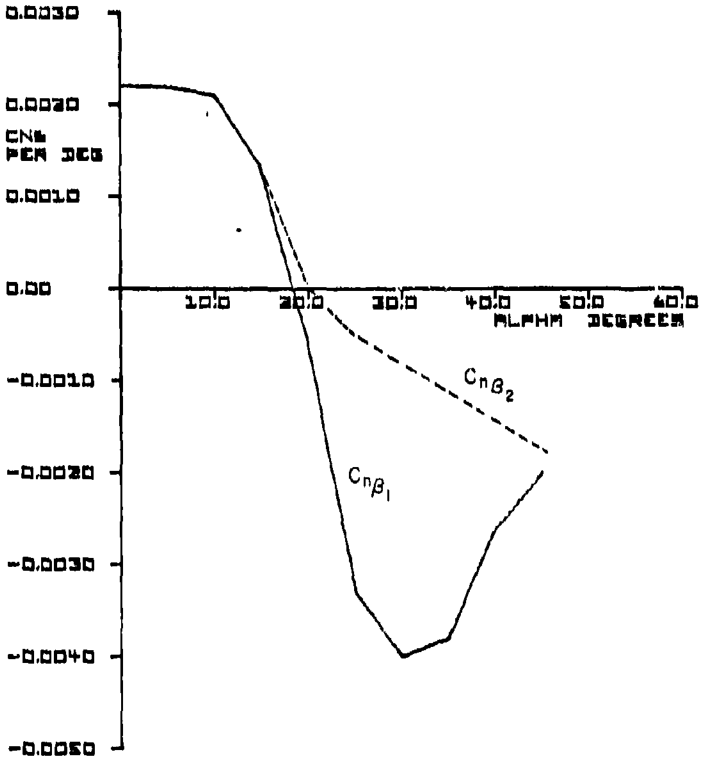

Figure 60. Change in C_{n_β} for Configuration D

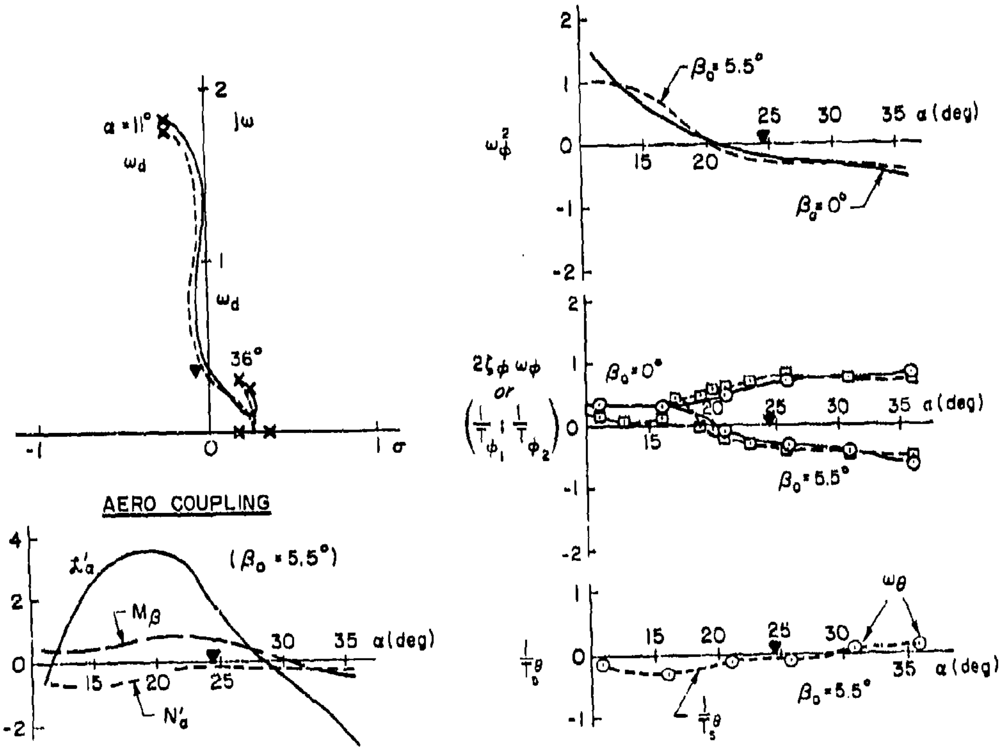

Figure 61. Key Parameters for Configuration D

5. Anticipated High AOA Maneuver-Limiting Characteristics

Review of the preceding four configurations should go a long way toward sorting out the relative importance of denominator (open-loop) vs. numerator (closed-loop) characteristics on high AOA departure susceptibility and severity. Configurations A, B, and C have nearly identical RHP numerator root locations and therefore should have similar closed-loop divergence tendencies, although the motion (i.e., roll vs. yaw) may differ somewhat due to C_{ℓ_p}, C_{ℓ_β}, and C_{ℓ_α} changes. On the other hand, the Configuration D numerator roots do not penetrate so far into the RHP and are relatively insensitive to sideslip. Thus one might expect this vehicle to appear less susceptible to or have less severe departure.

Alternately, if departure susceptibility or tendency should turn out to be strongly influenced by dutch roll (open-loop) root location, then one would expect Configurations C and D to be similar since both are near neutral stability and relatively insensitive to sideslip. Any differences between Configurations A and B would be dependent upon sideslip.

The dynamic stability parameter, $C_{n_{\beta_{dyn}}}$, has been referred to previously. The AOA at which this parameter becomes negative was identified in Figures 55, 57, and 61. Figure 62 presents plots of $C_{n_{\beta_{dyn}}}$ vs. α for the four configurations. Based upon the criterion of $C_{n_{\beta_{dyn}}} > 0.002$ for departure resistance (Reference 31), then only Configuration C should be resistant, Configurations A and B should be quite departure prone, and Configuration D might be mildly departure prone.

Another criterion, Reference 32, employs both open- and closed-loop parameters, i.e.,

$$\frac{\text{LCDP}}{C_{n_{\beta_{dyn}}}} = \frac{C_{n_\beta}\left[1 - \left(C_{n_{\delta_a}} C_{\ell_\beta} / C_{\ell_{\delta_a}} C_{n_\beta}\right)\right]}{C_{n_\beta} \cos\alpha - (I_z/I_x) C_{\ell_\beta} \sin\alpha} \sim \frac{\omega_\phi^2}{\omega_d^2}$$

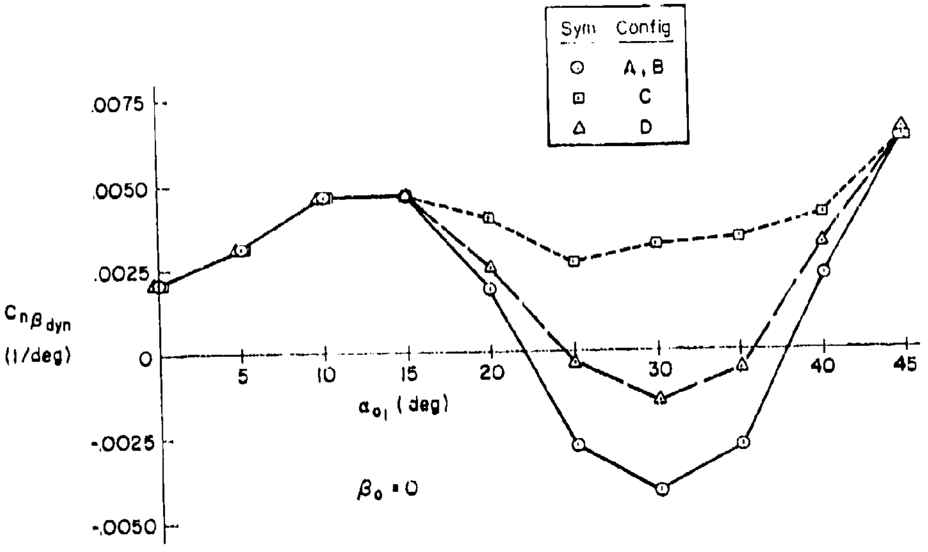

Figure 62. $C_{n_{\beta_{dyn}}}$ for Configurations Simulated

For a number of years it has been recognized (Reference 33) that undesirable $(\omega_\phi^2/\omega_d^2)$ ratios lead to roll reversal and pilot-aggravated wing rock (PIO). However, in Reference 32 Weissman plots $C_{n_{\beta_{dyn}}}$ vs. LCDP and identifies four regions of increasing departure and spin susceptibility and severity (Figure 63) based upon experience with a number of airframe configurations. The loci of our unaugmented airframe parameter values over the range of $16 < \alpha < 35$ deg are shown in Figure 63; circles represent Configurations A and B (since C_{ℓ_p} has no influence on either parameter), squares represent Configuration C, and triangles Configuration D. The criteria predict high departure/spin susceptibility with strong rolling departures for Configurations A and B, low spin susceptibility and mild rolling departures for Configuration C, and no departures for Configuration D. Thus, all regions of departure susceptiblity and severity are exercised with the aerodynamics selected.

The Figure 63 prediction that Configuration D should be less susceptible to departure is in agreement with the first assessment above based on numerator root locations.

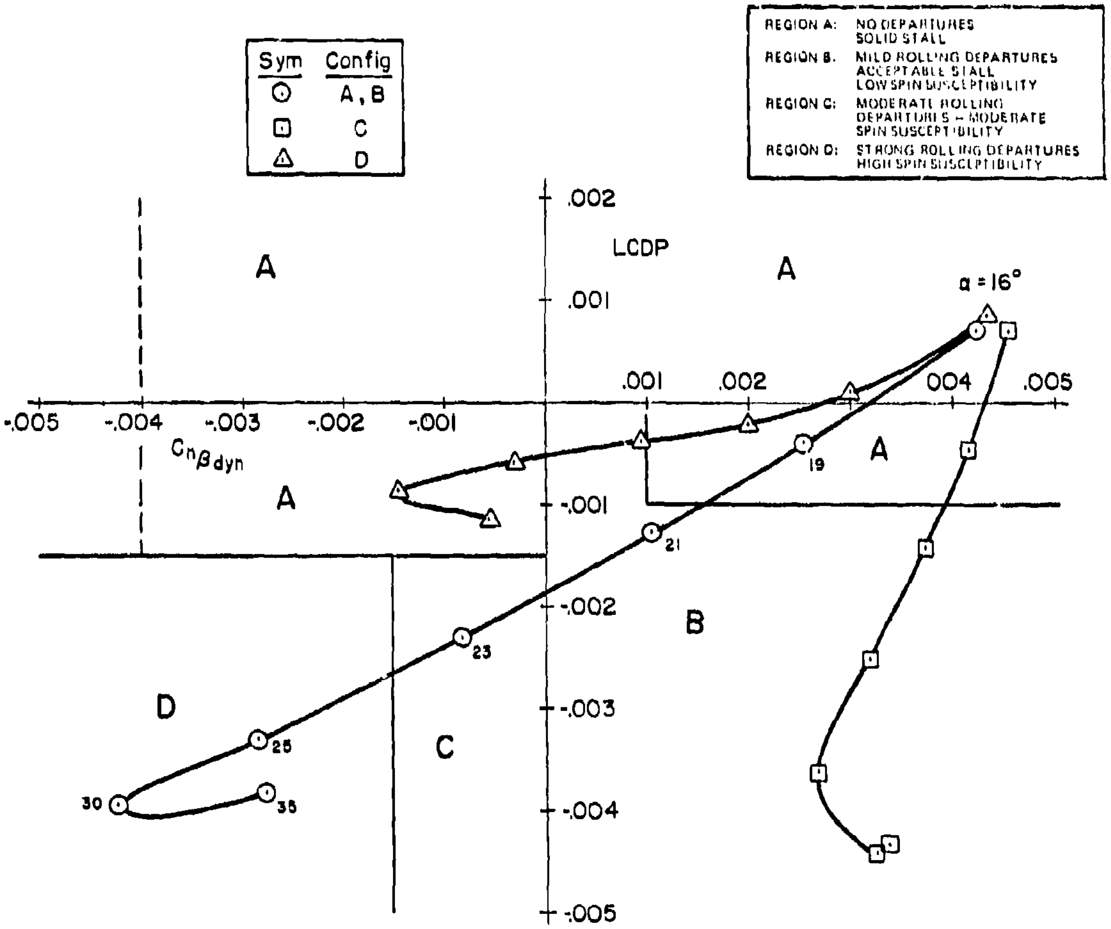

Figure 63. Weissman Criterion Predictions for the Simulation Configurations

B. AUGMENTED CONFIGURATIONS

Lateral-directional augmentation was synthesized for Configuration A (the most departure prone) and for Configuration C ($C_{n_{\beta_{dyn}}}$ always positive). The augmented configurations are identified as A_2 and C_2, respectively, while the unaugmented configurations will be referred to as A_1 and C_1. The augmentation mechanization is representative of that used in current high-performance fighters to improve both open- and closed-loop handling parameters, i.e., washed-out yaw rate and lateral acceleration feedbacks to rudder to increase dutch roll damping; roll rate feedback to differential stabilator to reduce or eliminate wing rock and augment dutch roll damping; and lateral stick to rudder crossfeed (SRI) to reduce or eliminate adverse aileron yaw for pilot inputs, thereby providing a positive shift in the closed-loop parameters LCDP, ω_ϕ^2, and $1/T_\phi$.

Undesirably, the roll damper also produces adverse yaw when opposing uncommanded roll; it may increase nose slice departure tendencies and pro-spin surface deflections. A block diagram for the augmentation mechanization is shown in Section V.

The root migration surveys for Configuration A_2 are shown in Figure 64. Comparison with Figure 55 shows that at $\beta = 0$ the dutch roll damping is increased considerably; it does not go unstable until AOA exceeds that for $C_{n_{\beta_{dyn}}}$ becoming negative (▲ symbol). Also, the AOA at which ω_ϕ^2 becomes negative has been increased approximately 5 deg and the negative values of both $1/T_{\phi_1}$ and $1/T_s^\theta$ have been reduced. Thus, within the augmentation system authority limits and near zero β, Configuration A_2 stability is increased and departure susceptibility decreased up to about 23 deg AOA. However, for $\beta \neq 0$ the augmentation benefits are overcome and the dynamic parameters revert back to airframe-alone values.

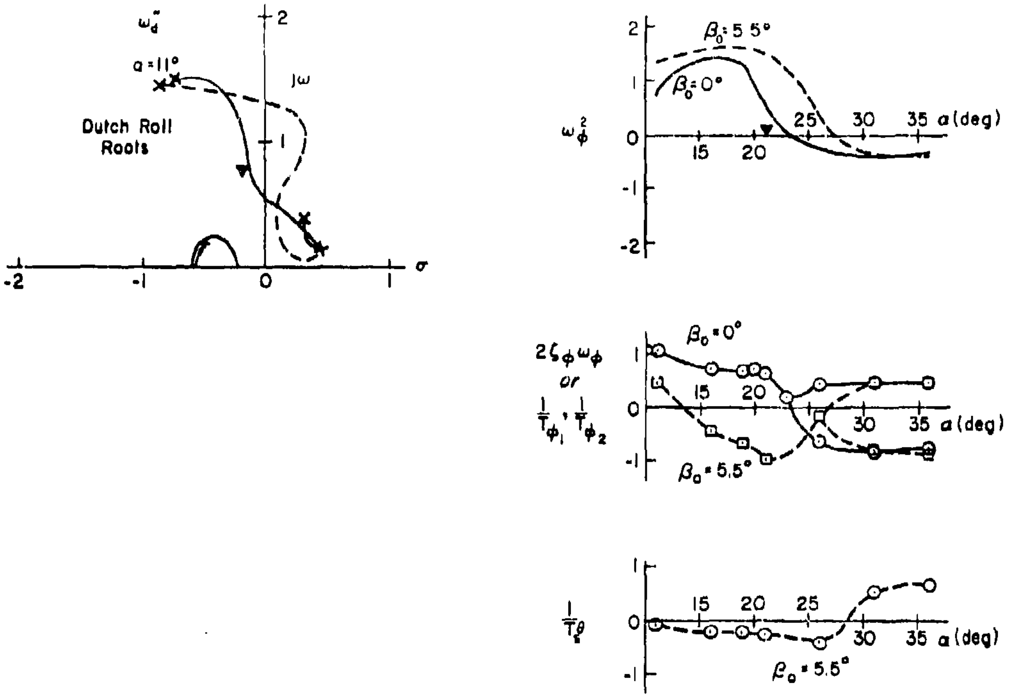

Figure 64. Key Parameters for Configuration A_2

Root migration survey plots for Configuration C_2 are presented in Figure 65. Comparison with Figure 57 again shows improvement in dutch roll stability. However, the most dramatic change is in ω_ϕ^2 which now remains positive up to 35 deg AOA (but note $\zeta_\phi \omega_\phi$ is small and negative beyond 31 deg AOA). Thus roll reversal problems are essentially eliminated and numerator root sensitivity to sideslip is decreased considerably — again subject to augmentation system authority limits.

The change in departure and spin characteristics cannot be predicted for these configurations using the static aerodynamic parameters of Figure 63 because the augmentation system influence is frequency dependent. But a somewhat similar plot can be constructed using the

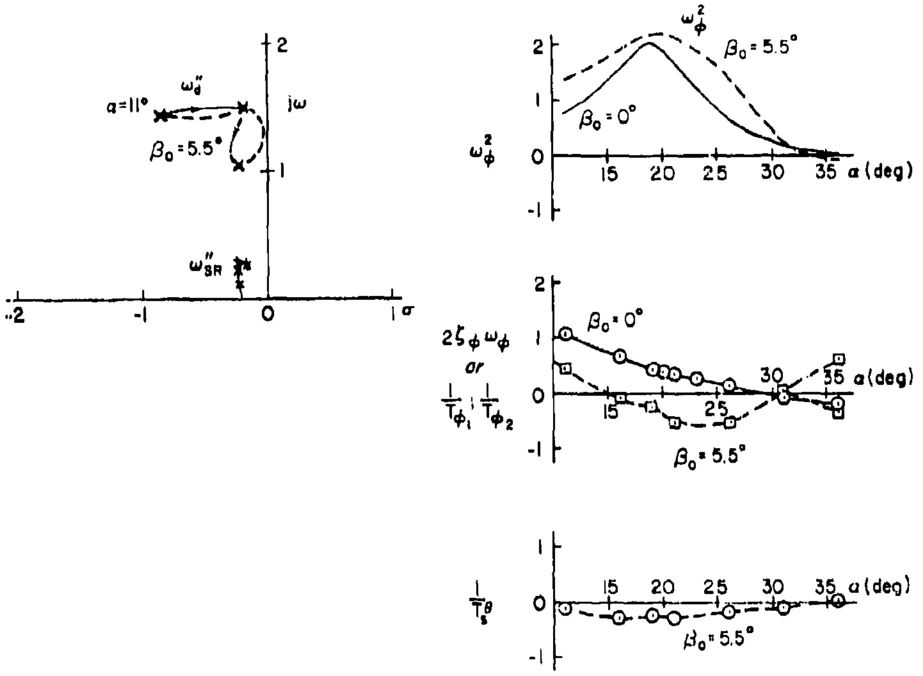

Figure 65. Key Parameters for Configuration C_2

parameters ω_ϕ^2 and $\zeta_d\omega_d$.* Such a plot is presented in Figure 66 for both unaugmented and augmented versions of Configurations A and C. The intercept of the ω_ϕ^2 axis with $\zeta_d\omega_d$ has been arbitrarily shifted to enhance similarity for the unaugmented configurations with Figure 63. Note that the root plots for the unaugmented Configurations A_1 and C_1 (solid lines) are quite similar to those of Figure 63. The plots (Figure 66) for Configurations A_2 and C_2 (dashed lines) are moved further into the upper right quadrant, which is identified as departure resistant in Figure 63. Similar interpretation would forecast A_2 to be departure resistant up to about 24 deg AOA but to have moderate to severe departure tendencies at higher AOA, while C_2 should have no departure tendencies.

---

*Despite the direct relationship between $C_{n_{\beta_{dyn}}}$ and ω_d^2, it is more appropriate to plot $\zeta_d\omega_d$ because the changes in sign (or lack thereof) of $C_{n_{\beta_{dyn}}}$ and ζ_d are in closer agreement.

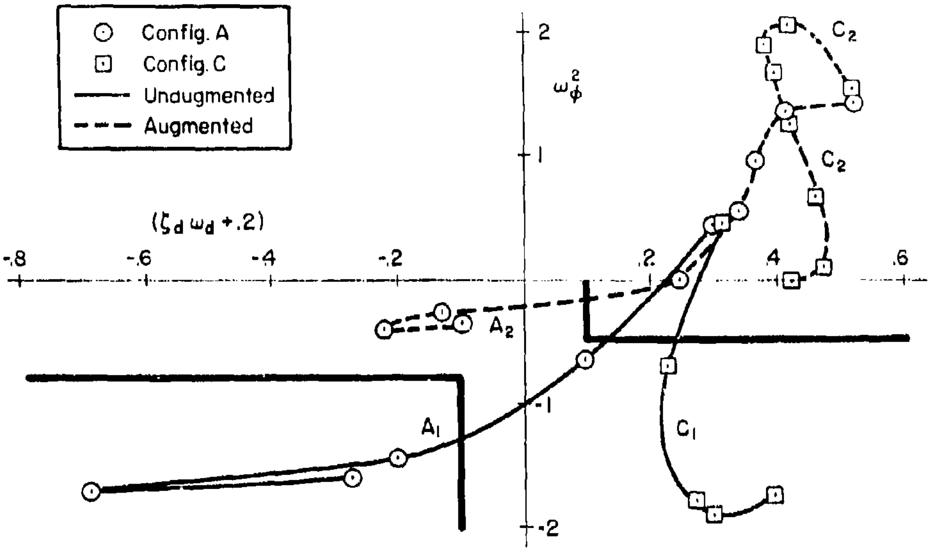

Figure 66. ω_ϕ^2 Versus $\zeta_d\omega_d$ for Augmented and Unaugmented Configurations A and C

C. SUMMARY OF CONFIGURATIONS AND PREDICTED HIGH α CHARACTERISTICS

Table 6 summarizes the six-configuration matrix employed in the piloted simulation. For A_1 a sequence of roll reversal, wing rock, nose slice, and finally strong rolling departure with high spin susceptibility is predicted with increasing AOA. For A_2 the augmentation system and crossfeed are expected to minimize or eliminate the roll reversal and wing rock predeparture warnings. The predicted characteristics are nose slice followed by moderate rolling departure. For B, predicted characteristics are roll reversal, nose slice, and strong rolling departure. Warning in the form of wing rock should not be present due to the large roll damping of this configuration. Note that Configurations A_2 and B allow comparison of high AOA stall/departure characteristics with high aerodynamic roll damping (Configuration B) and with artificially augmented roll damping (Configuration A_2).

The unagumented Configuration C_1 is predicted to exhibit roll reversal, wing rock, and mild rolling divergence with increasing AOA but to

TABLE 6. CONFIGURATION MATRIX

CONFIGURATION	FCS	AERODYNAMIC VARIANT	PREDICTED CHARACTERISTIC
A_1	Basic	Basic F-4J	Wing rock Roll reversal Nose slice Roll departure
A_2	Augmented		Nose slice Roll departure
B	Basic	Increased C_{ℓ_p}	Roll reversal Nose slice Roll departure
C_1	Basic	$\left.\begin{array}{l}\text{Increased } C_{\ell_\beta}\\ \text{Decreased } C_{\ell_\alpha}\end{array}\right\} 15 < \alpha < 45$	Wing rock Roll reversal Roll departure
C_2	Augmented		None $\begin{array}{l}C_{n_{\beta_{dyn}}} > 0\\ \text{LCDP} > 0\end{array}$
D	Basic	$\left.\begin{array}{l}\text{Increased } C_{n_\beta}\\ \text{Decreased } C_{n_\alpha}\end{array}\right\} \alpha > 15$ Positive C_{m_β}	Wing rock Roll reversal Pitch up

have no nose slice. Augmentation is employed with C_2 to improve maneuvering control and to determine if it will degrade the departure resistance of this configuration. On the basis of $C_{n_{\beta_{dyn}}}$ and ω_ϕ^2 (or LCDP), no departure tendency should be anticipated for C_2. Finally, D should exhibit roll reversal and wing rock warnings but little lateral-directional departure tendency. However, the change in sign of C_{m_β} to provide positive pitching moment with sideslip should result in pitch-up, which would be expected to aggravate any high AOA departure tendency. All other configurations have negative C_{m_β}, should pitch down with increasing sideslip, and hence should require more effort of the pilot to maintain high AOA (longitudinal stick cue).

SECTION V

PILOTED SIMULATION

The purposes of the piloted simulation were to validate the influences of the key aerodynamic coefficients in determining departure characteristics, evaluate the influences of varied maneuver limiting factors on high AOA maneuvering control, and identify potential flying qualities criteria. While aircraft motion is highly desirable for such validation and assessment, departure and post-stall gyration (PSG) severity obtained with the 6 DOF analytic models indicated that a moving-base simulation would offer very little benefit. Nose slice motion was so rapid that 130 deg/sec yaw rate could be reached within two seconds after departure onset; peak angular accelerations as large as

$$\dot{p} = 500 \text{ deg/sec}^2$$

$$\dot{q} = 200 \text{ deg/sec}^2$$

$$\dot{r} = 150 \text{ deg/sec}^2$$

were obtained. Washout requirements to prevent hitting displacement stops would have to be so rapid as to negate motion benefits. Therefore, a fixed-base simulation was selected having an unrestricted out-of-cockpit horizon display capable of such rates and accelerations. The aerodynamic model was also expanded to accommodate inverted flight maneuvers.

This section presents an overview of the simulator, including displays, airframe, and flight control system modeling, cockpit, and force and moment equations.

A. SIMULATOR

The simulation was performed in the McDonnell Aircraft Company's fixed-base Manned Air Combat Simulator dome, a 20 ft hemisphere identified as MACS-1. Physical aspects of the simulation are summarized in Figure 67. The horizon and target are projected on the inside of the hemisphere. The cockpit is located at the center of the dome. The out-the-window, head-up (HUD) and head-down (HDD) displays, and cockpit layout are as indicated in Figure 67. Seat cues consisted of normal acceleration and buffet motion provided through an inflatable seat bladder. The frequency and amplitude of the buffet oscillation varied as the aircraft angle of attack increased, starting at about 14 deg.

A TV projection of a gimballed model target aircraft provided a maneuvering tracking task. Target motion equations provided realistic maneuvers while allowing the aircraft to fly well beyond the departure region for the test aircraft. The target was controlled by the computer operator via a special control panel.

B. HEAD-UP DISPLAY

The head-up display (HUD) provided information on aircraft attitude, heading, airspeed, altitude, and trim conditions. Figure 68 illustrates the HUD presentation as originally installed. Display of normal acceleration provided a reference for trimming longitudinal control to 1 g prior to the start of a run. Trim thrust was set by adjusting throttles until change from trim thrust registered near zero. The Flight Path Angle Ladder displayed both flight path elevation angle and roll attitude. Orientation of the total velocity vector was provided through the Velocity Vector Indicator; when the velocity vector was outside the HUD field of view, the Indicator remained at the edge of the HUD and blinked.

At pilot request, the HUD was simplified late in the simulation program. Airspeed, Heading, and Altitude bar displays were removed.

The fixed reticle tracking gunsight was a part of the HUD.

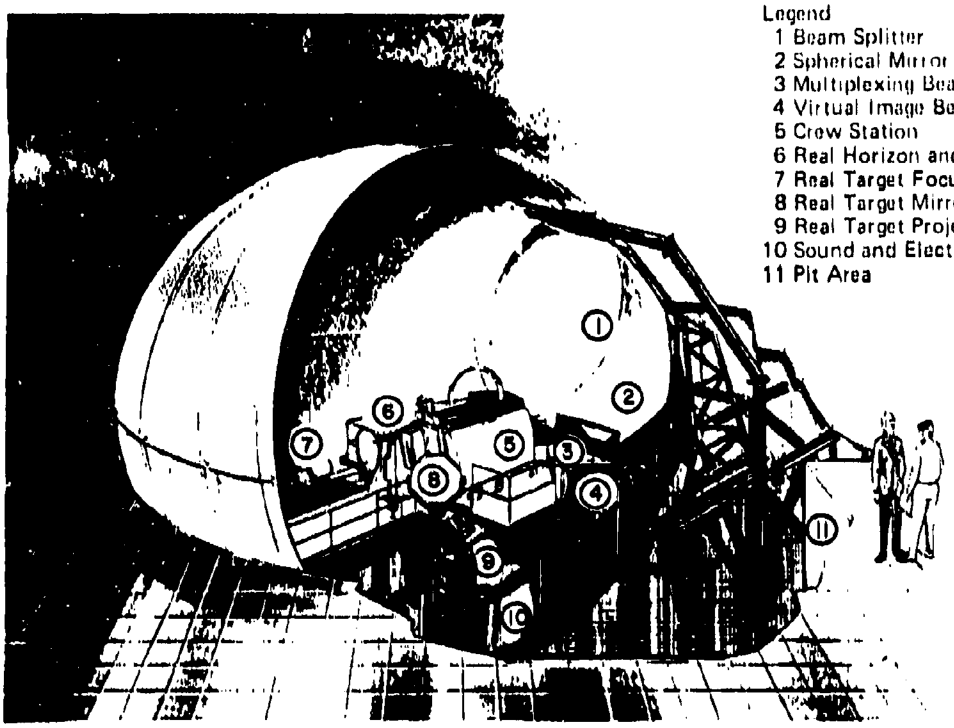

Legend
1 Beam Splitter
2 Spherical Mirror
3 Multiplexing Beam Splitter
4 Virtual Image Beam Splitter
5 Crew Station
6 Real Horizon and Missile Projector
7 Real Target Focus Lenses
8 Real Target Mirrors
9 Real Target Projector
10 Sound and Electronic Equipment
11 Pit Area

QP76-0287-4

Displays:	Horizon - 360 deg ϕ, θ, ψ HUD - CAS, h, ψ, velocity vector HDD - ϕ, θ, ψ, α, M, etc. Sight - fixed reticle
Cockpit:	Basic F-4
Seat Cues:	Load factor, buffet
Target:	Gimballed model TV projection

Figure 67. Manned Air Combat Simulator I

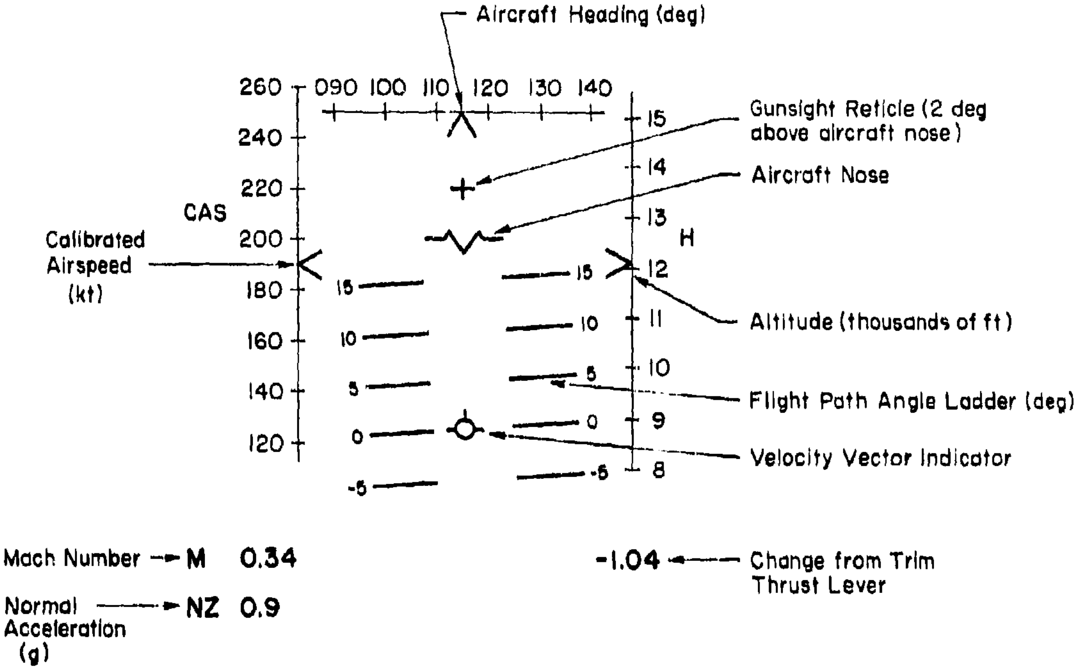

Figure 68. Head-Up Display (HUD) Used in Simulation

C. FLIGHT CONTROL SYSTEM

The manual flight control mechanization (stick, pedals, surface deflections and rates, etc.) represented the basic F-4 aircraft (e.g., see Figure 2).

A special lateral-directional stability and command augmentation system (SCAS) was mechanized as shown in Figure 69. The SCAS feedback gains are production F-4 values. The stick-to-rudder crossfeed gain and shaping were optimized for $10 < \alpha < 20$ deg and faded to zero at $\alpha \leq 10$ deg to prevent adversely influencing the low AOA handling qualities.

D. EQUATIONS OF MOTION

Slightly modified versions of the standard McDonnell Aircraft Company piloted simulation equations of motion were used. These are essentially the same as those presented in Appendix I, Part III, i.e., moment

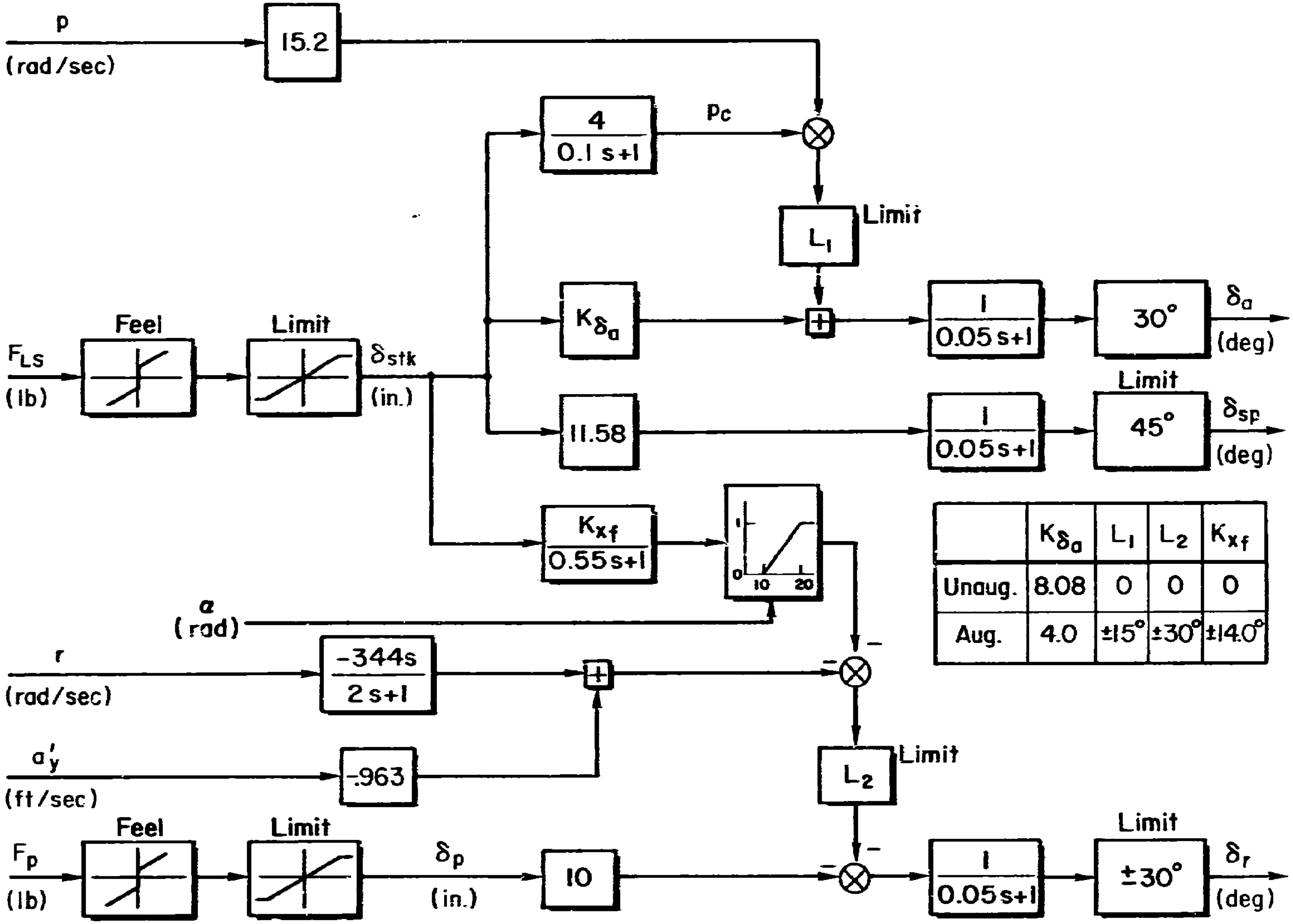

	K_{δ_a}	L_1	L_2	K_{x_f}
Unaug.	8.08	0	0	0
Aug.	4.0	±15°	±30°	±14.0°

Figure 69. Lateral-Directional Control System

equations in body centerline axes, force equations in wind axes, and aircraft orientation in standard Euler axes. The only change required was to expand the small angle α and β assumptions and to eliminate the tan β and $\cos^{-1}\beta$ expressions of the $\dot{\alpha}$ equation which gave discontinuity problems as β approached 90 deg. This required substituting the $\dot{w}$-equation for $\dot{\alpha}$, i.e.,

$$\dot{\alpha} = q - \tan\beta(p\cos\alpha + r\sin\alpha) + Z_w/(mV_T\cos\beta)$$

$$\dot{w} = qV_T\cos\beta - V_T\sin\beta(p\cos\alpha + r\sin\alpha) + Z_w/m$$

and using the simple expressions $\alpha = \sin^{-1}(w/V_T)$ and $\beta = \sin^{-1}(v/V_T)$ for entry into the aerodynamic look-up tables.

E. AERODYNAMIC MODELS

Since the major interest in the simulation was the analysis of departure onset, particular attention was given to realistically modeling aerodynamic data for the range of $0 < \alpha < 45$ deg and $\beta < \pm 30$ deg. The basic aerodynamic coefficients were selected with the goal of providing a reasonably accurate dynamic model of the F-4J over this α and β range. To allow greater aircraft motion freedom typical of severe departures, post-stall gyrations, and spins without encountering unrealistic discontinuities in the data, certain approximations were made for $\alpha > 45$ deg, $\alpha < 0$ deg, and $\beta > \pm 30$ deg, i.e.,

- For $\alpha > 45$ deg the coefficients were faired to 110 deg, then extended to 180 deg by either maintaining the value at 110 deg or fading the coefficient to zero at $\alpha = 180$ deg.
- The coefficients were assumed to be similar in value for positive and negative AOA so that all derivatives were taken to be even functions of AOA (i.e., mirror images about $\alpha = 0$) and the coefficients C_L and C_m to be odd functions of AOA.
- Variation of the coefficients with β was assumed to be linear for $\beta > 30$ deg.

The resulting aerodynamic coefficients are shown in Figure 70.

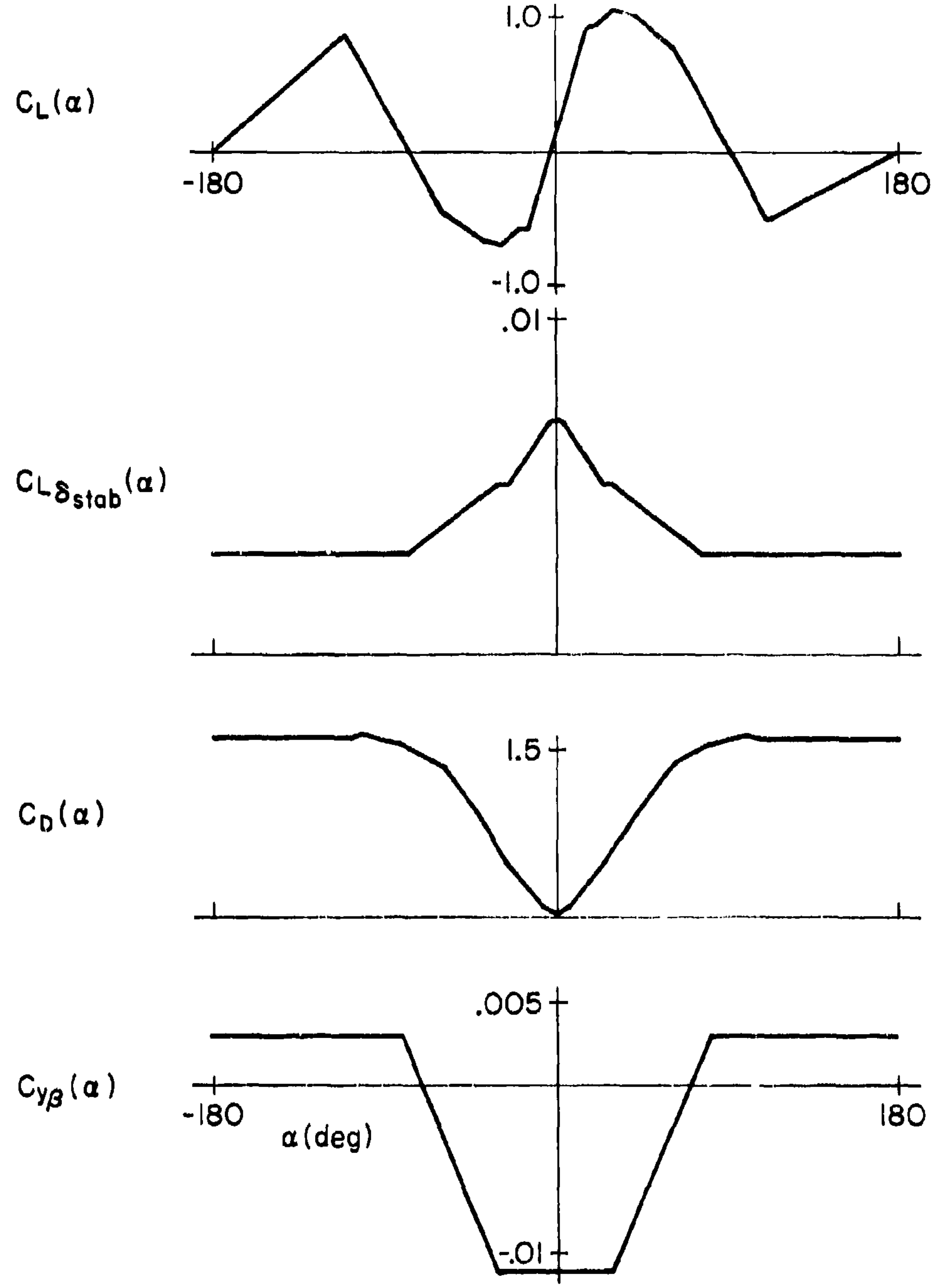

Figure 70. Coefficients as Extended for $|\alpha| \leq 180$ deg and $|\beta| \leq 90$ deg

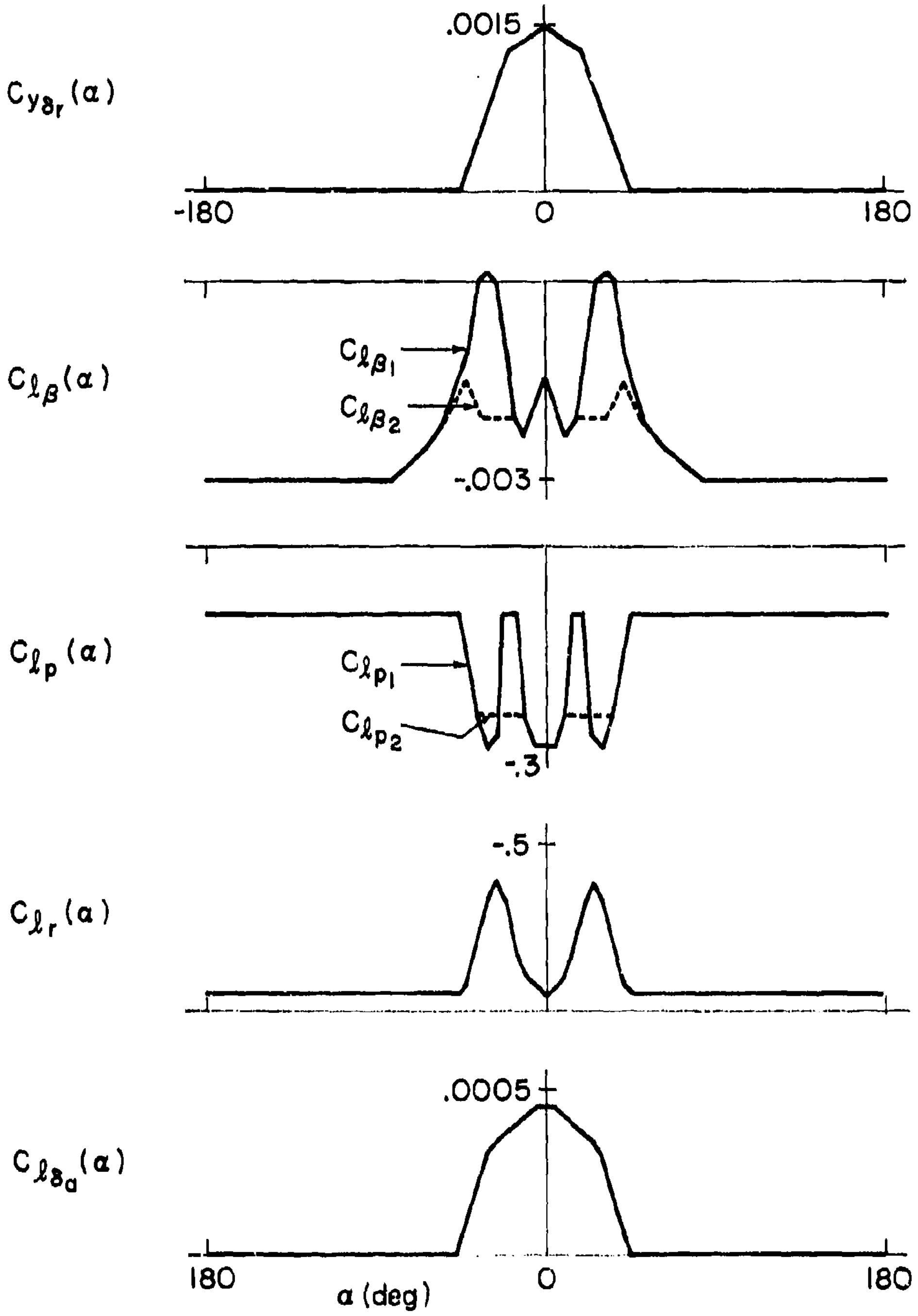

Figure 70. (Continued)

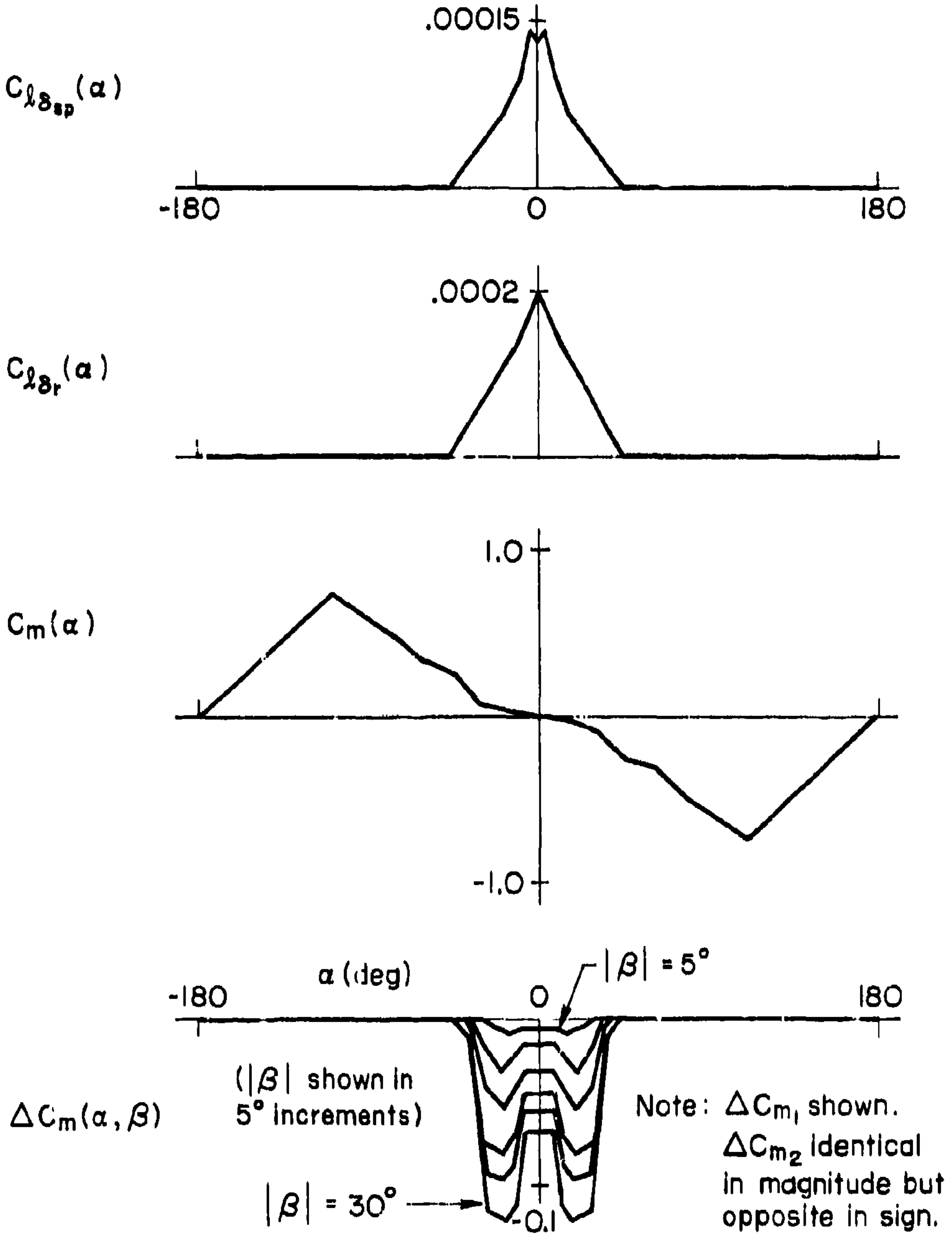

Figure 70, (Continued)

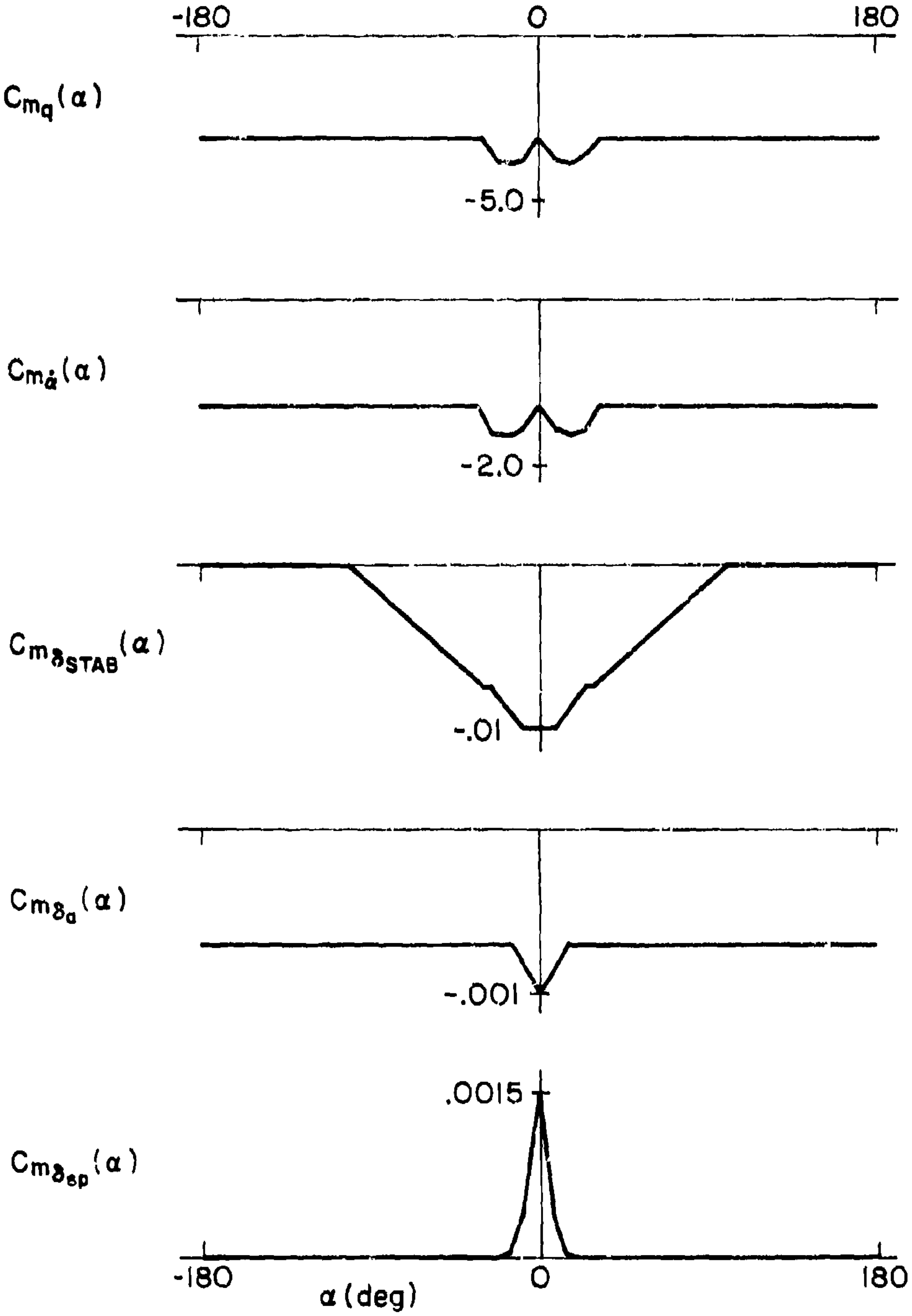

Figure 70. (Continued)

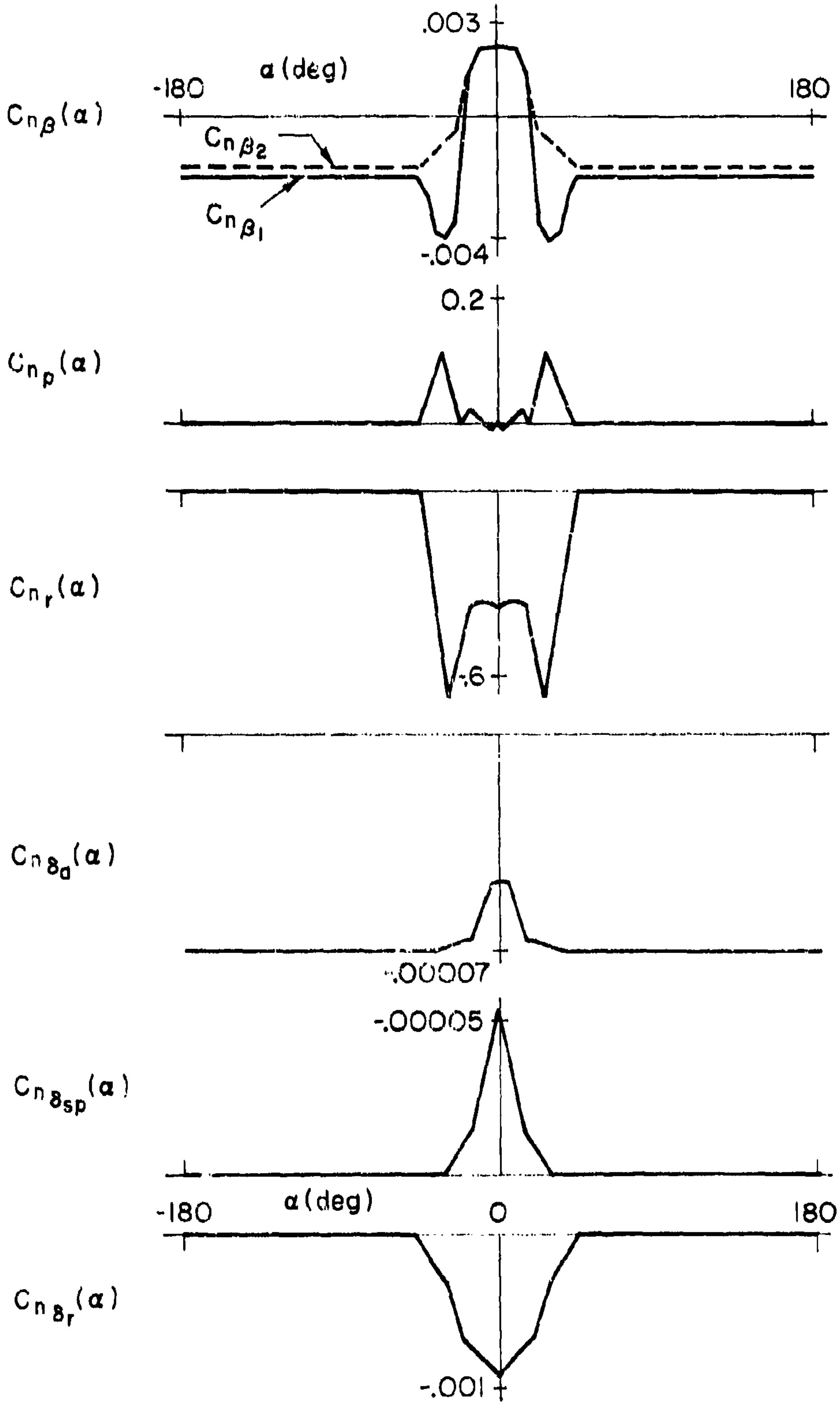

Figure 70. (Concluded)

It is recognized that the assumptions made above could result in considerable error for extreme angles of attack and sideslip; however, the use of full-ranged data allowed the simulation to be operated throughout a violent departure without demanding an immediate return to initial conditions when lower aerodynamic data limits were reached.

The aerodynamic data were stored in the digital computer as look-up tables. Total forces and moments were computed digitally and fed to the analog systems of the simulator to drive the cockpit displays.

Physical dimensions of the airplane were based upon the F-4J. Inertias and weights are summarized in Section II.

F. DATA RECORDED

Parametric data were recorded via three eight-channel Brush recorders. All Euler angles, body axis rates, and control deflections were recorded, as well as accelerations, altitude, velocity, and thrust settings.

For a limited number of runs the total body axis accelerations $(\dot{p}, \dot{q}, \dot{r})$ were recorded and inertial and aerodynamic components of $\dot{q}$ were also recorded separately.

G. TASKS AND MANEUVERS

Piloting tasks were selected which exercised the open- and closed-loop departure parameters of interest. These were divided into two phases. The first consisted of familiarization maneuvers typical of "feeling out" stall/departure motions, warning, etc., of a new airframe. These are modeled after the suggested test matrix of Reference 34 plus an additional aggravated input maneuver for determining departure susceptibility, proposed in Reference 35. The second phase consisted of tracking tasks and maneuvers as suggested in Reference 36.

1. Handling Familiarization and Assessment

Five basic familiarization (F) maneuvers were employed:

- Straight-ahead stall (F_1): 1 g, fixed thrust, longitudinal stick pull to produce $\dot{\alpha} \approx 1$ deg/sec until stall departure.
- Constant attitude stall (F_2): 1 g, wings level, holding constant pitch attitude while slowly reducing thrust until stall/departure.
- Bank-to-bank turns (F_3): Constant altitude, ±60 deg bank-to-bank turns at increasing AOA until departure; rudder coordination optional.
- Wind-up turn (F_4): Constant thrust, wind-up turn to stall departure.
- Full-stick-deflection maneuver (F_5): From 60 deg bank, rapidly ramp full aft longitudinal stick followed by full lateral stick out of the bank. After 8 sec neutralize controls.

With the exception of maneuver F_5 there was no restriction on the type or magnitude of controls used by the pilots. In fact, pilots were advised to investigate various control techniques just as they would in a stall evaluation of a new aircraft. Maneuver F_5 (from Reference 35) was evaluated as an indicator of departure susceptibility.

2. Precision Tracking Evaluation

The target aircraft (a TV picture of a model airplane, projected onto the dome at the proper aspect and size) was programmed to perform three basic maneuvers during a slow pull-up. Target climb rate was fixed to produce $\dot{\alpha} \approx 1$ deg/sec to guide the subject pilots into repeatable tracking runs of approximately 30 sec minimum duration before departure. The tasks started with the subject aircraft trimmed at $\alpha = 12$ deg, essentially in trail. The pilot attempted to stay in the target's 6 o'clock position as if trying to overextend a firing solution. The tracking (T) maneuvers were:

- Straight-ahead pullup (T_1): Constant-thrust, straight-ahead pullup keeping pipper on target until aircraft no longer controllable.

- Climbing roll-reversals (T_2): Track target aircraft through series of climbing roll reversals ($\phi \doteq \pm 40$ deg) until aircraft no longer controllable. Constant thrust.

- Wind-up turn (T_3): Starting wings-level, track target into constant-thrust 60 deg bank wind-up turn until aircraft no longer controllable.

3. Departure Recovery

Recovery techniques employed were at the discretion of the pilots, based upon their experiences in fighter aircraft. Recoveries were initiated either:

- Immediately upon positive indication of uncommanded motion (R_1), or

- After about a 3 sec delay (R_2).

Recoveries were also attempted in the SCAS-on configurations (Cases A_2 and C_2) by turning the SCAS off upon departure (R_3).

H. FLYING QUALITY RATING SCALES

Previous stall/departure simulations for flying quality assessment (e.g., Reference 5) have shown the familiar Cooper-Harper scale (Figure 71) to be inadequate because departure is centered on the first step in the decision tree, i.e., controllability instead of performance. It was preordained for this simulation that control would be lost (CH = 10) because the configurations were specifically selected to provide differing departure warning, severity, and recovery in order to identify gradations in these attributes. Therefore, one requirement of this program was to develop and validate a more appropriate stall/departure flying quality rating scale.

The Reference 37 experimental program succeeded in developing rating scales for a similar loss-of-control and recovery situation induced by flying into a very strong wake vortex. This experience indicated

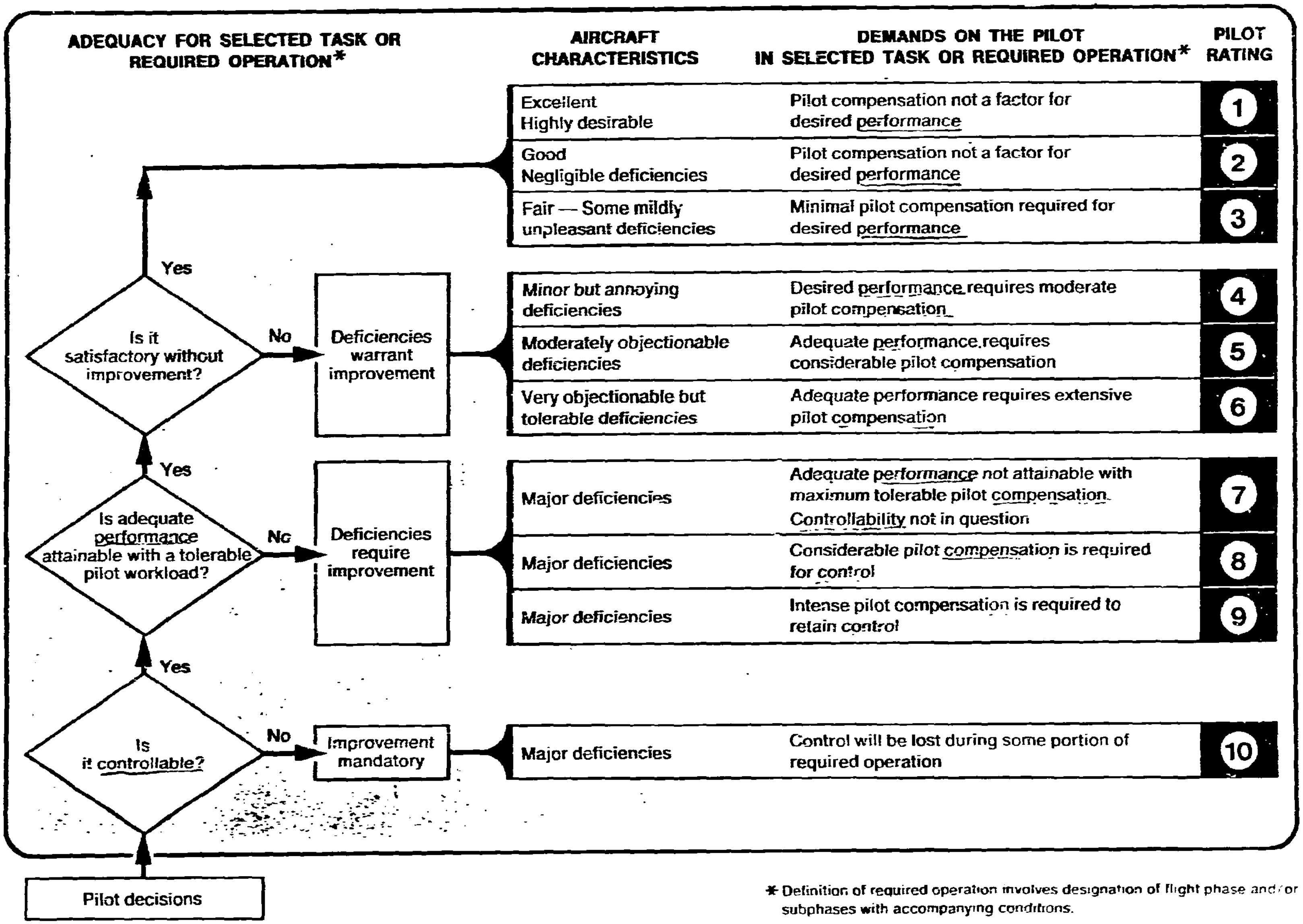

* Definition of required operation involves designation of flight phase and/or subphases with accompanying conditions.

Figure 71. Cooper-Harper Handling Qualities Rating Scale

that each attribute must be evaluated individually and then the overall hazard assessed. Figure 72 is a tentative departure rating scale adapted from the wake vortex experience. Here the stall/departure attributes are divided into four open-ended scales. The first is departure onset warning — clarity or lack of warning. Next, the attitude and attitude rate excursions are evaluated. Recovery characteristics are separately evaluated (whether the recovery was rapid and achieved by simple control application or whether it degraded down to the point of no recovery). Finally, an overall assessment of hazard is rated.

In anticipation that overall hazard assessment (acceptability) might vary with aircraft primary mission, provision is made for indicating scalar differences between training and operational squadron usage. For example, an operational aircraft might have very clear warning of departure onset and extreme excursions if the pilot persisted, and be difficult to recover, but be given a relatively good hazard rating, i.e., a 2, on the basis of the very clear and consistent warning. Similarly, a training aircraft might have little warning of departure onset and relatively large attitude excursions, but recover very easily and quickly by merely releasing the controls, and again might have a relatively good overall hazard rating, such as a 2, on the basis of recovery.

As an adjunct to the rating scales, the pilot is also asked to provide qualitative information as to the nature of the aircraft motions observed.

Although the rating scale of Figure 72 was conceived to cover both open- and closed-loop situations and specifically is not spin oriented, it was employed in a separate departure/spin susceptibility piloted simulation (Reference 38) to obtain an early assessment of its usefulness. Results were somewhat inconclusive since the Reference 38 task involved preprogrammed, open-loop pilot inputs to assess the departure/spin susceptibility of an airframe having variations in surface authority and actuator rate limiting characteristics. Nevertheless, valuable comments were obtained (Reference 39) along with a recommended expansion and restructuring of the pilots' qualitative assessment to provide greater flexibility and provoke additional commentary to identify what

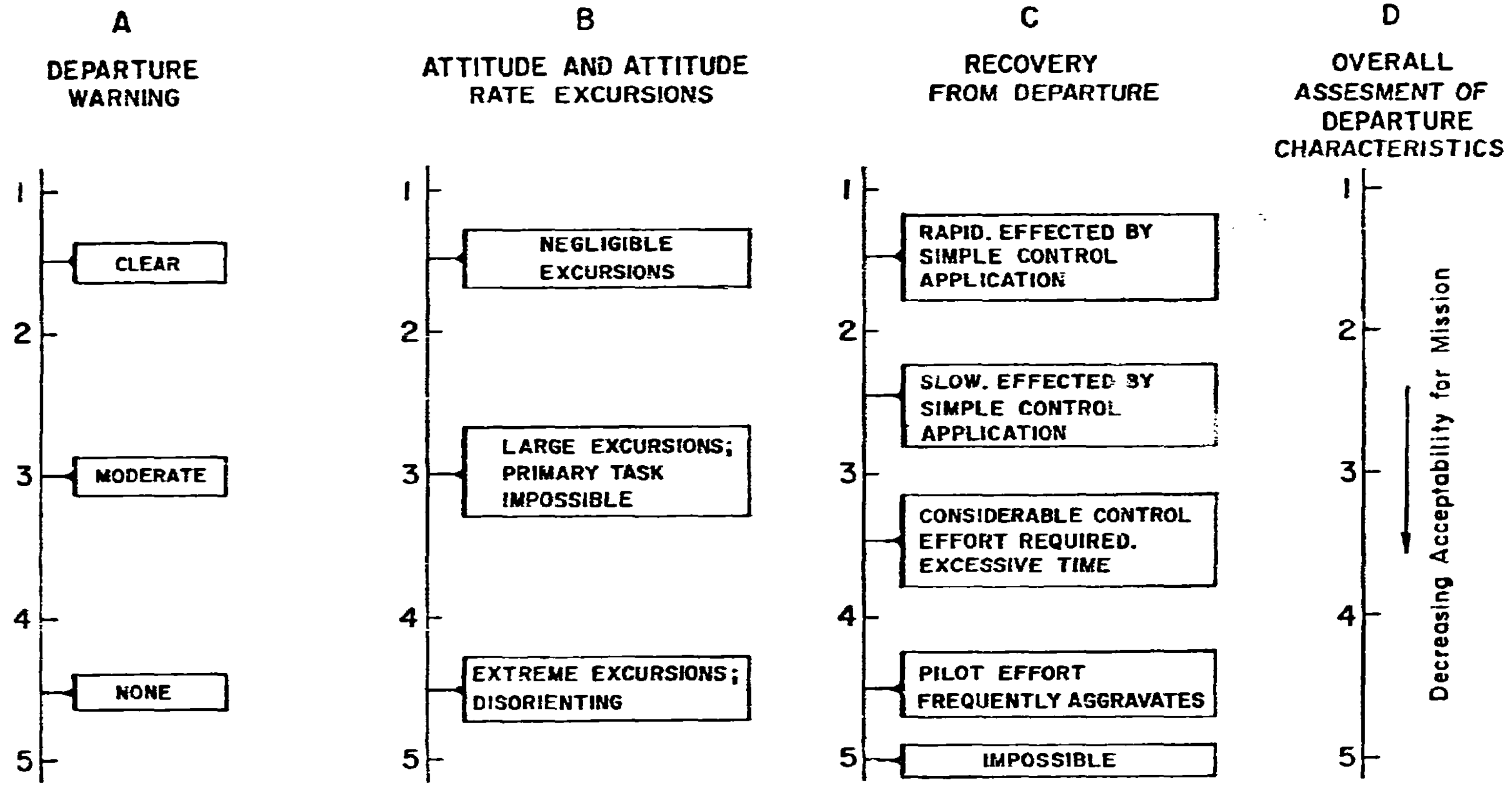

- Describe warning
- Did warning interfere with primary task? If so, to what extent?

- *Describe departure sequence*
  1. Nose slice
  2. Wing rock
  3. Rolling departure
  4. Pitch up
- What was primary departure variable? $(\theta, \dot{\theta}, \psi, \dot{\psi}, \phi, \dot{\phi})$

- Was altitude loss primarily due to a path divergence or to attitude excursions?

- Fighter
- Trainer

Figure 72. Tentative Departure Rating Scale

the pilot is rating. Accordingly, a loss-of-control/departure/recovery debriefing guide was prepared, Table 7, to augment the rating chart. This guide addresses the four topics of the Figure 72 rating scale plus an additional section devoted to post stall gyrations (PSG) characteristics and severity. Provision is made under each topic for the numerical rating (STI) from the Figure 72 scale. The pilot is requested to answer those questions appropriate for the maneuver flown. Most questions pertain to characteristics of the vehicle motion and are constructed to encourage simple yes/no, multiple choice, or short written answers. Cooper-Harper (CH) ratings are also requested for the two tasks which involve pilot effort to exert control on the vehicle (i.e., prevent departure and accomplish recovery). Finally, it should be noted that the questionnaire was prepared for use in flight as well as simulation. Thus, some questions are not appropriate for fixed-base simulation (e.g., assessment of vehicle acceleration).

TABLE 7. LOSS OF CONTROL/DEPARTURE/RECOVERY DEBRIEFING GUIDE

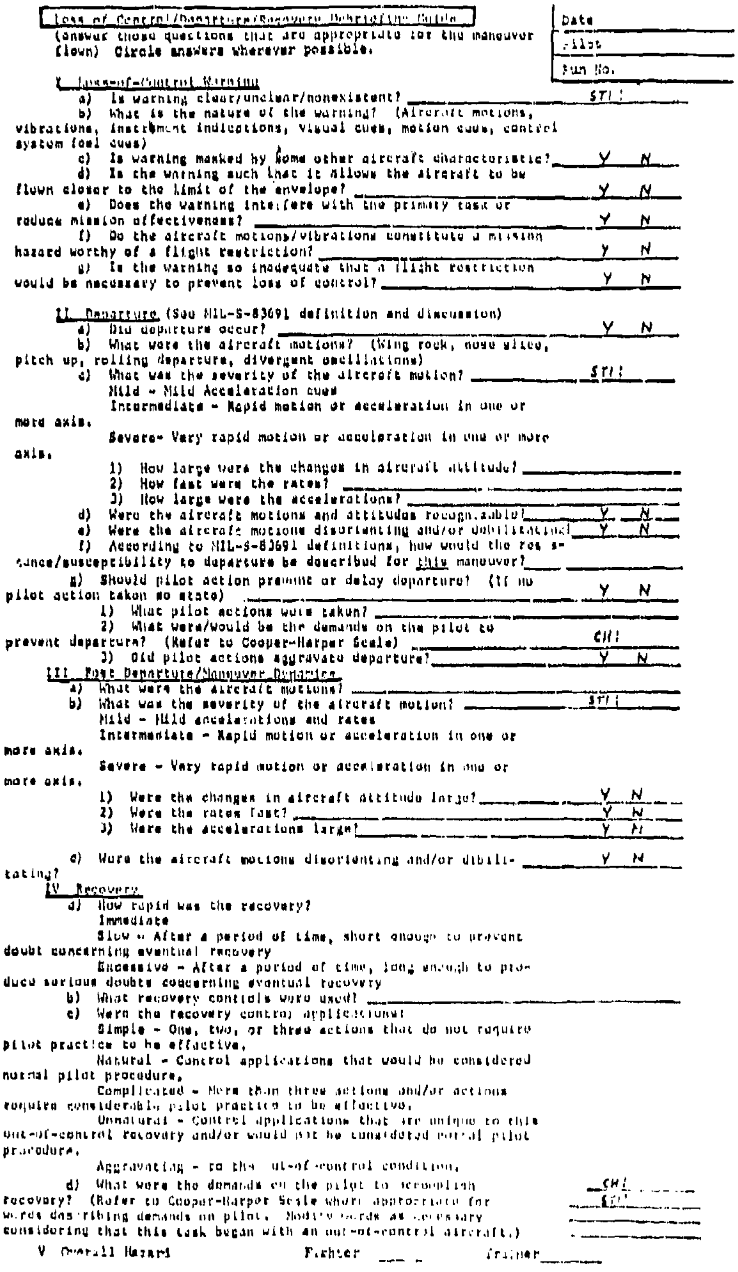

Loss of Control/Departure/Recovery Debriefing Guide

(answer those questions that are appropriate for the maneuver flown) Circle answers wherever possible.

Date ______
Pilot ______
Run No. ______

I Loss-of-Control Warning

a) Is warning clear/unclear/nonexistent? ______ STI ______

b) What is the nature of the warning? (Aircraft motions, vibrations, instrument indications, visual cues, motion cues, control system feel cues)

c) Is warning masked by some other aircraft characteristic? ______ Y N

d) Is the warning such that it allows the aircraft to be flown closer to the limit of the envelope? ______ Y N

e) Does the warning interfere with the primary task or reduce mission effectiveness? ______ Y N

f) Do the aircraft motions/vibrations constitute a mission hazard worthy of a flight restriction? ______ Y N

g) Is the warning so inadequate that a flight restriction would be necessary to prevent loss of control? ______ Y N

II Departure (See MIL-S-83691 definition and discussion)

a) Did departure occur? ______ Y N

b) What were the aircraft motions? (Wing rock, nose slice, pitch up, rolling departure, divergent oscillations)

c) What was the severity of the aircraft motion? ______ STI ______

Mild - Mild Acceleration cues

Intermediate - Rapid motion or acceleration in one or more axis.

Severe - Very rapid motion or acceleration in one or more axis.

1) How large were the changes in aircraft attitude? ______

2) How fast were the rates? ______

3) How large were the accelerations? ______

d) Were the aircraft motions and attitudes recognizable? ______ Y N

e) Were the aircraft motions disorienting and/or debilitating? ______ Y N

f) According to MIL-S-83691 definitions, how would the resistance/susceptibility to departure be described for this maneuver? ______

g) Should pilot action prevent or delay departure? (If no pilot action taken so state) ______ Y N

1) What pilot actions were taken? ______

2) What were/would be the demands on the pilot to prevent departure? (Refer to Cooper-Harper Scale) ______ CH ______

3) Did pilot actions aggravate departure? ______ Y N

III Post Departure/Maneuver Dynamics

a) What were the aircraft motions? ______

b) What was the severity of the aircraft motion? ______ STI ______

Mild - Mild accelerations and rates

Intermediate - Rapid motion or acceleration in one or more axis.

Severe - Very rapid motion or acceleration in one or more axis.

1) Were the changes in aircraft attitude large? ______ Y N

2) Were the rates fast? ______ Y N

3) Were the accelerations large? ______ Y N

c) Were the aircraft motions disorienting and/or debilitating? ______ Y N

IV Recovery

a) How rapid was the recovery?

Immediate

Slow - After a period of time, short enough to prevent doubt concerning eventual recovery

Excessive - After a period of time, long enough to produce serious doubts concerning eventual recovery

b) What recovery controls were used? ______

c) Were the recovery control applications:

Simple - One, two, or three actions that do not require pilot practice to be effective.

Natural - Control applications that would be considered normal pilot procedure.

Complicated - More than three actions and/or actions require considerable pilot practice to be effective.

Unnatural - Control applications that are unique to this out-of-control recovery and/or would not be considered normal pilot procedure.

Aggravating - to the out-of-control condition.

d) What were the demands on the pilot to accomplish recovery? (Refer to Cooper-Harper Scale where appropriate for words describing demands on pilot. Modify words as necessary considering that this task began with an out-of-control aircraft.) ______ CH ______ STI ______

V Overall Hazard Fighter ______ Trainer ______

SECTION VI

HIGH AOA FLYING QUALITIES ASSESSMENTS

Effects of the maneuver-limiting factors on high-angle-of-attack flying qualities were assessed by three pilots utilizing the prescribed set of non-tracking and tracking maneuvers. The two principal pilots were highly qualified U.S. Air Force fighter test pilots, graduates of the Air Force Test Pilot School at Edwards AFB, with a broad range of practical experience. The first pilot, RC, has flown a varied selection of aircraft, from the F-4 to the B-52; the second pilot, JF, was experienced in operational fighter and attack aircraft, including the A-9 stall/spin evaluation, and is a former instructor at the Test Pilot School responsible for stall/spin curricula. The third pilot, RH, was a handling quality engineer/general aviation pilot who also accomplished all of the initial simulation debugging, procedural checkout, primary pilot briefings and debriefings, etc.

The combination of airframe configurations, familiarization and tracking maneuvers, and recoveries resulted in the 98-cell matrix of Table 8. This matrix was flown first as a sequence of runs progressing horizontally across the various maneuvers for a given airframe. After the complete matrix had been accomplished once, a second series was performed progressing vertically through the airframe configurations for each tracking task.

A total of 1088 formal runs were conducted. These were fairly evenly divided between the various configurations and pilots, as indicated by Table 9.

One of the first tasks of the simulation was to validate or modify the ratings scale and debriefing questionnaire to the satisfaction of the evaluation pilots. The final versions were used throughout the remainder of the simulation. Accordingly, this section starts with the rating scale assessment and then presents the airframe configuration assessments.

TABLE 8. RUN MATRIX FOR PILOTED SIMULATION

CON-FIG.	TASK/RECOVERY TECHNIQUE																				
	F_1			F_2			F_3			F_4			F_5	T_1			T_2			T_3	
	R_1	R_2	R_3	R_1	R_2	R_3	R_1	R_2	R_3	R_1	R_2	R_3		R_1	R_2	R_3	R_1	R_2	R_3	R_1	R_2	R_3
A_1	x	x		x	x		x	x		x	x		x	x	x		x	x		x	x	
A_2	x	x	x	x	x	x	x	x	x	x	x	x	x	x	x	x	x	x	x	x	x	x
B	x	x		x	x		x	x		x	x		x	x	x		x	x		x	x	
C_1	x	x		x	x		x	x		x	x		x	x	x		x	x		x	x	
C_2	x	x	x	x	x	x	x	x	x	x	x	x	x	x	x	x	x	x	x	x	x	x
D	x	x		x	x		x	x		x	x		x	x	x		x	x		x	x	

TABLE 9. NUMBER OF RUNS

CONFIGURATION	PILOT			TOTAL
	RC	JF	RH	
A_1	59	79	79	217
A_2	68	48	79	195
B	61	94	58	213
C_1	44	77	40	161
C_2	53	62	58	173
D	35	62	32	129
TOTAL	320	422	346	1088

A. RATINGS SCALE AND QUESTIONNAIRE ASSESSMENT

The debriefing questionnaire was answered at the completion of the familiarization runs and again at the completion of the first set of tracking runs. During this period modifications were worked out for the rating scale. The modified scale was then used for the final set of tracking runs.

1. Questionnaire

The debriefing questionnaire proved essential to obtaining a consistent set of information for interpretation of results. However, the simple yes or no answers requested did not suffice. The tasks and resulting aircraft motions were so complex as to require considerable explanation. For example, more than a single mode of departure or spin was observed in some cases. Departure warning and severity also varied with rate of stall onset ($\dot{\alpha}$) and pilot usage of controls. Thus accomplishment of the questionnaire often became quite time-consuming, with several pages of accompanying explanation. This was augmented by tape recordings made, on-line, of pilot commentary while performing the simulation runs. As a consequence, pilot responses were so lengthy — and in so many cases repetitive —— that it is not practical to incorporate them in this report.

However, the basic conclusion reached by both pilots and experimentors was that such a questionnaire is highly desirable for stall/departure/recovery investigation. The only change in format deemed necessary is provision of more space to accommodate lengthy answers.

2. Rating Scales

As in the previous simulation (Reference 5), the pilots felt that the Cooper-Harper rating scale was inappropriate for stall/departure/recovery evaluation where aircraft characteristics rather than task performance are being assessed. On the other hand, the overall concept of the Figure 72 departure ratings scale was appreciated, although some alterations were required before this scale met with full approval. In particular, the pilots did not like the open-ended aspects of the scales (the scale extends beyond the first and last descriptors). This clearly gave problems, and they preferred that the scale be bounded with a simple descriptor at each end. Second, the time required to recover and the control application necessary to effect recovery needed to be separated. Recovery controls also deserved a further breakdown, with one rating for required control complexity and a second rating for control application timing. Finally, it was decided that an assessment of hazard was difficult to make because this changes with situations such as low versus high altitude. The pilots preferred to provide an overall assessment based upon the acceptability of the flying characteristics at high angles of attack. The end point descriptors selected by the pilots were, in their jargon, "Sierra Hotel," meaning they would like to fly the aircraft at high AOA and "Delta Sierra," meaning unacceptable flying characteristics. The resulting rating scale is shown in Figure 73. Both test pilots were happy with this final form and considered that it covered all key factors, minimized the descriptor conflicts, and did not constrain the pilot's quantitative evaluation.

The rating scale of Figure 73 was employed in the final set of tracking tasks. Resulting characteristic assessments for the six

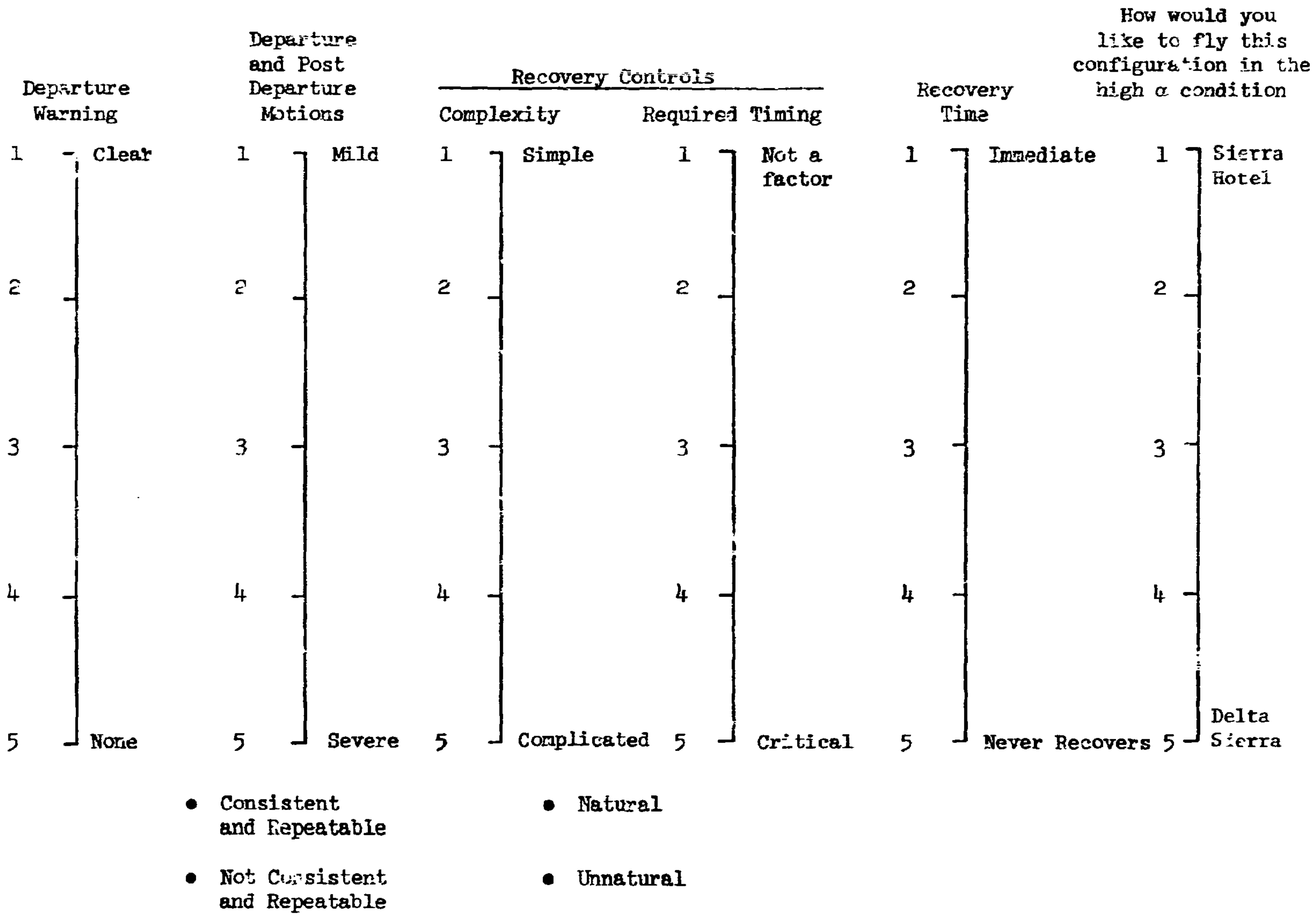

Figure 73. Modified Departure Rating Scale (Mod II)

vehicle configurations are summarized in Figure 74. The numerical ratings shown for each pilot are the averages of separate ratings given for each of the three tracking tasks (T_1 through T_3). Considering the small statistical run sampling and the fact that all configurations were intended to have basic handling deficiencies, the results are considered to be very good. It is to be expected that all ratings would tend toward the poor (high numerical value) end of the scales and they generally are. Most importantly, they also reflect the specific dynamic and handling variations intended to be exhibited between configurations and, in most instances, the ratings of RC and JF demonstrate agreement in variational differences if not in absolute levels. The ratings of pilot RH tend to vacillate between those of RC and JF and also (except for recovery control timing) tend to agree with the poorer rating. This downrating probably reflects pilot RH's relative inexperience in departure/spin/recovery and the violent PSGs which high-performance fighters often exhibit. Thus the ratings of RC and JF are considered the more significant.

The separation between RC and JF ratings on warning and motion severity is consistent with differences in piloting techniques. Generally JF is about one rating point harsher than RC because of a more rapid pull into departure and spin. This will be discussed in more detail later.

Recovery control timing assessment shows very good agreement between the pilots except for Configuration C_2. This primarily reflects timing of control release. The differential is about one rating point or less except Configuration C_2 where RC had difficulty with the two different spin modes the aircraft could have. Timing of control release determined whether an oscillatory (recoverable) or flat (unrecoverable) spin was obtained.

Time to recover and overall rating show almost identical trends and thus reflect predominant concern for loss of altitude in any departure/spin situation. Configuration C_1 had an oscillatory, recoverable spin. Configuration D did not spin but could end up with appreciable altitude loss if the pilot kept fighting the "wallowing" departure mode

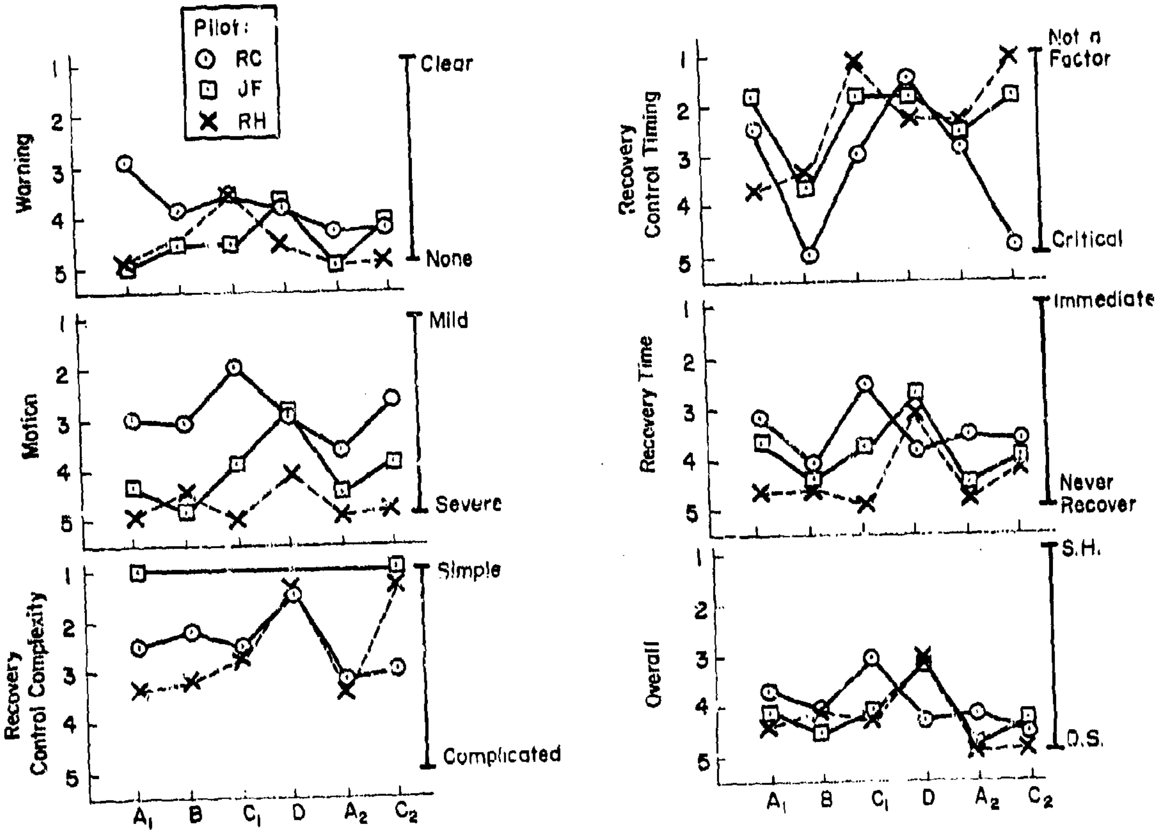

Figure 74. Rating Comparison Between Pilots

(described in Subsection II.B). All other configurations had flat spin modes that were difficult if not impossible to stop. The significant disapproval of the Configuration D pitch-up is also evident for pilot RC on both of these ratings.

The rating scale for recovery control complexity may need additional refinement. Pilot JF rated all configurations at 1 because he merely released controls to initiate recovery and, by definition, this is as simple as things can be. Pilot RC, with less severe departures, was able to discern some influence of the stick and rudder in effecting recovery and this was also reflected in his being more critical of recovery control timing.

However, aspects pertaining to recovery (control usage and recovery time) for configurations other than D are not necessarily significant because the simulation cannot be considered valid for spin and spin recovery. The motions were generally so violent and the out-the-windscreen sky/earth display so featureless that the pilots had to resort to the all-attitude ball for recovery. This is not completely unnatural for the military pilots, but did make the task more difficult. Additionally, the aerodynamic coefficients employed in the simulation do not represent steady spin conditions. Probably the most that can be attributed to recovery evaluations is that they exercised the rating scales.

In summary, the departure rating scales of Figure 73 were accepted and supported by the pilots and, based upon this small statistical sample, the numerical ratings given reflect characteristics "designed into" the vehicle configurations. The spread in ratings between the Air Force test pilots (generally about 0.5 on a 5-point scale) is consistent with spreads normally expected in Cooper-Harper ratings (about 1.0 on a 10-point scale). Greater spreads generally reflect sensitivity to piloting technique; that sensitivity itself may be an attribute of the scales.

Since vehicle attributes rather than a task performance level are being rated, use of the rating scales <u>must</u> be accompanied by a qualitative assessment/description. The qualitative information should include, as a minimum, the following:

- Warning
  - Type
  - Clarity
  - Margin
- Departure
  - Resistance (susceptibility)
  - Type
  - Severity
  - Ability of pilot to delay or prevent
    - Control action taken
    - Demands on the pilot
- Post-Departure Motion
  - Type of aircraft motion
  - Severity
- Recovery
  - Rapidity
  - Recovery controls
  - Demands
    - Ability to recognize
    - Ability to perform necessary control action

B. CONFIGURATION ASSESSMENTS

As noted previously, the goals were to validate the influence of the key aerodynamic coefficients in determining departure characteristics; evaluate the influence of varied maneuver-limiting factors on high AOA maneuvering control; and identify potential flying quality criteria in terms of departure resistance, warning, and severity for possible application to the flying quality specification. In this subsection, predicted vs. observed characteristics are reviewed and demonstrate that the above goals have been achieved, although there were some surprises in the process. The unaugmented airframe configurations will be assessed first, and then the augmented cases.

It is necessary to rely heavily on qualitative statements contained in the debriefing questionnaire and commentary taped on-line as the pilots talked themselves through the runs. The questionnaires were filled in only during the initial progression through the test matrix. At that time the pilots were "feeling out" the various configurations and produced voluminous commentary on each, covering the primary observations plus variations due to different control applications, techniques, rates of onset, tracking maneuvers, etc. The assessments reported in the following paragraphs have been distilled to the simplest possible factors consistent with the goals of the simulation.

Only assessments of the fighter test pilots are reported because RC and JF are most experienced in stall/departure/spin testing and were more observant of differences between configurations. It became apparent early in the data analysis that the two test pilots were employing almost opposite approaches to stall/departure. RC employed a cautious, slow increase in AOA and generally was able to detect subtle changes in vehicle stability or response characteristics. JF used an aggressive, rapid AOA increase which did not give time to detect such warnings. As a consequence, he generally pulled to a higher AOA with less speed bleedoff and obtained more severe post-stall gyrations (PSG). Thus, differences in pilot closed-loop control techniques produced a confounding influence which must be recognized before delving into other details: departure warning and severity are a function of pull-up rate and lateral-directional controls application immediately preceding departure.

1. Unaugmented Airframe

a. Configuration A_1

Predicted versus observed pre- and post-departure characteristics are shown in Table 10. The warning Pilot RC observed with increasing AOA is consistent with the graceful (gradual) degradation suggested by the open-loop dutch roll and roll numerator root migrations of Figure 55. It appears the negative C_{m_β} contribution was observed as a

TABLE 10. CONFIGURATION A_1 MANEUVER-LIMITING FACTORS

PREDICTED	OBSERVED	
	RC	JF
Warning: Wing rock ($16 < \alpha < 22$ deg)	Wing rock low amplitude, high frequency	None
Roll reversal ($\alpha > 18$ deg)	Roll reversal ($\alpha > 20$ deg); g-break (20-22 deg α)	None; g-break
	Wing rock large amplitude, low frequency	
Rating:	2.8	4.8
Departure: Nose slice ($\alpha > 22$ deg)	Nose slice followed by roll	Nose slice and roll
Post stall gyrations	Large yaw, pitch, roll oscillation and spin	Violent oscillations and spin
Severity Rating:	2.2	4.6
Departure/Spin Susceptibility (Weissman criterion): $\alpha < 21$ deg: mild or no departure	Release $\alpha \doteq 20$ deg; yaw initially slow, builds rapidly	
$21 < \alpha < 24$ deg: moderate rolling departure		Release $\alpha \doteq 23$ deg; abrupt nose slice, builds exponentially
$\alpha > 24$ deg: strong rolling departure, high spin susceptibility		
Rating:	Resistant	Extremely Susceptible
Comments:	Maneuvers tend to mask warning; not masked if pay attention	Most violent post stall gyration oscillations of any configuration

"g-break." The nose slice departure is as predicted, but the onset is noticed prior to $C_{n_{\beta_{dyn}}}$ becoming negative. Thus onset might be influenced by pilot control, and thus associated with negative $1/T_{\phi_1}$. Pilot RC considered the configuration departure resistant (R) because of ample warning and his tendency to initiate recovery at $\alpha \doteq 20$ deg where the Weissman criterion predicts mild or no departure. Pilot RC therefore gave fairly good high AOA ratings.

Pilot JF saw no warning except the "g-break." He obtained an abrupt nose slice and violent post-stall gyration (PSG). The tendency to flat spin may be due to the large negative C_{n_β} and small C_{ℓ_β} at his recovery initiation point and the further destabilizing influence of sideslip on the denominator and numerator roots, all of which portend high body-axis yaw rate and little roll. Inertia effects would tend to raise the nose and align the yaw rotational axis with the velocity vector —— a flat spin.

This configuration also exhibited violent oscillatory spin characteristics which could be reduced if a large nose-down pitch rate developed as the nose was slicing. This could be produced via forward stick coinciding with the "g-break." The resulting rq inertia cross-coupling produced a large roll acceleration and quite wild gyrations (e.g., Figure 75). Pilot JF noted this configuration to have the most violent PSG characteristics of any configuration and rated it extremely susceptible (ES) to departure.

While the Weissman criterion correctly predicted the spin susceptibility, the initial departure was in yaw rather than roll. The maneuver-limiting factors are the strong nose slice and spin characteristics. The causal factors are combined open- and closed-loop (roll) instabilities accompanied by signifcant negative C_{m_β}.

b. Configuration B

As predicted, this configuration is similar to Configuration A, but with less departure warning (see Table 11). The low-frequency yaw/roll oscillation that Pilot RC observed above 21 deg AOA is consistent with

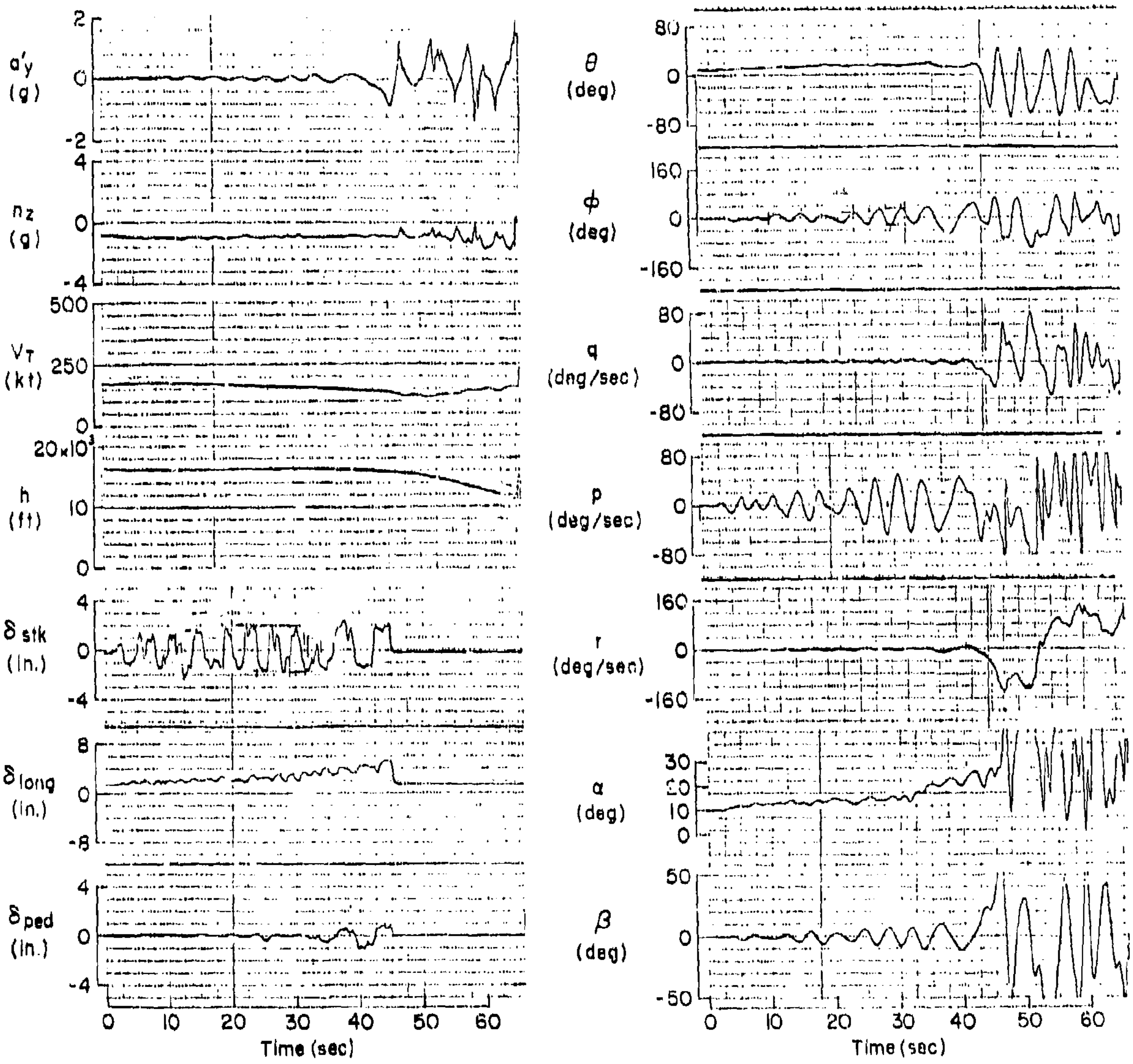

Figure 75. Configuration A_1 Departure and PSG from Wings Level Tracking Task; Pilot RC

TABLE 11. CONFIGURATION B MANEUVER-LIMITING FACTORS

PREDICTED	OBSERVED	
	RC	JF
Warning: Roll reversal ($\alpha > 18$ deg)	Resists roll command; g-break Low frequency yaw/roll 21 deg α	No warning
Rating:	4.2	4.8
Departure: Nose slice ($\alpha > 22$ deg)	Nose slice	Nose slice
Post stall gyrations	Violent roll reversal or spin	Severe and violent oscillation
Severity Rating:	2.7	4.5
Departure/Spin Susceptibility (Weissman Criterion) $\alpha < 21$ deg: mild or no departure	Release $\alpha \doteq 21$ deg; yaw followed by roll and pitch down	
$21 < \alpha < 24$ deg: moderate rolling departure		Release $\alpha \doteq 24$ deg
$\alpha > 24$ deg: strong nose slice, high spin susceptibility		Nose drift followed by roll; prone to flat spin
Rating:	Susceptible	Extremely Susceptible
Comments:	Cannot discern onset of departure; insidious	Low acceleration in nose slice

open-loop dutch roll dynamics (see Figure 57). The lower frequency resulted in less acceleration into the nose slice. Coupled with roll reversal, this apparently masks the departure onset. Although he initiated recovery at about the same AOA and thought the departure severity (pilot rating = 2.7) is about the same as Configuration A_1, he considered Configuration B to be departure susceptible (S) because of the poor warning (PR = 4.2). Pilot JF could see little difference between A_1 and B except the increased tendency to flat spin due to the combined high aerodynamic roll rate damping and strong directional divergence. He again rated it extremely susceptible (ES).

This configuration exhibited all anticipated flying characteristics. The Weissman criterion correctly identified departure and spin severity but not type. Again, the maneuver-limiting factors are the severe nose slice and flat spin tendencies. The causal factors are the open- and closed-loop directional instabilities aggravated by high negative C_{ℓ_p}.

c. Configuration C_1

Configuration C_1 (Table 12) with positive dynamic stability (due to large negative C_{ℓ_β}) had a much greater tendency to develop roll oscillations. Both pilots noted that any lateral control input excited wing rock and produced a tendency to lateral PIO. Since this sensitivity persisted over a wide AOA range, it was not considered a warning but actually a masking of departure onset. Both pilots considered the warning to be poor (PR > 4).

This configuration is stable open-loop and driven unstable and into departure by closing the attitude loops. Departure characteristics are less consistent (predictable) because the nature of departure depends upon pilot control activity. It exhibited at least two and possibly three different types of departure onset, which further aggravated the poor warning. The lateral phugoid mode could contribute the additional departure mode (see Figure 59). One pilot detected more tendency to yaw and the other more tendency to roll. However, they generally were in

TABLE 12. CONFIGURATION C_1 MANEUVER-LIMITING FACTORS

PREDICTED	OBSERVED	
	RC	JF
Warning: Wing rock ($16 < \alpha < 26$ deg)	Wing rock: any disturbance	Wing rock: tendency to low frequency pilot-induced oscillation
Roll reversal ($\alpha > 18$ deg)	Low frequency, high amplitude oscillation masks departure	
Rating:	4.3	4.0
Departure:		Two distinct types:
Roll departure	Nose slice	a) roll, little yaw;
Post-stall gyrations	Roll	b) yaw, followed by roll
Severity Rating:	1.6	3.7
Departure/Spin Susceptibility: (Weissman Criterion) $\alpha < 21$ deg: no departure		
$\alpha > 21$ deg: mild rolling departure, low spin susceptibility	Release $\alpha \triangleq 32.5$ deg, nose slice and roll	Release $\alpha \triangleq 25.5$ deg, milder departure, oscillatory spin
Rating:	Susceptible	Susceptible
Comments:	Takes time to see yaw is not going to stop	Not prone to flat spin

closer agreement for this configuration concerning warning, nature, and severity of and susceptibility to departure, probably due to the positive dynamic stability which prolonged the time period the airplane could be maintained under semi-control. Thus, both pilots had sufficient time to observe its high AOA characteristics fully before closed-loop instability predominated.

Both pilots considered the departure and PSG severity to be somewhat less than for either A_1 or B. The configuration was spin-prone, but spins were generally highly ocillatory with some possibility of recovery. It was not prone to flat spins. Departure and spin characteristics and susceptibility are in agreement with the Weissman criterion.

The initial or basic maneuver-limiting factor is the strong wing rock tendency which extends from relatively low AOA through departure and is aggravated by closed-loop instability (roll PIO). Departure is a secondary factor. Warning may also be adversely influenced by the low-frequency, large-amplitude, lateral phugoid oscillation.

d. Configuration D

This configuration (Table 13) had less directional instability but did have sideslip-induced pitch-up. The expected wing-rock tendency from a lightly damped dutch roll was not observed by either pilot. Both noted departure onset as a slow, persistent yaw (nose slice) accompanied by mild roll reversal and pitch-up. The onset was sufficiently mild that departure was semi-controllable throughout the achievable AOA range. A poor departure warning rating (PR > 3.5) resulted.

Open- and closed-loop instability parameters (ω_d^2 and ω_ϕ^2 or $C_{n_{\beta_{dyn}}}$ and LCDP) are small for this configuration and lead to sloppy control and low-frequency wallowing which masks departure. At the same time, the wallowing does not generate sufficiently rapid motion to excite inertia cross-coupling and PSG. All pilots tended to continue fighting to maintain control well past full stall, incurring excessive altitude loss. However, if controls were released at any time the aircraft would immediately go into a nose-low spiral and recover by itself.

TABLE 13. CONFIGURATION D MANEUVER-LIMITING FACTORS

PREDICTED	OBSERVED	
	RC	JF
Warning:		
Wing rock ($16 < \alpha < 26$ deg)		
Roll reversal ($\alpha > 20$ deg)	Yaw, roll reversal, pitch up Sloppy control, large θ and ϕ overshoots mask departure	Large definite yaw followed by reversal and pitch up
Rating:	4.0	3.5
Departure:		
Pitch up	Nose slice/pitch up	Nose slice/pitch up
Post stall gyration	None, never spin	Mild, no spin
Departure/Spin Susceptibility (Weissman Criterion):		
All α: no departure	Release $\alpha \triangleq 27.6$ deg, slow nose slice, pitch up, some roll	Release $\alpha \triangleq 27.6$ deg; slow consistent nose slice, roll, departure nose high
Rating:	Resistant	Resistant
Comments:	Do not like pitch up at departure; cannot get nose down	Always recoverable if release controls

Departure warning was considered poor (e.g., 4.0) by RC because of the wallowing, but at the same time the configuration was considered departure resistant (R). Pilot JF assessed it as resistant primarily because it would not spin. Pilot RC's principal objection to this configuration was the positive C_{m_β}. Even though it eliminated the severe pitch-down in nose slice and the resulting inertia-coupled PSG exhibited by other configurations, he did not like the nose rising, no matter how mildly, when in or near departure conditions.

The maneuver-limiting factor for this configuration is the wallowing —– a general insensitivity to or sloppiness of response to pilot control inputs <u>prior</u> to the departure AOA. The key causal factors are considered to be the relatively small ω_d^2 (due to small C_{n_β} and C_{ℓ_β}) which produces very low DC gain in the roll frequency (Bode) domain and positive C_{m_β} which apparently contributed to overcontrol in pitch.

e. Summary

The intended high AOA departure characteristics were obtained in the four unaugmented airframe configurations. The results demonstrated the influences that changes in the six key aerodynamic coefficients can have on departure warning, severity, and susceptibility. The susceptibility of Configuration C_1 to departure was somewhat revealing: the open-loop parameter $C_{n_{\beta_{dyn}}}$, by itself, is not a sufficient indicator of departure resistance. However, when combined with the closed-loop parameter LCDP (or ω_ϕ^2), the two are quite accurate indicators of departure susceptibility and severity as advanced by Weissman.

Departure severity also appears influenced by the static cross-coupling derivatives $\mathcal{L}_{\dot{\alpha}}$, $N_{\dot{\alpha}}$, and M_β. Severe departure and PSG were obtained for the two configurations in which combinations of these derivatives shifted lateral-directional denominator and numerator roots into the right half-plane of the root locus plot with $\beta \neq 0$ (Figures 55 and 57). Less severe departure was obtained for combinations which primarily shifted numerator roots into the right half-plane (Figure 59), and the mildest departure was obtained for combinations which produced very little shift of lateral denominator and numerator roots with sideslip (Figure 61). The literal approximate factors developed in Section III indicate that the small shifting is due to the combined influence of small N'_{δ_a} and positive M_β. However, the nose rise associated with large positive M_β was disconcerting to one pilot.

The simulation results also demonstrated that wing rock or lateral PIO is not a satisfactory warning of impending departure if there is sufficient elevator power to pull through the warning region rapidly or if the AOA range in which it occurs is too wide.

2. Augmented Airframe

a. Configuration A_2

The flight control augmentation was configured to provide a high level of roll rate damping, and to improve roll maneuvering response via roll rate command (p_c) and reduced adverse aileron yaw (SRI). This augmentation was also expected to eliminate all cues of impending departure. The departure was anticipated to be a strong nose slice due to increasingly negative C_{n_β} as AOA increased and, once sideslip started to build, it was expected that the characteristics would be very similar to those of Configuration A_1.

Results summarized in Table 14 for Pilot JF are very much as anticipated. However, Pilot RC detected a pre-nose-slice resistance to roll commands (at AOA above approximately 21 deg) when attempting to track the maneuvering target. This resistance was observed only during the initial tracking sets and resulted in the pilot's neutralizing all controls before the directional instability became severe (rating 1.8). The second set of tracking runs were done more hurriedly, the warning was not obtained (rating 4.3), and more severe departures ensued (rating 3.7). The susceptibility assessment as resistant (R) by Pilot RC was given only on the initial set of runs.

The maneuver-limiting factor for this configuration is the nose slice. But, since there is no warning, an AOA limit would have to be set to provide a safety margin against inadvertent departure. The key

TABLE 14. CONFIGURATION A_2 MANEUVER-LIMITING FACTORS

PREDICTED	OBSERVED	
	RC	JF
Warning: None	Resists ϕ_c above 21 deg α Clear warning with target	None
Rating:	2.8 (4.3 on reruns)	4.8
Departure: Nose slice	Nose slice	Nose slice Roll and severe PSG
Severity Rating	1.8 (3.7 on reruns)	4.5
Departure/Spin Susceptibility $\alpha < 23$ deg: no departure		
$\alpha > 23$ deg: nose slice and revert to Configuration A_1 characteristics	Release $\alpha \hat{=} 25$ deg; smooth, slow yaw followed by roll	Release $\alpha \hat{=} 32$ deg; exponential yaw divergence tendency to flat spin
Rating:	Resistant	Extremely Susceptible
Comments:	Depart without pilot aware; only cue is resistance to ϕ_c against target	Easier to fly Rate of yaw dependent upon $\dot{\alpha}$ or g

causal factors are the strong static directional divergence and the elimination of departure warning by the augmentation system.

Time traces of a Configuration A_2 departure from a wings-level pull-up are shown in Figure 76. The lateral stick trace reflects about the same activity prior to departure as in Figure 75 but far less sideslip and roll oscillation. After pilot neutralization of controls, the augmentation loops continue to deflect the lateral and directional control surfaces and apparently aid recovery (again compare with Figure 75). Interestingly, the actual departure and PSG motions of Figure 76 are remarkably similar to Reference 38 flight traces for the F-4E with augmentation systems on (Figure 77). Prior to departure the traces of the two figures are not comparable because the stick to rudder interconnect in the simulation reduced sideslip excitation and provided better roll attitude control.

b. Configuration C_2

Based on the positive $C_{n_{\beta_{dyn}}}$ and improved ω_ϕ^2 (or LCDP), this augmented configuration was expected to have the best high AOA flight characteristics and little or no departure tendency. It did allow both pilots to consistently maintain control to higher AOA than did any other configuration, though abrupt nose slice departures were common (Table 15). In this case the roll damper countered the C_{ℓ_β} dynamic stability contribution and allowed the large negative C_{n_β} static instability to predominate. The aircraft responses by themselves provided no warning of impending departure, although Pilot RC was able to extract some low-frequency PIO cues with respect to the target aircraft. He rated the configuration departure resistant (R) because of this cue and the mild (to him) nose slice motion. Without the target he rated the configuration departure susceptible (S), as did Pilot JF.

This configuration was also spin-prone and, similar to C_1, exhibited two distinct spin modes as noted in Table 15. It appeared to be more prone to spin flat than was the unaugmented configuration (C_1), because the roll rate CAS automatically opposed any uncommanded roll.

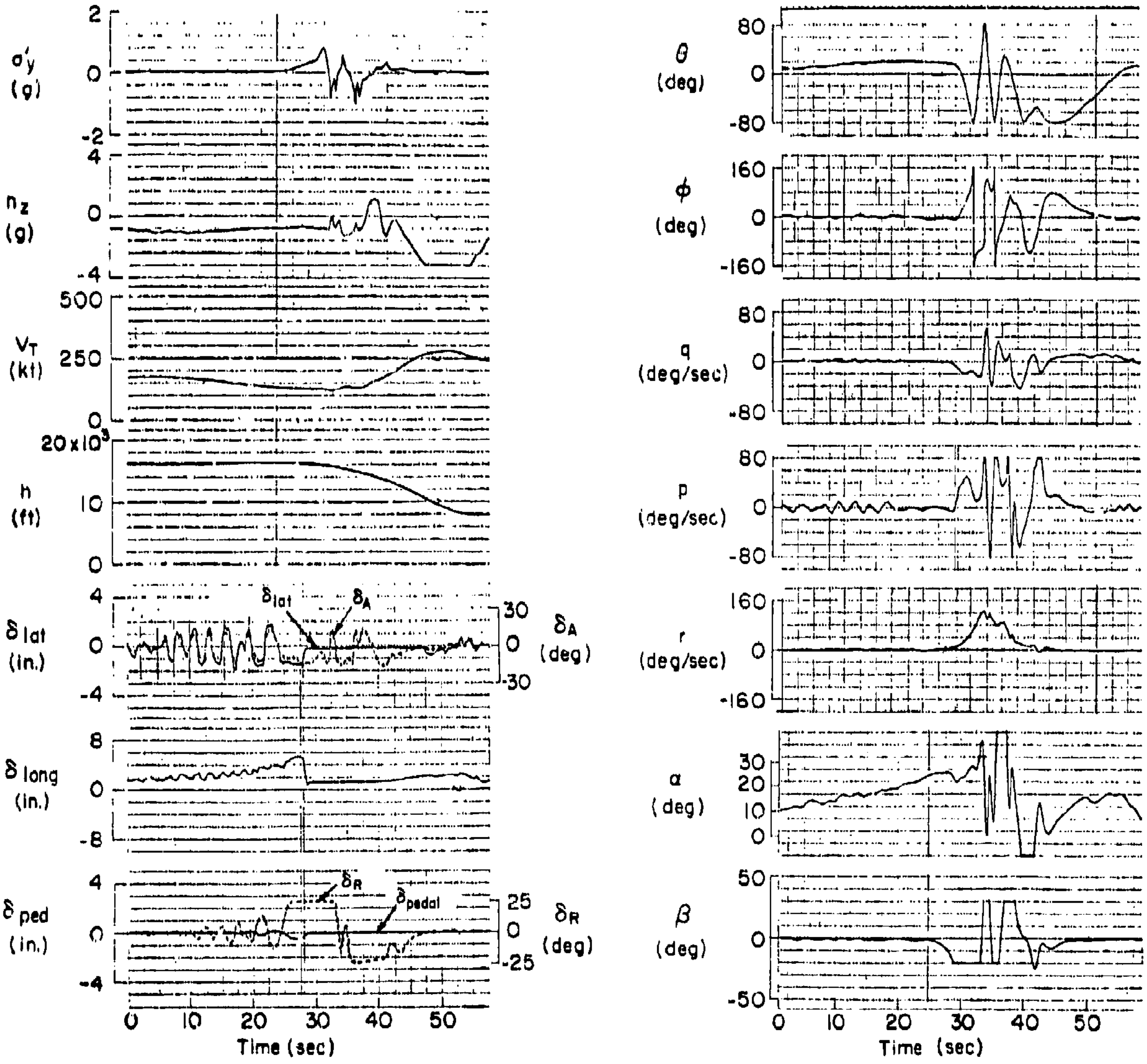

Figure 76. Configuration A_2 Departure and PSG from Wings Level Tracking Task; Pilot RC

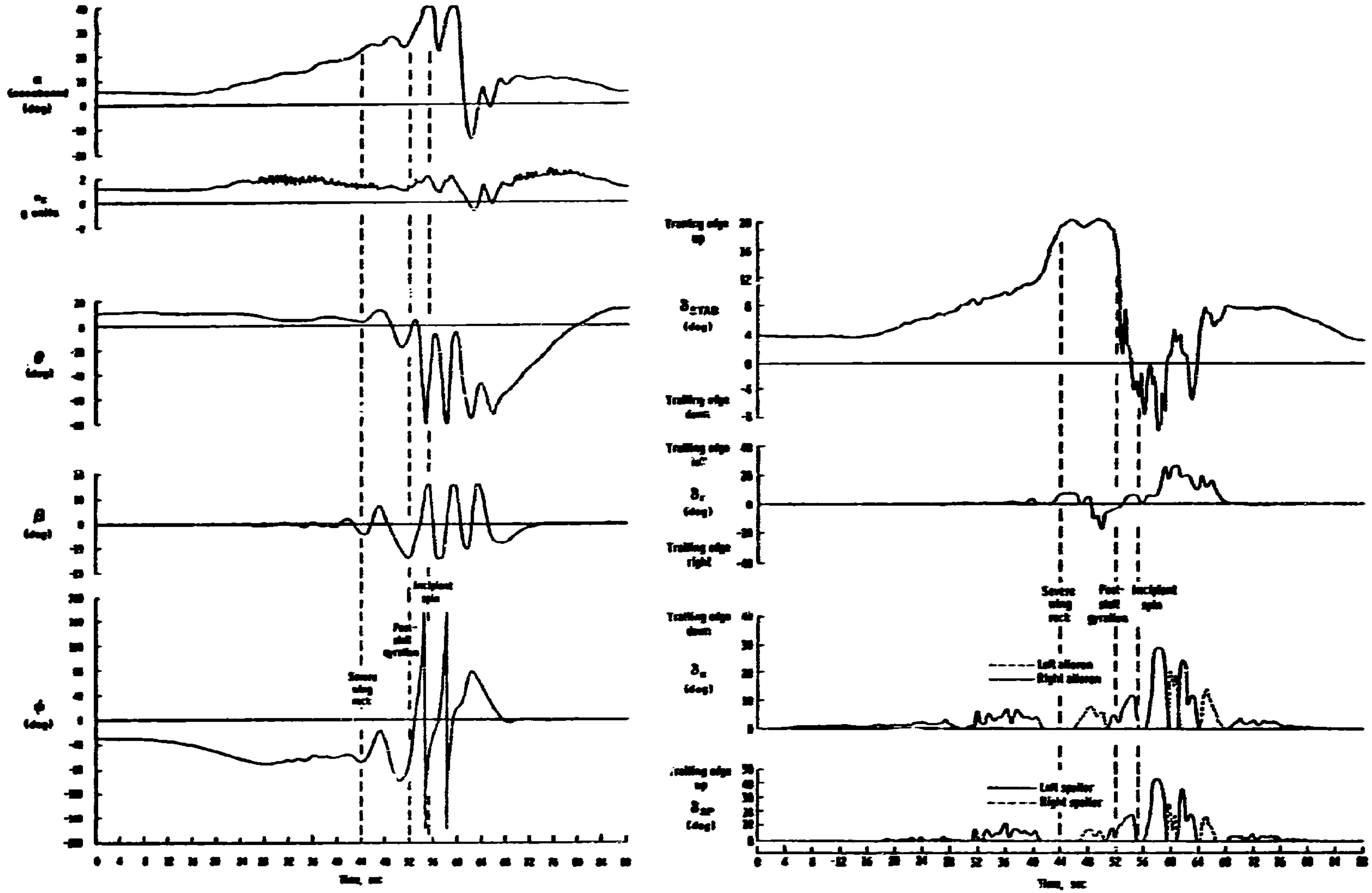

Flight Variables

Control-Surface Deflections

Figure 77. Typical F-4E Roll Departure/Spin Entry

TABLE 15. CONFIGURATION C_2 MANEUVER-LIMITING FACTORS

PREDICTED	OBSERVED	
	RC	JF
Warning: None	Low frequency pilot-induced oscillation; g-break	None, very steady
Rating:	3.2	4.8
Departure: None	Nose slice followed by roll and pitch down	Abrupt nose slice
Severity Rating:	1.5	3.8
Departure/Spin Susceptibility: Resistant	Release $\alpha \doteq 31$ deg; slow nose slice; almost always spin	Release $\alpha \doteq 30$ deg; abrupt nose slice; two spin modes: a) oscillatory (recoverable) b) flat (nonrecoverable)
Rating:	Resistant	Susceptible
Comments:	Resistant because target gives cue; without target is Susceptible	Better flying qualities prior to departure

The maneuver-limiting factor for this configuration is the nose slice departure. The positive $C_{n_{\beta_{dyn}}}$ and ω_ϕ^2 throughout the achievable AOA range did allow it to be controlled to considerably higher AOA than the other configurations. In this respect it was less susceptible to departure. However, at the higher AOA directional instability eventually required full opposing rudder deflection, which was immediately followed by departure.

c. Overall Assessment

The augmented flight control system designed to enhance characteristics in normal flight improved pre-departure control precision, reduced departure warning, and increased the tendency to flat spin. The roll rate CAS and the SRI together improved lateral-directional control, which allowed higher AOA to be reached before sideslip became significant. The major portion of this benefit derived from the SRI. For Configuration C_2 the roll rate damper suppressed the $\mathcal{L}'_\beta \beta$ contribution to dynamic stability and thus increased the nose-slice departure and flat spin tendencies. Thus, this augmentation function actually degraded high AOA characteristics.

C. SUMMARY

The intended high AOA departure characteristics were obtained in the four bare-airframe and two augmented configurations. The results demonstrate the strong influence changes in the six key aerodynamic coefficients ($\mathcal{L}'_\alpha$, $\mathcal{L}'_\beta$, $\mathcal{L}'_p$, N'_α, N'_β, and M_β) can have on departure warning, severity, and susceptibility. The simulation plus literal approximate factors of Section III show:

- The most violent departure characteristics and flat spin tendencies to be associated with large negative N'_α, N'_β, and M_β.
- The least violent departure characteristics and greatest spin resistance to be associated with small to moderate negative N'_α and N'_β and positive M_β.

- The tendency to inconsistent departure/spin characteristics (possibly several modes) to be associated with positive $C_{n_{\beta_{dyn}}}$ brought about by large negative C_{ℓ_β} and continued large adverse yaw (ω_ϕ^2, LCDP).

However, the observed high AOA stall, departure, and spin dynamic characteristics also depended significantly on pilot control technique. This is consistent with actual flight experience in which it has been observed, for example, that spin characteristics and recovery techniques can be quite different, depending upon the maneuver from which the spin occurred.

The final high AOA departure/spin rating scale of Figure 73 was accepted and supported by the pilots. Results of this first application showed consistent reflection of both the airframe dynamic characteristics and any sensitivity to difference in piloting technique. However, the ratings must be accompanied by detailed qualitative description of the characteristics observed, i.e., what is being rated.

In this vein, it might be noted that there are some differences between ratings for the initial familiarization and tracking runs reported in Subsection B and for the final tracking runs reported in Subsection A. These are due to several factors. First, Pilot RC was working with the original open-ended scale (Figure 72) during the initial runs and the closed-ended scale (Figure 73) during the reruns; Pilot JF used the close-ended scale for both sets of runs. Second, during the first sequence of runs Pilot RC was unhurried in investigating the characteristics of each configuration. However, for the repeat runs he was under some pressure to complete the series of maneuvers and configurations within time constraints. Thus, the rate at which he approached stall/departure was more rapid and this influenced his assessment of warning and motion severity, as demonstrated in Table 16. The greatest differences are for the augmented flight control configurations, where RC saw considerably less warning and more severe departure during the reruns. Results for JF, shown for comparison, reflect quite consistent ratings between the sets, since he always used a rapid pullup technique.

TABLE 16

COMPARISON OF PILOT RATINGS, INITIAL VS. RERUNS

CONFIGURATION	RC				JF			
	WARNING		MOTION SEVERITY		WARNING		MOTION SEVERITY	
	INITIAL	RERUN	INITIAL	RERUN	INITIAL	RERUN	INITIAL	RERUN
A_1	2.8	2.9	2.2	3.0	4.8	5.0	4.6	4.3
B	4.2	3.9	2.7	3.1	4.8	4.6	4.5	4.8
C_1	4.3	3.6	1.6	2.0	4.0	4.6	3.7	3.9
D	4.0	3.8	3.5	3.0	3.5	3.7	1.5	2.9
A_2	2.8	4.3	1.8	3.7	4.8	5.0	4.6	4.5
C_2	3.2	4.2	1.5	2.7	4.8	4.1	3.8	3.9

SECTION VII

DEPARTURE SUSCEPTIBLITY CRITERION

Pitch control techniques and aggressiveness had obvious influences on the departure warning and susceptibility assessments shown in the previous section. When asked about specific cues and personal criteria which would prompt the pilot to acknowledge departure and therefore to initiate recovery, vague answers were obtained, e.g., "persistent or continued uncommanded roll or yaw" or "sudden, rapid uncommanded motion — somewhere around 20-30 deg/sec." However, detailed scrutiny of the time traces failed to reveal correlation between release of back stick and various motion quantities (p, r, $\dot{\phi}$, $\dot{\psi}$, β, etc.). These quantities were always changing rapidly and timing became a big factor. Deviations of fractions of a second in initiating recovery (or reading the traces) produced a large variation in the motion amplitudes (e.g., see Figures 57 and 58). The greatest correlation was found in AOA itself — possibly because its rate of change was the slowest of all and therefore could be read and correlated with the greatest accuracy with what the pilots saw.

Since the piloting task required closed-loop attitude control, and there was considerable evidence of LCDP or ω_{ϕ}^2 being a key parameter, attention was turned to the possibility of a closed-loop criterion. A simple analysis of theoretical roll loop stability was found to agree quite well with frequencies, damping ratios, and divergences obtained from the time traces. Furthermore, the results corroborated the differences in pilot techniques and observed warning reported in the previous section.

This section summarizes the relationship obtained between the closed-loop analysis and the piloted simulation time traces and presents a closed-loop criterion which is consistent with and explains the seemingly diverse departure susceptibility assessments given by the two Air Force test pilots.

A. CLOSED-LOOP ANALYSIS

The lateral stick time trace of Figure 57 (Configuration A_1) is typical of most runs for Pilot RC. The phasing between ϕ excursions and stick deflections indicates little, if any, lead being generated during the PIO at $\alpha = 16$ deg and above. Therefore, the simple block diagram of Figure 78 was chosen to model the unaugmented airframe, control system, and pilot. A Bode-root locus closed-loop survey plot for Configuration A_1 at $\alpha = 16$ deg and $\beta = 0$ deg is presented in Figure 79. Closed-loop gains and frequencies obtained from strip chart recordings of simulation runs for Pilot RC are shown on the Bode amplitude plot by the several horizontal lines (K_ϕ) and tic marks (–+–). [For example, at 16 deg AOA the traces of Figure 57 show a pilot gain $K_\phi \doteq 4.5$ (13 dB) and frequency $\omega \doteq 1.8$ rad/sec.] The frequency of the undamped oscillation obtained from the strip chart is in remarkable agreement with the frequency for 180 deg phase of the analytical predictions, validating the assumptions that this pilot is adopting neither lead nor lag in attempting to control roll attitude. Rather, he is merely reacting with a normal time delay with stick proportional and opposite to bank angle excursions.

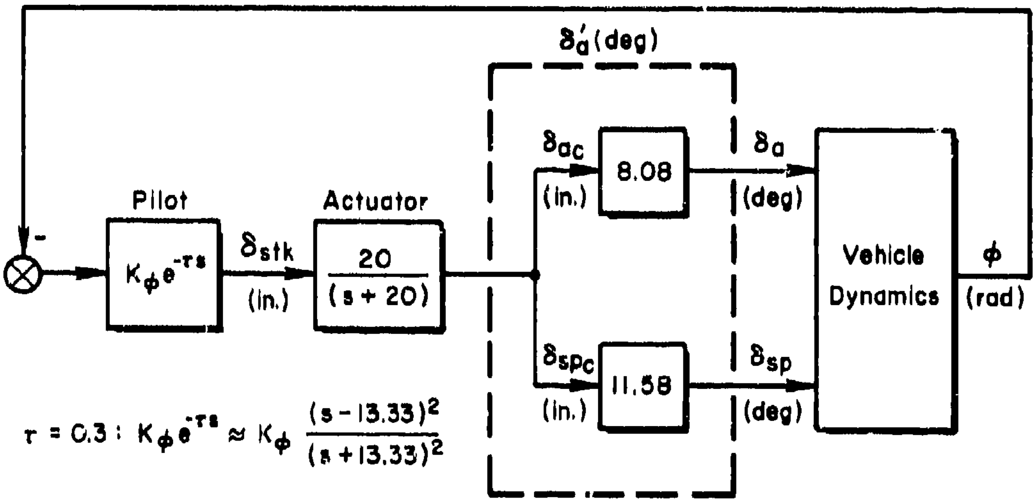

Figure 78. Assumed Pilot Lateral Loop Closure; $\phi \rightarrow \delta_{stk}$

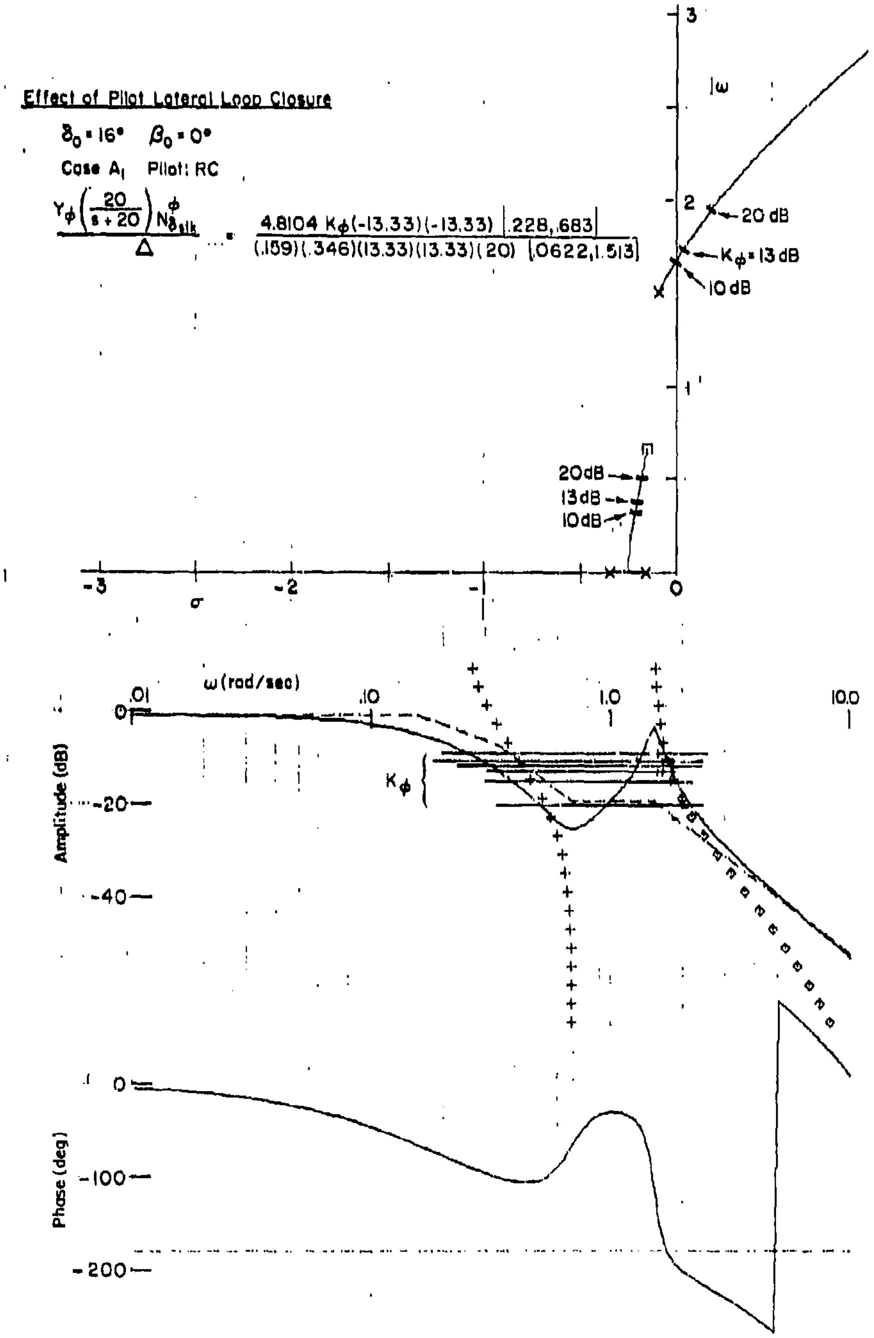

Figure 79. Survey Plot for Roll Loop Closure; $\alpha_o = 16$ deg, $\beta_o = 0$ deg

The measured gains range from about 10 to 20 dB. This variation, identified on the root locus plot of Figure 79, indicates but small influence on dutch roll divergence. The 13 dB gain point indicates a mild divergence which is also in agreement with the traces of Figure 57 at 16 deg AOA.

As AOA is increased in Figure 57, the lateral stick amplitude remains fairly constant but the ϕ excursions increase. Thus, the loop gain (K_ϕ) decreases slightly, the oscillation period increases to about 6 seconds ($\omega \doteq 1$ rad/sec), and a yaw rate divergence develops. Again, a closed-loop survey plot for $\alpha = 23$ deg (Figure 80) shows excellent agreement, i.e., $\omega_d' \doteq 1$ rad/sec and a first-order spiral divergence of $T_s' \doteq 2$ sec which results from the spiral mode being driven toward the RHP zero $1/T_{\phi_1}$.

Similar trends were obvious from Pilot RC run traces for most configurations. He appeared to be following the neutral stability boundary of the oscillatory mode and initiating recovery when the first-order divergence mode exceeded some as yet unidentified divergence rate. Therefore, using the same pilot model, the maximum K_ϕ boundary for stable modes was calculated and plotted as shown in Figure 81. This shows two boundaries. The upper is the gain not to be exceeded at $\beta = 0$ and the lower is the reduced limit gain for $\beta = 5.5$ deg. To the right (higher AOA) of either boundary a lateral or directional instability exists and if AOA is increased K_ϕ must be decreased to maintain stability.

The roll loop gains employed by both pilots were determined from the time traces and located on similar stability boundary plots drawn for each vehicle configuration. Figure 82 is the plot for Configuration A_1 again, but now showing gain bands for each pilot. The band for RC shows that he tended to keep his gain within 10 dB above the maximum stable boundary and to decrease his gain as AOA was increased. On the other hand, JF started with a lower gain and tended to keep it constant during the pull-up.

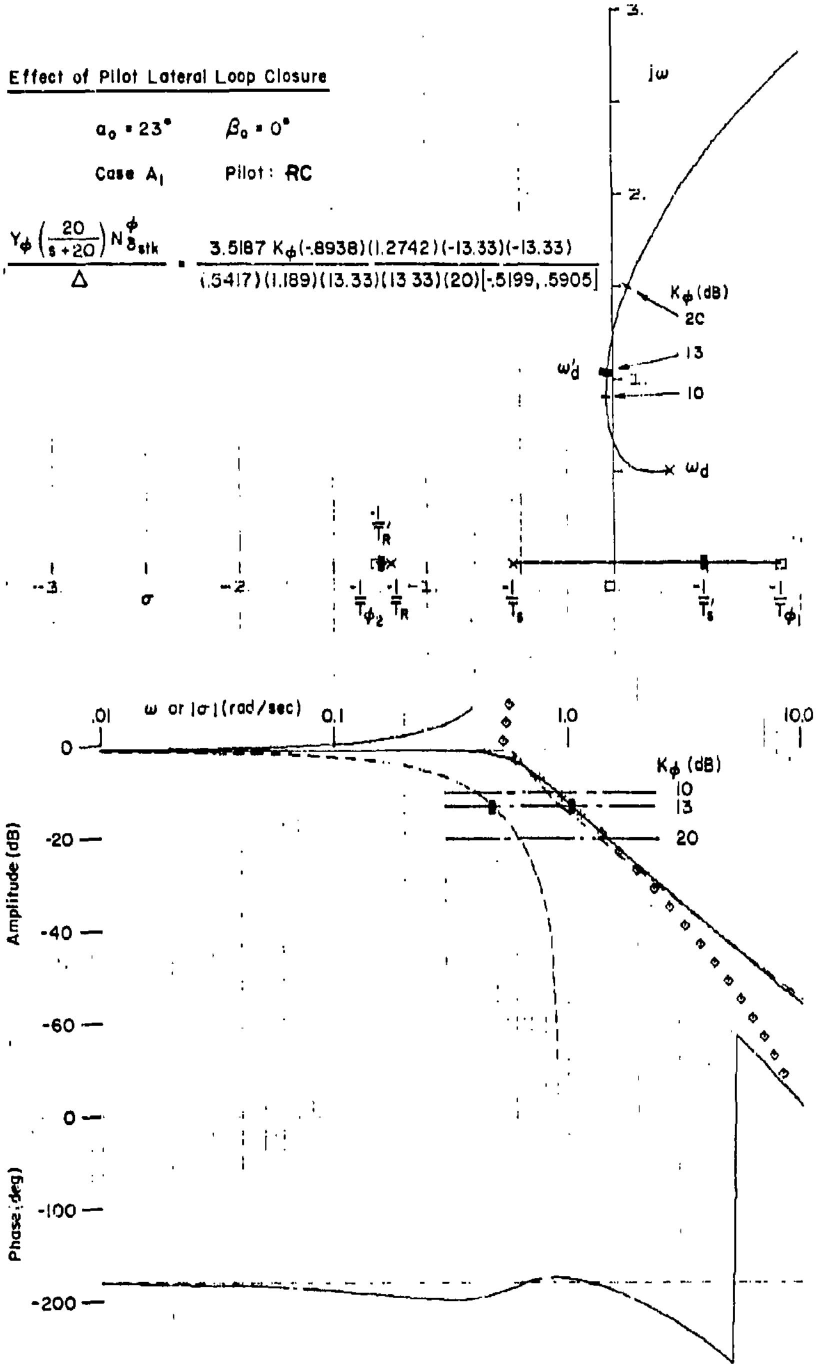

Figure 80. Survey Plot for Roll Loop Closure; α_0 = 23 deg, β_0 = 0 deg

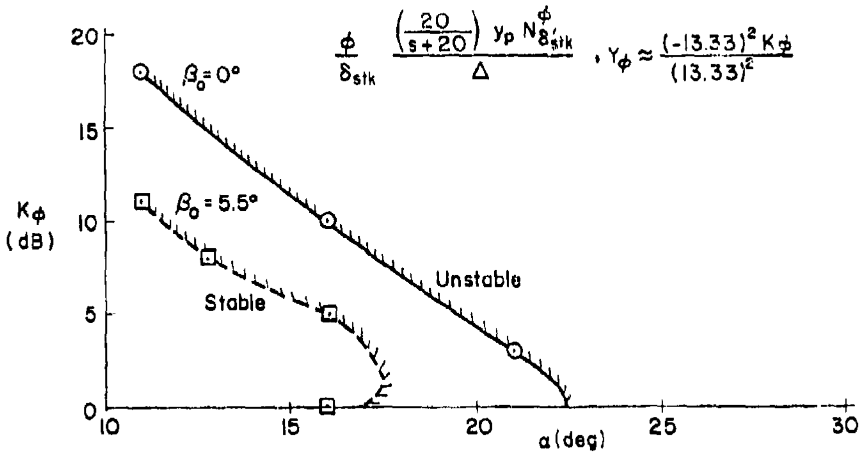

Figure 81. Maximum Pilot Gain for Stable $\phi \rightarrow \delta_{stk}$ Closure; Configuration A_1

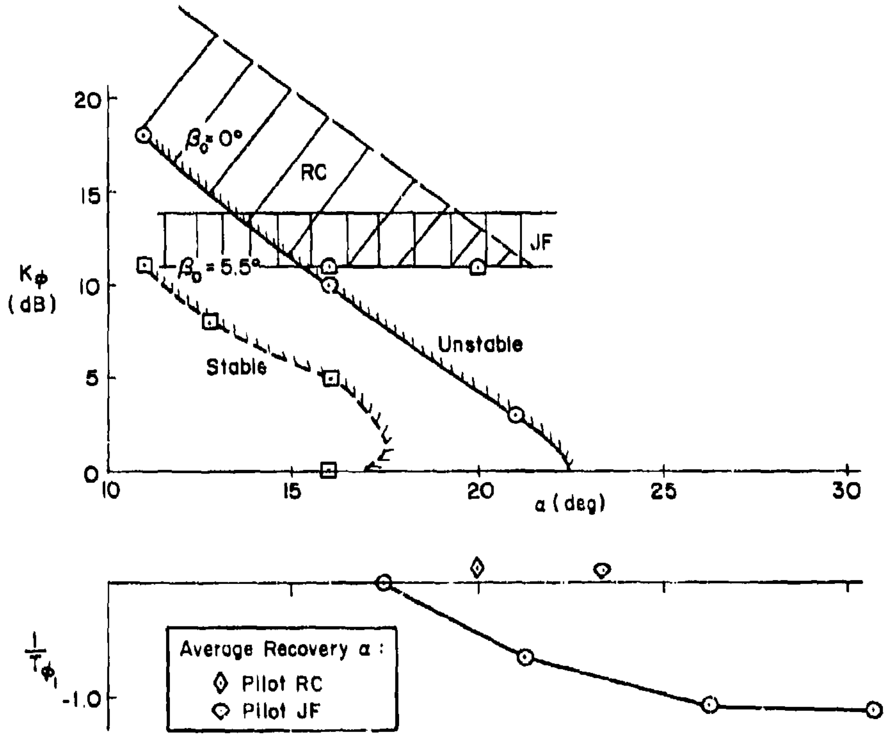

Figure 82. Roll Loop Closure Gains Employed with Configuration A_1

Figure 83 is the gain plot for Configuration A_2. Again JF used a lower, constant gain while RC tended to follow the stability boundary until the sudden drop. Figure 84 is the plot for Configuration C_1, showing results similar to those for Configuration A_1. This configuration is somewhat unusual in that a second stable region exists for $\beta \neq 0$ at very high AOA. Figure 85 for Configuration C_2 is similar to Configuration A_2 except there is no dropoff in stability boundary at high AOA. The results for Configuration D (Figure 86) are consistent: Pilot RC followed the stability boundary and hence should detect departure onset; Pilot JF used a lower, constant gain which suddenly crosses the boundaries as AOA is increased. He therefore obtained little warning. The plot for Configuration B is presented in Figure 87. This vehicle is so well damped in roll that it was difficult to obtain the necessary data from time traces except for one run by RC.

At the bottom of Figures 82-87 negative values of the open-loop roll numerator root $1/T_{\phi_1}$ are plotted versus α (at $\beta = 0$). Figure 85 does not show this extra plot because ω_ϕ^2 is positive to $\alpha > 35$ deg for this configuration. Also identified on each plot is the average AOA at which recovery was initiated by Pilots RC (◇ symbol) and JF (○). It will be noted that:

- In most instances a decrease in the K_ϕ boundary is related to $1/T_{\phi_1}$ becoming negative (RHP zero).
- In all but one case recovery is initiated by both pilots after exceeding the K_ϕ boundary and experiencing negative $1/T_{\phi_1}$ (the only exception is Configuration C_2 for which the numerator roots always lie in the LHP and there is no dropoff in K_ϕ).
- Pilot RC always employs higher roll loop gain, always follows the K_ϕ boundary, and generally initiates recovery at lower AOA. However, for Configurations C_1 and C_2 he did explore higher AOAs before recovery.
- Pilot JF tended to adopt a lower roll loop gain and kept it constant during his more rapid (aggressive) pull-up. He generally saw little or no warning and penetrated further into instability regions before initiating recovery.

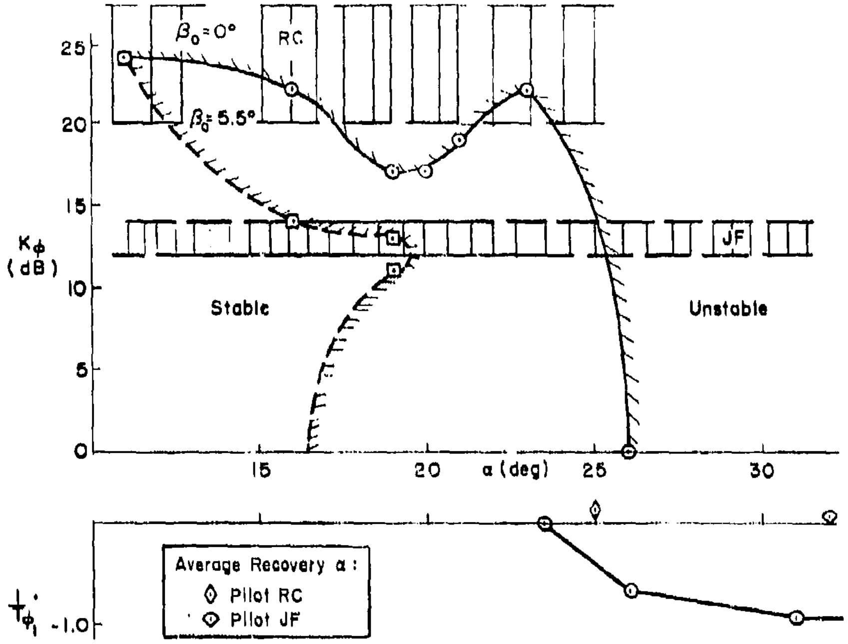

Figure 83. Roll Loop Closure Gains Employed with Configuration A_2

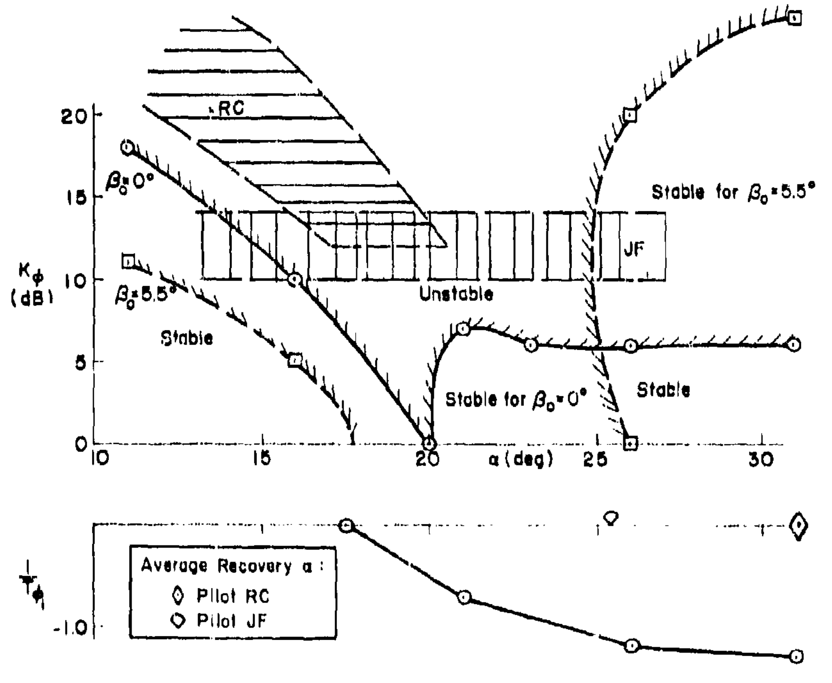

Figure 84. Roll Loop Closure Gains Employed with Configuration C_1

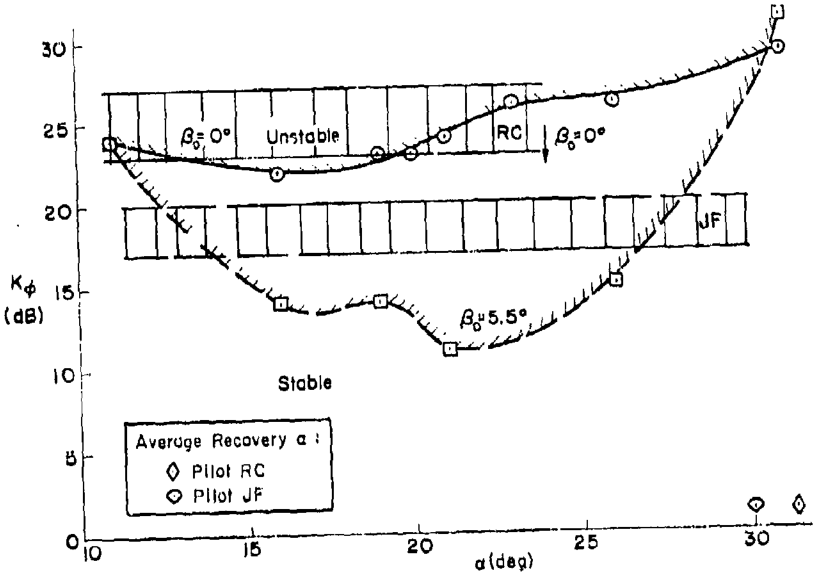

Figure 85. Roll Loop Closure Gains Employed with Configuration C_2

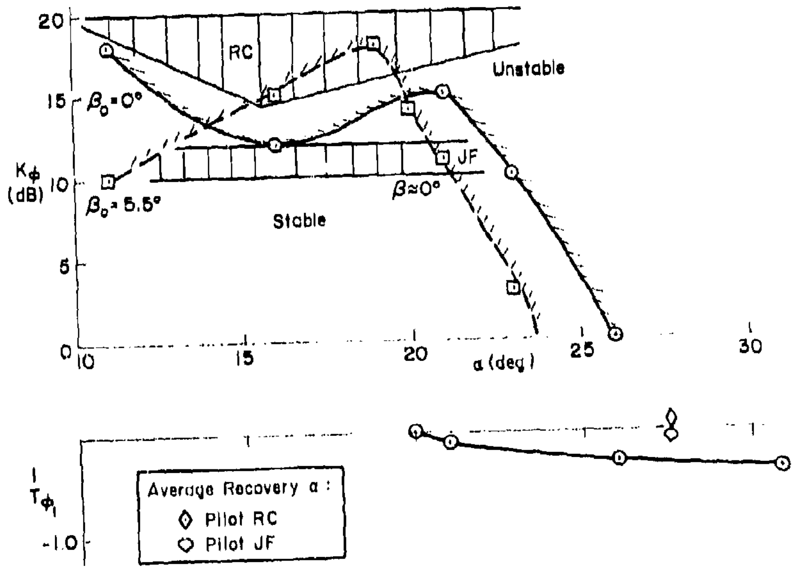

Figure 86. Roll Loop Closure Gains Employed with Configuration D

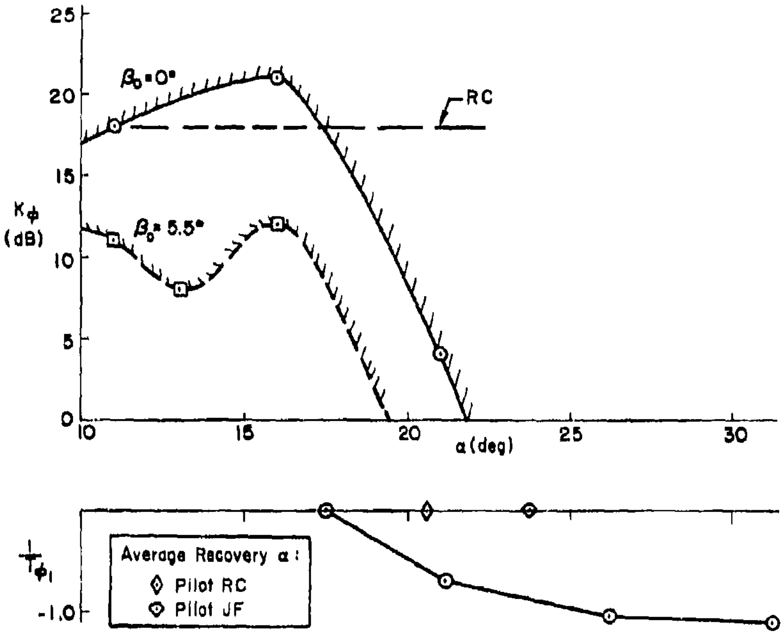

Figure 87. Roll Loop Closure Gain Employed with Configuration B

The foregoing observations appear to form the basis for each pilot's definition of departure susceptibility (cf. Section VI):

RC: Departure resistant (R) if warning is clear and consistent

Departure susceptible (S) if warning is unclear, masked, or inconsistent

JF: Departure resistant (R) if always recovered

Departure susceptible (S) if sometimes recovered

Departure extremely susceptible (ES) if never recovered

Thus each pilot is viewing different aspects of the departure. Fortunately, this difference serves to increase the information potential of the simulation program. This is probably typical of flight test, and indicative of why such stall/spin programs should be flown by more than one pilot.

B. POSSIBLE DEPARTURE SUSCEPTIBILITY CRITERIA

A comparison between departure/spin susceptibility predicted by the Weissman criterion and the assessments provided by the two pilots is shown is Table 17. Assessments substantially in agreement with prediction are shown in boxes. Obviously the aggressive pilot observed the worst possible characteristics of each unaugmented configuration as predicted by the criterion. The less aggressive pilot experienced something quite different. As noted previously, the criterion does not lend itself to prediction of the frequency-dependent augmented airframe charcteristics, but these configurations were expected to be less susceptible to departure. This influence was observed only by the less aggressive pilot.

TABLE 17

COMPARISON OF PREDICTED AND ACTUAL DEPARTURE SUSCEPTIBILITY ASSESSMENTS

DEPARTURE SUSCEPTIBILITY			
CONFIGURATION	PREDICTED	RC	JF
A_1	ES	R	$\boxed{\text{ES}}$
B	ES	S	$\boxed{\text{ES}}$
C_1	S	$\boxed{\text{S}}$	$\boxed{\text{S-ES}}$
D	R	$\boxed{\text{R}}$	$\boxed{\text{R}}$
A_2	NA	R	ES
C_2	NA	R	S

R = Resistant
S = Susceptible
ES = Extremely susceptible
NA = Not applicable

One important difference between prediction and simulation was the nature of departure. Figure 63 predicts predominantly rolling departure with no indication of yaw departure. Our Configurations A, B, and D exhibited initial yaw excursions sometimes followed by roll. Configuration C exhibited two or even three different departure modes which were dependent upon control application at onset of departure. However, a rolling type motion did predominate. Thus, the Weissman criterion was not as useful in predicting the nature of departure observed by the pilot.

The closed-loop analysis to identify causal factors behind the widely differing pilot ratings for departure/spin susceptibility produced a strong relationship between pilot ratings <u>for both pilots</u> and penetration of the roll numerator into the RHP. Figure 88 shows the value of the real part of the numerator root at the instant the pilot decided he had departed, or was about to depart, and initiated recovery. These values are plotted against the AOA at which recovery was started. (Note this is <u>not</u> the usual root locus $j\omega$ axis.) The points represent all six vehicle configurations as evaluated by both pilots.

The division between departure-resistant (R) and susceptible (S) ratings is seen to lie at roughly −0.5 rad/sec. This corresponds to a time to double amplitude of approximately 1.4 sec. Zeros which lie to the left of this line apparently limit the first-order divergence to a rate slow enough for pilots to respond and recover. Zeros to the right of the line apparently allow divergence rates so fast that the pilots cannot prevent departure. Again this is consistent with the previously noted definition of departure whereby both pilots indicated a threshold on rate of motion; however, the pilots were vague as to the value (e.g., "maybe 20 or 30 deg/sec"). One data point in Figure 88 violates the boundary. This is the augmented Configuration C_2. In this case the SRI eliminated adverse yaw and thus made the vehicle more departure resistant (as viewed by RC). However, it could be departed; and then the augmentation produced pro-spin control. Pilot JF rated <u>spin</u> susceptibility (and recovery) and apparently rated this configuration accordingly.

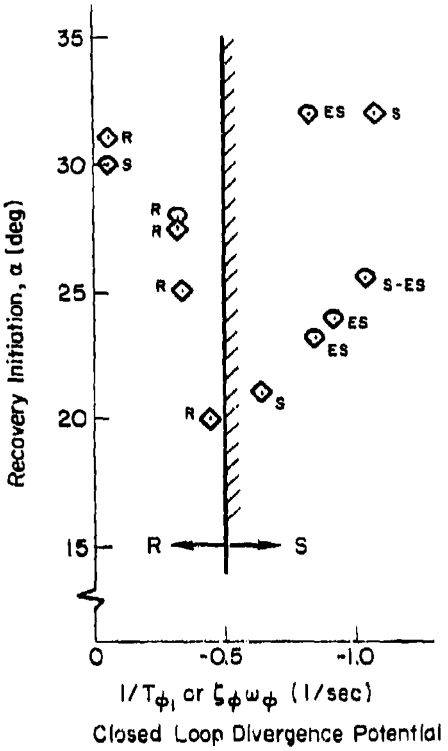

Figure 88. Departure Susceptibility Rating Versus Lateral Closed-Loop Divergence Potential

The implication is that if the combined aerodynamics and flight control system design is such that $1/T_{\phi_1}$ never exceeds −0.5 throughout the achievable AOA range, the airplane will be departure-resistant. It should be noted that this criterion places no restriction on open-loop stability. For example, $C_{n_{\beta_{dyn}}}$ can be negative and, in fact, is negative for Configuration D (see Figure 62) which is rated departure-resistant (see Table 13) by both pilots.

Since ω_ϕ^2 is the dimensional form of LCDP and since, in general, $|1/T_{\phi_1}|^2 \doteq |\omega_\phi^2|$, then one can relate the above $1/T_{\phi_1}$ boundary to an equivalent LCDP. For the flight conditions, inertias, etc., employed in this simulation, $1/T_{\phi_1}$ of −0.5 corresponds to LCDP of −0.001. This coincides with Weissman's boundary between Regions A and B for positive

$C_{n_{\beta_{dyn}}}$, see Figure 89; however, it is a little more conservative at negative $C_{n_{\beta_{dyn}}}$. Thus, the results of our simulation are compatible with and support Weissman's empirically derived LCDP boundary. The key difference in the criterion is that $1/T_{\phi_1}$ is not restricted to airframe lateral-directional static coefficients but can be applied to the completely coupled 6 DOF airframe with a full complement of augmentation, stick-to-rudder crossfeed, etc., throughout the aircraft development cycle.

In addition, results of our simulation tend to indicate that another boundary might be appropriate in the upper left quadrant of Figure 89 to create two additional regions, E and F, as suggested in Reference 40. Region E would be classified as mild directional divergence and moderate spin tendency. Region F might be classified as severe directional divergence and strong spin tendency. Note from Figure 63 that our aircraft Configuration D, which had mild departure characteristics but little or no spin tendency, would extend into Region E.

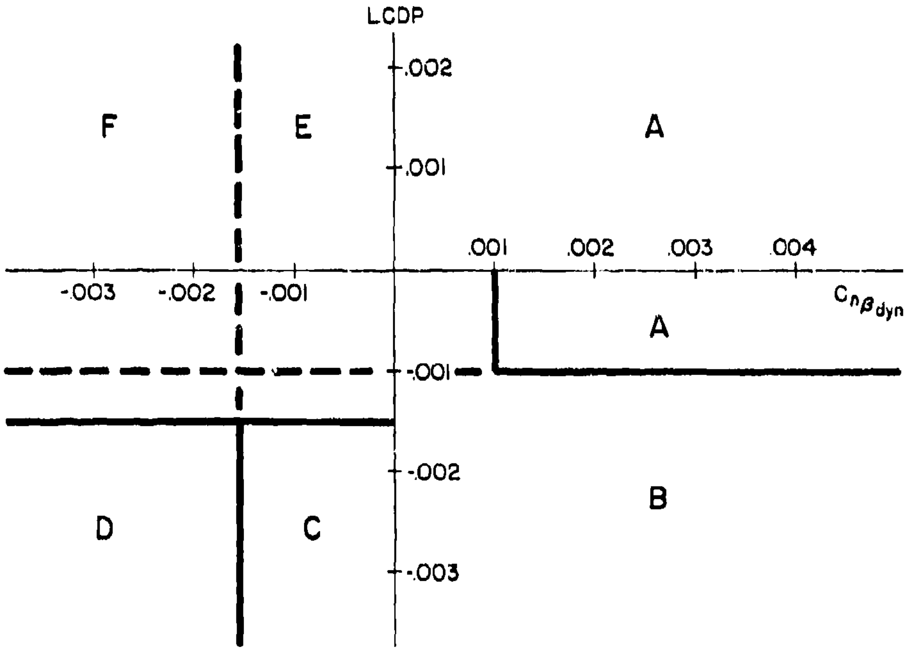

Figure 89. Possible Modifications to Weissman Criterion

Additional support for the limit on $1/T_{\phi_1}$ can be drawn from the current MIL-F-8785C spiral divergence limit. The Level 3,[*] Category A and C Flight Phases requirement is that time to double amplitude be not less than 4 sec. This limit came, in part, from the Reference 41 investigation in which aircraft configurations having various spiral divergence rates were rated by twelve pilots in a landing approach task. Results of that investigation, shown in Figure 90, indicate that divergences having a time to double amplitude of less than 2.4 sec were considered intolerable. The time to double amplitude (T_2) can be converted to an equivalent first-order time constant (T) by the relationship

$$T_2 \doteq 0.74T$$

A plot of pilot rating versus spiral-mode inverse time constant (1/T) is presented in Figure 91. The current -8785C Level 3 spiral limit is shown along with the proposed $1/T_{\phi_1}$ limit.

The two limits are in good agreement when it is remembered that $1/T_s$ represents a pole (modal response) while $1/T_{\phi_1}$ represents a zero. Under closed-loop roll control the migration of an airframe pole toward $1/T_{\phi_1}$ would be dependent upon pilot gain; infinite loop gain would be required to obtain a closed-loop pole exactly at the zero location. A more realistic situation is shown in Figure 92, which is a Bode-siggie plot for Configuration A_1 at $\alpha = 21$ deg, $\beta = 0$ deg. The dashed line terminating at $1/T_{\phi_1} = -0.6$ is the locus of the closed-loop first-order divergence root for increasing gain, K_ϕ. Two typical gain lines for Pilot RC extracted from simulation traces at $\alpha = 21 \pm 1$ deg are shown. These closures result in closed-loop roots at -0.2 and -0.33 rad/sec. Referring back to Figure 91, it may be observed that these straddle the

---

[*] Level 3: "Flying qualities such that the airplane can be controlled safely, but pilot workload is excessive or mission effectiveness is inadequate, or both. Category A Flight Phases can be terminated safely, and Category B and C Flight Phases can be completed."

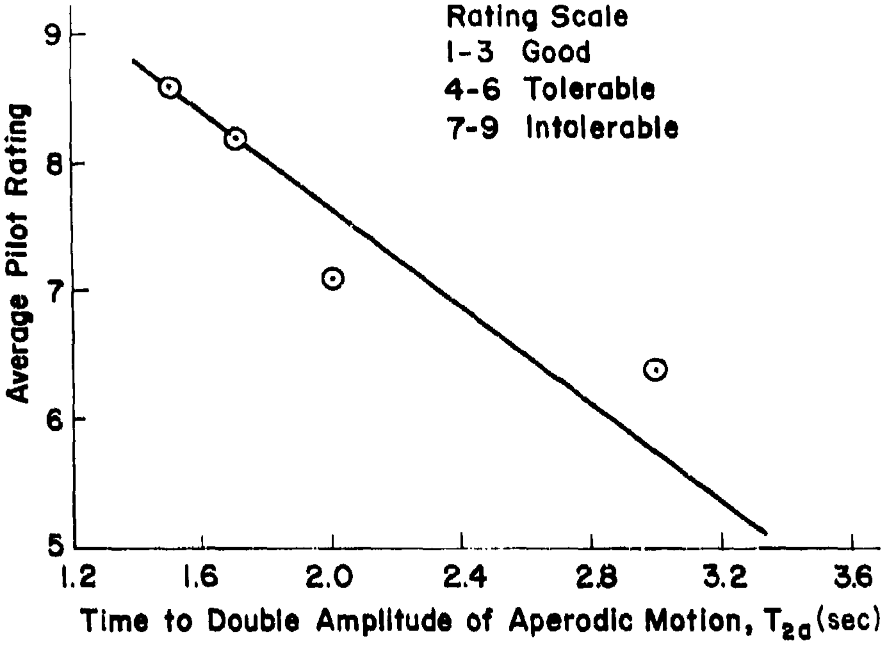

Figure 90. Variation of Pilot Ratings with Time to Double Amplitude of Aperiodic Motion; Landing Approach Condition (from Ref. 40)

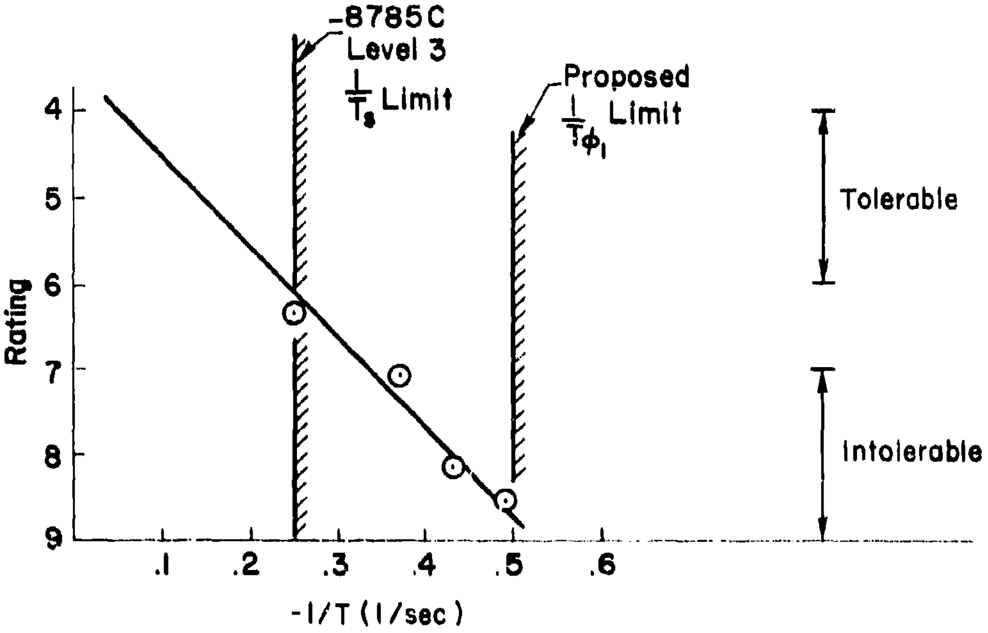

Figure 91. Variation of Pilot Ratings with Equivalent Aperiodic Inverse Time Constants

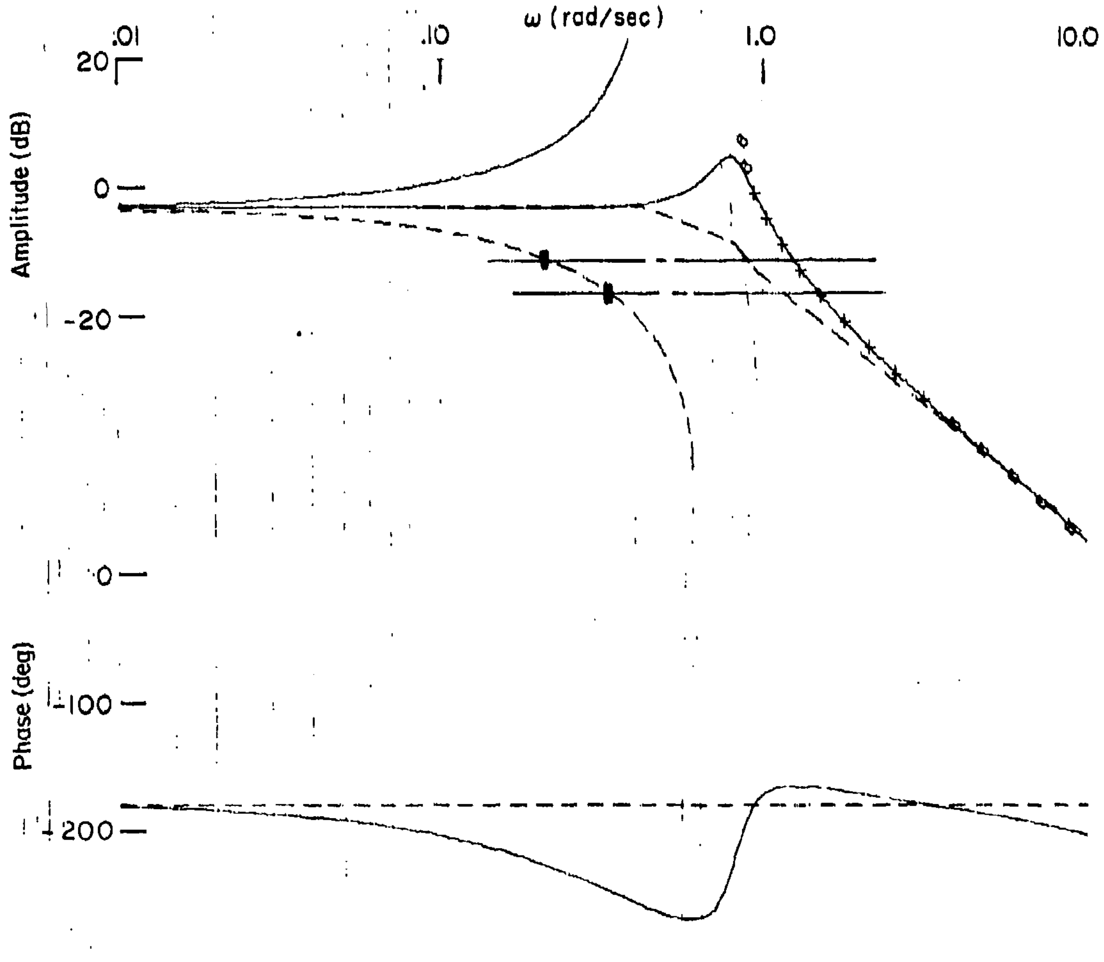

Figure 92. Migration of Closed-Loop Pole into RHP with Typical Roll Loop Gains

$1/T_s$ boundary and are consistent with the Reference 40 division between tolerable and intolerable handling. Again, our Pilot RC considered Configuration A_1 to be departure-resistant (R).

The above discussion tends to show that the $1/T_{\phi_1}$ limit selected (-0.5) may not be conservative, since a very tight roll loop closure could result in closed-loop roots in the intolerable range of Figure 91. Further investigation will be required to determine if the limit should be reduced.

C. SUMMARY

Analysis and piloted simulation have shown that:

- The pilot's perception of departure susceptibility was found to be correlated with movement of one root of the roll numerator for lateral stick control into the RHP of the root locus, i.e., a nonminimum-phase zero. If pilots could fly the aircraft to such AOAs, they rated high AOA configurations which produced a zero, $1/T_{\phi_1}$, more negative than -0.5 departure-susceptible. If this boundary was not or could not be exceeded, the aircraft was considered departure-resistant. This rating is not a function of the sign or magnitude of the dynamic stability parameter $C_{n_{\beta_{dyn}}}$.
- A value of $1/T_{\phi_1} = -0.5$ corresponds for the airframe tested to an effective LCDP of -0.001 and thus is consistent with and supports the empirically derived LCDP departure boundary developed by Weissman. However, results of the simulation were not in agreement with the types of departure predicted by Weissman in that negative $C_{n_{\beta_{dyn}}}$ regions produced yaw or nose-slice type departures.
- A value of $1/T_{\phi_1} = -0.5$ also is compatible with the current MIL-F-8785C Level 3 limit for spiral divergence in Category A and C Flight Phases.

It is suggested that as the aircraft design/development cycle progresses past the static wind tunnel phase the Weissman criterion for departure/spin susceptibility be replaced by a negative $1/T_{\phi_1}$ limit.

SECTION VIII

CONCLUSIONS AND RECOMMENDATIONS

The goals of this research program were to:

- Identify key design parameters that limit high-angle-of-attack maneuverability for contemporary high-performance attack and fighter-type aircraft.
- Postulate fundamental aerodynamic and control system design methodologies that will alleviate the limiting conditions.
- Formulate handling qualities requirements for high-angle-of-attack maneuvering flight to be incorporated in MIL-F-8785C, "Flying Qualities of Piloted Airplanes."

It should be borne in mind that the results are based on variations on a single nonlinear aerodynamic model representing a region dominated by phenomena that are highly configuration-dependent. Therefore, the generalizations drawn are in need of further substantiation.

A. KEY MANEUVER-LIMITING FACTORS

The most crucial factors pertain to limiting the safe flight envelope, i.e., departure from controlled flight. By varying static aerodynamic coupling and cross-coupling coefficients, the nature of high AOA characteristics and susceptibility to departure were changed to reflect nose slice, rolling, and pitch-up departures.

Nose slice (yaw) departures predominated for configurations having $Cn_{\beta_{dyn}}$ large, negative. Analysis and prior simulation have shown that nose slice can be aggravated once sideslip starts by the static aerodynamic coefficients C_{ℓ_α} and C_{n_α}. These aerodynamic coupling terms can cause a cross-coupled RHP zero to appear in the pitch numerator, $N^{\theta}_{\delta_{stab}}$. Any simultaneous attempt to control pitch attitude then produces or further aggravates directional divergence. The large negative $C_{n_{\beta_{dyn}}}$ configurations were prone to flat spins.

Rolling departures predominated when a large C_{ℓ_β} component made $Cn_{\beta_{dyn}}$ positive. These configurations also were prone to wing rock and lateral PIO. They exhibited at least two different PSG and spin modes, and were sensitive to maneuver and pilot activity at departure onset.

Pitch due to sideslip, C_{m_β}, of either positive or negative sign can adversely influence departure and handling characteristics. Positive C_{m_β} can produce pitch-up which tends to mask a "g-break" stall warning cue and oppose pilot attempts to prevent stall/departure via forward stick. Negative C_{m_β} tends to augment "g-break" stall warning but reinforces pilot-commanded recovery pitching moment to the point that pitch-roll-yaw coupling may produce violent PSG. The presence of appreciable C_{m_β} can be detected from flight traces of motion about a nominal zero sideslip via a longitudinal oscillation at twice the dutch roll frequency.

Unstable open-loop characteristic modes (poles) alone were not found to limit the safe flight envelope. If the pertinent control numerator zeros were favorably located (LHP), the pilot could prevent divergence. If the zeros were unfavorably located (RHP) divergence could not be prevented; in this case the presence of open-loop instability increased departure severity. Thus, pole-zero locations had influence on departure susceptibility and severity. In turn, pole-zero locations were shifted by static aerodynamic cross-coupling derivatives ($\mathcal{L}'_\alpha$, N'_α, M_β) when the magnitudes of these coefficients approached those of the common static stability derivatives ($\mathcal{L}'_\beta$, N'_β, M_α):

- $\mathcal{L}'_\alpha$, N'_α, and M_β, in combination, influence the high-frequency modes of both the lateral and longitudinal denominators.
- N'_α and M_β, in combination, influence the zeros of $N^{\phi}_{\delta_{stk}}$.
- N'_α and $\mathcal{L}'_\alpha$, in combination, influence the zeros of $N^{\theta}_{\delta_{stab}}$.

B. ADDITIONAL FINDINGS AND CONCLUSIONS

One major contribution has been identification and validation that pilot perception of lateral-directional departure susceptibility is related to one zero of the numerator $N^{\phi}_{\delta_{stk}}$ becoming negative. Root magnitudes more negative than −0.5 rad/sec were consistently rated as departure-susceptible, while those less negative (or positive) are rated as departure-resistant. This criterion reflects a closed-loop divergence rate limit related to the pilot's threshold for uncommanded motion or ability to cope. As such it is a pilot-centered criterion which should be applicable for any flight situation, although it has been identified in a low-Mach-number, fixed-base simulation. It is consistent with the empirically established airframe-alone departure/spin criterion boundaries of Weissman and extends applicability of that criterion to highly augmented airframe cases. It is also consistent with previous in-flight simulation of maximum controllable aperiodic divergence rates. Finally, it serves as both a design guide and a flying quality specification item.

The "unstable" (RHP) zero generally results from negative (adverse) Cn_{β} and $Cn_{\delta_{stk}}$. It therefore can be alleviated by aircraft configuration and flight control system modifications which principally alter those coefficients. As noted above, the zero also can be highly influenced by the static aerodynamic cross-coupling coefficients $C_{n_{\alpha}}$ and $C_{m_{\beta}}$.

A second major contribution has been the development and partial validation of a flying quality rating scale applicable to the stall/departure/recovery flight regime. It is believed that the scale has potential for defining the aircraft permissible flight envelope in much the same manner as the Cooper-Harper scale is now used in defining flying quality bounds.

The simulation demonstrated the importance of loss-of-control warning in pilot assessment of high AOA flying qualities and departure susceptibility. A gradual and consistent degradation in stability and controllability was found to provide the best warning; however, the realization of such warning can be highly dependent upon pitch control power. Oscillations such as wing rock or lateral PIO cannot be counted on for departure warning in air combat if the aircraft can be pulled through the "warning" region before the oscillation becomes apparent to the pilot.

Low-frequency dutch roll or lateral phugoid oscillation was found to mask departure onset. Roll about the velocity vector at high AOA produces significant "nose" yaw. The pilot has considerable difficulty differentiating between nose slice onset and low-frequency roll oscillation about the velocity vector. High roll rate damping (natural or augmented) was also found to reduce high AOA departure warning and increase flat spin tendency.

A flight control or augmentation system mechanization which improves and extends the aircraft controllability range by removing natural warning can actually be a detriment if the aircraft can still reach some departure AOA. To be of real benefit such a flight control system must also prevent departure.

A stick-to-rudder interconnect (SRI) can be beneficial in reducing adverse "aileron" yaw, thereby providing more favorable LCDP or $1/T_\phi$ values. However, if static aerodynamic cross-coupling is strong, the analysis of Configuration A_2 has shown that even small sideslip can shift the numerator roots in a manner to negate the SRI contribution. These results also imply that a finite-authority β-limiter may be of little benefit as a departure preventer if one or more RHP zeros occur in control loops the pilot is closing. That is, pilot control can drive the vehicle into a divergence which may exceed the β-limiter's capability.

Results of this study demonstrate that linear or quasi-linear frozen-point analysis is applicable to high AOA situations, but considerable caution must be exercised in the interpretation of results where aerodynamics are strong functions of angles of attack and sideslip. Any analysis pertaining to such regions must be based on a 6 DOF model with aerodynamic and kinematic cross-coupling terms, must include non-zero-sideslip trim points, must view transfer-function numerator as well as characteristic-equation parameters, and must be supported by nonlinear simulations.

In particular, the results demonstrated the power of vector polygon and closed-loop root extraction analytic techniques for identifying cause-effect relationships in highly coupled dynamic systems. The techniques facilitated development of transfer-function literal approximate factors for the F-4 in high AOA, non-zero-sideslip flight conditions.

C. PROPOSED MIL-F-8785C MODIFICATIONS

Based upon results of this program it is recommended that modifications to MIL-F-8785C requirements be considered in three areas.

1. Departure from Controlled Flight

The current paragraph (3.4.2.2.1) simply requires that "all Classes of aircraft be extremely resistant to departure from controlled flight, post-stall gyrations and spins....The aircraft shall exhibit no uncommanded motion which cannot be arrested promptly by simple application of pilot control."

The "uncommanded motion" requirement should be strengthened to require that, for roll control input within the service flight envelope (SFE) the following stability axis parameter values shall be no more negative than:

$$\text{Unaugmented airframe:} \quad \text{LCDP} = C_{n_\beta} - \frac{C_{n_{\delta_a}}}{C_{\ell_{\delta_a}}} C_{\ell_\beta} > -0.01$$

$$\text{Augmented airframe:} \quad 1/T_{\phi_1} > -0.5$$

An alternate requirement might be that the aircraft should exhibit no aperiodic uncommanded motion which exceeds 20 deg/sec and cannot be arrested promptly by simple application of pilot control. [The value selected here is based on a rough average of the simulation pilots' commentary as to their definitions of departure, the spiral divergence mode limit of Reference 40, and the $1/T_{\phi_1}$ limit above.]

Since the SFE specifically excludes stall and departure, the above criteria would automatically cover high AOA, pre-stall flight. Other potential locations for such wording are paragraphs 3.4.2.1.1, Stall Approach, and 3.4.2.1.2, Stall Characteristics.

2. Stall Definition

The current paragraph (3.4.2.1) allows definition of stall to be based on $C_{L_{max}}$; abrupt uncontrollable pitching, rolling, or yawing; or intolerable buffet. The results of our piloted simulation indicate that any abrupt aperiodic rolling or yawing motion which occurs without being preceded by noticeable "g-break" is considered to be a departure, not a stall, and results in severely downgraded flying qualities. Thus, abrupt roll or yaw motion should be deleted as an allowable definition of stall and should not occur prior to stall. If such characteristics cannot be achieved with the airframe alone, then the flight control system should prevent reaching the AOA at which the abrupt rolling or yawing motion is obtained.

3. Departure Warning

The current paragraphs (3.4.1.1, 3.4.2.1.1.1, and 3.4.2.1.1.2) covering warning pertain mainly to stall. But, since abrupt uncommanded roll or yaw is also considered to define stall, the Paras. 3.4.2.1.1.1 and 3.4.2.1.1.2 requirements, in effect, define departure warning. These requirements are based upon fixed margins of V_{stall} or $C_{L_{stall}}$ and do not take into account the severity of any post-stall/departure motion, uncontrolled altitude loss, or mission phase.

Results of this simulation indicated that stall/departure warning margin should be related to the severity of any uncommanded motion or PSG. Time and altitude loss prior to recovery were heavily dependent upon the initial departure severity; pilot commentary indicated the overall departure ratings obtained were heavily influenced by altitude loss and mission phase. Quite obviously, consequences of stall/departure in a ground attack phase can be more catastrophic than in high-altitude air combat. Unfortunately, insufficient data were obtained to establish a specific departure warning criterion.

4. Compliance Demonstration

The current specification (Para. 4.1) allows compliance with all requirements of Section 3 to be demonstrated through analysis. Although compliance with many of the requirements will be demonstrated by simulation, test, or both, this analysis and simulation program has demonstrated that linearized, frozen-point analytic results may be midleading or extemely difficult to interpret for flight regions where the airframe may exhibit large static aerodynamic cross-coupling moments. Therefore, it is recommended that the requirement be changed so that compliance with paragraphs pertaining to stall/departure must be demonstrated via simulation and/or flight.

REFERENCES

1. Sisk, T. R., D. A. Kier, and P. C. Carr, *Factors Affecting Tracking Precision of Fighter Aircraft*, NASA TM X-2248, Mar. 1971.

2. *Stall/Post-Stall/Spin Symposium*, proceedings of conference sponsored by ASD/AFFDL at Wright-Patterson AFB, Ohio, 15-17 Dec. 1971.

3. Weissman, Robert, *Criteria for Predicting Spin Susceptibility of Fighter-Type Aircraft*, ASD-TR-72-48, June 1972.

4. Pelikan, R. J., "Evaluation of Aircraft Departure Divergence Criteria with a Six-Degree-of-Freedom Digital Simulation Program," AIAA Paper 74-88, Jan. 1974.

5. Johnston, Donald E., Irving L. Ashkenas, and Jeffrey R. Hogge, *Investigation of Flying Qualities of Military Aircraft at High Angles of Attack. Vol. I: Technical Results*, AFFDL-TR-74-61, June 1974.

6. Teper, Gary L., and Donald E. Johnston, *F4J Data Package*, Systems Technology, Inc., WP-2041-1, June 1974.

7. Burris, W. R., and J. T. Lawrence, "Aerodynamic Design and Flight Test of US Navy Aircraft at High Angles of Attack," *Fluid Dynamics of Aircraft Stalling*, AGARD CP-102, Nov. 1972, pp. 25-1 to 25-10.

8. Bowser, D. K., *F-4 High-AOA Data Package*, McDonnell Aircraft Co., Rept. MDC A0005, Vol. II, 15 Aug. 1969 (digitized data).

9. Grafton, Sue B., and Charles E. Libbey, *Dynamics Stability Derivatives of a Twin-Jet Fighter Model for Angles of Attack from -1° to 110°*, NASA TN D-6091, Jan. 1971.

10. Meintel, Alfred J., Jr., Jack E. Pennington, and Walter W. Hankins III, *Differential Maneuvering Simulator Validation*, NASA TM X-2827, Oct. 1973.

11. Rutan, Elbert L., Collet E. McElroy, and Jerauld R. Gentry, *Stall/Near Stall Investigation of the F-4E Aircraft*, FTC-TR-70-20, Aug. 1970.

12. Brady, C. C., and J. Hodgkinson, *Validation of the Flying Qualities Requirements of MIL-F-008785A(USAF)*, AFFDL-TR-70-155, Jan. 1971.

13. Chapman, G. T., E. R. Keener, and G. N. Malcolm, "Asymmetric Aerodynamic Forces on Aircraft Forebodies at High Angles of Attack — Some Design Guides," *Stall/Spin Problems of Military Aircraft*, AGARD CP-199, June 1976.

14. Cord, T. J., *Hysteresis Induced Wing Rock*, AFFDL-TM-75-76-FGC, June 1975.

15. Hall, W. E., Jr., *Identification of Aircraft Stability Derivatives for the High Angles of Attack Regime*, Systems Control, Inc., Tech. Rept. No. 1, June 1973.

16. Hamel, P., "A Systems Analysis View of Aerodynamic Coupling," *J. Aircraft*, Vol. 7, No. 6, Nov.-Dec. 1970, pp. 567-569.

17. Orlick-Ruckemann, K. J., "On Aerodynamic Coupling Between Lateral and Longitudinal Degrees of Freedom," AIAA Paper 77-4, Jan. 1977.

18. Kalviste, Juri, "Aircraft Stability Characteristics at High Angles of Attack," *Dynamic Stability Parameters*, AGARD CP-235, May 1978.

19. Rutan, E. L., and J. R. Gentry, *Category II Stability and Control Evaluation of the F-4E Aircraft*, AFFTC-SD-69-14, July 1969.

20. McRuer, Duane, Irving Ashkenas, and Dunstan Graham, *Aircraft Dynamics and Automatic Control*, Princeton Univ. Press, 1973.

21. Sewell, C. A., *F-14 Erect Spin Characteristics*, Grumman Aerospace Corp., unpublished document.

22. Weber, C. L., A. L. Burgess, and M. J. Humphrey, *Model F-14A Airplane High Angle of Attack Flying Qualities Evaluation, Vol. I*, NATC Rept. SA-C11R-77, Dec. 1977.

23. Gilbert, William P., L. T. Nguyen, and R. W. Van Gunst, *Simulator Study of Applications of Automatic Departure and Spin-Prevention Concepts to a Variable-Sweep Fighter Airplane*, NASA TM X-2928, Nov. 1973.

24. Bihrle, William, Jr., and A. C. Hegman, *F-14 Spin Avoidance/Prevention Program, Final Report, Vol. II*, Grumman Aerospace Corp., A51-335-R-72-1, Mar. 1972.

25. Grafton, Sue B., and E. L. Anglin, *Dynamic Stability Derivatives at Angles of Attack from -5° to 90° for a Variable-Sweep Fighter Configuration with Twin Vertical Tails*, NASA TN D-6909, Oct. 1972.

26. Bihrle, William, Jr., and B. Barnhart, *Effects of Several Factors on Theoretical Predictions of Airplane Spin Characteristics*, NASA CR-137521, Aug. 1974.

27. Boisseau, Peter C., and Joseph R. Chambers, *Lateral-Directional Characteristics of a 1/10-Scale Free-Flight Model of a Variable Sweep Fighter Airplane at High Angles of Attack*, NASA TM SX-2649, Dec. 1972.

28. Kelly, C. P., *F-14 Flight Test Data*, Grumman Aerospace Corp., EG-GC-LTR-76-02, Nov. 1976.

29. Porter, R. F., and J. P. Loomis, "Examination of an Aerodynamic Coupling Phenomenon " *J. Aircraft*, Vol. 2, No. 6, Nov.-Dec. 1965, pp. 553-556.

30. Polhamus, E. C., *Some Factors Affecting the Variation of Pitching Moment with Sideslip of Aircraft Configurations*, NASA TN D-4016, Aug. 1958.

31. Titiriga, A., Jr., J. S. Ackerman, and A. M. Skow, "Design Technology for Departure Resistance of Fighter Aircraft," *Stall/Spin Problems of Military Aircraft*, AGARD CP-199, June 1976, pp. 5-1 through 5-14.

32. Weissman, R., "Status of Design Criteria for Predicting Departure Characteristics," AIAA Paper 74-791, Aug. 1974.

33. Ashkenas, Irving L., and Duane T. McRuer, *Approximate Airframe Transfer Functions and Application to Single Sensor Control Systems*, WADC TR-58-82, June 1958.

34. *Stall/Post-Stall/Spin Flight Test Demonstration Requirements for Airplanes*, MIL-S-83691A(USAF), 15 Apr. 1972.

35. Bihrle, W., Jr., and B. Barnhart, *Design Charts and Boundaries for Identifying Departure Resistant Fighter Configurations*, NADC-76154-30, July 1978.

36. Twisdale, Thomas R., and David L. Franklin, *Tracking Test Techniques for Handling Qualities Evaluation*, AFFTC-TD-75-1, May 1975.

37. Hoh, Roger H., *A Pilot Rating Scale for Vortex Hazard Evaluation*, NASA CR-143836, June 1975.

38. *HAME Research Simulation*, AFFDL-FGC and AFFTC, Apr. 1977.

39. Wood, R. A., High AOA Departure Rating Scales, AFFTC/TEEEP letter to Mr. R. O. Anderson, AFFDL/FGC, 12 Sept. 1978.

40. Skow, A. M., and A. Titiriga, Jr., "A Survey of Analytical and Experimental Techniques to Predict Aircraft Dynamic Characteristics at High Angles of Attack," Dynamic Stability Parameters, AGARD CP-235, Nov. 1978.

41. Liddell, C. J., B. Y. Creer, and R. D. Van Dyke, Jr., A Flight Study of Requirements for Satisfactory Lateral Oscillatory Characteristics of Fighter Aircraft, NACA RM A51E16.

☆U.S.Government Printing Office: 1981 — 757-002/608